TUDelft

Delft University of Technology

From Cue to Construct

Cues, Mechanisms, and Stability in Haptic Perception

Driller, K.K.

Important note
To cite this publication, please use the final published version (if applicable).
Please check the document version above.

FROM CUE TO CONSTRUCT

CUES, MECHANISMS, AND STABILITY IN HAPTIC PERCEPTION

FROM CUE TO CONSTRUCT

CUES, MECHANISMS, AND STABILITY IN HAPTIC PERCEPTION

Dissertation

for the purpose of obtaining the degree of doctor
at Delft University of Technology
by the authority of the Rector Magnificus, prof. dr. ir. T.H.J.J. van der Hagen,
chair of the Board for Doctorates
to be defended publicly on
Friday 6 December 2024 at 15:00 o'clock

by

Karina Kirk DRILLER

Master of Science in Psychology, Aarhus University, Denmark
born in Flensburg, Germany

This dissertation has been approved by the promotors.

Composition of the doctoral committee:

Rector Magnificus,	chairperson
Prof.dr.ir. **R.H.M. Goossens**,	Delft University of Technology, *promotor*
Dr. **J. Hartcher-O'Brien**,	Delft University of Technology, *copromotor*
Prof.dr. **V. Hayward †**,	Sorbonne Université, *promotor*

Independent members:

Prof.dr. **Y. Visell**,	University of California, Santa Barbara
Prof.dr. **M. Wexler**,	CNRS, Université de Paris
Dr. **M. Di Luca**,	University of Birmingham
Prof.dr. **D.V. Keyson**,	Delft University of Technology

Additional member:

Prof.dr. **G. Bailly**,	CNRS, Sorbonne Université, *non-independent member*

In memory of **Vincent Hayward**, who provided invaluable guidance and support as supervisor and promotor.

CONTENTS

SUMMARY

Haptic perception serves as one of our primary interfaces to the physical world. Without it, our ability to understand and respond to a world full of objects and physical beings would be profoundly impaired. This dissertation addresses how we reconstruct perceptually what is in contact with our skin from mechanical inputs that are behaviorally relevant during haptic interactions. Behaviorally relevant information is defined as the kind of information that allows the sensory system to achieve its goals. A primary goal of the somatosensory system is to enable the exploration and dexterous manipulation of objects.

Following an introduction (Chapter 1), which covers fundamental concepts related to the emergence of stable haptic percepts, the dissertation comprises a series of experimental studies aimed at uncovering the essential cues and mechanisms used by the sensory system to perceptually reconstruct different haptic interactions. Because most haptic interactions start with the detection of contact, the first challenge taken in Chapter 2 is to identify what information the sensory system uses to detect basic impact events. This first part of the dissertation uncovers an intensity metamer in the encoding of such impact events, in which the duration and amplitude of the impact can be interchanged for the same perceptual outcome. The work further suggests that while the total amount of energy transferred by a force (i.e., the mechanical work) is an important cue, it is not the sole determinant in the perceptual decomposition of haptic skin-object interactions.

The focus then moves towards more complex everyday-like skin-object interactions. Because texture and material cues are critical to grasp and sliding behavior, the dissertation places special emphasis on haptic texture and material perception (i.e., roughness and compliance perception), spanning three full chapters. Given the high-dimensional nature of haptic material and texture perception, Chapter 3 explores how we can capture the complexity of haptic interactions with naturalistic surfaces without compromising on the experimental control needed to link specific cues to perceptual phenomena. This problem is addressed via the development of a dual-property stimulus database containing well-characterized stimuli that resemble the statistics of naturally occurring rough and compliant surfaces. In a following experiment, Chapter 4 then explores the contribution of vibratory propagation waves in perceptually reconstructing these surfaces by eliminating cutaneous information using local anesthesia of the index finger. We identify propagation waves as both a behaviorally relevant cue and a sufficient cue for roughness perception, though this finding applies only to some participants. The perceived softness of these surfaces, on the other hand, is strongly diminished when local tactile information is removed. Chapter 5 subsequently explores the combined influence of surface features and material elasticity in mediating roughness and softness perception and highlights a perceptual confound in the reconstruction of surface roughness. The work uncovers roughness metamers, that is, regions where different combinations of elasticity and surface roughness lead to identical perceptual outcomes.

The final empirical chapter of this dissertation (Chapter 6) examines how the perceived time of dynamic haptic interactions changes when behaviorally relevant local tactile cues are removed. A temporal-binding task is used to illuminate the role of cutaneous cues in estimating the time course of a mechanical skin-button interaction and its sensory outcomes.

Together, the dissertation uncovers essential cues and mechanisms underlying the perceptual reconstruction of haptic interactions, emphasizing the importance of accurately identifying the physical, mechanical, and neural cues, as well as the mechanisms, that shape our world of touch.

SAMENVATTING

Haptische perceptie dient als een van onze primaire interfaces met de fysieke wereld. Zonder dit vermogen zou ons vermogen om een wereld vol objecten en fysieke wezens te begrijpen en erop te reageren ernstig worden aangetast. Deze scriptie behandelt hoe we perceptueel reconstrueren wat in contact is met onze huid vanuit gedrag-relevante mechanische input tijdens haptische interacties. Gedrag-relevante informatie wordt gedefinieerd als het soort informatie dat het sensorische systeem in staat stelt zijn doelen te bereiken, en een primair doel van het somatosensorische systeem is het mogelijk maken van de exploratie en vaardige manipulatie van objecten.

Na een inleiding (Hoofdstuk 1), die fundamentele concepten met betrekking tot het ontstaan van stabiele haptische percepties behandelt, omvat de scriptie een reeks experimentele studies gericht op het ontdekken van de essentiële aanwijzingen en mechanismen die worden gebruikt om verschillende haptische interacties perceptueel te reconstrueren. Aangezien de meeste haptische interacties beginnen met het detecteren van contact, is de eerste uitdaging in Hoofdstuk 2 om te identificeren welke informatie het sensorische systeem gebruikt om het begin van huidcontact tijdens basisimpactgebeurtenissen te detecteren. Dit eerste deel van de scriptie onthult een basisintensiteitmetameer voor de codering van impactgebeurtenissen en suggereert dat de totale hoeveelheid energie die door een kracht wordt overgedragen (d.w.z. de geleverde mechanische arbeid) een belangrijke aanwijzing is, maar niet de enige bepalende factor bij de perceptuele ontleding van haptische huid-objectinteracties.

De focus verschuift vervolgens naar meer complexe alledaagse huid-objectinteracties. Omdat textuur- en materiaalaanwijzingen cruciaal zijn voor grijpen en glijgedrag, wordt speciale nadruk gelegd op haptische textuur- en materiaalperceptie (d.w.z. ruwe en zachte perceptie), die drie volledige hoofdstukken van dit proefschrift beslaan. Gezien de hoge dimensionaliteit van haptische materiaal- en textuurperceptie, onderzoekt Hoofdstuk 3 eerst hoe we de complexiteit van haptische interacties met naturalistische oppervlakken kunnen vastleggen zonder concessies te doen aan de experimentele controle die nodig is om specifieke aanwijzingen te koppelen aan perceptuele fenomenen. Dit probleem wordt aangepakt door de ontwikkeling van een stimulusdatabase met dubbele eigenschap die goed gekarakteriseerde stimuli bevat die lijken op de statistieken van natuurlijk voorkomende ruwe en zachte oppervlakken. In een volgend experiment verkent Hoofdstuk 4 vervolgens de bijdrage van vibratiepropagatiegolven bij het perceptueel reconstrueren van deze oppervlakken door cutane informatie te elimineren met behulp van lokale anesthesie van de wijsvinger. We identificeren propagatiegolven als een gedrag-relevante variabele voor ruwe perceptie voor sommige, maar niet alle deelnemers. De waargenomen zachtheid van deze oppervlakken daarentegen wordt sterk verminderd wanneer lokale tactiele informatie wordt verwijderd. Vervolgens verkent Hoofdstuk 5 de gecombineerde invloed van oppervlaktekenmerken en materiaaleigenschappen bij het

bemiddelen van ruwe en zachte perceptie en benadrukt een perceptuele verwarring bij de reconstructie van oppervlakteruwheid. Het werk vindt ruwheidsmetameren, dat wil zeggen gebieden waar verschillende combinaties van aanwijzingen leiden tot identieke perceptuele uitkomsten.

Het laatste empirische hoofdstuk van deze scriptie (Hoofdstuk 6) onthult het gevolg van de waargenomen timing van dynamische haptische interacties wanneer gedrag-relevante lokale tactiele aanwijzingen worden verwijderd. Een temporele-bindende taak wordt gebruikt om de rol van cutane aanwijzingen bij het schatten van het tijdsverloop van mechanische huid-knopinteractie te verduidelijken.

Gezamenlijk benadrukt het werk in deze scriptie het belang van het correct bepalen van de bijdragen van fysieke, mechanische en neurale niveau aanwijzingen en mechanismen bij het begrijpen van de reconstructie van onze tastwereld.

Résumé

La perception haptique constitue l'une de nos interfaces principales avec le monde physique. Sans elle, notre capacité à comprendre et à répondre à un monde rempli d'objets et d'êtres physiques serait profondément altérée. Cette thèse aborde la façon dont nous percevons ce qui est en contact avec notre peau lors d'interactions haptiques, grâce aux informations mécaniques comportementalement pertinentes générée sur la peau. L'information comportementalement pertinente est définie comme le type d'information qui permet au système sensoriel d'atteindre ses objectifs. Un des objectifs principaux du système somatosensoriel est de permettre l'exploration et la manipulation dextre des objets.

Après une introduction (Chapitre 1), qui couvre les concepts fondamentaux liés à l'émergence des percepts haptiques stables, la thèse comprend une série d'études expérimentales visant à découvrir les éléments et mécanismes essentiels utilisés par le système sensoriel pour reconstruire perceptuellement différentes interactions haptiques. Comme la plupart des interactions haptiques commencent par la détection d'un contact, le premier défi du Chapitre 2 est d'identifier quelles informations le système sensoriel utilise pour détecter des événements d'impact basiques. Cette première partie de la thèse met en évidence un métamère d'intensité dans l'encodage des événements d'impact, où la durée et l'amplitude de l'impact peuvent être interchangées tout en produisant le même résultat perceptif. Les résultats suggèrent en outre que bien que la quantité totale d'énergie transférée par une force (c'est-à-dire le travail mécanique) soit un indice important, ce n'est pas le seul déterminant dans la décomposition perceptuelle des interactions peau-objet haptiques.

La seconde partie de la thèse rapporte des résultats des interactions peau-objet plus complexes, semblables à celles du quotidien. Comme les éléments de texture et de matériau sont essentiels pour la préhension et le comportement de glissement, la thèse met particulièrement l'accent sur la perception haptique de la texture et du matériau (c'est-à-dire la perception de sa rugosité et de sa déformabilité), qui est développé sur trois chapitres entiers. Étant donné la nature multidimensionnelle de la perception haptique des matériaux et des textures, le Chapitre 3 explore comment nous pouvons capturer la complexité des interactions haptiques avec des surfaces naturelles sans compromettre le contrôle expérimental nécessaire pour relier des éléments spécifiques aux phénomènes perceptifs. Ce problème est abordé via le développement d'une base de données de stimuli à double propriété contenant des stimuli bien caractérisés qui reflètent les statistiques des surfaces rugueuses et déformables présentes dans la nature. Dans l' expérience suivante, le Chapitre 4 explore ensuite la contribution des ondes de propagation vibratoire dans la reconstruction perceptuelle de ces surfaces en éliminant l'information cutanée par anesthésie locale de l'index. Nous identifions les ondes de propagation comme étant à la fois un indice comportementalement pertinent et un indice suffisant pour la percep-

tion de la rugosité, bien que cette découverte ne s'applique qu'à certains participants. La perception de la souplesse de ces surfaces, en revanche, est fortement diminuée lorsque l'information tactile locale est supprimée. Enfin, le Chapitre 5 explore l'influence combinée des caractéristiques de surface et de l'élasticité du matériau dans la médiation de la perception de la rugosité et de la souplesse, et met en évidence une confusion perceptuelle dans la reconstruction de la rugosité de surface. Le travail révèle des métamères de rugosité, c'est-à-dire des régions où différentes combinaisons d'élasticité et de rugosité de surface conduisent à des résultats perceptuels identiques.

Le dernier chapitre, empirique, de cette thèse (Chapitre 6) examine comment la perception temporelle des interactions haptiques dynamiques est modifiée lorsque les éléments tactiles locaux comportementalement pertinents sont supprimés. Une tâche de liaison temporelle est utilisée pour éclairer le rôle des éléments cutanés dans l'estimation du déroulement temporel d'une interaction mécanique entre la peau et un bouton-poussoir, ainsi que ses effets sensorielles.

Dans son ensemble, cette thèse met en lumière les éléments et mécanismes essentiels qui sous-tendent la reconstruction perceptive des interactions haptiques, en soulignant l'importance d'identifier avec précision les indices physiques, mécaniques et neuronaux, ainsi que les mécanismes, qui façonnent notre monde tactile.

1

INTRODUCTION

Science and technology multiply around us.
To an increasing extent they dictate the languages in which we speak and think.
Either we use those languages, or we remain mute.

– J.G. Ballard

Author: Karina Kirk Driller

1.1. About this Dissertation

Haptic perception, that is the perception relating to the sensing of physical objects or their properties using touch and proprioception, plays a fundamental role in our experience of the world. It serves as the main tool for navigating our physical environment and constitutes the foundation for our own sense of physical presence. Without it, our ability to interact with and understand our physical surroundings would be profoundly impaired.

This dissertation is aimed at identifying behaviorally relevant cues and mechanisms used by the human sensory system in creating stable haptic percepts during skin-object interactions. **Behaviorally relevant** information is defined as information that allows the sensory system to draw *useful inferences about* and *efficiently interact with* the physical world. Because the ultimate goal of the sensory system is to reconstruct the environment to be able to interact with it, we can decompose this reconstruction process into physical, mechanical, and neural-level cues and mechanisms.

Fundamental to this dissertation is the idea that variation and noise are inherent to interactions with the physical environment and their perceptual reconstruction. As a finger slides across a surface, the speed, load, and orientation of the finger, as well as its hydration level and temperature, will typically vary—not only across different sliding interactions but even within a single sliding contact. Furthermore, even the simplest perceptual experiences (such as the perceived intensity of a contact or the roughness of a surface) are rarely informed by just a singular physical cue. Instead, they are typically the result of a combination of multiple cues relevant to behavior. Consider the well-known example of the perceived weight of an object, which can depend not only on its mass but also on its volume and temperature [1–3].

In order to identify the information used by the sensory system to detect relevant changes in skin-object interactions within this myriad of information and create stable percepts of interesting events, I adopt the concept of invariance. It is assumed that stability in the perceptual system's response to a given cue across some type of change is a key indicator to its behavioral relevance. By systematically manipulating the available cue space as well as the conditions under which cues are presented, it is possible to gain insights into the cues and mechanisms used by the sensory system to draw stable and behaviorally relevant haptic inferences. Within this framework, a special focus is directed towards the disclosure of so-called metamers. Metamers are instances in which physically distinct inputs give rise to the same perceptual experiences. They can provide insights about what information matters to the sensory system in creating perceptual inferences.

This dissertation provides empirical insights about such cues and mechanisms within three specific contexts. The first part of this dissertation is targeted at uncovering behaviorally relevant cues at the most basic level, namely for the detection of mechanical contact, which constitutes the foundation for largely any behaviorally relevant haptic interaction. The focus then shifts to haptic texture and material perception. Here we uncover and explore cues for the perceptions of roughness and softness during dynamic-touch interactions. Finally, in the last part of this dissertation,

we discover the consequences of the perceived timing of events when behaviorally relevant haptic cues are removed during dynamic skin-object interactions.

Before embarking on this endeavor, however, Section 1.2 and Section 1.3 of this introductory chapter equip the reader with the essential background information and key terminology needed to understand the emergence of stable haptic percepts. I start with the fundamentals of hand physiology and mechanical skin-object interactions, as well as key aspects of the somatosensory system in processing haptic inputs. From there, I provide a detailed account of several critical themes within the study of haptic perception. These include commonly investigated haptic qualities or "dimensions," the concepts of perceptual constancy and invariance, the integration of cues, and the idea of perceptual or sensory metamers. Armed with this foundational knowledge, readers will be well prepared for the specific motivations, research questions, and methodologies that drive this dissertation, which are detailed at the end of this introduction.

1.2. THE MECHANICS AND PHYSIOLOGY OF TOUCH

The haptic perception of external objects and their properties is first and foremost dictated by mechanical contact with them. This stems from the basic fact that solid objects do not interpenetrate [4]. This section addresses the most important concepts concerning the mechanics and physiology of touch. It begins with an overview of basic hand physiology, followed by an account of the mechanics of skin-object interactions, and concludes by addressing how the human somatosensory system processes these mechanical inputs.

1.2.1. HAND PHYSIOLOGY

Although behaviorally relevant haptic interactions can involve the entire body, the undoubtedly most relevant sensory "tool" when it comes to object manipulation and haptic exploration is the human hand. Its anatomical configuration and biomechanical properties have evolved to optimally facilitate object interactions and haptic perception [5, 6]. Concurrently, its inherent physiology also conditions the mechanics of touch interactions and imposes natural constraints on them.

The human hand is constituted of an assembly of bones, joints, muscles, tendons, ligaments, subcutaneous tissues, nerves, and skin. The skeletal structure comprises the bones in the fingers, known as the proximal, middle, and distal **phalanges**, as well as the **carpal** and **metacarpal** bones of the wrist and hand [7]. It provides a rigid framework connected by joints that in total give the human hand and wrist 21 degrees of freedom of movement [5]. Depending on how one considers certain subdivisions, between 29 and 38 muscles are generally said to be responsible for these movements [5, 8]. Most of these muscles are located in the forearm while some are located in the palm. The fingers themselves do not contain any muscles other than arrector pili, which are small muscles attached to hair follicles [7, 9].

Motor function and sensory innervation of the hand are provided by the radial, median, and ulnar nerves; each branching out extensively. The **radial nerve** primarily

innervates the dorsolateral part of the hand, while the **median nerve** innervates a large area of the volar surface as well as the lateral three-and-a-half fingers. The **ulnar nerve** innervates the volar and dorsal surfaces of the medial one-and-a-half fingers. However, considerable variation between individuals is common [7, 10]. Figure 1.1 shows the bone and muscular structure as well as innervation of the hand.
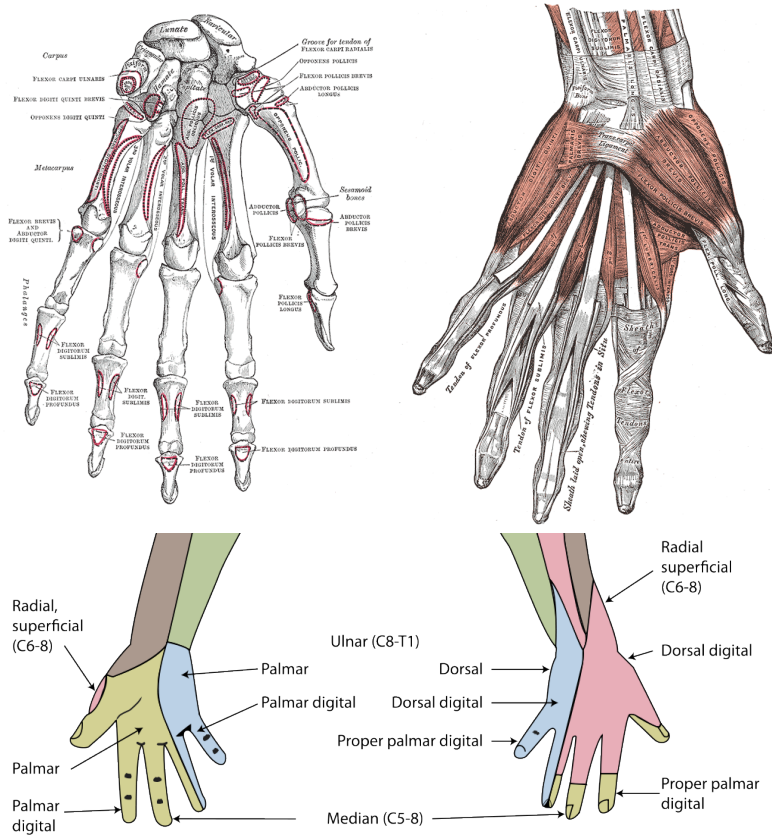
Figure 1.1. Top: Bones and muscles of the hand. Bottom: Innervation of the hand by the radial, medial, and ulnar nerves [11].

The properties of the skin itself, as well as the subcutaneous tissues of the hand and fingers, also shape the mechanics of touch during haptic interactions. The skin on the volar surface of the hand is referred to as **glabrous skin**. It is composed of the outer **epidermis** and the deeper **dermis**. Below the dermis lies the **hypodermis**, a layer of fatty, subcutaneous tissue that connects the dermis with the muscles and bones of the hand [5, 12]. While the dermis consists of two sub-layers, the epidermis of glabrous skin consists of five sub-layers, with the keratinous **stratum corneum** making up the protective outermost layer. Glabrous skin is generally thicker than the hairy skin found on the dorsal surface of the hand and most other body parts [13–15].

It also distinguishes itself from hairy skin through its high innervation of specialized mechanoreceptors (see Section 1.2.3) facilitating discriminative touch [16, 17]. On the surface, it features **papillary ridges**, likely playing a functional role in grip- and moisture regulation and in enhancing tactile sensitivity [18–20], and, compared to other areas of the skin, the glabrous skin contains a much higher density of **sweat glands** [21, 22]. Together, the soft tissue and skin on the volar surface of the hand are often referred to as **pulp** [23, 24]. Finally, on the dorsal side of the fingertips, the fingernail connects directly to the bone, providing a rigid link to it [10]. Notably, many of the biomechanical properties of the skin change with age, making the aging skin thinner and less flexible [25–27].

1.2.2. MECHANICS OF HAPTIC INTERACTIONS

The mechanical response of the hand during skin-object interactions, particularly with attention to the fingertips, has been studied extensively. One line of research has focused on determining the **mechanical impedance** of the fingertip, that is, the frequency-dependent link between force and resulting movement [28]. The bulk surface of the volar hand is capable of withstanding extraordinarily high deformation without damage [29]. In fact, a single fingertip can withstand forces of several hundred of Newtons, while maintaining the sensitivity to detect a needle [30]. Due to its complex structure, the fingertip is generally considered non-homogeneous, anisotropic, and non-linear, and there is general agreement that the fingertip pulp is best modeled as a **viscoelastic material** (e.g., [30–33]). At lower frequencies (below 100Hz) elasticity is dominant while viscosity becomes dominant for higher frequencies up until 400Hz. At even higher frequencies the origin of the fingertip structural dynamics is uncertain [30, 34, 35]. Similarly, the relaxation behavior of the skin after indentation is non-linear [32]. Next to protecting the fingertips against shock, this behavior of the pulp gives it the ability to conform to touched surfaces by enlarging the contact area. While the **real contact area** refers to the sum of the microscopic points of contact, the gross or **apparent contact area** refers to the overall, elliptic contact region.

Another well-studied aspect of skin-object mechanics is finger-pad **friction** and its role in grip and touch. **Friction** refers to the reaction force of two surfaces moving against each other. Physically, it is commonly expressed through **the coefficient of friction**, that is the ratio of frictional resistance between two bodies and the normal force applied [36]. Friction is crucial for haptic interactions. Without it, many types of object manipulation would be practically impossible [30]. Friction also shapes the nature of the vibrations generated when a fingertip slides across a surface, which consequently shapes the perception of the surface [37–39]. Two important stages of friction are often discussed in the literature. The first one is known as **stick**, which happens when the contact between the two surfaces is retained (such as when holding and handling objects), while the second one is called **slip**, which occurs when the contact is overcome by the force and breaks during lateral motion (such as when exploring a texture) [37, 40–42]. Finally, the intermediate state where slippage occurs only at the periphery of the contact area before spreading to the center is often

1

referred to as incipient slip or **partial slip**, a state that is said to act as a warning signal about potential grip loss [43–46].

The dynamics of friction during skin-object interactions are complex. Two major components of the friction force are commonly described in the literature [36, 37, 39, 47]. The first one of these is molecular **adhesion**, which is shaped by the chemical properties of the bodies in contact as well as the presence of interfacial fluids (such as sweat) [37, 44, 48]. Adhesion is predominant in flat materials where the friction force becomes proportional to the real contact area between the two bodies [49]. In the specific context of the volar skin, the presence of fluids furthermore hydrates the stratum corneum, whose elastic modulus can, as a consequence, drop dramatically, thus increasing the real contact area [50]. The second major component of the friction force is **deformation**. In this context, **ploughing** generally refers to the temporary displacement of local volumes within a (visco)elastic body by the asperities of the other, less elastic body [51–53].

In the specific case of sliding friction, such as when a fingertip slides across a surface with a given roughness, the asperities of this surface will induce oscillating forces resulting in displacement waves which propagate into the bodies [47]. Such **propagating waves**, that travel through the human hand during haptic interactions, have been shown to be crucial for the haptic perception of, for instance, fine textures. It has in fact been suggested that the biomechanical properties of the human hand have evolved to effectively compress this tactile information, thereby facilitating later perceptual processes [6, 54–56].

Notably, such propagation waves do not only travel through the human hand but also enable tool-mediated haptic sensing. By using rigid, handheld probes, humans can perceive various properties of the environment, such as texture and material properties, distance, position, and impact location [57–59].

1.2.3. THE SOMATOSENSORY SYSTEM

Haptic perception is mediated by the **somatosensory system**, a network of neural structures within the body and brain with the overarching function of informing about the mechanical state of the body that it inhabits [30].

During dynamic touch interactions, the mechanics of this contact give rise to spatiotemporal input features as described in the previous section that are picked up by receptors in the skin and transformed into neural signals. This stage of the perceptual process is generally referred to as **transduction** (cf. Figure 1.3), and a variety of receptor types are involved in this task during haptic perception. These include thermoreceptors (responding to changes in temperature), nociceptors (responding to noxious mechanical, thermal, or chemical stimuli), and, importantly, a number of different **mechanoreceptors** (responding to innocuous skin deformation) [60–62]. Next to free nerve endings and hair follicle receptors, four different types of mechanoreceptors are often discussed in the literature, all differing in their response properties or preferences, commonly referred to as **tuning**, as well as their location within and across the skin [63, 64]. While *Merkel's discs* are exquisitely responsive to fine skin displacement and low-frequency (5–15 Hz) vibrations, *Meissner's corpuscles*

show strong responses to intermediate frequency vibrations (10–60 Hz). *Ruffini endings*, on the other hand, are sensitive to skin stretch and a wide range of frequencies, although their specific response properties are more poorly understood. Finally, *Pacinian corpuscles* are extremely sensitive to higher frequency vibrations delivered to large contact areas, with a peak sensitivity around 200–250 Hz. The different mechanoreceptors are furthermore innervated by different types of fibers or **afferents**, similarly differing in their properties. While Merkel's discs and Ruffini endings are innervated by slowly adapting type 1 and 2 (SA1 & SA2) afferents, producing a sustained response to sustained skin deformation, Meissner's corpuscles are innervated by rapidly adapting (RA) afferents, producing a transient response to changes in skin indentation. Pacinian corpuscles are innervated by PC afferents, which produce transient responses to the onset and offset of skin indentation (e.g., [30, 62, 65, 66]). Merkel's disks and Meissner's corpuscles are located in or just beneath the epidermis of the glabrous skin, where Merkel's disks are neatly aligned with the papillae that lie beneath the papillary ridge. Ruffini endings, on the other hand, are located deeper in the skin as well as in ligaments and tendons. Finally, Pacinian corpuscles are located deep in the dermis and have big diffuse receptive fields, allowing them to pick up propagating vibratory cues far away from the contact location [6, 55, 67]. Together, these mechanosensitive channels thus transform mechanical deformation into neural signals conveying information about the initiation and breaking of contact, object shape, weight, material properties, and more. Despite their distinctness, however, which has received a great amount of attention in the haptic literature, it is important to note that all receptors and afferent types tend to be activated during even the most basic haptic interactions, conveying information about largely any object feature. No singular experience is correlated with the activation of only one type of receptor and their afferents [68–70]. Figure 1.2 shows an illustration of the human skin structure.
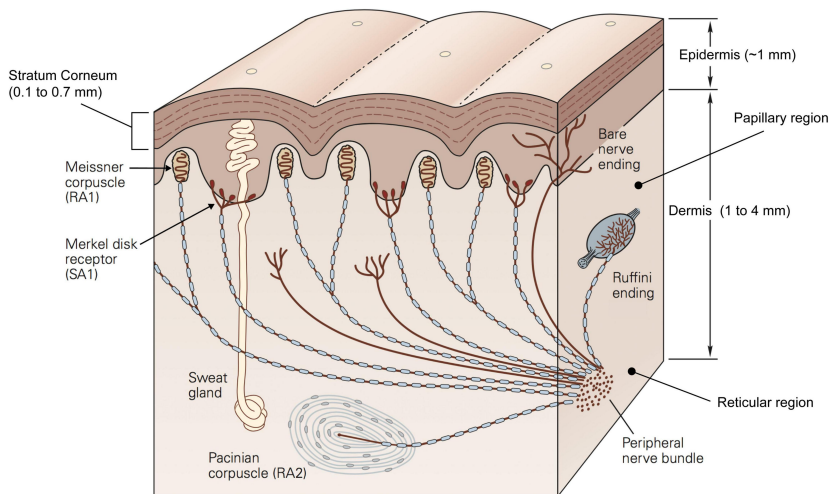
Figure 1.2. Mechanoreceptors and skin structure [71].

1

After mechanotransduction, the resulting nerve spike outputs propagate into the central nervous system, where their firing rate and periodicity communicate information about the skin deformation that has taken place. Many aspects of this process remain poorly understood. Most generally, however, distinct input features are first segregated and encoded sub-cortically in the cuneate nucleus and then transmitted to the thalamus. From the thalamus, the sensory information is sent further to the neocortex, where the formation of percepts of skin-object interactions is taking place [72–74]. While the **somatosensory cortex** is generally referred to as the region in the neocortex specialized to process and represent haptic information [66, 75, 76], recent research indicates that information about the specific features of tactile inputs is present in largely any region of the neocortex [77].

1.3. HAPTIC PERCEPTION

In the previous section, I have addressed how the physiology of the human hand and the somatosensory system are exquisitely tuned to generate, pick up, and process behaviorally relevant haptic cues and transform them into haptic percepts. Figure 1.3 summarizes the whole haptic perceptual pathway during skin-object interactions.

In this section, I will address some of the most widely investigated cues and perceptual dimensions within the study of haptic perception. Additionally, I will introduce several fundamental concepts within the study of perception that are integral to this dissertation, including the concepts of perceptual constancy or invariance, cue integration, and metamers.

1.3.1. HAPTIC STIMULI AND CUES

First and foremost, one generally refers to the **distal stimulus** when speaking about physical changes in the object or feature of perceptual interest itself. In the context of haptic perception, this could, for instance, be the avocado displayed in Figure 1.3 or some of its physical features such as its shape, surface, and material properties. Conversely, the **proximal stimulus** refers to the energy impinging on the observer's sensory system, thereby informing it about the distal stimulus [68, 78, 79]. In the context of haptic perception, proximal stimuli will most generally be the spatiotemporal input features generated during mechanical skin-object interactions as described in Section 1.2.2. When speaking about perceptual or sensory **cues**, on the other hand, I refer to basic features within the distal or proximal stimulus that are identified as communicating behaviorally relevant information about it. While the notion of cues in sensory or perceptual processing is widely used, no precise definition of it exists, and the concept is often dealt with as implicitly understood [80].

The inevitable proximity between the distal and proximal stimulus in haptic perception, I would argue, has furthermore given rise to a few common notions about haptic stimuli and cues, relevant to address here. These are notions that I have observed reappearing in the haptic perceptual literature and that will intermittently emerge throughout this dissertation as well. The first one of these notions is the distinction between **spatial and temporal** stimulus characteristics (i.e., of the proximal
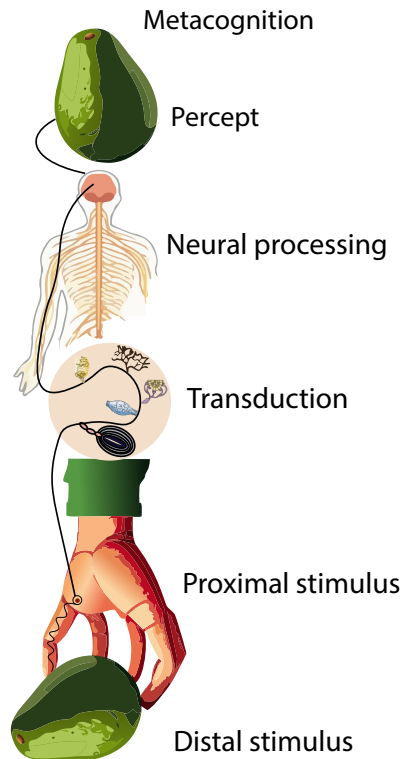
Figure 1.3. The haptic perceptual pathway from distal stimulus to final percept. Mechanical interactions with an object result in spatiotemporal input features which are transformed into neural signals via receptors in the skin, joints, and muscles. These signals are subsequently filtered and processed by the peripheral nervous system and the brain, resulting in a final percept.

stimulus) and corresponding coding mechanisms. This distinction refers to the understanding that some (often larger) stimulus features are best coded via spatial patterns of activation of a population of mechanoreceptors, while other stimulus features are best coded via a temporal code present in the vibratory information created during interactions like lateral motion [81–83]. It is an important and conceptually meaningful distinction that has received a vast amount of attention, especially within the literature on texture perception [81–85]. Yet, it has also nourished the idea of functionally distinct receptor systems. I would therefore like to highlight that any behaviorally relevant proximal haptic stimulus is by definition both

spatial and temporal in its extent and will involve an interplay between these neural mechanisms [69, 70, 86].

A related distinction following the previous one is the one between **static and dynamic** touch. The former is often used to describe sustained input, such as during sustained pressing with a single finger, while the latter describes interactions like stroking or tapping, which, in addition to local deformation, create vibration (e.g., [81, 83, 87, 88]). Thus, static touch is often said to give access to spatial cues, while dynamic touch gives rise to temporal cues. Needless to say, any touch interaction in daily life has static and dynamic moments, and there is no clear cutoff between the two.

Finally, the distinction between **local and propagating** cues will be made repeatedly in this dissertation. This distinction is related to the assumption that some afferents are tuned to picking up information that propagates far away from the immediate contact area between skin and object during haptic interactions, while others have very limited receptive fields and thus a more "local" range. Due to the principles of contact mechanics, however, tactile stimulation leads to mechanical gradients within the skin that are fundamentally nonlocal, even when assuming quasistatic conditions. Consequently, the processing of any input is likely to involve various submodalities and receptive fields [4, 74]. While the propagation of haptic proximal cues and their resulting percepts strongly depend on the active exploration of the contacting body, even highly local contact interactions have far-reaching consequences [89]. It is therefore, again, a conceptual distinction referring to two extremes regarding the range or traveling distance of a relevant proximal cue relative to the interaction contact surface itself.

Having addressed the specific nature of haptic stimuli and cues, the following section focuses on the behaviorally relevant perceptual qualities or "dimensions" that can be derived from them.

1.3.2. Haptic Perceptual Dimensions

Perceptual dimensions are defined here as perceptual qualities or properties of common behavioral interest. Behaviorally relevant perceptual dimensions are thus frequently linked to corresponding adjectives as descriptors. A full account of the dimensionality of haptic perception does not presently exist [4], however, I will here briefly address some of the most studied haptic perceptual dimensions as well as the sensory cues informing them. A particular focus will be given to the dimension relevant to the empirical chapters of this dissertation.

Stimulus Magnitude

Perceived **stimulus magnitude** is one of the most basic perceptual dimensions, and its behavioral relevance can hardly be questioned, as it directly links to the perceived intensity or presence of a mechanical contact during haptic events. The adjectives best describing this dimension in the haptic domain would be *strong and weak* at the supra-threshold level and probably *present and absent* at the threshold level. The perceived magnitude of a stimulus is most commonly associated with *stimulus*

amplitude as a cue; however, other cues, such as ***indentation speed***, ***stimulus duration***, and the ***stimulus area***, are well-known for communicating stimulus magnitude as well (e.g., [90–98]). The effects of stimulus duration and stimulus area on the perceived stimulus magnitude are sometimes referred to as temporal and spatial summation. Chapter 2 of this dissertation, as well as Appendix A, provide examples of the former for two very different haptic events.

In the specific context of **vibrotactile stimuli**, which have been used extensively in the study of haptic perception, ***stimulus frequency*** plays a significant role in the perceived intensity of that stimulus (e.g., [63, 99–101]). This is related to the earlier addressed assumption that different afferent populations are tuned to different stimulus characteristics. A higher perceived intensity or lower detection threshold has thus commonly been reported for vibrations around 200–250 Hz, which has been linked to the strong frequency dependency of Pacinian corpuscle afferents [65, 102–105].

On a neural level, the perceived intensity of a stimulus can be associated more or less directly with the spiking pattern of the involved afferents. However, there is general agreement that signals from various afferent types are integrated to determine the perceived intensity of a stimulus [101, 104, 106].

SHAPE

The shape of an object is behaviorally relevant because it shapes possible interactions with it [68]. Shape serves as the primary factor in object categorization, while object categories are often associated directly with relevant motor interactions [107, 108]. Throwing a ball, grasping a door handle, or threading a needle all require not only seeing but also "feeling" the shape of the respective objects. In contexts like fumbling for a key in a cluttered bag or reading braille, the significance of haptic shape perception becomes even more evident. As these examples demonstrate, shape information is present at multiple scales, starting with signals from single finger pads to whole-hand interactions and beyond [109]. Many adjectives can be linked to shape perception. A few examples being round, pointed, angular, curved, flat, or deep. Haptic shape perception is a large research field that has received much attention, but because it is not within the scope of any of the empirical chapters in this dissertation, it is only addressed very briefly here.

Most generally, relevant haptic shape cues within the distal stimulus are the configuration and orientation of ***edges*** and ***bumps*** as well as the ***slope*** and ***curvature*** of object surfaces. Somewhat less is known about the coding of larger, 3D object shape, although it likely involves integrating cutaneous signals from these cues with proprioceptive information about movement and configuration of the hand during interactions [109–113]. Within or approaching the proximal stimulus, ***force*** (such as the force relating to the slope of a bump when sliding across it) and ***position*** information (such as that of the finger when following the geometry of a bump or curve) have been identified as relevant cues for haptic shape perception [88, 114–116]. Appendix B provides an example of one of the most basic cues to shape perception—the relative arrangement of two points in space. However, this work also

highlights the challenges that arise when trying to render haptic shape without direct mechanical contact, using a stimulus of low behavioral relevance for communicating object shape.

At a very small scale, individual shapes can be said to become elements of texture.

MATERIAL AND TEXTURE

The terms material and texture are often used interchangeably. However, when it comes to the distal stimulus itself, I will refer to **material** as the general matter of which something is composed, exhibiting certain properties, and **texture** as the surface characteristics, such as its asperity and the topographical arrangement of elements on a surface. The haptic perception of material and texture is behaviorally relevant for a number of reasons. First and foremost, since the material and texture characteristics of an object shape important properties such as the friction during interactions with it (cf. Section 1.2.2), they also shape our behavior toward that object. We very intuitively adjust our grip to accommodate the surface and material properties of objects that we interact with [37, 117–119]. A sturdy mug is thus naturally held differently than a flimsy plastic cup. Material and texture furthermore matter when we try to identify different material types, such as when distinguishing wood from plastic or silk from cotton, and they communicate information about the state of certain objects, such as the ripeness or freshness of certain food products. Unsurprisingly, a vast amount of research has been conducted to gain a better understanding of haptic texture and material perception. Chapter 3 through Chapter 5 of this dissertation also contribute to this aim.

Haptic texture and material perception clearly possess multiple dimensions. This has, among others, been revealed by studies using multidimensional-scaling (MDS) analyses. The dimensions most frequently uncovered by these studies are **roughness** and **compliance**, while other dimensions sometimes uncovered are temperature and stickiness or slipperiness [87, 120–122]. Each of these is addressed separately below.

- **Roughness:** Roughness is often described as one of the most salient object properties. The adjectives describing this dimension are *rough* and *smooth* and it is most frequently estimated using lateral motion [81, 123]. Common measures of surface roughness include the so-called arithmetic average (Rα) and root mean square average (Rq or rms) of the profile height deviations from the mean line. However, no singular definition or predictive roughness feature has been identified to date. Perceived roughness can be influenced by various factors [38, 124–126]. Relevant cues at the level of the distal stimulus of manufactured surfaces include the ***groove width, ridge height, particle diameter, as well as the spacing of raised dots*** [127–130]. Perceived roughness has furthermore been suggested to correlate with the ***friction*** created during surface interactions [38, 120, 131, 132]. The ***amplitude of the vibrations*** created during surface interactions weighted with the ***frequency response of Pacinian receptors*** [133, 134], as well as the ***average rate of change of the tangential force*** [135], are other cues that have been associated with perceived roughness. An important distinction is commonly drawn between the perception of **coarse**

1

and fine roughness features, some researchers having argued that they may by themselves be considered as distinct dimensions [121]. While coarse roughness features can be assessed using static touch, giving rise to *spatial cues*, fine roughness features require dynamic touch (i.e., lateral motion) and the generation of frictional and vibratory or *temporal cues* to be felt [83, 128, 136] (cf. Section 1.3.1). Using lateral motion, it has thus been shown that humans are able to detect surface features down to the nanoscale [137]. The so-called *duplex theory* has explained this difference by functionally linking it to distinct receptor systems (i.e., the Pacinian and non-Pacinian channels) [83, 85], although such a strict binary classification in mediating perceived roughness has since been challenged (e.g., [69, 70, 86]). Overall, however, there is a general consensus that roughness perception is largely influenced by vibratory cues. This is not the least evidenced by the fact that roughness perception using direct (bare finger) and indirect (tool) touch tends to be strongly correlated [58, 70, 133, 134, 136, 138].

- **Compliance:** Compliance refers to a material's compressibility or deformability and is best described by the adjectives *hard* and *soft* [87, 120, 121]. At the level of the distal stimulus, a material's compliance can be determined via its *stiffness* (the ratio between applied force and displacement), *elasticity* (the ratio between stress and strain) or *indentation hardness* (resistance to indentation) [87, 139, 140]. Material compliance tends to be assessed using pressing or squeezing but can be available using dynamic tapping or stroking, too [123, 141–143]. Numerous studies have highlighted the critical role of *cutaneous cues*, such as local *deformation* in mediating the perception of compliance [139, 141, 144]. It follows that local shape cues (i.e., curvature) can sometimes communicate compliance as well [145]. However, there is also evidence suggesting that vibrotactile feedback can influence compliance perception under certain conditions [143, 146–148].

- **Other texture dimensions:** Multidimensional-scaling studies have sometimes reported two other dimensions in addition to roughness and compliance. The first one is **temperature**, with its adjectives *cold* and *warm*. The role of thermal cues in material perception can hardly be neglected and can quite generally be attributed to the thermal conductivity of different materials and the resulting *heat transfer* between a surface and the skin as a cue [81, 121, 149]. The second one of these dimensions is **stickiness** with the adjectives *sticky* and *slippery*. This dimension has been reported to be quite well-related to *friction* as a cue [87, 121, 122, 150]. Like roughness and compliance, the stickiness of a surface is not only accessible via direct touch but can be assessed using a rigid probe as well [58]

TIME AND MOTION

Because touch interactions take place in space and time, two further perceptual dimensions that I wish to address here are the perception of time and motion. The two are by no means independent. While the adjectives accurately describing

perceived time (or duration) would be *long* and *short*, the adjectives most frequently describing perceived motion would be *fast* and *slow*. Because motion refers to change in position over time, and the velocity and acceleration of it can vary within a single movement, their rate of change in motion gives rise to other adjectives describing different qualities or dimensions of movement. Some examples include *smooth, steady, irregular*, or *jerky*.

Time and motion perception are crucial across the senses. Understanding the occurrence of events within time is functional in linking them together and inferring causality within and across senses [151–153]. Within the context of motor interactions, the ability to generate precisely timed movements within the physical world is critical for any successful interaction and thus survival. To adapt to a dynamic environment, mobile organisms like humans need to accurately determine both when and where to move, and this requires a strong sense of time [123, 154, 155].

Cues informing **haptic motion perception** have been studied for a long time [156]. However, one most generally distinguishes between ***tactile or cutaneous cues*** (such as during the successive activation of mechanoreceptors with neighboring receptive fields on the skin) and ***proprioceptive or kinaesthetic cues*** (such as through signals from joints, muscles, tendons, and skin stretch) [157–159].

The primary cue for the **perceived time** or duration of an event, unsurprisingly, is ***time***. However, a great number of other cues have been identified as affecting subjective time. Only a few examples include ***attention and memory*** [160, 161], ***emotional state*** [162, 163], ***body temperature*** [164, 165], ***age*** [166, 167], general stimulus ***change*** [168, 169], and as mentioned, ***motion*** [170, 171]. Furthermore, while I have already addressed how the duration of an event can affect the perceived intensity of it, the reverse phenomenon, where the ***intensity*** of an event provides a cue to its subjective duration, has similarly been reported across modalities [172–174].

One major focus within the research on time perception has been the link between subjective time and ***action***. While actions and movements are closely related, actions refer to larger-scale events directed at the environment, commonly including not only motion but also causal relationships [175]. Actions exert a multitude of effects on subjective time before, during, and after an action [155, 176–178]. In fact, the close link between motor actions and time perception has led researchers as far as to suggest that the main timing mechanism may reside within the motor system. From this viewpoint, the motor system is thought to not only affect but also more directly encode our sense of time [176].

One well-known effect of action on subjective time is the phenomenon of ***temporal or intentional binding***. Temporal binding refers to a compression of the perceived time between a voluntary action and its sensory outcome [177, 179, 180]. The primary mechanism initially proposed for this distortion of subjective time was intentional action, giving rise to the term "intentional binding." Consequently, temporal binding has frequently been regarded as an implicit indicator of agency [177, 180]. However, recent studies have challenged this association, suggesting instead that temporal binding might represent a phenomenon of more general multisensory causal integration [181, 182]. In either case, voluntary motor interactions commonly imply

both tactile and proprioceptive cues. The last chapter (Chapter 6) of this dissertation explores the consequences of extinguishing some of these cues on temporal binding.

WEIGHT AND SIZE

The perceived weight of an object is most generally linked to its physical **mass** as a cue, while the perceived size of an object is mostly linked to its physical **volume**, the adjectives best describing these two dimensions being *heavy/light* and *large/small*. However, haptic size-weight and temperature-weight illusions are well-known phenomena, where smaller and colder objects tend to feel heavier than larger and warmer objects of the same mass [1–3, 30, 183, 184]. While the haptic perception of weight and size is not within the scope of this dissertation, the above provide beautiful examples of how a single perceptual dimension is rarely linked to just a single stimulus cue but is often informed by several cues at the same time.

As these examples demonstrate, inferences about even the most basic haptic qualities or dimensions are rarely drawn from just one single cue or physical descriptor. Moreover, variations in mechanical state caused by changing exploration conditions can lead to potentially ambiguous mechanical cues derived from contact with the same object. So how does the perceptual system reconstruct a stable and robust world of touch? In the following section, I will address the problem of how the sensory system deals with such a multitude of behaviorally relevant cues as well as irrelevant changes within them and how perceptual stability can still be ensured under such conditions.

1.3.3. PERCEPTUAL CONSTANCY AND INVARIANCE

By now, it has become clear that it is a misconception about perception that single cues or physical descriptors can be linked more or less directly to corresponding perceptual dimensions. As Shockley writes:

> "*A recurring theme in the study of perception is that the currently available physical descriptions of the constraints on perception are adopted without question even though the understanding of perception that follows from them is often close to solipsism.*" [185] p. 105.

The problem of **perceptual constancy** or invariance is a problem that has occupied the minds of psychologists and perceptual scientists for many centuries. When we interact with and perceive the world around us, the proximal stimuli that inform us about it constantly change. This largely happens as a result of task-irrelevant physical fluctuations and the changing availability of relevant cues. Yet, we do not experience the world or distal stimuli of interest as changing constantly. The most well-known examples of this phenomenon come from visual shape and object perception. As we move towards or alongside an object, such as a door, the shape and size of the image of that object projected on our retina steadily change. However, we are still perceiving the door as staying true to its size and rectangular shape as this happens. Other well-known examples can be found in the auditory domain, such as in speech

perception, where acoustic variations of the same phoneme can yield the same perceptual outcomes (e.g., [186–188]). Finally, as will become clear in this dissertation, perceptual constancy can be found and plays an important role in perception in the haptic domain too.

The two terms, perceptual constancy and invariance, are frequently used interchangeably. They can both, largely, be conceptualized as stability in a perceptual response under varying (physical, mechanical, or physiological) conditions [68, 189]. Here I will refer to **constancy** as the global perceptual experience of something (such as a color, a pitch, or a texture) remaining constant during change and **invariance** (or an invariant) as a feature that is not changing and hence, mechanistically speaking, may be underlying the former. As Gibson writes:

> *"The transformations of the anatomical pattern of excited receptors have subjective reference; the invariants of adjacent and successive order in the overall input specify the invariants of stimulation and thereby the invariants [constancy] of the world."* [68] p.284.

Such invariance can be found on several levels during the perceptual process. Assuming *variance* at the level of the **distal stimulus**, that is, physical changes in the object or feature of interest itself, invariance might occur as early as in the **proximal stimulus**, that is, within the energy impinging on the observer's sensory system, informing it about the former [68, 78, 79]. Subsequently, invariance may also be observed at an early sensory or a neural computational level (cf. Figure 1.3).

The overarching function of constancy mechanisms is therefore to help our sensory system extract behaviorally relevant information about the physical environment across irrelevant changes in the proximal stimulus [190]. Mechanisms of constancy have, in fact, been proposed to mark the very difference between mere sensory systems and perceptual systems and thus constitute a requirement for perceptual representation [191, 192].

While researchers still disagree on the fundamental mechanisms behind perceptual constancy, I here adopt the notion of constancy as proposed by Greens [193]. This notion posits that true constancy must distinguish itself from 1) mere sensory stability through proximal filtering, 2) sensory stability through irrelevant proximal change, and 3) perceptual categorization of a distal dimension. Attunement to, as well as behavioral relevance of, the respective cues are thus key for true perceptual constancy.

A key assumption guiding this dissertation is that understanding and discovering instances of invariance within haptic perception can provide insights into which cues and perceptual dimensions matter for behavior. If we can identify a constancy mechanism, I believe this would suggest that the cue, mechanical feature, neural correlate, or perceptual quality showing consistency is important for behavior in some way.

1.3.4. CUE INTEGRATION AND METAMERS

Not unlike other senses, the sense of touch thus frequently deals with a multitude of cues relevant for a single perceptual dimension. Sometimes these cues work in

collaboration to convey a specific perceptual quality. However, it is not uncommon for such cues to be ambiguous either. **Ambiguity** in one relevant cue is in this context frequently disambiguated using another relevant cue. However, different cues do not only have differing influence due to their very nature but also due to their **salience**, a term that can be borrowed from visual perception research to describe the most conspicuous cues within a stimulus [194–196]. Examples of such events were provided in Section 1.3.2, such as when the curvature of an object becomes a more salient cue to the object's compliance than its elasticity or when the duration of an event provides a more salient cue to the intensity of it than its amplitude. Importantly, the perceptual outcome of complex stimuli often does not simply correspond to the sum of the individual cues but relies on non-linear summation mechanisms driven by stimulus salience [196, 197].

A sensory apparatus with limited processing capabilities but a rich set of inputs from a range of cues and sensing conditions necessitates multiple ways to combine inputs. **Metamers** are instances in which distinct (physical) cue combinations lead to similar perceptual outcomes because they produce the same response at some stage of sensory processing. They are a specific type of perceptual constancy that emerges when cues are subject to mandatory fusion prior to the resulting percept. The most well-known examples of this phenomenon can again be found in the visual domain, where color metamers refer to the perceived matching of colors under some but not other lighting conditions [198–201]. Yet, a few examples can be drawn from the haptic domain too. Consider the previous scenario provided regarding weight perception. A cold marble with a smaller mass might consequently feel similarly heavy as a warmer marble with a larger mass, thus constituting a "weight metamer" [184]. Another example would be the compliance of objects varying in both their shape and elasticity. Because both of these cues can affect the perceived compliance of an object, a less elastic but concave object may be perceived as similarly soft as a more elastic but flat object [145].

Because constancy mechanisms that govern perceptual inferences about haptic or other perceptual events can occur on multiple levels of processing, a useful distinction can here be drawn between sensory and perceptual metamers [190]. Physically distinct cues that are processed similarly during the early peripheral stage of the perceptual pathway (cf. Section 1.2.3) may thus be referred to as **sensory metamers**. On the other hand, physically distinct cues that are first processed individually and then integrated at a later central stage of the perceptual pathway can be called **perceptual metamers** [190]. Importantly, and in accordance with Green's notion about invariance [193], these confounds do *not* arise as a consequence of insensitivity to a cue but due to the simultaneous sensitivity to multiple cues concerning a single perceptual dimension. In this manner, metamers can in essence be regarded as instances of constancy. And just like other types of constancy, metamers provide a unique opportunity to evaluate what matters to our perceptual system when making certain judgments. Changing behaviorally relevant stimulus cues without changing the resulting percept can in this way be used to uncover the stimulus-driven activity, that is, what matters to the somatosensory system in drawing haptic perceptual inferences. Chapter 2 and Appendix A of this dissertation uncover metamers relating to the

1

perceived intensity of haptic events, while Chapter 5 reveals a previously unreported metamer related to the perception of roughness.

Knowingly, cues do not only combine within but also across senses. Merging of sensory information within and across senses in real-world interactions is crucial for reducing perceptual ambiguity and improving the precision of perceptual judgments [80]. The research presented in this dissertation primarily focuses on haptic stimuli and cues. As is customary in a controlled experimental context, relevant cues from other modalities (such as vision and audition) are thus mostly masked or prohibited for experimental control. However, behaviorally relevant haptic interactions in the real world most frequently take place in a multisensory context. In Chapter 6 of this dissertation, we discover the effects of removing behaviorally relevant information from one sensory modality in a multisensory interaction on the perceived timing of the events within this interaction.

1.4. METHODOLOGICAL APPROACHES

To irrefutably identify the role of different haptic cues in perception, we need to be able to measure the consequences of changes in the cue space on what human observers perceive. This section will give a brief introduction to the methodologies commonly used to navigate these challenges and provide an outline of the methodological framework adopted in this dissertation.

1.4.1. THE CONTROLLED EXPERIMENT AND PSYCHOPHYSICS

The research presented in this dissertation covers a series of experimental studies (Chapters 2–6) alongside this theoretical introduction (Chapter 1) and a conclusion (Chapter 7). **The controlled experimental method**, where the effect of one or more independent variable(s) (e.g., a cue, stimulus parameter, or exploration condition) on a dependent variable (i.e., the perceptual outcome) is investigated, thus constitutes the main approach to answer the research questions and the primary methodological framework of this dissertation. In these experiments, I particularly draw on psychophysical methods. **Psychophysics** can be described as a sub-field of experimental psychology that investigates how our sensory system maps changes in the parameters of our physical environment to changes in the probability of detecting or discriminating said changes. It can thus help answer questions about how we perceive the physical world around us and how our perception relates to these physical stimuli. It is the premier research method for studying the quantitative relationship between stimulus and sensation [202]. In psychophysics, stimulus inputs are selected under the assumption that these stimulus parameters embody the parameters to which a particular perceptual mechanism is tuned.

A very important concept within psychophysical research is the one of thresholds. **Detection thresholds** (or absolute thresholds) describe the magnitude of a stimulus at which a subject is able to detect the stimulus a certain amount of time (e.g., 50% or 75% of the time). **Discrimination thresholds**, on the other hand, describe the amount of change in the magnitude of a stimulus needed to detect a difference

between two stimuli a certain amount of time. Discrimination thresholds are also commonly referred to as difference limen or just-noticeable differences (JNDs) [203]. In this context, researches often seek to determine the **psychometric function**, an inferential psychometric model describing the stimulus-response relationship [204]. Thresholds are computed in Chapters 2 through 5 of this dissertation, as well as in the Appendices A and B.

Classical psychophysical methods as originally described by Fechner [203] include the method of limits, the method of constant stimuli, and the method of adjustment. In **the method of limits**, subjects indicate detection or discrimination as stimulus magnitudes are presented in either ascending or descending order. In **the method of constant stimuli** a set of stimuli of varying intensities is presented in random order, and the subject's responses are used to determine the threshold at which the stimulus is detected or discriminated a certain percentage of the time. In **the method of adjustment** subjects are asked to adjust the magnitude of the stimuli until reaching detection or discrimination thresholds.

Next to these, **adaptive psychophysical methods** are often used. These methods dynamically adjust stimulus parameters based on participants' previous responses and have the advantage of being more efficient in converging on the threshold levels, thereby reducing the number of trials needed and improving the accuracy and speed of the experimental process. **staircase-procedures** make up the most simple procedures within this class of methods. Here, stimulus magnitude is increased or decreased stepwise according to a set rule based on the participant's detection or discrimination in the previous trial. Another adaptive method or group of methods is **Bayesian or model-based active-learning methods**. In contrast to staircase procedures, such methods most generally incorporate a probabilistic or statistical framework to learn from participant's previous responses and update and select the stimulus correspondingly. Such methods commonly start with a prior and then calculate the probability of the threshold's location based on this prior and the history of responses. Subsequent trial's stimulus levels are selected to maximize information gain, often incorporating a prior probability distribution in Bayesian approaches. [205, 206].

The research presented in this dissertation incorporates both classical psychophysical methods, such as the method of constant stimuli, and adaptive methods, such as staircase procedures and model-based active learning algorithms, to determine the probabilities of detecting or discriminating events. In several of my studies, I particularly draw on a model-based active learning algorithm called AEPsych, which uses non-parametric Gaussian Process models to efficiently estimate psychometric fields by dynamically adjusting experimental conditions based on the responses from previous trials and regions of high uncertainty in the field [207]. In addition to these psychophysical methods, I also utilize behavioral techniques more commonly employed in experimental psychology. These techniques do not examine the relationship between physical stimuli and perceptual mechanisms but instead investigate broader cognitive or behavioral processes. Such methods are adopted in Chapter 6. In Chapter 3, I also employ methods of mechanical characterization where different assumptions drive the metrics used to understand the stimulus space.

Finally, in Chapter 4 and Chapter 5, confidence ratings are used as a metacognitive measure to capture participants' subjective confidence about their responses.

1.4.2. MANIPULATING THE AVAILABLE CUE SPACE

Understanding and controlling the stimulus is fundamental for conducting controlled experiments, presenting a unique challenge in haptic perception research. In haptic interactions, spatiotemporal input signals from our skin, joints, and muscles carry an enormous flow of information to be transformed into neural signals and made sense of by our brain. The intrinsic link between movement execution, physical contact, and the proximal stimulus makes capturing these signals and presenting them in a controlled, yet ecologically valid, fashion in an experiment extraordinarily challenging. This difficulty is not in the least evidenced by the absence of devices capable of fully capturing haptic experiences in the way that sound or images are captured, rendered, and shared.

The research presented in this dissertation includes cue manipulation at three different levels of the haptic perceptual pathway (cf. Figure 1.3): 1) at an early, distal-stimulus level, 2) at an interaction or proximal-stimulus level, and 3) at the level of transduction or neural processing. Cue manipulation at these three levels is briefly discussed below.

MANIPULATING DISTAL STIMULI

(Haptic) perceptual experimentation most traditionally involves manipulation of the cue space at a distal stimulus level, that is, physical changes in the stimulus properties of interest such as their shape, weight, temperature, or material properties. When examining the relationship between physical cues and a perceptual outcome, a stringent physical characterization of stimulus material is key. Chapters 3, 4, and 5 of this dissertation include manipulations of the cue space at the distal level.

SHAPING PROXIMAL STIMULI

Next to manipulating the distal cue space, it is possible to manipulate the proximal cue space in several ways. One way of doing so is by manipulating the interaction conditions under which the distal stimuli are explored. Tapping an object rather than stroking it or sensing with a probe rather than using direct touch will, in this way, generate different proximal cues relating to the same distal stimulus material. Chapter 5 of this dissertation makes use of this method.

Another way of manipulating (or approaching a direct manipulation of) the proximal stimulus in haptic interactions is through haptic interfaces or devices. Haptic interfaces generate mechanical signals that stimulate receptors relevant to our sense of touch [208]. Using such interfaces, it is therefore possible to *simulate* interactions with distal stimuli by creating proximal input features that resemble those of "real" haptic interactions. In Chapter 2 of this dissertation, we make use of such an interface in simulating basic contact events. The two studies included in the appendices of this dissertation (Appendix A and Appendix B) also make use

of a haptic interface that creates proximal input features on user's skin without mechanical contact. Transparency of the interface and rigorous control over the stimulus is key when aiming at simulating distal interactions through proximal cues and at characterizing perceptual mechanisms.

SHAPING TRANSDUCTION AND NEURAL PROCESSING

Finally, it is possible to shape the somatosensory system's response to stimuli at the stage of mechanotransduction or neural processing (cf. Figure 1.3). One way of doing so at an early processing level includes methods of desensitization, such as mechanoreceptor adaptation to sustained stimulation (e.g., [85, 209–211]) or cooling [212]. Another way of doing so is via drug use, altering the physiological response to haptic stimuli. At an early processing stage, local anesthetics can be used to inhibit the propagation of action potentials. In Chapters 4 and 6, we use this method to investigate the perceptual response when behaviorally relevant local tactile cues are removed. Evidently, neural processing can also be shaped at later stages using drugs or by imposing certain mental states like tiredness or distraction.

Together, while often impossible to manipulate and characterize cues at every level of the perceptual process, transparency of a stimulus and interface as well as an awareness of the level of cue manipulation are key for understanding perceptual mechanisms.

1.4.3. STATISTICAL ANALYSES

The statistical analyses used in this dissertation include both traditional frequentist and Bayesian statistical methods. Under the frequentist approach, hypothesis testing is conducted to evaluate the null hypothesis (indicating no effect or no difference) against the alternative hypothesis. This is done using both parametric and non-parametric hypothesis tests, which are standard in significance testing and evaluating the impact of independent variables on dependent variables. For instance, non-parametric tests such as the Wilcoxon signed-rank test are employed in Chapter 4 to assess differences between conditions where data do not meet parametric assumptions. In Chapter 6, paired-sample t-tests and ANOVA with repeated measures are used to evaluate differences between conditions, with appropriate adjustments for sphericity and multiple comparisons.

In addition to these frequentist techniques, Bayesian methods are employed in Chapters 2, 3, 4, and 5. These methods can incorporate prior knowledge and are particularly valuable for their ability to handle complex models and small sample sizes, allowing for a more nuanced interpretation of data. Gaussian Process (GP) models are used, which provide a flexible approach to modeling without strict parametric assumptions. These models allow for the simultaneous analysis of multiple tasks or conditions and offer insights into individual-level variations and conditional effects.

1

1.4.4. A NOTE ABOUT SMALL-N STUDIES

Readers may note the relatively low sample sizes in certain chapters of this dissertation, specifically in Chapter 2 and Chapter 5. In psychology and neuroscience research, the prevalent approach involves large-N studies aimed at enabling inferences about the strength of an effect in an average population, typically using null-hypothesis significance testing. However, small-N studies, especially within a psychophysical framework, can provide valuable insights that are often obscured by the broad averages of large-N studies. By treating individual participants as replication units, it is possible to gain insights that are robust and replaceable. This approach leverages the assumption that the experiment probes a fundamental processing mechanism considered to be universal. Additionally, by either making numerous repetitions of the same data point or using a model to estimate the probability of a response at a given point, we can achieve robust predictions about whether the outcomes will generalize. Many research questions can in this way be answered by asking whether a phenomenon investigated is universal to human perception rather than inferring the average effect of an effect in a population [213, 214].

1.5. RESEARCH QUESTIONS AND CONTRIBUTION

The overarching questions guiding this dissertation can be formulated as follows:

A. Which cues and mechanisms does the human somatosensory system use to robustly detect relevant changes in the mechanical state of the body and the world during dynamic touch events?

B. How does our sensory system ensure stable haptic percepts that inform us about the state of these events under changing conditions and cues?

The sub-questions guiding the chapters of this dissertation fall into three categories and can be formulated as follows:

Detection of contact (Chapter 2)

1. Can we identify metamers of duration and intensity in the detection of transient contact events? And if so, can they be associated with invariant states of mechanical energy transfer?

Material and texture perception (Chapters 3–5)

2. Can we determine behaviorally relevant and naturalistic cues to texture perception that are realizable in manufactured stimuli?

3. Do mechanical propagation waves provide a behaviorally relevant and sufficient cue to roughness and softness perception?

4. Does surface roughness provide a relevant cue to softness perception, and does material elasticity provide a relevant cue to roughness perception? And to what extent are these mechanisms local to the contact and invariant to contact conditions?

Time perception during haptic interactions (Chapter 6)

    5. How does the absence of local tactile feedback during a behaviorally relevant motor interaction affect the perception of the timing of contact and its outcomes?

By systematically combining, removing, or bringing cues into conflict and investigating the resulting perceptual changes, we can answer these questions and understand which cues and mechanisms our perceptual system uses to draw stable and behaviorally relevant haptic inferences.

Gaining a better understanding of these fundamental aspects of human experience is relevant in its own right, but can furthermore have implications for understanding individuals with sensory disorders, helping individuals with certain impairments (such as amputees), and improving user experiences in human-computer interactions. By knowing which components of sensory feedback are used by the somatosensory system to reconstruct contact interactions, we can, for example, optimize feedback patterns provided for amputees and reproduce haptic experiences based purely on a small subset of mechanical inputs for seamless human-computer interactions.

1.6. THESIS OUTLINE AND STRUCTURE

This dissertation consists of five empirical chapters (2–6), this introduction (Chapter 1), and a concluding chapter (7).

Chapter 2 addresses the question of what information the somatosensory system responds to when detecting a change in the state of the mechanical world at the most basic level; namely in the detection of extremely short contact events. A metamer is defined in which the duration (or frequency) of a signal can be interchanged with the signal amplitude for the same perceptual outcome. The research suggests the total energy content of dynamic touch events as one important factor but not the sole informant to the somatosensory system in its decomposition of dynamic touch events.

Chapter 3 explores the possibilities of creating a stimulus space for behaviorally relevant and naturalistic texture and material interactions without compromising on experimental control. The goal of this work is to provide a highly controlled stimulus space facilitating the decomposition of the relevant behavioral components for roughness and compliance perception. The chapter documents the conceptualization, design, and validation of such a stimulus database, as well as initial insights into its behavioral relevance, providing stimuli that are systematically covaried in their statistical microscale roughness and material elasticity.

In **Chapter 4**, we utilize this stimulus database to pursue two objectives: 1) we investigate the relative roles of local and propagating haptic cues in the perception of surface roughness and material compliance, and 2) we examine potential combined effects of surface roughness and material elasticity on determining subjective roughness and softness. The findings illustrate that roughness perception can remain invariant during the dynamic exploration of naturalistic surfaces, even when local cues are eliminated through regional anesthesia, although a large between-subject variability raises questions about the specific conditions under which this is possible.

1

Conversely, the perception of softness is more generally disrupted under the same conditions. However, we do not observe a combined influence of surface roughness and material elasticity on either perceptual outcome.

In **Chapter 5**, the joint influence of material elasticity and surface roughness on the perceived roughness and compliance is investigated in more detail, using an updated stimulus space and differing interaction modes. We discover a metameric relationship where different combinations of surface roughness and material elasticity result in indistinguishable percepts and uncover the conditions under which this metamer arises for both direct- and indirect-touch interactions. No mixed-cue effects are found for the perceived softness of the same surfaces.

The final empirical **Chapter 6** of this dissertation explores the effects of removing local tactile feedback on the perceived timing of behaviorally relevant haptic object interactions using local anesthesia. We uncover an increase in a perceptual (temporal) illusion under these conditions—a possible mechanism to ensure the linking of causally related events.

The dissertation ends with a general discussion and conclusion in (**Chapter 7**).

Included in the appendices A and B of this dissertation are two further empirical studies, together delving into the spatial and temporal constraints of the perception of a rather novel haptic stimulus, namely, ultrasonic mid-air haptic (UMH) stimuli. While holding potential for some applications and perceptual phenomena, UMH stimuli represent a less suitable choice for mimicking naturalistic skin-object contact, particularly under the aim of understanding the somatosensory system's responses to naturalistic and behaviorally relevant touch interactions. While the contribution of this additional work is primarily interface-related, it is included as an appendix to this dissertation because it provides examples of the challenges that can arise when exploring haptic perceptual phenomena using a stimulus of low behavioral relevance.

REFERENCES

[1]   Weber, E. H. *Der Tastsinn und das Gemeingefühl*. Ed. by Wagner, R. 3rd ed. Vieweg und Sohn: Braunschweig, 1846.

[2]   Stevens, J. C. and Green, B. G. Temperature–touch interaction: Weber's phenomenon revisited. *Sensory Processes* **2** (1978), 206–219.

[3]   Amazeen, E. L. and Turvey, M. T. Weight perception and the haptic size–weight illusion are functions of the inertia tensor. *Journal of Experimental Psychology: Human Perception and Performance* **22** (1996), 213–232. DOI: 10.1037/0096-1523.22.1.213.

[4]   Hayward, V. Is there a 'plenhaptic' function? *Philosophical Transactions of the Royal Society of London. Series B, Biological Sciences* **366** (2011), 3115–3122. DOI: 10.1098/rstb.2011.0150.

[5]   Jones, L. A. and Lederman, S. J. *Human Hand Function*. Oxford ; New York: Oxford University Press, 2006.

[6]   Manfredi, L. R., Baker, A. T., Elias, D. O., Iii, J. F. D., Zielinski, M. C., Polashock, V. S., and Bensmaia, S. J. The effect of surface wave propagation on neural responses to vibration in primate glabrous skin. *PLOS ONE* **7** (2012), e31203. DOI: 10.1371/journal.pone.0031203.

[7]   Taylor, C. L. and Schwarz, R. J. The Anatomy and Mechanics of the Human Hand. *Artif Limbs* **2** (1955), 22–35.

[8]   Alexander, R. M. *The Human Machine: How the Body Works*. Columbia University Press, 1992.

[9]   Torkamani, N., Rufaut, N., Jones, L., and Sinclair, R. The arrector pili muscle, the bridge between the follicular stem cell niche and the interfollicular epidermis. *Anatomical Science International* **92** (2017), 151–158. DOI: 10.1007/s12565-016-0359-5.

[10] Glover, N. M., Black, A. C., and Murphy, P. B. "Anatomy, Shoulder and Upper Limb, Radial Nerve". In: StatPearls. Treasure Island (FL): StatPearls Publishing, 2024.

[11] Gray, H. and Carter, H. *Gray's Anatomy: The Anatomical Basis of Medicine and Surgery*. 20th ed. David McKay Company, 1918.

[12] Montagna, W., Kligman, A. M., and Carlisle, K. S. *Atlas of Normal Human Skin*. Springer-Verlag, 1992.

1

[13] Olausson, H., Wessberg, J., Morrison, I., McGlone, F., and Vallbo, A. The neurophysiology of unmyelinated tactile afferents. *Neuroscience and Biobehavioral Reviews* **34** (2010), 185–191. DOI: `10.1016/j.neubiorev.2008.09.011`.

[14] McGlone, F. and Reilly, D. The cutaneous sensory system. *Neuroscience and Biobehavioral Reviews* **34** (2010), 148–159. DOI: `10.1016/j.neubiorev.2009.08.004`.

[15] Gould, J. Superpowered skin. *Nature* **563** (2018), S84–S85. DOI: `10.1038/d41586-018-07429-3`.

[16] Mountcastle, V. B. *The Sensory Hand: Neural Mechanisms of Somatic Sensation.* Harvard University Press, 2005.

[17] McGlone, F., Wessberg, J., and Olausson, H. Discriminative and Affective Touch: Sensing and Feeling. *Neuron* **82** (2014), 737–755. DOI: `10.1016/j.neuron.2014.05.001`.

[18] Cartmill, M. The volar skin of primates: its frictional characteristics and their functional significance. *American Journal of Physical Anthropology* **50** (1979), 497–509. DOI: `10.1002/ajpa.1330500402`.

[19] Hamrick, M. W. Functional and adaptive significance of primate pads and claws: evidence from New World anthropoids. *American Journal of Physical Anthropology* **106** (1998), 113–127. DOI: `10.1002/(SICI)1096-8644(199806)106:2<113::AID-AJPA2>3.0.CO;2-R`.

[20] Yum, S.-M., Baek, I.-K., Hong, D., Kim, J., Jung, K., Kim, S., Eom, K., Jang, J., Kim, S., Sattorov, M., Lee, M.-G., Kim, S., Adams, M. J., and Park, G.-S. Fingerprint ridges allow primates to regulate grip. *Proceedings of the National Academy of Sciences of the United States of America* **117** (2020), 31665–31673. DOI: `10.1073/pnas.2001055117`.

[21] O'Leary, E., Slaney, J., Bryant, D. G., and Fraser, F. C. A simple technique for recording and counting sweat pores on the dermal ridges. *Clinical Genetics* **29** (1986), 122–128. DOI: `10.1111/j.1399-0004.1986.tb01234.x`.

[22] Taylor, N. A. and Machado-Moreira, C. A. Regional variations in transepidermal water loss, eccrine sweat gland density, sweat secretion rates and electrolyte composition in resting and exercising humans. *Extreme Physiology & Medicine* **2** (2013), 4. DOI: `10.1186/2046-7648-2-4`.

[23] Serina, E. R., Mockensturm, E., Mote, C. D., and Rempel, D. A structural model of the forced compression of the fingertip pulp. *Journal of Biomechanics* **31** (1998), 639–646. DOI: `10.1016/s0021-9290(98)00067-0`.

[24] Hauck, R. M., Camp, L., Ehrlich, H. P., Saggers, G. C., Banducci, D. R., and Graham, W. P. Pulp nonfiction: Microscopic anatomy of the digital pulp space. *Plastic and Reconstructive Surgery* **113** (2004), 536–9. DOI: `10.1097/01.PRS.0000101053.03572.26`.

[25] Pawlaczyk, M., Lelonkiewicz, M., and Wieczorowski, M. Age-dependent biomechanical properties of the skin. *Advances in Dermatology and Allergology/Postępy Dermatologii i Alergologii* **30** (2013), 302–306. DOI: 10.5114/pdia.2013.38359.

[26] Park, S. Biochemical, structural and physical changes in aging human skin, and their relationship. *Biogerontology* **23** (2022), 275–288. DOI: 10.1007/s10522-022-09959-w.

[27] Lynch, B., Pageon, H., Le Blay, H., Brizion, S., Bastien, P., Bornschlögl, T., and Domanov, Y. A mechanistic view on the aging human skin through ex vivo layer-by-layer analysis of mechanics and microstructure of facial and mammary dermis. *Scientific Reports* **12** (2022), 849. DOI: 10.1038/s41598-022-04767-1.

[28] Griffin, M. J. "Whole-Body Vibration". In: Encyclopedia of Vibration. Ed. by Braun, S. Oxford: Elsevier, 2001, pp. 1570–1578. DOI: 10.1006/rwvb.2001.0082.

[29] Everett, J. S. and Sommers, M. S. skin viscoelasticity: Physiologic mechanisms, measurement issues, and ppplication to nursing science. *Biological research for nursing* **15** (2013), 338–346. DOI: 10.1177/1099800411434151.

[30] Hayward, V. "A Brief Overview of the Human Somatosensory System". In: Musical Haptics. Ed. by Papetti, S. and Saitis, C. Cham: Springer International Publishing, 2018, pp. 29–48. DOI: 10.1007/978-3-319-58316-7_3.

[31] Skalak, R. and Chien, S. *Handbook of Bioengineering*. New York: McGraw Hill Higher Education, 1987.

[32] Wang, Q. and Hayward, V. In vivo biomechanics of the fingerpad skin under local tangential traction. *Journal of Biomechanics* **40** (2007), 851–860. DOI: 10.1016/j.jbiomech.2006.03.004.

[33] Jindrich, D. L., Zhou, Y., Becker, T., and Dennerlein, J. T. Non-linear viscoelastic models predict fingertip pulp force-displacement characteristics during voluntary tapping. *Journal of Biomechanics* **36** (2003), 497–503. DOI: 10.1016/s0021-9290(02)00438-4.

[34] Wiertlewski, M. and Hayward, V. Mechanical behavior of the fingertip in the range of frequencies and displacements relevant to touch. *Journal of Biomechanics* **45** (2012), 1869–1874. DOI: 10.1016/j.jbiomech.2012.05.045.

[35] Hayward, V. A brief taxonomy of tactile illusions and demonstrations that can be done in a hardware store. *Brain Research Bulletin* **75** (2008), 742–752. DOI: 10.1016/j.brainresbull.2008.01.008.

[36] Goossens, R. H. M. "Fundamentals of Pressure, Shear and Friction and Their Effects on the Human Body at Supported Postures". In: Bioengineering Research of Chronic Wounds: A Multidisciplinary Study Approach. Ed. by Gefen, A. Berlin, Heidelberg: Springer, 2009, pp. 1–30. DOI: 10.1007/978-3-642-00534-3_1.

[37] Adams, M. J., Johnson, S. A., Lefèvre, P., Lévesque, V., Hayward, V., André, T., and Thonnard, J.-L. Finger pad friction and its role in grip and touch. *Journal of The Royal Society Interface* **10** (2013), 20120467. DOI: 10.1098/rsif.2012.0467.

1

[38] Arvidsson, M., Ringstad, L., Skedung, L., Duvefelt, K., and Rutland, M. W. Feeling fine - the effect of topography and friction on perceived roughness and slipperiness. *Biotribology*. Special issue on the 3rd International Conference on Biotribology. **11** (2017), 92–101. DOI: 10.1016/j.biotri.2017.01.002.

[39] Van Kuilenburg, J., Masen, M. A., and van der Heide, E. A review of fingerpad contact mechanics and friction and how this affects tactile perception. *Proceedings of the Institution of Mechanical Engineers, Part J: Journal of Engineering Tribology* **229** (2015), 243–258. DOI: 10.1177/1350650113504908.

[40] Nakano, K. Two dimensionless parameters controlling the occurrence of stick-slip motion in a 1-DOF system with Coulomb friction. *Tribology Letters* **24** (2006), 91–98. DOI: 10.1007/s11249-006-9107-7.

[41] Nakano, K. and Maegawa, S. Stick-slip in sliding systems with tangential contact compliance. *Tribology International*. Special Issue: 35th Leeds-Lyon Symposium **42** (2009), 1771–1780. DOI: 10.1016/j.triboint.2009.04.039.

[42] Derler, S. and Rotaru, G.-M. Stick-slip phenomena in the friction of human skin. *Wear* (2013), 324–329. DOI: 10.1016/j.wear.2012.11.030.

[43] Barrea, A., Delhaye, B. P, Lefèvre, P., and Thonnard, J.-L. Perception of partial slips under tangential loading of the fingertip. *Scientific Reports* **8** (2018), 7032. DOI: 10.1038/s41598-018-25226-w.

[44] André, T., Lévesque, V., Hayward, V., Lefèvre, P., and Thonnard, J.-L. Effect of skin hydration on the dynamics of fingertip gripping contact. *Journal of the Royal Society Interface* **8** (2011), 1574–1583. DOI: 10.1098/rsif.2011.0086.

[45] Delhaye, B., Lefèvre, P., and Thonnard, J.-L. Dynamics of fingertip contact during the onset of tangential slip. *Journal of the Royal Society, Interface* **11** (2014), 20140698. DOI: 10.1098/rsif.2014.0698.

[46] Delhaye, B. P., Schiltz, F., Crevecoeur, F., Thonnard, J.-L., and Lefèvre, P. Fast grip force adaptation to friction relies on localized fingerpad strains. *Science Advances* **10** (2024), eadh9344. DOI: 10.1126/sciadv.adh9344.

[47] Persson, B. N. J. Theory of rubber friction and contact mechanics. *The Journal of Chemical Physics* **115** (2001), 3840–3861. DOI: 10.1063/1.1388626.

[48] Persson, B. N. J. *Sliding Friction*. Ed. by Von Klitzing, K. and Wiesendanger, R. NanoScience and Technology. Berlin, Heidelberg: Springer Berlin Heidelberg, 2000. DOI: 10.1007/978-3-662-04283-0.

[49] Bowden, F. P., Tabor, D., and Taylor, G. I. The area of contact between stationary and moving surfaces. *Proceedings of the Royal Society of London. Series A. Mathematical and Physical Sciences* **169** (1997), 391–413. DOI: 10.1098/rspa.1939.0005.

[50] Sparr, E., Björklund, S., Pham, Q. D., Mojumdar, E. H., Stenqvist, B., Gunnarsson, M., and Topgaard, D. The stratum corneum barrier – From molecular scale to macroscopic properties. *Current Opinion in Colloid & Interface Science* **67** (2023), 101725. DOI: 10.1016/j.cocis.2023.101725.

[51]   Spurr, R. T. The "ploughing" contribution to friction. *British Journal of Applied Physics* **7** (1956), 260. DOI: `10.1088/0508-3443/7/7/305`.

[52]   Derler, S., Preiswerk, M., Rotaru, G. M., Kaiser, J. P., and Rossi, R. M. Friction mechanisms and abrasion of the human finger pad in contact with rough surfaces. *Tribology International*. The International Conference on BioTribology 2014 **89** (2015), 119–127. DOI: `10.1016/j.triboint.2014.12.023`.

[53]   Tomlinson, S. E., Lewis, R., Carré, M. J., and Franklin, S. E. Human finger friction in contacts with ridged surfaces. *Wear*. Wear of Materials 2013 **301** (2013), 330–337. DOI: `10.1016/j.wear.2012.12.039`.

[54]   Mackevicius, E. L., Best, M. D., Saal, H. P., and Bensmaia, S. J. Millisecond precision spike timing shapes tactile perception. *Journal of Neuroscience* **32** (2012), 15309–15317. DOI: `10.1523/JNEUROSCI.2161-12.2012`.

[55]   Andrews, J. W., Adams, M. J., and Montenegro-Johnson, T. D. A universal scaling law of mammalian touch. *Science Advances* **6** (2020), eabb6912. DOI: `10.1126/sciadv.abb6912`.

[56]   Shao, Y., Hayward, V., and Visell, Y. Compression of dynamic tactile information in the human hand. *Science Advances* **6** (2020), eaaz1158. DOI: `10.1126/sciadv.aaz1158`.

[57]   Klatzky, R. L. and Lederman, S. J. Tactile roughness perception with a rigid link interposed between skin and surface. *Perception & Psychophysics* **61** (1999), 591–607. DOI: `10.3758/bf03205532`.

[58]   Yoshioka, T., Bensmaïa, S. J., Craig, J. C., and Hsiao, S. S. Texture perception through direct and indirect touch: An analysis of perceptual space for tactile textures in two modes of exploration. *Somatosensory & Motor Research* **24** (2007), 53–70. DOI: `10.1080/08990220701318163`.

[59]   Miller, L. E., Montroni, L., Koun, E., Salemme, R., Hayward, V., and Farnè, A. Sensing with tools extends somatosensory processing beyond the body. *Nature* **561** (2018), 239–242. DOI: `10.1038/s41586-018-0460-0`.

[60]   Schepers, R. J. and Ringkamp, M. Thermoreceptors and thermosensitive afferents. *Neuroscience and Biobehavioral Reviews* **34** (2010), 177–184. DOI: `10.1016/j.neubiorev.2009.10.003`.

[61]   Dubin, A. E. and Patapoutian, A. Nociceptors: the sensors of the pain pathway. *The Journal of Clinical Investigation* **120** (2010), 3760–3772. DOI: `10.1172/JCI42843`.

[62]   Deflorio, D., Di Luca, M., and Wing, A. M. Skin and Mechanoreceptor Contribution to Tactile Input for Perception: A Review of Simulation Models. *Frontiers in Human Neuroscience* **16** (2022), 862344. DOI: `10.3389/fnhum.2022.862344`.

[63]   Gescheider, G., Bolanowski, S., and Verrillo, R. Some characteristics of tactile channels. *Behavioural Brain Research* **148** (2004), 35–40. DOI: `10.1016/S0166-4328(03)00177-3`.

1

[64] Dayan, P. and Abbott, L. F. *Theoretical Neuroscience: Computational and Mathematical Modeling of Neural Systems*. The MIT Press, 2005.

[65] Johansson, R. S., Landström, U., and Lundström, R. Responses of mechanoreceptive afferent units in the glabrous skin of the human hand to sinusoidal skin displacements. *Brain Research* **244** (1982), 17–25.

[66] Delhaye, B. P., Long, K. H., and Bensmaia, S. J. Neural Basis of Touch and Proprioception in Primate Cortex. *Comprehensive Physiology* **8** (2018), 1575–1602. DOI: 10.1002/cphy.c170033.

[67] Delhaye, B., Hayward, V., Lefèvre, P., and Thonnard, J.-L. Texture-induced vibrations in the forearm during tactile exploration. *Frontiers in Behavioral Neuroscience* **6** (2012). DOI: 10.3389/fnbeh.2012.00037.

[68] Gibson. *The Senses Considered as Perceptual Systems*. James J. Gibson. *The Quarterly Review of Biology* **44** (1969), 104–105. DOI: 10.1086/406033.

[69] Saal, H. P. and Bensmaia, S. J. Touch is a team effort: interplay of submodalities in cutaneous sensibility. *Trends in Neurosciences* **37** (2014), 689–697. DOI: 10.1016/j.tins.2014.08.012.

[70] Weber, A. I., Saal, H. P., Lieber, J. D., Cheng, J.-W., Manfredi, L. R., Dammann, J. F., and Bensmaia, S. J. Spatial and temporal codes mediate the tactile perception of natural textures. *Proceedings of the National Academy of Sciences of the United States of America* **110** (2013), 17107–17112. DOI: 10.1073/pnas.1305509110.

[71] Kandel, E., Schwartz, J., Jessell, T., Siegelbaum, S., and Hudspeth, A. *Principles of Neural Science*. 5th ed. New York, NY: McGraw Hill Education, 2013.

[72] Jones, E. G. Cortical and subcortical contributions to activity-dependent plasticity in primate somatosensory cortex. *Annual Review of Neuroscience* **23** (2000), 1–37. DOI: 10.1146/annurev.neuro.23.1.1.

[73] Abraira, V. E. and Ginty, D. D. The Sensory Neurons of Touch. *Neuron* **79** (2013), 10.1016/j.neuron.2013.07.051. DOI: 10.1016/j.neuron.2013.07.051.

[74] Jörntell, H., Bengtsson, F., Geborek, P., Spanne, A., Terekhov, A. V., and Hayward, V. Segregation of tactile input features in neurons of the cuneate nucleus. *Neuron* **83** (2014), 1444–1452. DOI: 10.1016/j.neuron.2014.07.038.

[75] Purves, D., Augustine, G. J., Fitzpatrick, D., Katz, L. C., LaMantia, A.-S., McNamara, J. O., and Williams, S. M. "The Somatic Sensory Cortex". In: Neuroscience. 2nd edition. Sinauer Associates, 2001.

[76] Raju, H. and Tadi, P. "Neuroanatomy, Somatosensory Cortex". In: StatPearls. Treasure Island (FL): StatPearls Publishing, 2024.

[77] Enander, J. M. D. and Jörntell, H. Somatosensory cortical neurons decode tactile input patterns andl location from both dominant and non-dominant digits. *Cell Reports* **26** (2019), 3551–3560.e4. DOI: 10.1016/j.celrep.2019.02.099.

[78] Gibson, J. J. *The Ecological Approach to Visual Perception: Classic Edition*. New York: Psychology Press, 1979. DOI: 10.4324/9781315740218.

[79] Snyder, D. M. *On the relationship between proximal and distal stimuli and an example of its significance to physics. Preprint. arXiv.* 2001. DOI: `10.48550/arXiv.physics/0110036`.

[80] Ernst, M. O. and Bülthoff, H. H. Merging the senses into a robust percept. *Trends in Cognitive Sciences* **8** (2004), 162–169. DOI: `10.1016/j.tics.2004.02.002`.

[81] Katz, D., Krueger, L. E., and Krueger, L. E. *The World of Touch.* New York: Psychology Press, 1989. DOI: `10.4324/9780203771976`.

[82] Gescheider, G. A. Evidence in support of the duplex theory of mechanoreception. *Sensory Processes* **1** (1976), 68–76.

[83] Hollins, M. and Risner, S. R. Evidence for the duplex theory of tactile texture perception. *Perception & Psychophysics* **62** (2000), 695–705. DOI: `10.3758/bf03206916`.

[84] Blake, D., Hsiao, S., and Johnson, K. Neural coding mechanisms in tactile pattern recognition: the relative contributions of slowly and rapidly adapting mechanoreceptors to perceived roughness. *The Journal of Neuroscience* **17** (1997), 7480–9. DOI: `10.1523/JNEUROSCI.17-19-07480.1997`.

[85] Hollins, M., Bensmaïa, S. J., and Washburn, S. Vibrotactile adaptation impairs discrimination of fine, but not coarse, textures. *Somatosensory & Motor Research* **18** (2001), 253–262. DOI: `10.1080/01421590120089640`.

[86] Grigorii, R. V., Colgate, J. E., and Klatzky, R. The spatial profile of skin indentation shapes tactile perception across stimulus frequencies. *Scientific Reports* **12** (2022), 13185. DOI: `10.1038/s41598-022-17324-7`.

[87] Bergmann Tiest, W. M. Tactual perception of material properties. *Vision Research.* Perception and Action: Part I **50** (2010), 2775–2782. DOI: `10.1016/j.visres.2010.10.005`.

[88] Wijntjes, M. W. A., Sato, A., Hayward, V., and Kappers, A. M. L. Local Surface Orientation Dominates Haptic Curvature Discrimination. *IEEE Transactions on Haptics* **2** (2009), 94–102. DOI: `10.1109/TOH.2009.1`.

[89] Bochereau, S., Dzidek, B., Adams, M., and Hayward, V. Characterizing and Imaging Gross and Real Finger Contacts under Dynamic Loading. *IEEE transactions on haptics* **10** (2017), 456–465. DOI: `10.1109/TOH.2017.2686849`.

[90] Werner, G. and Mountcastle, V. B. Neural activity in mechanoreceptive cutaneous afferents: stimulus-response relations, weber functions, and information transmission. *Journal of Neurophysiology* **28** (1965), 359–397. DOI: `10.1152/jn.1965.28.2.359`.

[91] Verrillo, R. T. Temporal summation in vibrotactile sensitivity. *The Journal of the Acoustical Society of America* **37** (1965), 843–846. DOI: `10.1121/1.1909458`.

[92] Verrillo, R. T. and Verrillo, R. T. Effect of contactor area on the vibrotactile threshold. *Journal of the Acoustical Society of America* **35** (1963), 1962–1966. DOI: `10.1121/1.1918868`.

[93] Poulos, D., Mei, J., Horch, K., Tuckett, R., Wei, J., Cornwall, M., and Burgess, P. The neural signal for the intensity of a tactile stimulus. *The Journal of Neuroscience* **4** (1984), 2016–2024. DOI: 10.1523/JNEUROSCI.04-08-02016.1984.

[94] Gescheider, G. A., Berryhill, M. E., Verrillo, R. T., and Bolanowski, S. J. Vibrotactile temporal summation: probability summation or neural integration? *Somatosensory & motor research* **16** (1999), 229–242. DOI: 10.1080/08990229970483.

[95] Barlow, H. B. Temporal and spatial summation in human vision at different background intensities. *The Journal of Physiology* **141** (1958), 337–350.

[96] Gescheider, G. A., Güçlü, B., Sexton, J. L., Karalunas, S., and Fontana, A. Spatial summation in the tactile sensory system: Probability summation and neural integration. *Somatosensory & Motor Research* **22** (2005), 255–268. DOI: 10.1080/08990220500420236.

[97] Franzén, O. On spatial summatin in the tactual sense. A psychophysical and neurophysiological study. *Scandinavian Journal of Psychology* **10** (1969), 193–208. DOI: 10.1111/j.1467-9450.1969.tb00027.x.

[98] Stevens, J. C. and Marks, L. E. Spatial summation and the dynamics of warmth sensation. *Perception & Psychophysics* **9** (1971), 391–398. DOI: 10.3758/BF03210236.

[99] Verrillo, R. T., Fraioli, A. J., and Smith, R. L. Sensation magnitude of vibrotactile stimuli. *Perception & Psychophysics* **6** (1969), 366–372. DOI: 10.3758/BF03212793.

[100] Hollins, M. and Roy, E. A. Perceived intensity of vibrotactile stimuli: the role of mechanoreceptive channels. *Somatosensory & Motor Research* **13** (1996), 273–286. DOI: 10.3109/08990229609052583.

[101] Muniak, M. A., Ray, S., Hsiao, S. S., Dammann, J. F., and Bensmaia, S. J. The neural coding of stimulus intensity: linking the population response of mechanoreceptive afferents with psychophysical behavior. *The Journal of Neuroscience: The Official Journal of the Society for Neuroscience* **27** (2007), 11687–11699. DOI: 10.1523/JNEUROSCI.1486-07.2007.

[102] Bolanowski, S. J., Gescheider, G. A., Verrillo, R. T., and Checkosky, C. M. Four channels mediate the mechanical aspects of touch. *The Journal of the Acoustical Society of America* **84** (1988), 1680–1694. DOI: 10.1121/1.397184.

[103] Talbot, W. H., Darian-Smith, I., Kornhuber, H. H., and Mountcastle, V. B. The sense of flutter-vibration: comparison of the human capacity with response patterns of mechanoreceptive afferents from the monkey hand. *Journal of Neurophysiology* **31** (1968), 301–334. DOI: 10.1152/jn.1968.31.2.301.

[104] Bensmaia, S. J. Tactile intensity and population codes. *Behavioural brain research* **190** (2008), 165–173. DOI: 10.1016/j.bbr.2008.02.044.

[105] Verrillo, R. T. Investigation of some parameters of the cutaneous threshold for vibration. *The Journal of the Acoustical Society of America* **34** (1962), 1768–1773. DOI: 10.1121/1.1909124.

[106] Birznieks, I., McIntyre, S., Nilsson, H. M., Nagi, S. S., Macefield, V. G., Mahns, D. A., and Vickery, R. M. Tactile sensory channels over-ruled by frequency decoding system that utilizes spike pattern regardless of receptor type. *eLife* **8** (2019). Ed. by Ginty, D. D., King, A. J., and Lechner, S. G., e46510. DOI: 10.7554/eLife.46510.

[107] Rosch, E. "Principles of Categorization". In: Readings in Cognitive Science, a Perspective From Psychology and Artificial Intelligence. Ed. by Collins, A. and Smith, E. E. Morgan Kaufmann Publishers, 1978, pp. 312–22.

[108] Klatzky, R. L. and Lederman, S. J. Haptic object perception: spatial dimensionality and relation to vision. *Philosophical Transactions of the Royal Society B: Biological Sciences* **366** (2011), 3097–3105. DOI: 10.1098/rstb.2011.0153.

[109] Yau, J. M., Kim, S. S., Thakur, P. H., and Bensmaia, S. J. Feeling form: the neural basis of haptic shape perception. *Journal of Neurophysiology* **115** (2016), 631–642. DOI: 10.1152/jn.00598.2015.

[110] LaMotte, R. H., Friedman, R. M., Lu, C., Khalsa, P. S., and Srinivasan, M. A. Raised object on a planar surface stroked across the fingerpad: responses of cutaneous mechanoreceptors to shape and orientation. *Journal of Neurophysiology* **80** (1998), 2446–2466. DOI: 10.1152/jn.1998.80.5.2446.

[111] LaMotte, R. H. and Srinivasan, M. A. Neural encoding of shape: responses of cutaneous mechanoreceptors to a wavy surface stroked across the monkey fingerpad. *Journal of Neurophysiology* **76** (1996), 3787–3797. DOI: 10.1152/jn.1996.76.6.3787.

[112] Jenmalm, P., Birznieks, I., Goodwin, A. W., and Johansson, R. S. Influence of object shape on responses of human tactile afferents under conditions characteristic of manipulation. *The European Journal of Neuroscience* **18** (2003), 164–176. DOI: 10.1046/j.1460-9568.2003.02721.x.

[113] Hsiao, S. S. and Bensmaia, S. "6.04 - Coding of Object Shape and Texture". In: The Senses: A Comprehensive Reference. Ed. by Masland, R. H., Albright, T. D., Albright, T. D., Masland, R. H., Dallos, P., Oertel, D., Firestein, S., Beauchamp, G. K., Catherine Bushnell, M., Basbaum, A. I., Kaas, J. H., and Gardner, E. P. New York: Academic Press, 2008, pp. 55–66. DOI: 10.1016/B978-012370880-9.00345-5.

[114] Robles-De-La-Torre, G. and Hayward, V. Force can overcome object geometry in the perception of shape through active touch. *Nature* **412** (2001), 445. DOI: 10.1038/35086588.

[115] Drewing, K. and Ernst, M. O. Integration of force and position cues for shape perception through active touch. *Brain Research* **1078** (2006), 92–100. DOI: 10.1016/j.brainres.2005.12.026.

[116] Hayward, V. "Haptic shape cues, invariants, priors and interface design". In: Human Haptic Perception: Basics and Applications. Ed. by Grunwald, M. Basel: Birkhäuser Basel, 2008, pp. 381–392. DOI: 10.1007/978-3-7643-7612-3_31.

[117] Tomlinson, S. E., Lewis, R., and Carré, M. J. The effect of normal force and roughness on friction in human finger contact. *Wear*. 17th International Conference on Wear of Materials **267** (2009), 1311–1318. DOI: `10.1016/j.wear.2008.12.084`.

[118] Burstedt, M. K., Flanagan, J. R., and Johansson, R. S. Control of grasp stability in humans under different frictional conditions during multidigit manipulation. *Journal of Neurophysiology* **82** (1999), 2393–2405. DOI: `10.1152/jn.1999.82.5.2393`.

[119] Lewis, R., Menardi, C., Yoxall, A., and Langley, J. Finger friction: Grip and opening packaging. *Wear*. 16th International Conference on Wear of Materials **263** (2007), 1124–1132. DOI: `10.1016/j.wear.2006.12.024`.

[120] Bergmann Tiest, W. M. and Kappers, A. M. Analysis of haptic perception of materials by multidimensional scaling and physical measurements of roughness and compressibility. *Acta Psychologica* **121** (2006), 1–20. DOI: `10.1016/j.actpsy.2005.04.005`.

[121] Okamoto, S., Nagano, H., and Yamada, Y. Psychophysical dimensions of tactile perception of textures. *IEEE Transactions on Haptics* **6** (2013), 81–93. DOI: `10.1109/TOH.2012.32`.

[122] Hollins, M., Bensmaïa, S., Karlof, K., and Young, F. Individual differences in perceptual space for tactile textures: Evidence from multidimensional scaling. *Perception & Psychophysics* **62** (2000), 1534–1544. DOI: `10.3758/BF03212154`.

[123] Lederman, S. J. and Klatzky, R. L. Hand movements: A window into haptic object recognition. *Cognitive Psychology* **19** (1987), 342–368. DOI: `10.1016/0010-0285(87)90008-9`.

[124] Connor, C. E., Hsiao, S. S., Phillips, J. R., and Johnson, K. O. Tactile roughness: neural codes that account for psychophysical magnitude estimates. *The Journal of Neuroscience: The Official Journal of the Society for Neuroscience* **10** (1990), 3823–3836. DOI: `10.1523/JNEUROSCI.10-12-03823.1990`.

[125] Di Stefano, N. and Spence, C. Roughness perception: A multisensory/crossmodal perspective. *Attention, Perception & Psychophysics* **84** (2022), 2087–2114. DOI: `10.3758/s13414-022-02550-y`.

[126] Kahrimanovic, M., Bergmann Tiest, W. M., and Kappers, A. M. L. Context effects in haptic perception of roughness. *Experimental Brain Research* **194** (2009), 287–297. DOI: `10.1007/s00221-008-1697-x`.

[127] Lamb, G. D. Tactile discrimination of textured surfaces: psychophysical performance measurements in humans. *The Journal of Physiology* **338** (1983), 551–565. DOI: `10.1113/jphysiol.1983.sp014689`.

[128] Lederman, S. J. and Taylor, M. M. Fingertip force, surface geometry, and the perception of roughness by active touch. *Perception & Psychophysics* **12** (1972), 401–408. DOI: `10.3758/BF03205850`.

[129] Miyaoka, T., Mano, T., and Ohka, M. Mechanisms of fine-surface-texture discrimination in human tactile sensation. *The Journal of the Acoustical Society of America* **105** (1999), 2485–2492. DOI: 10.1121/1.426852.

[130] Tymms, C., Zorin, D., and Gardner, E. P. Tactile perception of the roughness of 3D-printed textures. *Journal of Neurophysiology* **119** (2018), 862–876. DOI: 10.1152/jn.00564.2017.

[131] Ekman, G., Hosman, J., and Lindstrom, B. Roughness, smoothness, and preference: A study of quantitative relations in individual subjects. *Journal of Experimental Psychology* **70** (1965), 18–26. DOI: 10.1037/h0021985.

[132] Gwosdow, A., Stevens, J., Berglund, L., and Stolwijk, J. Skin friction and fabric sensations in neutral and warm environments. *Textile Research Journal* **56** (1986), 574–580. DOI: 10.1177/004051758605600909.

[133] Bensmaïa, S., Hollins, M., and Yau, J. Vibrotactile intensity and frequency information in the pacinian system: a psychophysical model. *Perception & Psychophysics* **67** (2005), 828–841. DOI: 10.3758/bf03193536.

[134] Bensmaïa, S. J. and Hollins, M. The vibrations of texture. *Somatosensory & Motor Research* **20** (2003), 33–43. DOI: 10.1080/0899022031000083825.

[135] Smith, A. M., Chapman, C. E., Deslandes, M., Langlais, J.-S., and Thibodeau, M.-P. Role of friction and tangential force variation in the subjective scaling of tactile roughness. *Experimental Brain Research* **144** (2002), 211–223. DOI: 10.1007/s00221-002-1015-y.

[136] Roberts, R. D., Loomes, A. R., Allen, H. A., Di Luca, M., and Wing, A. M. Contact forces in roughness discrimination. *Scientific Reports* **10** (2020), 5108. DOI: 10.1038/s41598-020-61943-x.

[137] Skedung, L., Arvidsson, M., Chung, J. Y., Stafford, C. M., Berglund, B., and Rutland, M. W. Feeling small: exploring the tactile perception limits. *Scientific Reports* **3** (2013), 2617. DOI: 10.1038/srep02617.

[138] Klatzky, R. L., Lederman, S. J., Hamilton, C., Grindley, M., and Swendsen, R. H. Feeling textures through a probe: Effects of probe and surface geometry and exploratory factors. *Perception & Psychophysics* **65** (2003), 613–631. DOI: 10.3758/BF03194587.

[139] Bergmann Tiest, W. and Kappers, A. Cues for Haptic Perception of Compliance. *IEEE Transactions on Haptics* **2** (2009), 189–199. DOI: 10.1109/TOH.2009.16.

[140] Gent, A. N. On the relation between indentation hardness and young's modulus. *Rubber Chemistry and Technology* **31** (1958), 896–906. DOI: 10.5254/1.3542351.

[141] Friedman, R. M., Hester, K. D., Green, B. G., and LaMotte, R. H. Magnitude estimation of softness. *Experimental Brain Research* **191** (2008), 133–142. DOI: 10.1007/s00221-008-1507-5.

[142] Higashi, K., Okamoto, S., Yamada, Y., Nagano, H., and Konyo, M. Hardness perception based on dynamic stiffness in tapping. *Frontiers in Psychology* **9** (2019), 2654. DOI: 10.3389/fpsyg.2018.02654.

[143] Visell, Y. and Okamoto, S. "Vibrotactile Sensation and Softness Perception". In: Multisensory Softness: Perceived Compliance from Multiple Sources of Information. Ed. by Di Luca, M. Springer Series on Touch and Haptic Systems. London: Springer, 2014, pp. 31–47. DOI: 10.1007/978-1-4471-6533-0_3.

[144] Srinivasan, M. A. and LaMotte, R. H. Tactual discrimination of softness. *Journal of Neurophysiology* **73** (1995), 88–101. DOI: 10.1152/jn.1995.73.1.88.

[145] Hartcher-O'Brien, J., Edin, B., and Hayward, V. "Shape-elasticity tactile confound". In: Hand, Brain and Technology: The Somatosensory System CSF Conferenc. 2018, p. 1.

[146] Ikeda, A., Suzuki, T., Takamatsu, J., and Ogasawara, T. "Producing Method of Softness Sensation by Device Vibration". In: 2013 IEEE International Conference on Systems, Man, and Cybernetics. 2013, pp. 3384–3389. DOI: 10.1109/SMC.2013.577.

[147] Kildal, J. "3D-press: haptic illusion of compliance when pressing on a rigid surface". In: International Conference on Multimodal Interfaces and the Workshop on Machine Learning for Multimodal Interaction. ICMI-MLMI '10. New York, NY, USA: Association for Computing Machinery, 2010, pp. 1–8. DOI: 10.1145/1891903.1891931.

[148] Visell, Y., Giordano, B. L., Millet, G., and Cooperstock, J. R. Vibration influences haptic perception of surface compliance during walking. *PloS One* **6** (2011), e17697. DOI: 10.1371/journal.pone.0017697.

[149] Bergmann Tiest, W. M. and Kappers, A. M. L. Tactile perception of thermal diffusivity. *Attention, Perception, & Psychophysics* **71** (2009), 481–489. DOI: 10.3758/APP.71.3.481.

[150] Smith, A. and Scott, S. Subjective scaling of smooth surface friction. *Journal of neurophysiology* **75** (1996), 1957–62. DOI: 10.1152/jn.1996.75.5.1957.

[151] Freeman, W. J. Perception of Time and Causation Through the Kinesthesia of Intentional Action. *Integrative Psychological and Behavioral Science* **42** (2008), 137–143. DOI: 10.1007/s12124-007-9049-0.

[152] Straube, B. and Chatterjee, A. Space and time in perceptual causality. *Frontiers in Human Neuroscience* **4** (2010). DOI: 10.3389/fnhum.2010.00028.

[153] Murai, Y. and Yotsumoto, Y. Optimal multisensory integration leads to optimal time estimation. *Scientific Reports* **8** (2018), 1–11. DOI: 10.1038/s41598-018-31468-5.

[154] De Kock, R., Gladhill, K. A., Ali, M. N., Joiner, W. M., and Wiener, M. How movements shape the perception of time. *Trends in cognitive sciences* **25** (2021), 950–963. DOI: 10.1016/j.tics.2021.08.002.

[155] Balasubramaniam, R., Haegens, S., Jazayeri, M., Merchant, H., Sternad, D., and Song, J.-H. Neural Encoding and Representation of Time for Sensorimotor Control and Learning. *The Journal of Neuroscience: The Official Journal of the Society for Neuroscience* **41** (2021), 866–872. DOI: 10.1523/JNEUROSCI.1652-20.2020.

[156] Gibson, J. J. Observations on active touch. *Psychological Review* **69** (1962), 477–491. DOI: `10.1037/h0046962`.

[157] Pei, Y.-C. and Bensmaia, S. J. The neural basis of tactile motion perception. *Journal of Neurophysiology* **112** (2014), 3023–3032. DOI: `10.1152/jn.00391.2014`.

[158] Dupin, L., Hayward, V., and Wexler, M. Generalized movement representation in haptic perception. *Journal of Experimental Psychology: Human Perception and Performance* **43** (2017), 581–595. DOI: `10.1037/xhp0000327`.

[159] Edin, B. B. and Johansson, N. Skin strain patterns provide kinaesthetic information to the human central nervous system. *The Journal of Physiology* **487** (1995), 243–251.

[160] Block, R. A. and Gruber, R. P. Time perception, attention, and memory: A selective review. *Acta Psychologica*. Including Special section articles of Temporal Processing Within and Across Senses - Part-2 **149** (2014), 129–133. DOI: `10.1016/j.actpsy.2013.11.003`.

[161] Polti, I., Martin, B., and van Wassenhove, V. The effect of attention and working memory on the estimation of elapsed time. *Scientific Reports* **8** (2018), 6690. DOI: `10.1038/s41598-018-25119-y`.

[162] Lehockey, K. A., Winters, A. R., Nicoletta, A. J., Zurlinden, T. E., and Everhart, D. E. The effects of emotional states and traits on time perception. *Brain Informatics* **5** (2018), 9. DOI: `10.1186/s40708-018-0087-9`.

[163] Gable, P. A., Wilhelm, A. L., and Poole, B. D. How Does Emotion Influence Time Perception? A Review of Evidence Linking Emotional Motivation and Time Processing. *Frontiers in Psychology* **13** (2022). DOI: `10.3389/fpsyg.2022.848154`.

[164] Hancock, P. A. Body temperature influence on time perception. *The Journal of General Psychology* **120** (1993), 197–216. DOI: `10.1080/00221309.1993.9711144`.

[165] Wearden, J. H. and Penton-Voak, I. S. Feeling the heat: body temperature and the rate of subjective time, revisited. *The Quarterly Journal of Experimental Psychology. B, Comparative and Physiological Psychology* **48** (1995), 129–141. DOI: `10.1080/14640749508401443`.

[166] Wittmann, M. and Lehnhoff, S. Age effects in perception of time. *Psychological Reports* **97** (2005), 921–935. DOI: `10.2466/pr0.97.3.921-935`.

[167] Riemer, M., Wolbers, T., and van Rijn, H. Age-related changes in time perception: The impact of naturalistic environments and retrospective judgements on timing performance. *Quarterly Journal of Experimental Psychology (2006)* **74** (2021), 2002–2012. DOI: `10.1177/17470218211023362`.

1

[168] Gibson, J. J. "Events are Perceivable But Time Is Not". In: The Study of Time II: Proceedings of the Second Conference of the International Society for the Study of Time Lake Yamanaka-Japan. Ed. by Fraser, J. T. and Lawrence, N. Berlin, Heidelberg: Springer, 1975, pp. 295–301. DOI: 10.1007/978-3-642-50121-0_22.

[169] Block, R. A. Temporal judgments and contextual change. *Journal of Experimental Psychology. Learning, Memory, and Cognition* **8** (1982), 530–544. DOI: 10.1037//0278-7393.8.6.530.

[170] brown, S. W. Time, change, and motion: The effects of stimulus movement on temporal perception. *Perception & Psychophysics* **57** (1995), 105–116. DOI: 10.3758/BF03211853.

[171] Allingham, E., Hammerschmidt, D., and Wöllner, C. Time perception in human movement: Effects of speed and agency on duration estimation. *Quarterly Journal of Experimental Psychology (2006)* **74** (2021), 559–572. DOI: 10.1177/1747021820979518.

[172] Berglund, B., Berglund, U., Ekman, G., and Frankehaeuser, M. The Influence of Auditory Stimulus Intensity on Apparent Duration. *Scandinavian Journal of Psychology* **10** (1969), 21–26. DOI: 10.1111/j.1467-9450.1969.tb00003.x.

[173] Ekman, G., Frankenhaeuser, M., Berglund, B., and Waszak, M. Apparent duration as a function of intensity of vibrotactile stimulation. *Perceptual and Motor Skills* **28** (1969), 151–156. DOI: 10.2466/pms.1969.28.1.151.

[174] Goldstone, S., Lhamon, W. T., and Sechzer, J. Light intensity and judged duration. *Bulletin of the Psychonomic Society* **12** (1978), 83–84. DOI: 10.3758/BF03329633.

[175] Bobick, A. F. Movement, activity and action: the role of knowledge in the perception of motion. *Philosophical Transactions of the Royal Society B: Biological Sciences* **352** (1997), 1257–1265.

[176] Merchant, H. and Yarrow, K. How the motor system both encodes and influences our sense of time. *Current Opinion in Behavioral Sciences*. Time in perception and action **8** (2016), 22–27. DOI: 10.1016/j.cobeha.2016.01.006.

[177] Haggard, P., Clark, S., and Kalogeras, J. Voluntary action and conscious awareness. *Nature Neuroscience* **5** (2002), 382–385. DOI: 10.1038/nn827.

[178] Yarrow, K. and Rothwell, J. C. Manual chronostasis: tactile perception precedes physical contact. *Current biology: CB* **13** (2003), 1134–1139. DOI: 10.1016/s0960-9822(03)00413-5.

[179] Wenke, D. and Haggard, P. How voluntary actions modulate time perception. *Experimental Brain Research* **196** (2009), 311–318. DOI: 10.1007/s00221-009-1848-8.

[180] Moore, J. W. and Obhi, S. S. Intentional binding and the sense of agency: A review. *Consciousness and Cognition*. Beyond the Comparator Model **21** (2012), 546–561. DOI: 10.1016/j.concog.2011.12.002.

[181] Suzuki, K., Lush, P., Seth, A. K., and Roseboom, W. Intentional binding without intentional action. *Psychological Science* **30** (2019), 842–853. DOI: 10.1177/0956797619842191.

[182] Kirsch, W., Kunde, W., and Herbort, O. Intentional binding is unrelated to action intention. *Journal of Experimental Psychology. Human Perception and Performance* **45** (2019), 378–385. DOI: 10.1037/xhp0000612.

[183] Turvey, M. T., Shockley, K., and Carello, C. Affordance, proper function and the physical basis of perceived heaviness. *Cognition* **73** (1999), B17–B26. DOI: 10.1016/S0010-0277(99)00050-5.

[184] Shockley, K., Carello, C., and Turvey, M. T. Metamers in the haptic perception of heaviness and moveableness. *Perception & Psychophysics* **66** (2004), 731–742. DOI: 10.3758/BF03194968.

[185] Turvey, M., Whitmyer, V., and Shockley, K. Explaining Metamers: Right Degrees of Freedom, Not Subjectivism. *Consciousness and Cognition* **10** (2001), 105–116. DOI: 10.1006/ccog.2000.0480.

[186] Blumstein, S. E. and Stevens, K. N. Phonetic features and acoustic invariance in speech. *Cognition* **10** (1981), 25–32. DOI: 10.1016/0010-0277(81)90021-4.

[187] Cooper, F. S., Delattre, P. C., Liberman, A. M., Borst, J. M., and Gerstman, L. J. Some Experiments on the Perception of Synthetic Speech Sounds. *The Journal of the Acoustical Society of America* **24** (1952), 597–606. DOI: 10.1121/1.1906940.

[188] *Phonetic features and acoustic invariance in speech - ScienceDirect.*

[189] Cohen, J. "Perceptual Constancy". In: Oxford University Press, 2014. DOI: 10.1093/oxfordhb/9780199600472.013.014.

[190] Backus, B. T. "Perceptual Metamers in Stereoscopic Vision". In: Advances in Neural Information Processing Systems 14. Ed. by Dietterich, T., Becker, S., and Ghahramani. 2002, p. 8.

[191] Burge, T. *Origins of objectivity*. 1. ed. Oxford: Clarendon Press, 2010.

[192] Schulte, P. The nature of perceptual constancies. *Philosophy and Phenomenological Research* **103** (2021), 3–20. DOI: 10.1111/phpr.12693.

[193] Green, E. J. Perceptual constancy and perceptual representation. *Analytic Philosophy* **n/a** (2023). DOI: 10.1111/phib.12293.

[194] Treue, S. Visual attention: the where, what, how and why of saliency. *Current Opinion in Neurobiology* **13** (2003), 428–432. DOI: 10.1016/S0959-4388(03)00105-3.

[195] Van de Langenberg, R., Kingma, I., and Beek, P. J. Mechanical invariants are implicated in dynamic touch as a function of their salience in the stimulus flow. *Journal of Experimental Psychology. Human Perception and Performance* **32** (2006), 1093–1106. DOI: 10.1037/0096-1523.32.5.1093.

1

[196] Cataldo, A., Ferrè, E. R., di Pellegrino, G., and Haggard, P. Why the whole is more than the sum of its parts: Salience-driven overestimation in aggregated tactile sensations. *Quarterly Journal of Experimental Psychology (2006)* **72** (2019), 2509–2526. DOI: 10.1177/1747021819847131.

[197] Walsh, L., Critchlow, J., Beck, B., Cataldo, A., de Boer, L., and Haggard, P. Salience-driven overestimation of total somatosensory stimulation. *Cognition* **154** (2016), 118–129. DOI: 10.1016/j.cognition.2016.05.006.

[198] Billmeyer Jr., F. W. Color Science: Concepts and Methods, Quantitative Data and Formulae. *Color Research & Application* **8** (1983), 262–263. DOI: 10.1002/col.5080080421.

[199] Wandell, ©. B. A. and Use, S. U. |. T. o. *Foundations of Vision.*

[200] Akbarinia, A. and Gegenfurtner, K. R. Color metamerism and the structure of illuminant space. *Journal of the Optical Society of America. A, Optics, Image Science, and Vision* **35** (2018), B231–B238. DOI: 10.1364/JOSAA.35.00B231.

[201] Hillis, J. M. Combining Sensory Information: Mandatory Fusion Within, but Not Between, Senses. *Science* **298** (2002), 1627–1630. DOI: 10.1126/science.1075396.

[202] Gescheider, G. A. *Psychophysics: The Fundamentals.* 3rd ed. New York: Psychology Press, 1997. DOI: 10.4324/9780203774458.

[203] Fechner, G. T. *Elemente der Psychophysik.* Breitkopf und Härtel, 1860.

[204] Wichmann, F. A. and Hill, N. J. The psychometric function: I. Fitting, sampling, and goodness of fit. *Perception & Psychophysics* **63** (2001), 1293–1313. DOI: 10.3758/bf03194544.

[205] Treutwein, B. Adaptive psychophysical procedures. *Vision Research* **35** (1995), 2503–2522. DOI: 10.1016/0042-6989(95)00016-X.

[206] Leek, M. R. Adaptive procedures in psychophysical research. *Perception & Psychophysics* **63** (2001), 1279–1292. DOI: 10.3758/bf03194543.

[207] Owen, L., Browder, J., Letham, B., Stocek, G., Tymms, C., and Shvartsman, M. Adaptive nonparametric psychophysics. *arXiv* (2021). DOI: 10.48550/arXiv.2104.09549.

[208] Hayward, V., Astley, O. R., Cruz-Hernandez, M., Grant, D., and Robles-De-La-Torre, G. Haptic interfaces and devices. *Sensor Review* **24** (2004), 16–29. DOI: 10.1108/02602280410515770.

[209] Cohen, L. H. and Lindley, S. B. Studies in Vibratory Sensibility. *The American Journal of Psychology* **51** (1938), 44–63. DOI: 10.2307/1416415.

[210] Gescheider, G. A., Frisina, R. D., and Verrillo, R. T. Selective adaptation of vibrotactile thresholds. *Sensory Processes* **3** (1979), 37–48.

[211] Hollins, M., Lorenz, F., and Harper, D. Somatosensory Coding of Roughness: The Effect of Texture Adaptation in Direct and Indirect Touch. *The Journal of Neuroscience* **26** (2006), 5582–5588. DOI: 10.1523/JNEUROSCI.0028-06.2006.

[212] Lowrey, C. R., Strzalkowski, N. D. J., and Bent, L. R. Cooling reduces the cutaneous afferent firing response to vibratory stimuli in glabrous skin of the human foot sole. *Journal of Neurophysiology* **109** (2013), 839–850. DOI: 10.1152/jn.00381.2012.

[213] Smith, P. L. and Little, D. R. Small is beautiful: In defense of the small-N design. *Psychonomic Bulletin & Review* **25** (2018), 2083–2101. DOI: 10.3758/s13423-018-1451-8.

[214] Schwarzkopf, D. S. and Huang, Z. *A simple statistical framework for small sample studies.* preprint. Neuroscience, 2023. DOI: 10.1101/2023.09.19.558509.

2

METAMERIC STATES IN THE DETECTION OF TRANSIENT CONTACT EVENTS

Chapter 2, constituting the first empirical chapter of this dissertation, investigates the cues and mechanisms the somatosensory system uses to detect a change in the mechanical state of a touch event at the most basic level. It addresses the question: Can we identify metamers of duration and intensity in the detection of transient contact events? And if so, can they be associated with invariant states of mechanical energy transfer?

Authors: Karina Kirk Driller, Camille Fradet, James Andrews, Vincent Hayward and Jess Hartcher-O'Brien.

Abstract: The human somatosensory system's response to mechanical stimuli, particularly impulses or broadband transients, is critical for understanding dynamic touch and the system's linear and non-linear response properties. Traditionally, research has focused on its responses to non-transient, sinusoidal stimuli in the 200–250 Hz range. In contrast, this study investigates the somatosensory system's responsiveness to very short, broadband impulses and their mechanical energy. We conducted an experiment using quantitative stimulus-generation techniques and Bayesian psychophysical methods to identify the stimuli that result in the lowest detection thresholds. Our aim was to represent mechanical interactions, notably transient contact or impact events, to provide insights into skin-object interactions at a neural level. The study identifies intensity metamers specific to the encoding of impact events, expanding upon known intensity metamers across sensory systems. Our findings furthermore highlight the importance of the total amount of energy transferred by a force as an important mechanical feature driving the detection of brief contact events. However, varying energy at threshold level across different combinations of signal amplitude and duration suggests mechanisms beyond simple energy summation, possibly indicating a preferential encoding of specific temporal cues.

2.1. INTRODUCTION

Tactile perception is inherently ambiguous; multiple physical or mechanical input states can give rise to similar perceptual outcomes [1, 2]. We can refer to scenarios in which different physical input states result in the same sensory or perceptual outcome as metamers [3–5]. One fundamental example of such a metamer is the phenomenon of intensity summation over time, where altering the duration or amplitude of a stimulus can produce the same perceived magnitude or detection behavior of that stimulus. Perceptual temporal summation is well-documented across several sensory modalities, including vision, audition, pain, and thermal perception [6–17]. However, in the tactile domain, this phenomenon has predominantly been described for non-transient stimuli lasting between 100 and 900 ms, [18–22], and most commonly involving sinusoidal vibrations [18–20] (see Appendix A for a review of this literature).

A central challenge in the study of early touch in humans involves 1) generating behaviorally relevant yet well-controlled and repeatable stimuli and 2) accessing the underlying neural response transformations in detecting them from in vivo behavioral studies, without resorting to neuroimaging or electrophysiological techniques. One approach to this challenge is to consider how the somatosensory system might decompose manipulable mechanical stimuli into a subset of mechanical inputs or cues. A behaviorally relevant mechanical input or cue should produce a stable detection response, despite other input parameters changing, providing insights into meaningful mechanical quantities and thus perceptual "primitives" needed for triggering a response on a perceptual or neural level. Previous research has often exploited non-transient (500–1000 ms) sinusoidal stimuli for this purpose, showing a

U-shaped response curve with a peak sensitivity around 200–250 Hz, said to reflect the frequency response of Pacinian corpuscles [18, 23–25]. More specifically, based on this frequency specificity of mechanoreceptor populations, Bolanowski et al. [26] proposed a theory suggesting frequency as the primary stimulus dimension used by the somatosensory system to decompose behaviorally relevant touch events. While insightful, this theory has also led to a bias in investigating the focus on frequency in research on tactile perception, often overlooking other potentially behaviorally relevant cues that might influence the somatosensory response to changes in stimuli.

Furthermore, a recurrent challenge in many of these studies is a lack of verification and transparency of the stimulus once applied to the skin, and thus the resulting proximal stimulus. This issue is pervasive due to the inherent difficulties in ensuring accurate and consistent skin-coupled stimulation. For example, lack of control for potential decoupling from the skin [27] during stimulation raises the possibility that some prior findings might have been influenced by artifacts of the testing apparatus rather than solely reflecting processing mechanisms of the somatosensory system. Finally, studies have traditionally determined detection thresholds at the 50%-chance level, which corresponds to the region of highest uncertainty and thus evidences an unstable system response. A more stable representation, such as the 75% level, can minimize misrepresentation and provide a more robust threshold [28].

The study of sensory system's responses is best done using excitation signals that mimic those of real-world interactions. However, real-world haptic interactions are far from simple sinusoidal signals. Instead, they involve complex mechanical inputs, most commonly initiated by contact detection and its detection. Moreover, many common skin-object interactions are characterized by brief events. This is evident not only in brief actions like knocking on a door or typing on a keyboard, but also in sustained skin-object interactions such as when reading Braille or exploring textured surfaces with the fingertips, which consist of a series of minute impacts as the skin contacts various textural elements. Therefore, it is crucial to investigate the somatosensory system's response to transient broadband inputs, such as those arising from impact or brief contact events.

In the present study, we investigated the somatosensory system's response to stimuli that mimic brief contact events. We used a Gaussian function and its derivatives as a signal to simulate brief interactions between the skin and a solid object. Because such signals can effectively be characterized by two key parameters, namely their amplitude and duration, the approach provides an elegant method to investigate resulting perceptual metamers and gain insights into how the somatosensory system might decompose these events. Specifically, when considering intensity metamers in the context of such inputs, there may be several factors explaining why longer signals result in lower detection thresholds. One hypothesis is that the somatosensory system might decompose these impact events into their frequency components. Alternatively, the system might encode the energy or mechanical work – the total amount of energy transferred by a force – associated with the impact. Because the duration of a Gaussian function and its derivatives is inherently linked to its frequency content, each hypothesis would predict different combinations of inputs that the somatosensory system might use to drive perception. If frequency is a key factor in

the detection of these events, then signals with differing frequency content (inverse duration) but the same total energy content should *not* produce a stable detection response. Conversely, if mechanical work is a key feature driving behavioral responses to dynamic touch events, then the perceptual thresholds should remain stable (i.e., metameric) regardless of whether the mechanical energy is derived from changes in the frequency content (inverse duration) or the amplitude of the event.

Grounded in the hypothesis that humans are most sensitive to behaviorally relevant stimuli, and because good agreement has been established between psychophysical and physiological detection responses in certain body regions [29], our study sought to determine 75 % detection thresholds in the two-dimensional amplitude-duration space of our theoretically optimal Gaussian signals. From the literature [18–22] and our previous study (Appendix A), we assumed that the amplitude and duration dimensions are non-orthogonal for the perception of stimulus magnitude and that increases of duration and amplitude each increase the probability of detecting a contact event. We used a highly controlled, custom-made stimulator to deliver stimuli to the fingertips of participants and a model-based active learning algorithm called AEPsych [30] to efficiently estimate the probability of detection (i.e., the latent perceptual function for detection) of these events. In addition, in order to ensure that the amplitude of the signal corresponded with our predictions, and to characterize the precise mechanical work (MW) delivered to the skin, we conducted post-experimental characterizations of the stimuli. These efforts were undertaken to confirm that the perceptual thresholds measured were not merely reflecting the response characteristics of the apparatus but were instead accurately representing the perceptual workspace associated with the mechanical stimuli.

2.2. METHODS

2.2.1. PARTICIPANTS

Five healthy participants (4 male, 1 female, mean age 28.6 years (SD 3.14)) took part in the study. All participants reported being right-handed. Participants gave written informed consent for participation in the study. The study was performed in accordance with relevant guidelines at Sorbonne University and the Declaration of Helsinki.

2.2.2. APPARATUS

The apparatus was made and characterized by Vincent Hayward to create an accurate empirical model of the fingertip's dynamic response to mechanical stimuli. It was developed to overcome frequent shortcomings of studies exploring the skin displacement resulting from dynamic touch, including a previous focus on measuring only hairy skin (e.g., [31–34]), using only non-transient signals (e.g., [31, 32, 35]), and most importantly for the present study, a common lack of verification and transparency of the stimuli impinging on the skin and the control for potential leaks between the stimulator and the skin (e.g., [32, 36, 37]). The apparatus has been used previously to study the dynamics of skin tissue [38]. We here used it for

its precise excitation capabilities, enabling the investigation of the somatosensory system's response properties to highly controlled transient stimuli applied to the finger pad. The apparatus comprised the following components, as illustrated in Figure 2.1.
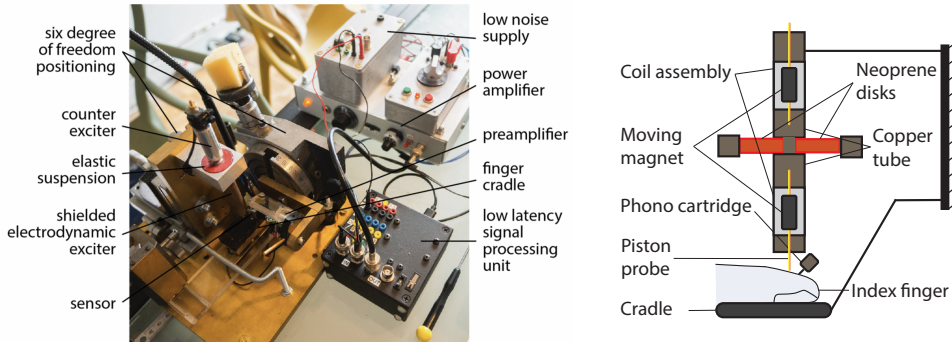
Figure 2.1. Full view of the apparatus and arrangement of components (left) and schematic close-up of the setup with a finger placed in the cradle (right). Note that the phono cartridge was used during characterization only and was not in contact with participants' skin during the experiment reported here.

- A six-axes positioning system where three displacements were allocated to position the exciter piston business end in space; two were allocated to orient the sensor around its tip; and one to elevate the cradle so the finger could be brought into contact with both the 1 mm piston and the sensor tip.
- A shielded electrodynamic exciter made of a modified vibrotactile actuator from Actronika model HC121238O. It was used in an inverted configuration with the moving magnet assembly extended with a piston probe and the coil assembly inserted in a copper tube to attenuate the high-frequency components of the magnetic field perturbations. The business end of the 2.0 mm diameter probe shaft was tapered to form a 1.0 mm contact area impinging on the skin.
- A counter-exciter of the same model. The exciter was supplied with the same signal as the main exciter but was wired to move in phase opposition, leading to zero total momentum. Hence, the reaction force on the support is zero, up to calibration errors.
- This dual exciter feature had two purposes. It minimized the energy leak from the exciter to the anatomy, which can find a path through the structure of the apparatus since the finger must be supported by a cradle. Also, some of this energy could leak directly to the sensor, which was also connected to the structure. This is a serious problem since the sensor was detecting movements down to the 10-nanometer range. Having near-zero reaction forces made it possible to suspend the assembly elastically (here, by two neoprene disks), realizing a mechanical low-pass filter with low cut-off (about 10 Hz). As a

bonus, suspending the dual exciter elastically allows it to be robust to inevitable perturbations when positioning the tested finger.

- A sensor that is a phono cartridge with a spherical diamond stylus (Ortofon, Pros S), sensitivity of 0.1 V·s/m. The sensor was shielded with soft iron foil to attenuate the low-frequency components of the magnetic field perturbations.
- A low latency signal processing unit of 16-bit resolution 44.1 kHz sampling rate, built around a Bela™ sound processor (itself built upon a BeagleBone™ single board computer running an AM335x 1GHz ARM® Cortex-A8 CPU). Residual latency was software compensated.
- A cradle to support the nail of a finger to minimize physiological movements.
- A custom-made 100x preamplifier that raised the sensitivity of the sensor to 10 V·s/m.
- A power amplifier built around a 100 W class D amplifier (Wondom™, model AA-AB31184, 24 V rail supply).
- A low-noise power supply (two D-size batteries).
- A phase-correct digital compensating filter that extended the usable frequency in the low range since the natural frequency of the exciter, which was about 70 Hz ($\sigma \approx 0.2$). The filter extended the bandwidth by one octave.

Figure 2.2 illustrates some example measurements of Ricker wavelets using the tapered piston and sensor positioned on the finger pad. A series of measurements performed for different signal durations and at different measurement distances from the source excitation can be found in Appendix C.

The measurements of the velocity vector using the phono cartridge close to the indentation location on the skin shown in Figure 2.2 and Appendix C are for reference only. They testify to the behavior of the skin-coupled device—the stimulus delivered to the skin and thus the proximal stimulus. During data collection of the study presented here, measurements with the phono cartridge were *not* carried out, as skin contact with the sensor might have biased the detectability of the stimuli. A series of post-experimental measurements using the phono cartridge on the precise stimulus parameters used in this study is described in Section 2.2.5.

2.2.3. STIMULUS

GAUSSIAN DISPLACEMENT AND THE RICKER WAVELET

The present study employed Gaussian indentations to stimulate the skin. Because the stimulator used in this study controls the acceleration of the piston probe, we used a normalized Ricker expression, mathematically defined as the second derivative of a Gaussian, as a stimulus for which the amplitude can be scaled using a simple multiplicative factor. This method allowed for the separate control of the amplitude and the duration of the stimulus. The relevant equations, beginning with Gaussian displacement, are as follows:

2
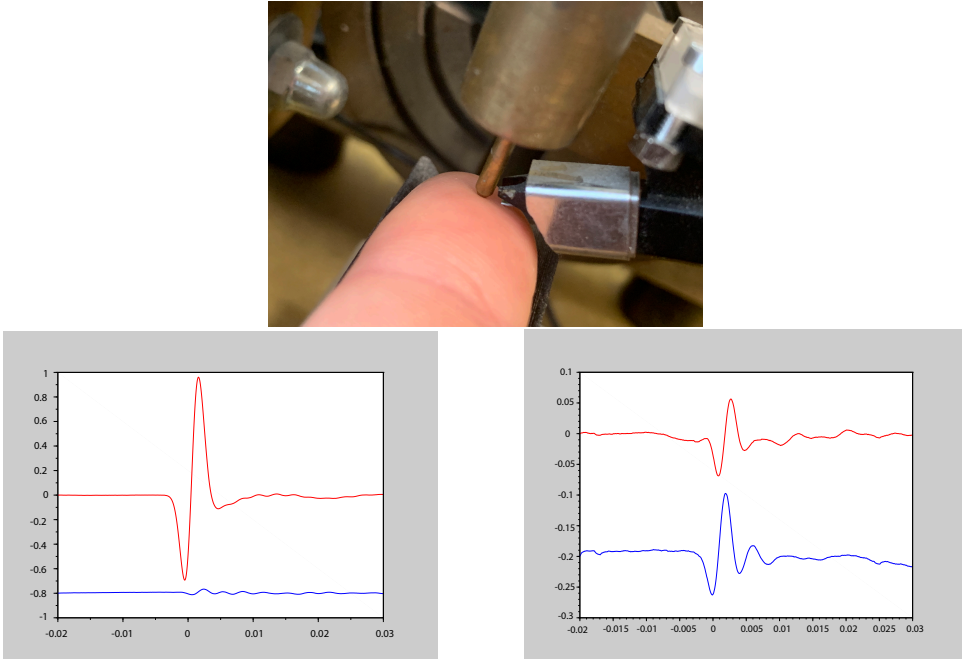
Figure 2.2. Top: Configuration for measurements of the velocity vector of skin movements in the median plane of the finger. Bottom left: Measurement of the velocity vector with the sensor of a Ricker wavelet with a σ of 1 ms measured directly at the stimulator. Vertical direction in red and horizontal direction in blue. Here, the velocity of the peak in the vertical direction corresponds to 1.0 m/s. Bottom right: Measurement of the same excitation on the skin, 4 mm from the locus of stimulation.

$$g(t) = \alpha \sigma^2 \exp\left(-\frac{t^2}{2\sigma^2}\right), \qquad G(\omega) = \alpha \sigma^3 \sqrt{2\pi} \exp\left(-\frac{\sigma^2 \omega^2}{2}\right), \quad \text{Gaussian} \quad (2.1)$$

$$s(t) = -\alpha\, t \exp\left(-\frac{t^2}{2\sigma^2}\right), \qquad S(\omega) = i\omega G(\omega), \qquad\qquad\qquad\quad (2.2)$$

$$r(t) = \alpha \left(\frac{t^2}{\sigma^2} - 1\right)\exp\left(-\frac{t^2}{2\sigma^2}\right), \qquad R(\omega) = -\omega^2 G(\omega), \qquad\qquad \text{Ricker} \quad (2.3)$$

$$j(t) = \alpha \frac{1}{\sigma^2}\left(3\,t - \frac{t^3}{\sigma^2}\right)\exp\left(-\frac{t^2}{2\sigma^2}\right), \qquad J(\omega) = -i\omega^3 G(\omega). \qquad\qquad (2.4)$$

In these equations, α represents the amplitude of the Ricker wavelet and plays a role in the amplitude of the associated derivatives, while σ determines the duration of each of the wavelets. The frequency content of each wavelet is given by its Fourier transform in the right column of eq. (2.1)–eq. (2.4).

Setting $\sigma = 1$ and $\alpha = 1$ produces the wavelets as shown in Figure 2.3.
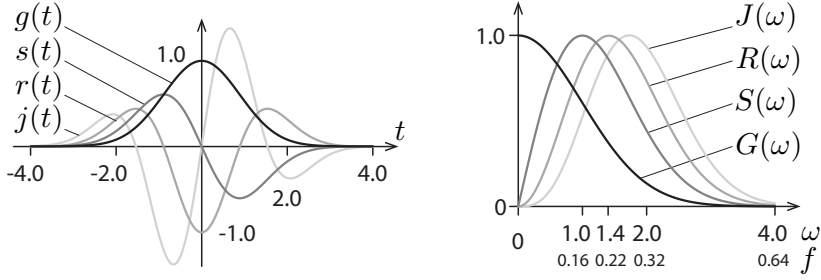
Figure 2.3. Left: The Gaussian wavelet g(t) and its three derivatives where $\sigma = 1$ and $\alpha = 1$. Right: the spectra of each wavelet, normalized by their maximum value. The graph of the wavelets scales with σ and their Fourier transforms shift with $1/\sigma$.

The side lobes of $r(t)$ are separated in time by $t_c = 3.4641\sigma$. The magnitude of the wavelets can be considered negligible beyond $\pm 4\sigma$. Each derivative increases the number of zero crossings by one and shifts the dominant frequency of the wavelets upwards by $\sqrt{2}/\sigma$. Since their spectra are small beyond $4/\sigma$ the frequency bands narrow with each derivative. The wavelets can be centered at t_0. For instance, a t_0-centered $r(t)$ is,

$$ r(t) = \alpha \left[\left(\frac{t - t_0}{\sigma} \right)^2 - 1 \right] \exp\left[-\frac{1}{2} \left(\frac{t - t_0}{\sigma} \right)^2 \right]. \tag{2.5} $$

MECHANICAL IMPACTS OF CONSTANT WORK

In the context of a brief and localized interaction between two solids, one significantly harder than the other, such as the tapered piston and the fingertip pulp in the present study, the deformation rate (velocity) is assumed to approach zero at the beginning and end of the event while passing through a maximum point. The evolution of the deflection over time can be represented by a Gaussian function, denoted as g(t). If it is further assumed that the interaction results in a viscous force proportional to the rate of deflection, with a proportionality factor b, then the work lost during the event is a function of the amplitude, α, and the duration, σ, of the interaction.

The viscous force work, as calculated in the way presented in Appendix D, can thus be determined as follows:

$$ \boxed{w(\alpha, \sigma) = \frac{\sqrt{\pi}}{2} b\alpha^2 \sigma^3} \tag{2.6} $$

Note: The fingertip pulp is best modeled as a viscoelastic material (e.g., [39–42]). At lower frequencies (below 100 Hz), the elastic properties dominate, while at higher

frequencies, the viscous properties become more significant (e.g., [43]). Given the high-frequency content of our brief signals, we assume a purely viscous response, which, although not entirely accurate, should serve as a good approximation.

APPLICATION IN THE PRESENT STUDY

The Ricker wavelet in the experiment was varied in its σ from 0.2 to 2 ms, spanning dominant frequency values (i.e., the frequency of highest amplitude) from 1125.4 Hz for the shortest signal to 112.5 Hz for the longest signal, following the conversion of dominant frequency $= \frac{\sqrt{2}}{2\pi\sigma}$. The time scale of the wavelet thus inversely affects its dominant frequency value, with shorter time scales (smaller σ) corresponding to higher dominant frequency values and longer time scales (larger σ) corresponding to lower dominant frequency values. The amplitude of the Ricker wavelet, α, in the experiment was varied from 0.01 to 1 (1–100% of the maximum admissible excitation) at an amplification level of 2 out of 9. Figure 2.4 shows the Ricker wavelet and its two parameters α and σ, used as the stimulus parameters for amplitude and duration in the present study.
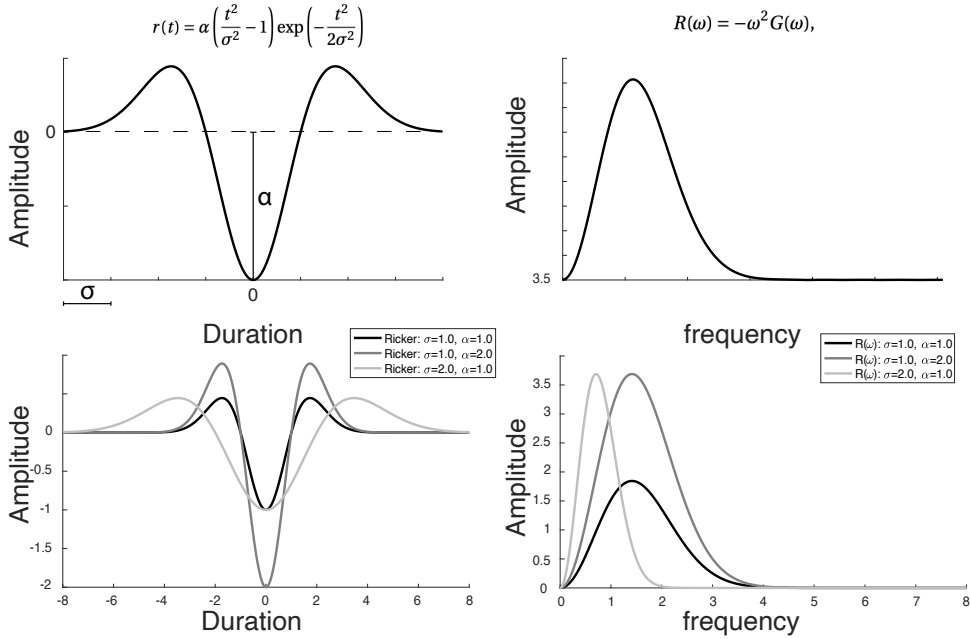
Figure 2.4. Top left: The Ricker wavelet depicts a brief contact incident between the skin and a solid object (i.e., its acceleration). Top right: The corresponding frequency spectrum, obtained via the Fourier transform. Bottom left: The Ricker wavelet with differing amplitudes α and duration σ. Bottom right: The corresponding frequency spectra of these wavelets.

In summary, the Ricker wavelet is essentially the second derivative of a Gaussian function, which makes it mathematically convenient and physically realistic for studying touch. In Section 2.2.3, we expressed the successive derivatives of the Gaussian function in both the time and frequency domains. When modeling the interaction between two solids (one much harder than the other, such as during the mechanical impact of a piston probe and a finger pad), the Ricker wavelet helps describe the deflection over time. This deflection can be represented by a Gaussian function, and the resulting viscous force (proportional to the rate of deflection) leads to energy loss, which can be calculated from the corresponding work of the viscous force.

If both σ and α affect perceptual detection of the signal, detection thresholds should be shaped by each of these parameters. Further, if the amount of work developed during the interaction is a key physical quantity for detection of the event, then the value of the work for the α and σ values should remain constant across the threshold line. It should then be the product of the amplitude squared (α^2) and the duration (σ^3).

2.2.4. EXPERIMENTAL DESIGN AND PROCEDURE

Participants were seated at a desk, wearing noise-canceling headphones (Bose QC45). Their left index finger was positioned in the cradle of the apparatus, the finger pad turned upwards, establishing light contact with the piston probe as illustrated in Figure 2.1. We used patafix to attach participants' fingernail to the cradle in order to reduce movement by the participants. Upon placing their index finger on the cradle, the cradle was slowly lifted until participants indicated detection of contact with the probe. The probe was then lowered 1 mm in order to ensure only light contact and a similar preloading of the skin between participants.

We used a non-parametric Bayesian optimization procedure called AEPsych with an underlying Gaussian-Process model [30, 44] to determine how the amplitude α and duration σ of the wavelet signal relate to the perceptual detection of an excitation. This active learning method allowed for the efficient sampling of a large stimulus space without prior expectations about the underlying shape of the relationship between stimuli and response. The method uses an adaptive stimulus selection policy and a level-set estimation objective, allowing us to model a single latent perceptual function for detecting a contact/impact event in the two-dimensional amplitude-duration input space defined by our theoretically optimal 2nd order Gaussian signal. The configuration file for this model is available in Appendix F.

We employed a one-alternative forced-choice (1AFC) "yes/no" task, in which participants had to indicate whether they felt a stimulus or not. Signal amplitude α and the duration σ were varied on a trial-by-trial basis depending on the participant's previous response and the model's areas of high uncertainty. Before the experiment proper, a few test trials were provided using pre-chosen stimuli from the middle of the distribution for participants to get acquainted with the nature of the stimulus. We adopted a 50-trial stopping criterion for threshold estimation, as simulations revealed

that, for a 2d 1AFC threshold estimation, the model would converge around this point. The experiment lasted approximately 3–4 minutes.

2.2.5. POST-EXPERIMENTAL CALIBRATION

The apparatus was characterized by Vincent Hayward with a view to achieving highly accurate Ricker wavelets in acceleration with a good representation of the parameter σ. From Appendix C it is evident that the input-output relationship for σ was well calibrated. Additional measurements performed by us confirmed this relationship. However, the parameter α of the signal can be modified in two ways, namely by changing the amplification level of the amplifier and by changing the input value in the Bela code (from 0–1). Post-experimental measurements of the output signal were therefore carried out to evaluate the input-output relationship for the parameter α across differences in σ for the specific amplification settings used in the experiment. These measurements were also necessary for correct calculations of the mechanical work of these signals as outlined in Section 2.2.3.

To evaluate the precise acceleration of our output signal and determine the multiplicative factor of the output-input amplitude relationship for any given excitation in the experiment, a series of post-experimental measurements was carried out using the phono cartridge, which measures velocity (cf. Figure 2.1). To this end, the needle of the phono cartridge was put in direct contact with the piston. The needle was placed below the tip of the piston, oriented at a $-45°$ angle to the horizontal line, as illustrated in Figure 2.5.
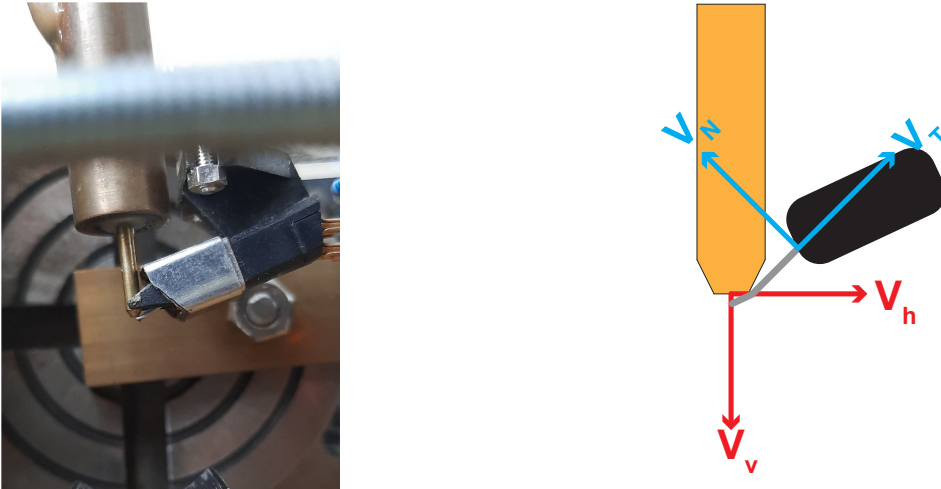
Figure 2.5. Setup for peak velocity measurements. The phono cartridge was placed in direct contact with the piston, positioned at a $-45°$ angle from below. The cartridge features two measurement axes, both tilted at a $-45°$ angle relative to the horizontal plane. Only the vertical velocity component (V_v) was of interest.

The arrangement illustrated in Figure 2.5 allowed for the separation of vertical and horizontal velocity components, respectively V_v and V_h, using the following transformations:

$$V_v = 0.707 \cdot V_T - 0.707 \cdot V_N \tag{2.7}$$
$$V_h = -0.707 \cdot V_T - 0.707 \cdot V_N \tag{2.8}$$

where V_T and V_N are the measurements of the tangential and normal velocity components in the reference frame of the cartridge. Here, only the vertical velocity component V_V was of interest, given the vertical movement of the piston. It will be referred to as V for the rest of the section.

A series of 10 Ricker impulses was sent, with different σ values, ranging from 0.0002 s to 0.002 s with steps of 0.0002 s at 50% of the maximum amplitude[1] at an amplification level of 2, corresponding to the device settings and stimulus parameters used in the experiment.

Velocity measurements contain two peaks from which the parameter α can be deduced using eq. (2.1)–eq. (2.4) provided in Section 2.2.3. For each measured impulse, the peak-to-peak value, denoted as V_{p2p}, was extracted. Using these values and following the calculation provided in Appendix E, the parameter α was calculated as follows:

$$\alpha_{out} = \frac{V_{p2p}}{2\exp\left(-\frac{1}{2}\right)} \tag{2.9}$$

Once extracted from the calibration measurements, the output acceleration amplitude α_{out} was compared to the amplitude of the command signal sent to the motor α_{in}. The ratio between these two amplitudes is shown in Figure 2.6 as a function of the second parameter, σ.

The relationship of the ratio $R_{IO} = \alpha_{out}/\alpha_{in}$ to the parameter σ was then estimated with a quadratic regression, allowing for the determination of the correct R_{IO} for any value of σ.

$$R_{IO}(\sigma) = \frac{\alpha_{out}(\sigma)}{\alpha_{in}} \tag{2.10}$$
$$= c_2\sigma^2 + c_1\sigma + c_0 \tag{2.11}$$
$$\Rightarrow R_{IO}(\sigma) = 1.9403 \times 10^7 \sigma^2 + -9.3989 \times 10^4 \sigma + 199.1421 \tag{2.12}$$
$$\alpha_{out}(\sigma) = R_{IO}(\sigma)\alpha_{in} \tag{2.13}$$

[1]it was verified that the relationship remained constant across different input amplitudes.
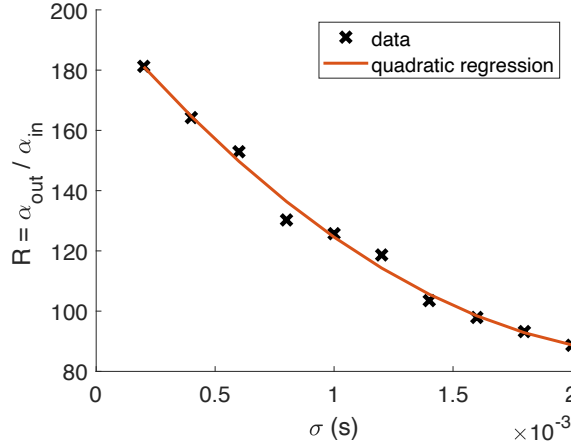
Figure 2.6. R_{IO}: Relationship between α_{in} and α_{out} as a function of σ. Here for an amplification level of 2 and an $\alpha_{in} = 0.5$. This relationship was found to be constant for different amplification and α_{in} levels.

with the regression coefficients found:

$$c_2 = 1.9403 \times 10^7 \tag{2.14}$$

$$c_1 = -9.3989 \times 10^4 \tag{2.15}$$

$$c_0 = 199.1421 \tag{2.16}$$

Figure 2.7 illustrates the relationship between the real acceleration amplitude α_{out} and the input signal parameters, α_{in} and σ.

Additionally, with the accurate α output space now determined, we can display the corresponding physical quantities associated with the stimuli, such as the resulting viscous work (cf. Figure 2.8).

2.2.6. STATISTICAL ANALYSES

We first fit the response values as a function of our two wavelet-input parameters, α and σ, with a Gaussian Process (GP)-kernel model using level set estimation (LSE) [30] to determine the .75 threshold for each participant. Means were calculated by averaging the model predictions across participants. To assess the data within the context of the post-experimental calibration of α, we first extracted the .75 threshold lines computed within the α-input space and subsequently mapped them onto the α-output space. Following this, we determined the viscous work corresponding to these threshold lines and plotted them as a function of σ and displayed our thresholds in a surface plot of the viscous work, corresponding to any stimulus combination in our stimulus space. Finally, we transformed the 2D-detection data into a 1D space of viscous work and re-fitted the detection responses with the GP model, determining 1D thresholds for each participant and the mean.
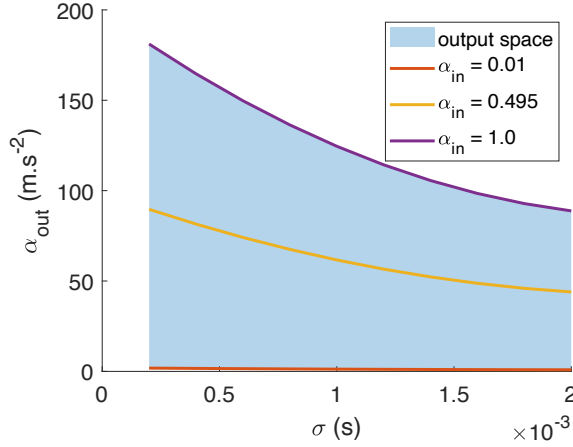
Figure 2.7. Output space. Display of α_{out} as a function of σ and α_{in}, testifying to an under-representation of the amplitude parameter α for longer signals.
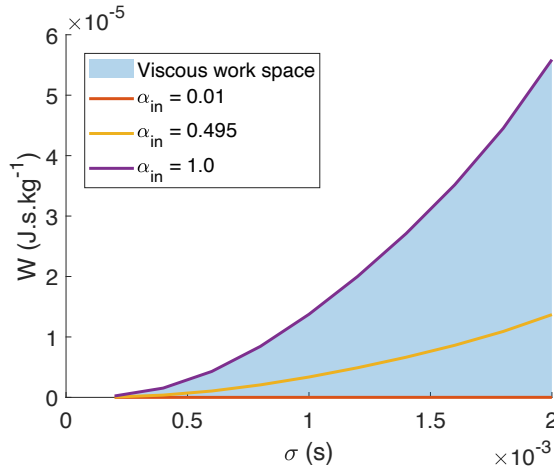
Figure 2.8. Viscous work output space. Display of the viscous work as a function of σ and α_{in}.

2.3. ANALYSIS AND RESULTS

2.3.1. PSYCHOMETRIC FIELDS FOR α AND σ

INPUT-SPACE THRESHOLDS

Psychometric field response curves for each participant are shown in Figure 2.9, while the mean across all participants is shown in Figure 2.10.
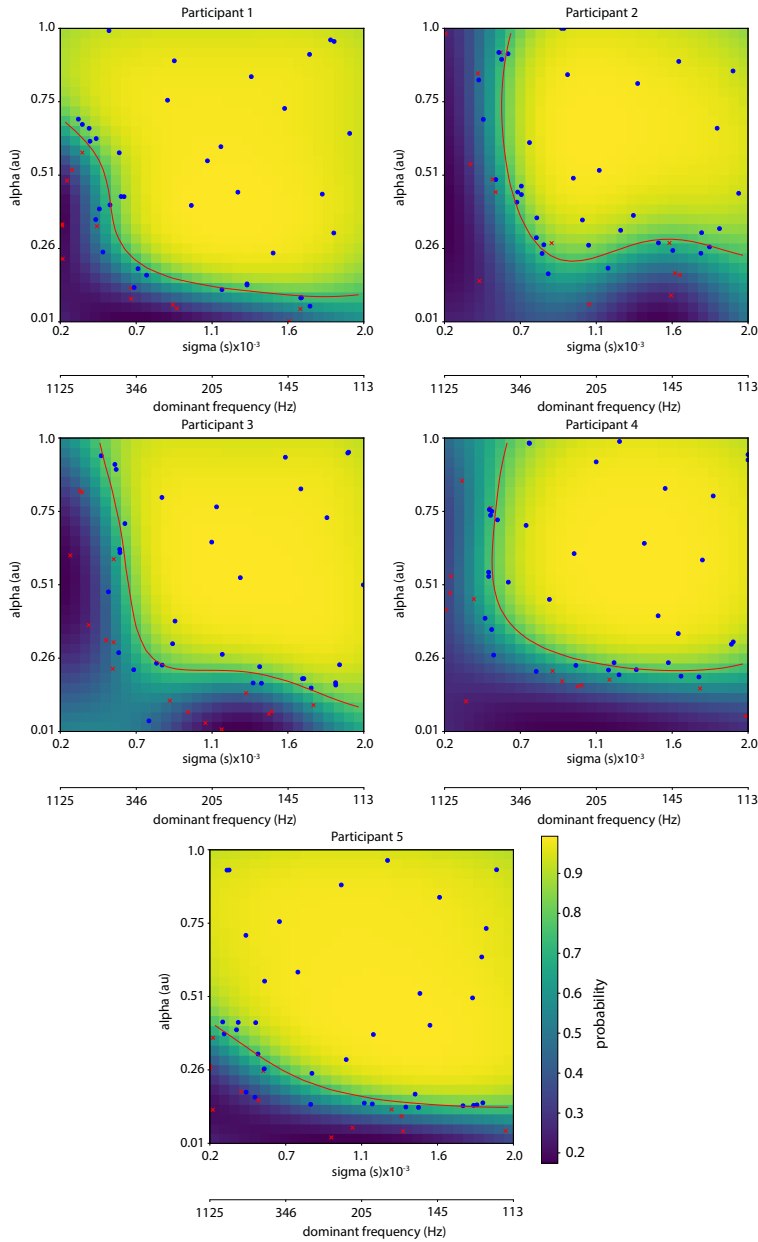
Figure 2.9. Psychometric field responses as a function of σ and input amplitude α. Dominant frequencies (inverse duration) are shown below the corresponding σ values. The probability of detecting the contact event is shown by different colors. The red isocontour line signifies the 75% threshold. Individual trials are marked in blue for detected events and red for those not detected.
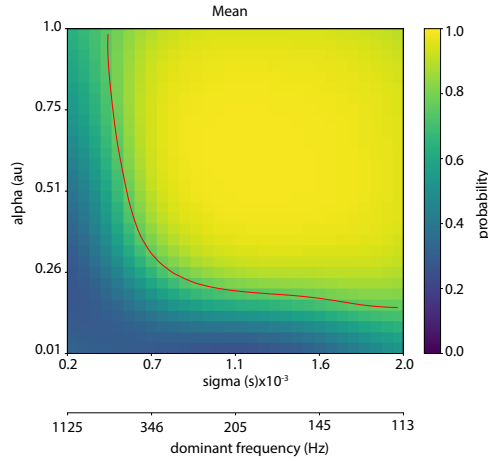
Figure 2.10. Mean probability plot across all subjects for the 2-dimensional input space.

Threshold predictions in Figure 2.9 and Figure 2.10 were made relative to the σ- and α-input space, which were the parameters fed to the active-learning algorithm during the data collection. The underlying Gaussian-Process model allowed us to identify the probability threshold of our 2-dimensional input space rapidly and reliably. Colors in these plots indicate the probability of detecting the contact event. The red isocontour lines represent the 75% thresholds. In the participant-wise psychometric fields (cf. Figure 2.9), trials and their outcomes are represented by blue (detected) and red (not detected) markers. The psychometric fields in Figure 2.9 and Figure 2.10 span sigmas σ from 0.02 to 2 ms, corresponding to dominant frequencies from 1125 to 113 Hz, and input amplitudes α_{in} from 0.01 to 1 (1–100% of the maximum admissible excitation). The 75%-probability-detected states, represented along the red contour lines, show that significantly larger input amplitudes α_{in} were needed for stimuli with a σ of approximately 0.7 ms or less to be felt. Accordingly, significantly longer signal durations σ were needed for low-amplitude α signals (0.25 or below) to be felt. This pattern was present for all participants, although individual differences are visible. Between-subject variability was largest for the shortest signals, where thresholds were close to the boundaries of our amplitude space. Consequently, for some participants, the shortest signals (0.4 ms or below) were never detected.

It is evident from these plots that there are combinations of σ and α_{in} that produce the same probability of detection. These physical confound states are metameric, meaning that different input parameter combinations can deliver the same perceptual outcome.

OUTPUT-SPACE THRESHOLDS

Upon extracting the 75% threshold lines shown in Figure 2.9 and Figure 2.10, and mapping them to the amplitude-output space α_{out} determined in Section 2.2.5, the following thresholds were achieved, as illustrated in Figure 2.11.
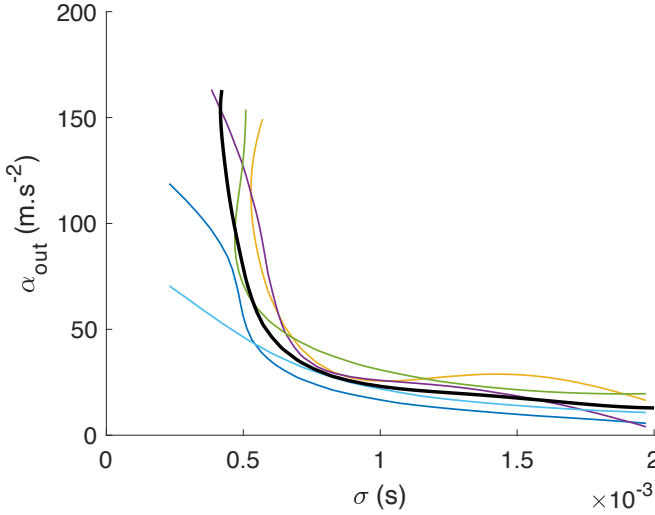
Figure 2.11. Individual and mean thresholds remapped to the α output space.

Figure 2.11 confirms that the metameric relationship between σ and α remains, following the remapping to the α_{out} space. A slight increase in α_{out} required to reach threshold can be observed as σ decreases from 2 ms to approximately 0.7 ms. After that, thresholds rise sharply for even shorter signals. On average, signals beyond 0.4 ms remained mostly undetected.

2.3.2. THRESHOLDS AS A FUNCTION OF MECHANICAL WORK

If perceived intensity or the ability to detect a change during an impact event is the result of mechanical work, then the observed metamer or confound could be seen as representing the somatosensory system's encoding of the viscous work done, rather than σ or α per se. In order to explore this hypothesis, we created plots displaying 1) the viscous work calculated for the σ and α_{out} values at threshold line and 2) the viscous work corresponding to any combination of σ and α_{in} of the input space of our experiment. For all calculations of the mechanical work, we used the α_{out} values obtained through the measurements of the piston velocity described in Section 2.2.5 and eq. (2.6) presented in the Section 2.2.3:

$$w(\alpha, \sigma) = \frac{\sqrt{\pi}}{2} b \alpha^2 \sigma^3$$

Figure 2.12 and Figure 2.13 show the results.
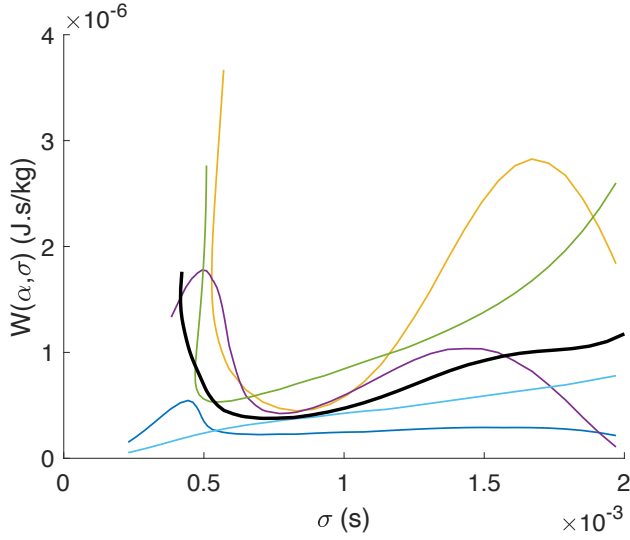
Figure 2.12. Viscous work vs sigma at 0.75 threshold for each subject (colored lines) and group mean (black line).
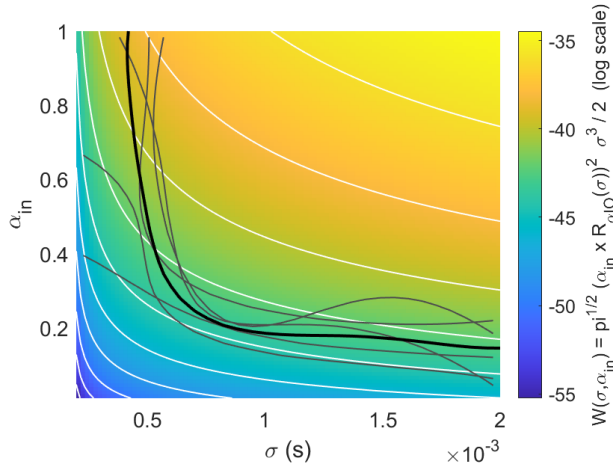
Figure 2.13. Surface plot depicting the viscous work across combinations of α_{in} and σ in log space from our experiment. Isocontours are shown at every 10th increment of viscous work. The plot also includes the 75%-probability threshold lines for each observer, as well as the mean. Note that the viscous work was accurately calculated using α_{out}, while the X- and Y-axes represent the corresponding input parameters of the experiment.

In Figure 2.12, an increase in noise or individual differences between participants is evident, likely due to the post-experimental transformations applied to the threshold values when calculating the corresponding viscous work. Differences in the α-σ representation map non-linearly to differences in the work-σ representation, due to the polynomial transformations of α and σ applied when calculating the viscous work. Figure 2.7 and Figure 2.8 help illustrate these points. Additionally, the sampling algorithm was tuned to sample for the original input space rather than the viscous-work space, meaning areas of high uncertainty in the latter may not have been adequately sampled. Although these data should thus be interpreted with caution, a clear minimum of viscous work can be observed at threshold for σ values between approximately 0.6 and 1 ms. This is in accordance with Figure 2.13, where the lowest thresholds appear around σ values of 0.6–1 ms when regarded relative to the white contour lines indicating equal levels of viscous work.

Finally, to directly fit our detection thresholds as a function of the viscous work, we transformed the 2D detection data into a 1D space, computing the viscous work done for σ and α_{out} of each individual trial via eq. (2.6) presented in the Section 2.2.3:

$$w(\alpha,\sigma) = \frac{\sqrt{\pi}}{2} b\alpha^2\sigma^3$$

Figure 2.14 shows the participant-wise probability of detecting the contact event as a function of the event's viscous work lost. Figure 2.15 shows model predictions for the same event from the aggregate data across all participants.

Figure 2.14 and Figure 2.15 clearly show how the probability of detecting the event rises sharply as the mechanical work of the event increases. On average, the 0.75 detection threshold is reached when the mechanical work is at approximately $2 \times 10^{-6}\,\text{J}\cdot\text{s}\cdot\text{kg}^{-1}$. Because the target value was set to 0.75 in the level set estimation (LSE) during data collection, and because the algorithm was tuned to sample for the original input space rather than the viscous-work space, model uncertainty, indicated by the shaded 95% credible intervals, was often larger in other regions of the parameter space. Note that the mechanical work is derived from multiple combinations of α and σ; it is therefore not possible to determine the individual effects of α and σ from these figures.

2.4. DISCUSSION

Historically, somatosensory neuroscience has been heavily shaped by classical psychophysical research on activation thresholds in neural units during passive touch (e.g., [26, 29, 45]). This focus has led to an emphasis on minimal, localized stimulation that is ideally suited to a single touch submodality. However, this approach often overlooked the complex computational challenges that arise when two solids interact. In the present study, we used a broadband transient signal, namely the Ricker wavelet, to simulate brief impact events on participants' finger pads. We determined the absolute detection threshold of these events, varying their amplitude α and duration σ. Our approach allowed us to quantify both the individual effects as well as the
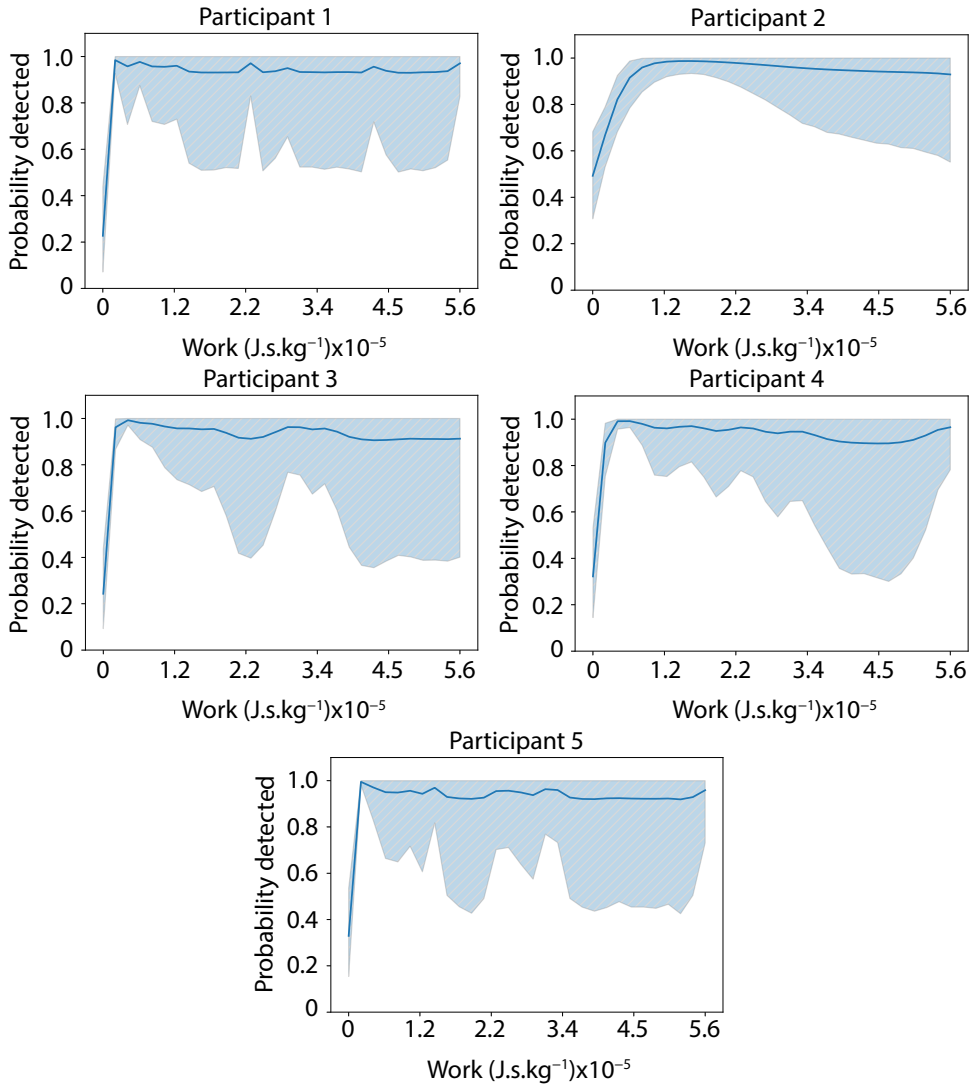
Figure 2.14. Participant-wise 1D psychometric response curves for viscous work. The shaded regions represent the 95% credible intervals, showing where the majority of the posterior distribution is concentrated, indicating the uncertainty associated with the model's predictions.

combined effect of our stimulus parameters. First, the data revealed an intensity metamer, in which different combinations of signal amplitudes and durations can be interchanged for the same perceptual outcome (i.e., probability of detection). Second, we evaluated these thresholds in light of the mechanical work produced by different combinations of the stimulus parameters σ and α. While a clear relationship
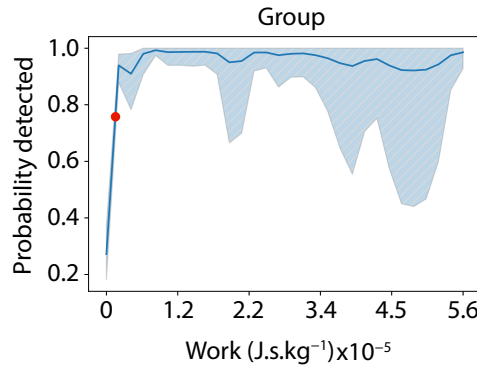
Figure 2.15. Group-level 1D psychometric response curve for viscous work. The shaded region represents the 95% credible interval, illustrating the uncertainty in the aggregated model predictions across participants. The red dot shows the 75% detection probability threshold.

between detection thresholds and the mechanical work of the signal was observed, the mechanical work appeared lower for some combinations of the parameters α and σ at the threshold line than for others. The findings are discussed in detail below.

2.4.1. AN INTENSITY METAMER

First and foremost, our results demonstrate the existence of an intensity metamer for tactile stimuli, specifically the detection of brief contact or impact events. Our data show how two distinct combinations of stimulus parameters – temporal duration/frequency and amplitude – can evoke the same perceptual response.

The existence of intensity metamers is well-established across various sensory modalities, including vision [6–9] and audition [10–12], but also pain [13–16] and thermal perception [17]. In the tactile domain, the phenomenon has mainly been described for non-transient stimuli in the range of 100–900 ms, most commonly sinusoidal vibrations (e.g., [18–20] and Appendix A), but also for pink noise Gabor wavelets [21] and stochastic vibratory stimuli [22] (see Appendix A for a review of this literature). We here demonstrated the phenomenon at a threshold level for extremely short transient impact events. The ubiquity and modality-independence of this phenomenon suggest that it might be a fundamental aspect of perception [17, 21]. Specifically, the phenomenon may be viewed as a basic constancy mechanism wherein the somatosensory system integrates temporal and amplitude parameters to maintain a stable perceptual outcome of intensity or magnitude. This capability to perceive constant intensity despite variations in temporal and amplitude characteristics supports the notion that constancy mechanisms are a fundamental aspect of our somatosensory system and perception. Our results indicate that the somatosensory system uses this fundamental integration to ensure reliable perception of tactile events, thereby enhancing our understanding of how sensory information is processed and maintained as consistent despite variations in the physical properties

of stimuli. A real-world illustration could, for instance, be when swiping a finger across a bump on a flat surface with differing speed. While the resulting duration and peak amplitude of the event in terms of its displacement, velocity, acceleration, and jerk will vary, the perceived intensity or perceived size of the bump will likely remain the same.

2.4.2. DETECTION OF CONSTANT WORK

From modifications of our amplitude parameter, α, and the increase in probability of detection as α increased, it appears clear that the energy content or magnitude of the signal matters for detection. However, the increase in probability of detection associated with the increase in the signal duration σ could in principle be accountable to at least two factors: 1) the temporal changes themselves, such as the duration and the related shift in the frequency content of the signal, or 2) the accompanying increase in energy. In other words, this ambiguity raises the fundamental question: Is the observed phenomenon a result of simple energy summation, or does it reflect the simultaneous processing and integration of two independent cues? If the phenomenon is a consequence of simple energy summation, we would expect the mechanical energy at threshold level to remain constant, regardless of whether the energy is derived from amplitude or duration changes of our stimulus. Conversely, if the system is to some degree attuned to both energy and temporal cues independently, we might observe a differing influence of the two stimulus parameters on detection sensitivity.

In the present study, a clear increase in the probability of detection was observed, as the mechanical energy of the event increased, testifying to a strong attunement to this mechanical cue (cf. Figure 2.14 and Figure 2.15). However, our data did not completely testify to a state of constant mechanical work at threshold level. We observed the lowest-energy thresholds for stimuli with σ values between approximately 0.6–1 ms (cf. Figure 2.8 and Figure 2.13). The dominant frequency of these signals lies between 225 Hz and 375 Hz, which is, in fact, not far from the region of highest sensitivity commonly described for Pacinian corpuscle (PC) afferents [26, 46–49]. For longer signals (containing lower dominant-frequency values and more concentrated frequency distributions), thresholds rose smoothly as a function of σ. For shorter signals (containing higher dominant-frequency values and generally wider frequency distributions), thresholds rose very steeply. It must be noted here, however, that thresholds for signals with σ values below 0.5 ms were generally very noisy and varied largely between participants. For three out of five participants, thresholds below σ values of 0.4 ms were never reached. Individual differences in detection thresholds are common and can be due to many factors, including between-subject differences in the mechanical properties of the skin [50] as well as a differing sensitivity across different locations of the fingertip itself [51, 52]. However, the specific increase in such differences for the shortest signals are likely related to the unequal effect of the parameter α on signals with differing σ values (cf. Figure 2.8). The amplitude needed for detection of these signals was thus close to or outside the admissible range for the device settings of the present study, and the sampling algorithm will have had limited

information here. The curves in this region should therefore be regarded with high caution.

It is here furthermore important to remember that all signals in this study were generally very brief, broadband signals, encompassing a wide range of frequencies (increasingly so for decreasing durations), which naturally limits our ability to speak about a single frequency in our signals. The dominant frequency therefore only constitutes one out of several descriptors of the frequency content of these signals. However, our findings do suggest that the duration of a brief impact event on the finger pad influences detection thresholds by mechanisms beyond simple energy summation. It therefore appears likely that, alongside intensity information, some type of temporal information is encoded by the mechanoreceptors. This hypothesis would align with previous research on vibrotactile stimuli, suggesting that Pacinian corpuscles may convey more than just intensity information, potentially including temporal or frequency information (e.g., [53–55]).

In sum, while the energy of such signals therefore undoubtedly constitutes an important cue in the detection of such events, our data does not presently suggest the total energy content of such signals as a mechanical invariant to their detection.

2.4.3. LIMITATIONS AND FUTURE DIRECTIONS

A number of limitations of the present study warrant consideration. First and foremost, our methodology relied on psychophysical data to make indirect inferences about underlying neural response transformations. A more comprehensive approach, integrating both psychophysical and physiological techniques, would be necessary to draw more direct and robust conclusions. Furthermore, while research has pointed towards good agreement between detection thresholds and afferent responses in the stimulus region tested, the present approach to assess detection thresholds relative to the mechanical energy of the stimuli assumes detection to take place over the complete course of the signal. However, it is possible that detection of a stimulus and the associated mechanoreceptor response do not depend on the total signal but on significant components of the signal. Efforts are presently being undertaken to compare perceptual outcomes to theoretical predictions for mechanoreceptor responses using Short-Time Fourier Transforms (STFT) of these signals.

Second, our calculations of mechanical work were based on an assumption of the skin as a viscous material. Given the high frequencies represented in our signals, we believe this assumption to have been a reasonable one. However, a future approach could involve considering the elastic properties of the skin that become increasingly relevant at lower frequencies.

Third, we employed an adaptive testing paradigm to efficiently explore a large stimulus space. While this approach allowed for broad coverage, model predictions were made based on comparatively few stimulus combinations within a large stimulus space. Given the non-linear relationship and interdependent nature of our stimulus parameters determined during post-experimental measurements of the stimulus, this sparsity may have introduced some noise into our model predictions. Consequently, while our results provide valuable insights, they are based on model approximations

and predictions that may not have captured fine differences in specific stimulus regions. This limitation is particularly relevant when considering effects beyond the direct influence of our two primary stimulus parameters, α and σ, such as when examining the impact on mechanical entities derived from them (i.e., the mechanical work).

A final limitation lies in the nature of the Gaussian signal used. Despite its many advantages, one drawback of the signal used is the interdependence of the duration and frequency content of the signals. Future research could bridge this gap by investigating detection thresholds of signals for which the duration and frequency content can be varied independently (such as the Morlet wavelet).

2.5. CONCLUSION

We investigated the somatosensory system's responsiveness to brief impact events using highly controlled Gaussian signals delivered to the fingertip. In doing so, we uncovered an intensity metamer for these events, in which different combinations of signal duration and intensity can be interchanged for the same perceptual outcome of stimulus magnitude (i.e., the same probability of event detection). The finding highlights the somatosensory system's flexibility in achieving stable perceptual representations of behaviorally relevant information across multiple cues or input states. We further evaluated these thresholds relative to a measure of the combined effect of our two stimulus parameters, namely the total mechanical energy of these stimuli. Our findings confirmed a strong relationship between detection thresholds and the mechanical energy content of our signals. However, they did not testify to a constant state of this feature at threshold level; the mechanical energy at threshold level was thus lower for some combinations of the parameters α and σ than for others. These results suggest that while energy is a crucial cue to trigger a neural and perceptual response, an attunement to other cues, likely the temporal aspects of the signals such as the duration itself or the corresponding frequency content, may play a role in detection. While our findings highlight that the somatosensory system is sensitive to energy, they do not provide proof that this is the only cue considered when reconstructing information about skin contact, prompting further investigation of tactile perception in terms of both energy and frequency or other temporal parameters. Beyond providing valuable insights into neural response characteristics and mechanisms of dynamic touch, the present findings have specific practical implications, such as when aiming to render haptic properties using prosthetic limbs or in virtual reality environments.

REFERENCES

[1] Ernst, M. O. and Bülthoff, H. H. Merging the senses into a robust percept. *Trends in Cognitive Sciences* **8** (2004), 162–169. DOI: 10.1016/j.tics.2004.02.002.

[2] Cataldo, A., Ferrè, E. R., di Pellegrino, G., and Haggard, P. Why the whole is more than the sum of its parts: Salience-driven overestimation in aggregated tactile sensations. *Quarterly Journal of Experimental Psychology (2006)* **72** (2019), 2509–2526. DOI: 10.1177/1747021819847131.

[3] Backus, B. T. "Perceptual Metamers in Stereoscopic Vision". In: Advances in Neural Information Processing Systems 14. Ed. by Dietterich, T., Becker, S., and Ghahramani. 2002, p. 8.

[4] Shockley, K., Carello, C., and Turvey, M. T. Metamers in the haptic perception of heaviness and moveableness. *Perception & Psychophysics* **66** (2004), 731–742. DOI: 10.3758/BF03194968.

[5] Hartcher-O'Brien, J., Edin, B., and Hayward, V. "Shape-elasticity tactile confound". In: Hand, Brain and Technology: The Somatosensory System CSF Conferenc. 2018, p. 1.

[6] Barlow, H. B. Temporal and spatial summation in human vision at different background intensities. *The Journal of Physiology* **141** (1958), 337–350.

[7] Baumgardt, E. and Hillmann, B. duration and size as determinants of peripheral retinal response. *Journal of the Optical Society of America* **51** (1961), 340. DOI: 10.1364/JOSA.51.000340.

[8] Ekman, G., Frankenhaeuser, M., Levander, S., and Mellis, I. The influence of intensity and duration of electrical stimulation on subjective variables. *Scandinavian Journal of Psychology* **7** (1966), 58–64. DOI: 10.1111/j.1467-9450.1966.tb01338.x.

[9] Kahneman, D. and Norman, J. G. The time-intensity relation in visual perception as a function of observer's task. *Journal of experimental psychology* **68** (1964), 215–220. DOI: 10.1037/h0046097.

[10] Kryter, K. D. and Pearsons, K. S. Some effects of spectral content and duration on perceived noise level. *The Journal of the Acoustical Society of America* **35** (1963), 866–883. DOI: 10.1121/1.1918620.

[11] Stévens, J. C. and Hall, J. W. Brightness and loudness as functions of stimulus duration. *Perception & Psychophysics* **1** (1966), 319–327. DOI: 10.3758/BF03215796.

[12] Zwislocki, J. J. Temporal summation of loudness: An analysis. *The Journal of the Acoustical Society of America* **46** (1969), 431–441. DOI: 10.1121/1.1911708.

[13] Shimizu, T. Tooth pre-pain sensation elicited by electrical stimulation. *Journal of Dental Research* **43** (1964), 467–475. DOI: 10.1177/00220345640430040201.

[14] Ekman, G., Frankenhaeuser, M., Berglund, B., and Waszak, M. Apparent duration as a function of intensity of vibrotactile stimulation. *Perceptual and Motor Skills* **28** (1969), 151–156. DOI: 10.2466/pms.1969.28.1.151.

[15] Koyama, Y., Koyama, T., Kroncke, A. P., and Coghill, R. C. Effects of stimulus duration on heat induced pain: the relationship between real-time and post-stimulus pain ratings. *Pain* **107** (2004), 256–266. DOI: 10.1016/j.pain.2003.11.007.

[16] Tran, T. D., Wang, H., Tandon, A., Hernandez-Garica, L., and Casey, K. L. Temporal summation of heat pain in humans: Evidence supporting thalamocortical modulation. *Pain* **150** (2010), 93–102. DOI: 10.1016/j.pain.2010.04.001.

[17] Dufour, A., Després, O., Pebayle, T., and Lithfous, S. Thermal sensitivity in humans at the depth of thermal receptor endings beneath the skin: validation of a heat transfer model of the skin using high-temporal resolution stimuli. *European Journal of Applied Physiology* **120** (2020), 1509–1518. DOI: 10.1007/s00421-020-04372-y.

[18] Gescheider, G. A. Evidence in support of the duplex theory of mechanoreception. *Sensory Processes* **1** (1976), 68–76.

[19] Gescheider, G. A., Berryhill, M. E., Verrillo, R. T., and Bolanowski, S. J. Vibrotactile temporal summation: probability summation or neural integration? *Somatosensory & motor research* **16** (1999), 229–242. DOI: 10.1080/08990229970483.

[20] Verrillo, R. T. Temporal summation in vibrotactile sensitivity. *The Journal of the Acoustical Society of America* **37** (1965), 843–846. DOI: 10.1121/1.1909458.

[21] Bochereau, S., Terekhov, A., and Hayward, V. "Amplitude and Duration Interdependence in the Perceived Intensity of Complex Tactile Signals". In: Haptics: Neuroscience, Devices, Modeling, and Applications. Ed. by Auvray, M. and Duriez, C. Lecture Notes in Computer Science. Springer Berlin Heidelberg, 2014, pp. 93–100.

[22] Fassihi, A., Akrami, A., Pulecchi, F., Schönfelder, V., and Diamond, M. E. Transformation of perception from sensory to motor cortex. *Current Biology* **27** (2017), 1585–1596.e6. DOI: 10.1016/j.cub.2017.05.011.

[23] Békésy, G. v. Über die Vibrationsempfindung. **4** (1939), 316–334.

[24] Verrillo, R. T. Investigation of some parameters of the cutaneous threshold for vibration. *The Journal of the Acoustical Society of America* **34** (1962), 1768–1773. DOI: 10.1121/1.1909124.

[25] Verrillo, R. T., Fraioli, A. J., and Smith, R. L. Sensation magnitude of vibrotactile stimuli. *Perception & Psychophysics* **6** (1969), 366–372. DOI: 10.3758/BF03212793.

[26] Bolanowski, S. J., Gescheider, G. A., Verrillo, R. T., and Checkosky, C. M. Four channels mediate the mechanical aspects of touch. *The Journal of the Acoustical Society of America* **84** (1988), 1680–1694. DOI: 10.1121/1.397184.

[27] Cohen, J. C., Makous, J. C., and Bolanowski, S. J. Under which conditions do the skin and probe decouple during sinusoidal vibrations? *Experimental Brain Research* **129** (1999), 211–217. DOI: 10.1007/s002210050891.

[28] Levitt, H. Transformed up-down methods in psychoacoustics. *The Journal of the Acoustical Society of America* **49** (1971), 467–477.

[29] Johansson, R. S. and Vallbo, A. B. Detection of tactile stimuli. Thresholds of afferent units related to psychophysical thresholds in the human hand. *The Journal of Physiology* **297** (1979), 405–422. DOI: 10.1113/jphysiol.1979.sp013048.

[30] Owen, L., Browder, J., Letham, B., Stocek, G., Tymms, C., and Shvartsman, M. Adaptive nonparametric psychophysics. *arXiv* (2021). DOI: 10.48550/arXiv.2104.09549.

[31] Von Gierke, H. E., Oestreicher, H. L., Franke, E. K., Parrack, H. O., and von Wittern, W. W. Physics of vibrations in living tissues. *Journal of Applied Physiology* **4** (1952), 886–900. DOI: 10.1152/jappl.1952.4.12.886.

[32] Moore, T. J. A Survey of the mechanical characteristics of skin and tissue in response to vibratory stimulation. *IEEE Transactions on Man-Machine Systems* **11** (1970), 79–84. DOI: 10.1109/TMMS.1970.299966.

[33] Delhaye, B., Hayward, V., Lefèvre, P., and Thonnard, J.-L. Texture-induced vibrations in the forearm during tactile exploration. *Frontiers in Behavioral Neuroscience* **6** (2012). DOI: 10.3389/fnbeh.2012.00037.

[34] Shao, Y., Hayward, V., and Visell, Y. Spatial patterns of cutaneous vibration during whole-hand haptic interactions. *Proceedings of the National Academy of Sciences* **113** (2016), 4188–4193. DOI: 10.1073/pnas.1520866113.

[35] Potts, R. O., Chrisman, D. A., and Buras, E. M. The dynamic mechanical properties of human skin in vivo. *Journal of Biomechanics* **16** (1983), 365–372. DOI: 10.1016/0021-9290(83)90070-2.

[36] Kirkpatrick, S. J., Duncan, D. D., and Fang, L. Low-frequency surface wave propagation and the viscoelastic behavior of porcine skin. *Journal of Biomedical Optics* **9** (2004), 1311–1319. DOI: 10.1117/1.1803843.

[37] Mridha, M., Odman, S., and Oberg, P. A. Mechanical pulse wave propagation in gel, normal and oedematous tissues. *Journal of Biomechanics* **25** (1992), 1213–1218. DOI: 10.1016/0021-9290(92)90077-e.

[38] Rongala, U. B., Seyfarth, A., Hayward, V., and Jörntell, H. The import of skin tissue dynamics in tactile sensing. *Cell Reports Physical Science* **5** (2024). DOI: 10.1016/j.xcrp.2024.101943.

[39] Skalak, R. and Chien, S. *Handbook of Bioengineering*. New York: McGraw Hill Higher Education, 1987.

[40] Hayward, V. "A Brief Overview of the Human Somatosensory System". In: Musical Haptics. Ed. by Papetti, S. and Saitis, C. Cham: Springer International Publishing, 2018, pp. 29–48. DOI: 10.1007/978-3-319-58316-7_3.

[41] Wang, Q. and Hayward, V. In vivo biomechanics of the fingerpad skin under local tangential traction. *Journal of Biomechanics* **40** (2007), 851–860. DOI: 10.1016/j.jbiomech.2006.03.004.

[42] Jindrich, D. L., Zhou, Y., Becker, T., and Dennerlein, J. T. Non-linear viscoelastic models predict fingertip pulp force-displacement characteristics during voluntary tapping. *Journal of Biomechanics* **36** (2003), 497–503. DOI: 10.1016/s0021-9290(02)00438-4.

[43] Wiertlewski, M. and Hayward, V. Mechanical behavior of the fingertip in the range of frequencies and displacements relevant to touch. *Journal of Biomechanics* **45** (2012), 1869–1874. DOI: 10.1016/j.jbiomech.2012.05.045.

[44] Song, X. D., Sukesan, K. A., and Barbour, D. L. Bayesian active probabilistic classification for psychometric field estimation. *Attention, Perception, & Psychophysics* **80** (2018), 798–812. DOI: 10.3758/s13414-017-1460-0.

[45] Vallbo, Å. B. and Johansson, R. "Skin mechanoreceptors in the human hand: Neural and psychophysical thresholds". In: Sensory Functions of the Skin in Primates. Ed. by Zotterman, Y. Wenner–Gren Center International Symposium Series. Pergamon, 1976, pp. 185–199. DOI: 10.1016/B978-0-08-021208-1.50021-7.

[46] Johansson, R. S., Landström, U., and Lundström, R. Responses of mechanoreceptive afferent units in the glabrous skin of the human hand to sinusoidal skin displacements. *Brain Research* **244** (1982), 17–25.

[47] Mountcastle, V. B., LaMotte, R. H., and Carli, G. Detection thresholds for stimuli in humans and monkeys: comparison with threshold events in mechanoreceptive afferent nerve fibers innervating the monkey hand. *Journal of Neurophysiology* **35** (1972), 122–136. DOI: 10.1152/jn.1972.35.1.122.

[48] Johnson, K. O. Reconstruction of population response to a vibratory stimulus in quickly adapting mechanoreceptive afferent fiber population innervating glabrous skin of the monkey. *Journal of Neurophysiology* **37** (1974), 48–72. DOI: 10.1152/jn.1974.37.1.48.

[49] Bolanowski, S. J. and Zwislocki, J. J. Intensity and frequency characteristics of pacinian corpuscles. I. Action potentials. *Journal of Neurophysiology* **51** (1984), 793–811. DOI: 10.1152/jn.1984.51.4.793.

[50] Kawai, A. and Tanaka, Y. "Individual Differences in Skin Vibration Characteristics and Vibrotactile Sensitivity at Fingertip". In: 2022 IEEE Haptics Symposium (HAPTICS). 2022, pp. 1–6. DOI: 10.1109/HAPTICS52432.2022.9765612.

[51] Keyson, D. V. and Houtsma, A. J. Directional sensitivity to a tactile point stimulus moving across the fingerpad. *Perception & Psychophysics* **57** (1995), 738–744. DOI: 10.3758/bf03213278.

[52]   Sobue, M., Kato, S., Mizoguchi, I., and Kajimoto, H. "Measuring the Distribution of Tactile Acuity at the Fingertips". In: Haptics: Understanding Touch; Technology and Systems; Applications and Interaction. Ed. by Kajimoto, H., Lopes, P, Pacchierotti, C., Basdogan, C., Gori, M., Lemaire-Semail, B., and Marchal, M. Cham: Springer Nature Switzerland, 2025, pp. 15–24. DOI: 10.1007/978-3-031-70061-3_2.

[53]   Bensmaïa, S. and Hollins, M. Pacinian representations of fine surface texture. *Perception & Psychophysics* **67** (2005), 842–854. DOI: 10.3758/BF03193537.

[54]   Bensmaïa, S., Hollins, M., and Yau, J. Vibrotactile intensity and frequency information in the pacinian system: a psychophysical model. *Perception & Psychophysics* **67** (2005), 828–841. DOI: 10.3758/bf03193536.

[55]   Bensmaia, S. J. Tactile intensity and population codes. *Behavioural brain research* **190** (2008), 165–173. DOI: 10.1016/j.bbr.2008.02.044.

2

3

CONCEPTION AND DESIGN OF A DUAL-PROPERTY HAPTIC STIMULI DATABASE INTEGRATING STOCHASTIC ROUGHNESS AND ELASTICITY

Chapter 2 examined the detection of basic contact event, uncovering a metamer in the detection of contact events and proposing mechanical work as an important cue but likely not sole determinant in the detection of such events. In the following three chapters, the focus shifts to more complex haptic interactions in investigating cues and mechanisms for detecting change and maintaining stability, namely the haptic perception of texture and material properties. Chapter 3 lays the foundation for these chapters by addressing the question: Can we determine behaviorally relevant and naturalistic cues to texture perception that are realizable in manufactured stimuli?

Abstract: Understanding the interplay between surface roughness and material elasticity in haptic texture perception is important. In the real world, these characteristics do not occur in isolation from one another; yet, the haptic perceptions of surface features and material properties are often investigated individually. This highlights the need for suitable stimulus material for haptic perceptual experiments. The present research details the manufacturing and validation of a database of stochastically rough, elastic stimuli tailored for haptic perceptual experiments. The stimulus set comprises 49 3D-printed samples, offering a systematic variation in stochastic microscale roughness and material elasticity, replicating natural surface features without compromising experimental control. The surfaces were generated using an algorithm that produces randomly rough surfaces with well-defined spectral distributions, demonstrating fractal properties over a large range of length scales. Controlled variations in elasticity were implemented via variations in the printing material composition. Finally, we present preliminary perceptual data from two observers, illustrating the discriminability of the stimulus space for roughness and softness discrimination. This database aims to facilitate haptic research on material and texture perception, offering a controlled yet naturalistic set of stimuli to explore the intricate interplay between surface roughness and material elasticity in shaping haptic texture perception.

3.1. INTRODUCTION

Most natural and engineered surfaces that we encounter during our everyday life are self-affine surfaces, exhibiting fractal properties over a range of length scales [2]. However, research on the perception of surface roughness has typically used simpler stimulus material (such as sandpapers or sinusoidal gratings) that can be varied easily in a controlled fashion (e.g., [3–6]). Furthermore, surface roughness tends to occur alongside other texture or material dimensions, such as material elasticity [7–9]. While the haptic perception of surface roughness and material elasticity (softness/hardness) has each been investigated extensively, the need for investigating the combined effects of different cues on perceptual outcomes is often stressed (e.g., [10]). More specifically, there is recent evidence suggesting that material elasticity and surface structure are sometimes not perceived independently [11]. While insightful, this research has employed relatively simple stimulus material, not reflecting the often complex nature of both engineered and natural surfaces. Conversely, when using databases of naturally occurring textures and materials (e.g., [7]), research faces a multitude of physical cues difficult to control in an experimental setting. This stresses the need for behaviorally relevant yet well-controlled stimulus material for haptic research on texture and material perception. Here we therefore present a database of 3D-printed stimuli varying systematically in their microscale roughness and material elasticity, intended for haptic perceptual experiments. The presented stimuli resemble natural textures in their surface statistics by exhibiting self-affine fractal properties over a range of length scales relevant to touch, while not compromising on the experimental

control needed due to thorough characterization. The database consists of seven different surfaces varying in their scale-dependent roughness (Hurst exponent) on a 0.03–5 mm scale, each available in seven different elasticities, together resulting in a final database of 49 3D-printed samples.

The surfaces in this database were generated using an algorithm that produces randomly rough surfaces with well-defined spectral distributions [12, 13], exhibiting fractal properties as described by Persson [2]. These surfaces are produced by a superposition of waves, where the amplitudes are derived from a height spectrum that is composed of a plateau for large wavelengths of equal amplitude (defining the macroscopic topography) while amplitudes of smaller wavelengths (defining the microscale topography) decay according to a power law. A smaller Hurst exponent, H, leads to a slower decay towards small length scales and thus results in a higher microscale roughness. This hyperbolic decay in topography wavelengths is expected to impose a similar pattern in the temporal spectral content of the friction-elicited vibrations during an interaction. Indeed, it has been observed that some spatial spectral properties of textures, like the hyperbolic wavelengths decay, are transmitted to the spectral content of the vibrotactile signal [14, 15]. Randomness is implemented in the phase shift between the superposed waves, which is controlled by a random number sequence. The final topographies are obtained by combining the parameterized spectrum and the random phase shift into a spatial frequency representation and applying an inverse Fourier transform. For the present sample set, the macroscale topography remained the same for all samples, as recent research has demonstrated such larger-scale topographic differences or "higher order statistics" to be of little relevance for tactile texture perception [16–18]. The Hurst exponent, H, on the other hand, has been shown to be a perceptually relevant parameter for the discrimination of roughness using the same surface algorithm, albeit on much larger length scales [18].

3.2. METHODS

3.2.1. GENERATION OF SURFACES

For the stimuli of the database presented here, the slope of the function for shorter wavelengths was varied in seven steps, spanning an H from 0.3 to 0.9 m while the random sequence remained the same. This resulted in seven surfaces with the same 'macroscale' topography but varying in their 'microscale' roughness or self-affinity. The longest wavelength was set to the longest side of the final stimuli (50 mm) while the shortest possible wavelength was set to 0.03 mm. This value was chosen because the PolyJet 735 used for 3D printing of the stimuli has a resolution of 0.0135 mm. Following the Nyquist-Shannon sampling theorem, it was therefore expected that it could present details down to approximately 0.027 mm. To create comparatively smooth (not rugged) stimuli, with little variation in the large wavelengths, the roll-off wavelength was set to a value of 5 mm, approximately corresponding to half of an average fingertip width. This value defined the cut-off between the plateau and the interval of wavelengths to which the fractal dimension was applied. The surfaces generated were 50x50 mm (note that one of the sides was later cropped to 31 mm for

the final 3D-printed samples). Figure 3.1 displays the model used from Müser et al. [13] to design the height spectrum of the generated surfaces and the steps taken to generate the surface topographies.
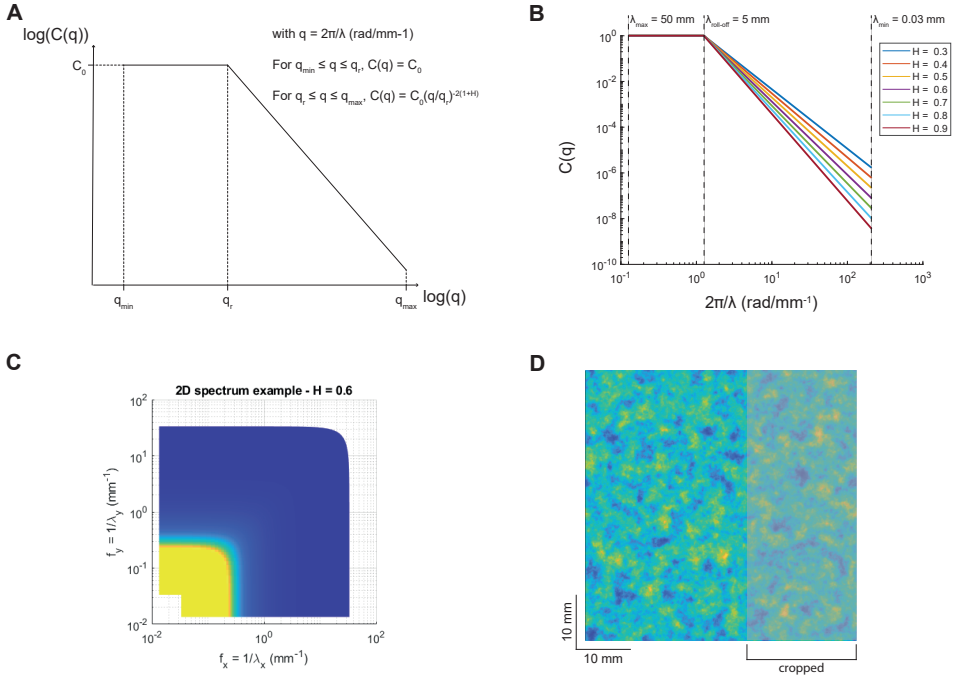
Figure 3.1. Topography generation. (A) The spatial spectrum model from Müser et al. [13]. (B) Parametrization of the spatial spectrum for the 7 surfaces of the present set. (C) An example of the resulting 2D spectrum (here showing only the strictly positive frequencies quarter, in log space which distorts the expected shape of the spectrum) obtained from $H = 0.6$. (D) The resulting topography obtained by applying an inverse Fourier transform to the example spectrum shown in graph C.

The global scale of the wavelength amplitude C_0 (Figure 3.1A) was set to 1 for all seven topographies generated. The spectra (Figure 3.1B) were then used to create a 2D spectral content of 3704 × 3704 samples. An inverse Fourier transform was applied using an inverse fast Fourier transform algorithm, and the result was then multiplied by $\frac{N^2}{2\pi}$, with N being the number of samples per dimension (3704). We then scaled the obtained topographies by 0.01 to generate topographic details of relevant size. This scaling factor was selected based on 3D visualizations as well as pilot discrimination studies of test stimuli, as we wished to produce stimuli with an approximate step size in change of a JND (just-noticeable difference) in perceived roughness. Contrary to Sahli et al. [18], we multiplied all topographies by the same factor. This resulted in the seven topographies having the same amplitude for the wavelengths larger than

the roll-off value, but a root mean square of heights decreasing with an increasing *H* value. This decision was based on perceptual pilot studies not reported here. The height matrices obtained were 50×50 mm, both dimensions with a sampling rate of 74.08 samples per millimeter (3704 samples for 50 mm). They were then cropped along one dimension to obtain 50×31 mm (3704×2296 samples). The spatial definition was set very high to match the theoretical minimum droplet size of the 3D printer, enabling the capture of microscale details at the closest possible approximation to their limits. The height matrices were then transformed to STL files in Python by loading the height matrices from a configuration file, converting them into 3D surfaces represented by vertices and then generating triangles by dividing each rectangular area between adjacent vertices into two triangles. The resulting mesh was then saved to an STL file. Since this produced file sizes larger than needed, we used the "Quadric Edge Collapse Decimation" simplification function of MeshLab to decimate each sample with a decimation ratio of 6% (options "Preserve Boundary of the mesh", "Preserve Normal", "Preserve Topology" applied). The quality threshold was set to 0.6, and the following settings were applied: "Preserve Boundary of the mesh", Preserve Normal", and "Preserve Topology". These parameters were chosen with respect to a minimal deviation between the initial and decimated STL files, as estimated using the Hausdorff Distance sampling method (deviation in % of diagonal of 3D object: max 0.025946, mean 0.00336, rms 0.004386). Although minimal, this decimation may have resulted in a slight smoothing effect on the STL files compared to the original height matrices.

3.2.2. 3D PRINTING

Each of these seven surfaces was then 3D printed in seven different elasticities using a Connex Stratasys Polyjet J735 with the printer software (GrabCAD Print 1.60). Different elasticities were achieved by combining the rigid *VeroYellow*™ and the flexible *Agilus30*™ in the proportions predefined by the printer software for Shore-A values 30, 35, 40, 50, 60, 70, and 85 (but see Table 3.1 for achieved shore-A values). All stimuli were sized $50 \times 31 \times 13$ mm including a rigid platform of 3 mm which was CAD-modeled underneath each stimulus in *VeroMagenta*™ to provide a stable base for the samples and for engraved text for identification of the stimuli. The stimuli were printed in glossy finish. However, to avoid head-bumper impacts during the printing process, as well as to achieve more flexible (i.e., more elastic) stimuli than standard settings allow, the 3D prints were printed with only half of the amount of UV-curing normally used (by enabling only one of the two UV lamps of the printer) and post-cured in a curing device (Formlabs Form Cure) for 30 seconds at an LED Radiant wattage of 9.1 W and an LED Wavelength of 405 nm [1]. This resulted in a final database of 49 samples (see Figure 3.2).

---

[1]The thickness of the stimuli and their comparatively flat surface leads to a large contact area with the roller of the printer, which increases the risk of head-bumper impacts, especially for the more flexible prints, where the roller cannot scrape away enough material and unwanted material gets stuck. Less curing results in the surface becoming less sticky during the printing process.
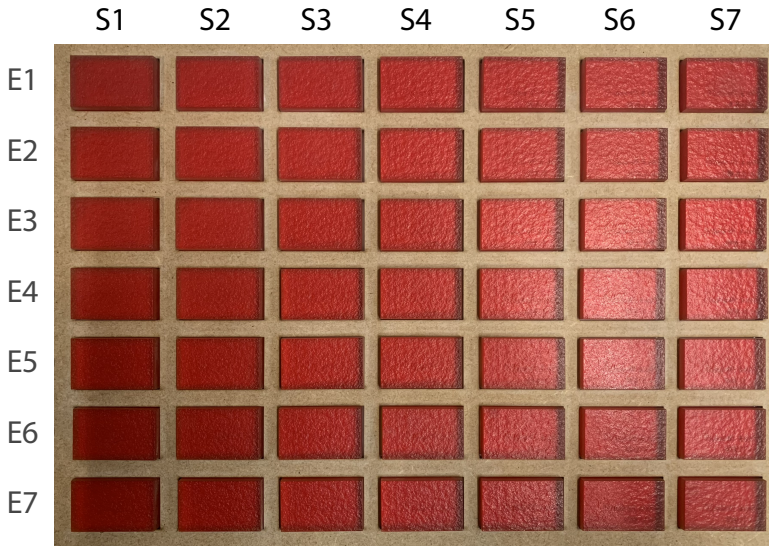
Figure 3.2. Image of the final database of 49 samples. Columns (S1–7) indicate changes in the surface statistics, corresponding to an *H* between 0.3 and 0.9. Rows (E1–7) indicate changes in the elasticity (cf. Table 3.1). All samples measure 50x31x13 mm (including the rigid platform below the flexible prints).

3.2.3. VERIFICATION PROCEDURE OF THE 3D-PRINTED SAMPLES

After fabrication, the samples were measured with a shore-A durometer (Teclock GS-709N) on their long axis for 20 seconds at a temperature of approximately 20°C. The Young's modulus was thereafter calculated using Gent's conversion equation [19]. Table 3.1 summarizes the defined and achieved elasticity parameters of the database.

Table 3.1. Elasticity parameters of the database. The shore-A values were measured with a shore-A durometer on the center of their long axis for 20 seconds. The values are the mean across all 7 surfaces, with standard deviation in parentheses. Young's moduli were calculated using Gent's conversion equation [19].

Elast. Nr.	E1	E2	E3	E4	E5	E6	E7
Shore A Target	30	35	40	50	60	70	85
Shore A Achieved	23.6 (0.55)	24.83 (0.41)	25.83 (0.41)	28.67 (0.52)	34 (0.71)	44.2 (1.48)	65.8 (1.1)
Y. Modulus (MPa)	0.121	0.122	0.128	0.144	0.179	0.264	0.611

To verify the surface statistics of the final 3D-printed stimuli, profilometry measurements were carried out on a subset of the samples. A key aim of this was to ensure that changes in the elasticity of the samples did not result in significant changes in the surface features. Due to the respective advantages and disadvantages

A

Theoretical topography
S4

B

Profilometry
S4 E4

C
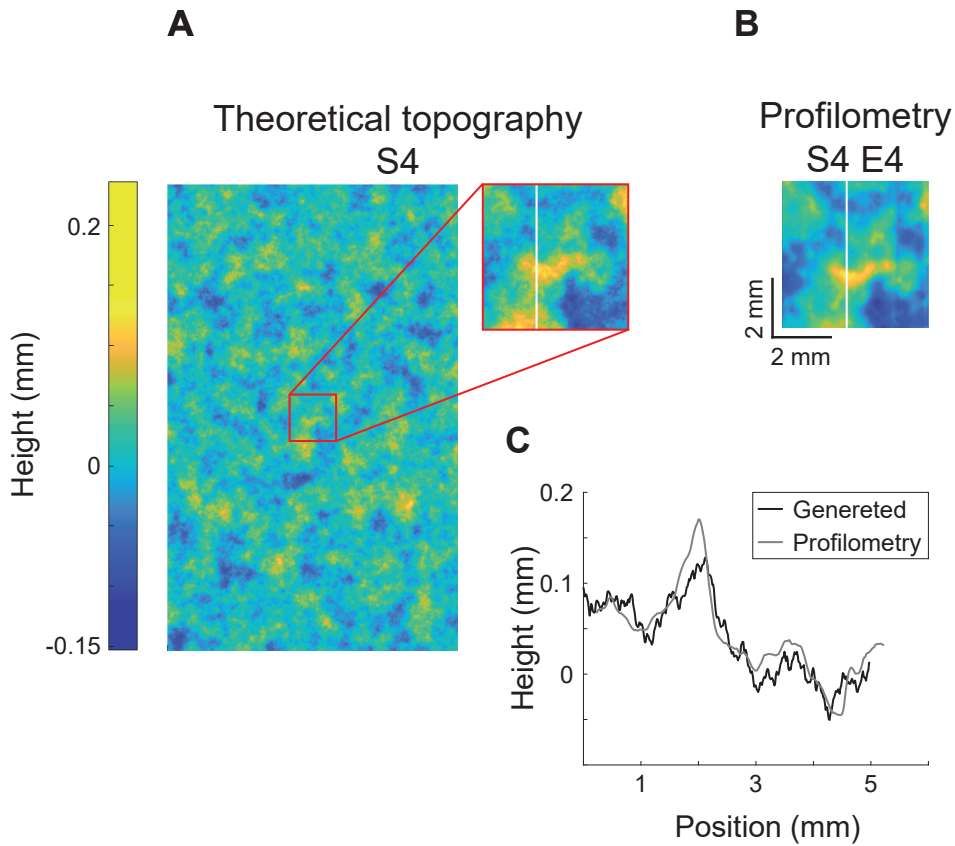
Figure 3.3. (A) Top view of example theoretical topography S4(H = 0.6) (height spectrum generated before decimation 3D and 3D printing). The red square indicates the corresponding 5x5 mm window in which contact profilometry measurements were carried out on the 3D-printed stimuli. (B) Plots of the height data achieved from the contact profilometry of the corresponding location on the same surface 3D printed at medium elasticity. (C) Profile view comparison between the theoretical and measured height data at matched coordinates. The position of the profile cut is indicated by a white line on graphs A and B.

of contact and optical profilometry, different subsets of the database were subjected to each of these methods. A smaller subset of five samples underwent contact profilometry. This method provided accurate topographical data of the same central location of different samples, allowing us to compare these directly. With this method, we could furthermore be sure that differences in translucency of the samples (resulting from the different mixing ratios of the two different printing materials) would not affect the measurements. Optical profilometry measurements were carried

out on a larger subset of nine samples, with three repeated measurements of each sample at random locations, allowing for overall conclusions about surface statistics and roughness parameters.

Contact profilometry measurements were carried out for surfaces S1 (H = 0.3), S4 (H = 0.6), and S7 (H = 0.9) at the medium elasticity of the parameter space (E4). To investigate the consistency of the topography over different elasticities, further measurements were taken on elasticities E1 and E7 of surface S4 (cf. Figure 3.2). Two of the surfaces (S4E4 and S4E7) were measured twice to estimate the test-retest reliability. The measurements were made using a Dektak 150 Surface Profiler. All measurements were taken in the center 5x5 mm of the surfaces, by taking the line crossing of diagonals drawn from the corners. The distance between each line of measurements was 30 μm while the distance between each measurement point was 4 μm. Plots of the measured compared to theoretical (before decimation and 3D printing) height data can be seen in Figure 3.3.

Figure 3.3 demonstrates the great resemblance between theoretical and measured height data. On Figure 3.3C, a certain amount of "smoothing out" of the finest details in the profile of the final 3D print is visible. While the height profiles follow the target topography closely, detail and prominence of the asperities are lost for the very smallest variations. This smoothing effect mainly concerns details within the micrometer range, however, and is to be expected due to (A) the decimation of the STL files and more importantly (B) the limited resolution of the 3D printer.

Optical profilometry was carried out on samples S1 (H = 0.3), S4 (H = 0.6), and S7 (H = 0.9) at elasticities E1, E4, and E7 (cf. Figure 3.2). On each of these samples, 3 different measurements were taken at 3 random locations. The measurements were made using a MarSurf CM Explorer. Each measurement comprised a 3.1 x 3.1 mm window. The lateral resolution was 1.33 μm at 10X with the pixel arrangement being 1200 x 1200 for a single scan. The measuring vertical range with the fine motor was 0.35 mm.

We used an online tool [20] to analyze all profilometry measurements (contact and optical) and the theoretical topographies. Figure 3.4 shows the height power-spectral density of the theoretical topographies and measurements of the final surfaces, respectively. As anticipated, a clear downward slope in frequency can be observed, changing with *H*. There is a clear difference in the power spectral density (PSD) from one *H* to another.

We then calculated the 2D RMS heights (known as Rq or Sq for the roughness of a surface), the RMS slope (gradient, RΔq), and the RMS curvature for all measurements. The values from the profilometry measurements were then compared to the values of all original theoretical surface files. Figure 3.5 and Table 3.2 summarize these data.

As can be seen in Figure 3.5A, the Rq values of profilometry measurements follow the predicted pattern, where a lower *H* leads to a higher Rq. The Pearson correlation coefficient is significant and indicates a strong relationship for both profilometry measurements (contact and optical). The same holds true for the root mean square of slope and curvature, although some grouping of the samples with different elasticities can be observed. This variance between samples of different elasticities is not larger than the variance observed for repeated measurements of the same sample, but
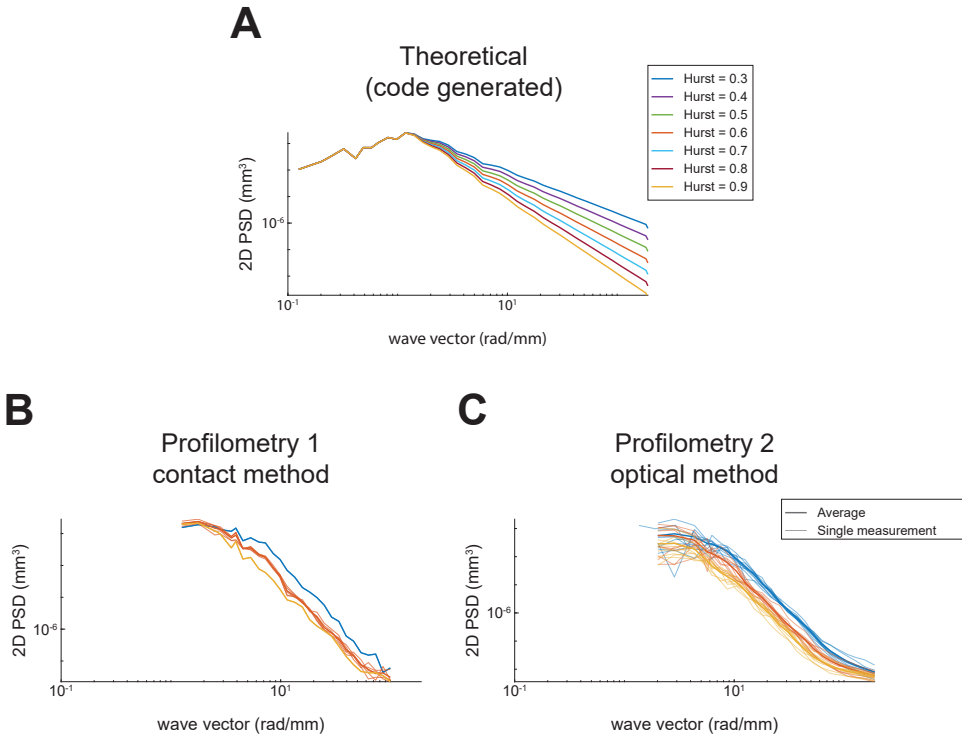
Figure 3.4. Height power-spectral density of (A) the 7 theoretical surfaces (before triangulation, decimation, and 3D printing), (B) contact profilometry measurements of the 5x5 mm window of 5 chosen final samples, and (C) optical profilometry measurements. The radial direction is used for all plots.

is within the general level of measurement noise, which expectedly increases as derivatives are applied. Such a degree of variance is expected, not the least due to the changes in measurement location during the optical profilometry. It must furthermore be noted for the contact profilometry data that, although the center of the surface was targeted for each measurement, slight offsets will likely be present as the samples were marked and placed by hand (cf. Figure 3.3). This is a likely source of noise, especially on the RMS of heights which, at this scale, will be highly sensitive to the exact position of measurement. Figure 3.5B demonstrates how changes in the elasticity of the samples do not result in a corresponding change in any of the roughness statistics. All Pearson correlation coefficients are below the significance level.

It must be noted that although these measurements testify to a significant relationship between the *H* and the measured roughness statistics (i.e., rms height, gradient, and curvature) for both profilometry measurements, a considerable
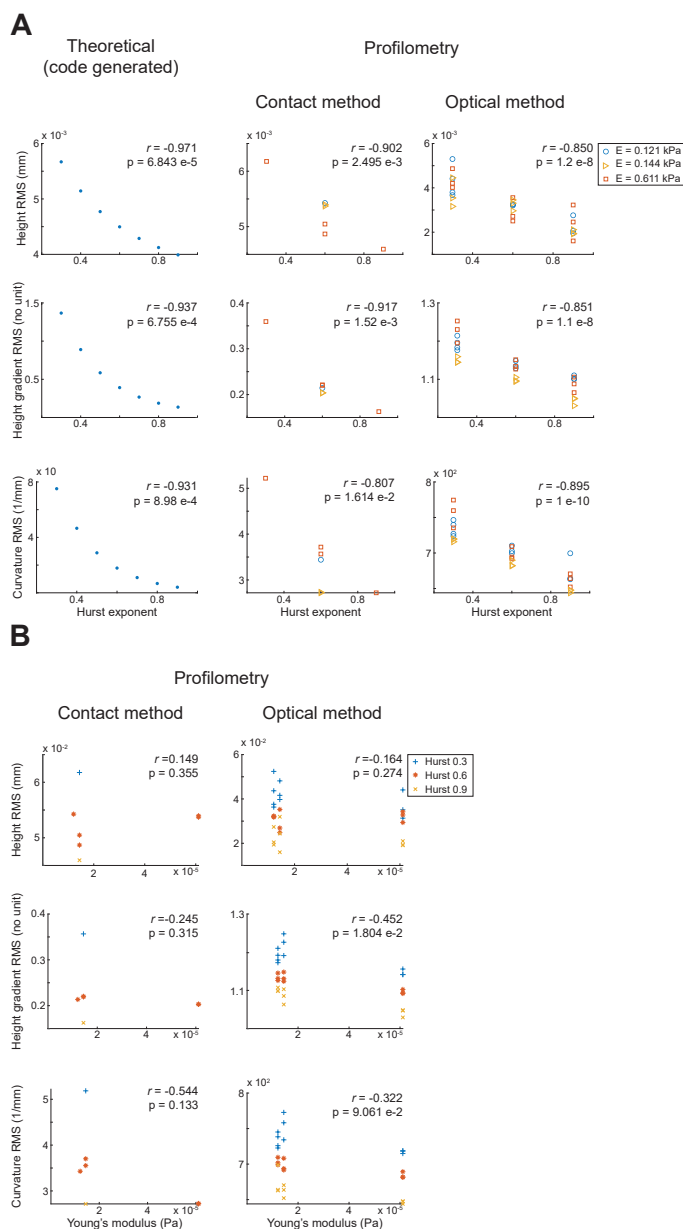
Figure 3.5. (A) The root mean square of heights (Rq), the root mean square of slope (gradient, RΔq), and the root mean square of the curvature, for contact profilometry, optical profilometry, and the theoretical topographies as a function of *H*. r = Pearson's correlation coefficient for the relationship between *H* and the respective roughness statistic. (B) The same statistics as a function of the sample elasticity.

Table 3.2. Roughness parameters of theoretical topographies and profilometry measurements of 3D-printed stimuli. Rq = RMS height, $R\Delta q$ = RMS slope. Measurements from contact profilometry are displayed in red.

Surface nr. (H)		S1 (H 0.3)	S2 (H 0.4)	S3 (H 0.5)	S4 (H 0.6)	S5 (H 0.7)	S6 (H 0.8)	S7 (H 0.9)
Theoretical $Rq\,[\times 10^{-2}\,\text{mm}]$		5.68	5.16	4.79	4.51	4.3	4.14	4.01
Profilometry 1 $Rq\,[\times 10^{-2}\,\text{mm}]$ Profilometry 2 $Rq\,[\times 10^{-2}\,\text{mm}]$	E1	3.8 3.67 5.3 4.41	N/A	N/A	5.43 3.21 3.24 3.26	N/A	N/A	2.06 1.95 2.76
	E4	6.18 4.02 4.21 4.87	N/A	N/A	4.87 5.05 2.5 3.56 2.71	N/A	N/A	4.59 1.61 2.56 3.23
	E7	3.54 3.16 4.45	N/A	N/A	5.37 5.39 3.45 2.96 3.31	N/A	N/A	2.11 1.92 1.94
Theoretical $R\Delta q$ (gradient)		1.38	0.9	0.6	0.4	0.28	0.2	0.15
Profilometry 1 $R\Delta q$ (gradient) Profilometry 2 $R\Delta q$ (gradient)	E1	1.18 1.18 1.21 1.20	N/A	N/A	0.21 1.13 1.13 1.15	N/A	N/A	1.10 1.11 1.10
	E4	0.36 1.25 1.23 1.19	N/A	N/A	0.22 0.22 1.15 1.13 1.13	N/A	N/A	0.16 1.09 1.07 1.11
	E7	1.14 1.14 1.16	N/A	N/A	0.2 0.2 1.10 1.11 1.09	N/A	N/A	1.03 1.05 1.05
Theoretical rms curvature $[\text{mm}^{-1}]$		75.72	47.16	29.45	18.44	11.59	7.31	4.63
Profilometry 1 rms curvature $[\text{mm}^{-1}]$ Profilometry 2 rms curvature $[\text{mm}^{-1}]$	E1	723.76 727.06 746.54 739.71	N/A	N/A	3.44 702.56 699.72 710.40	N/A	N/A	664.14 699.60 663.07
	E4	5.22 774.49 759.73 735.37	N/A	N/A	3.57 3.72 709.06 694.34 692.33	N/A	N/A	2.72 663.98 652.23 670.65
	E7	719.12 715.84 719.96	N/A	N/A	2.73 2.72 682.33 689.89 681.91	N/A	N/A	643.98 647.36 647.86

difference in absolute roughness values between the theoretical topographies and the measurements of the 3D-printed samples is present, which increases as the degree of derivation increases. A similar difference can be observed between the

contact and optical profilometry measurements, where the difference between the two methods is very small for the RMS of heights but increases strongly with successive derivation. This discrepancy might very well be due to the broader bandwidth in the optical method, capturing more noise and the physical limitations of the contact method's stylus missing fine details. As a general matter, the difficulty in capturing the topographies of the samples presented here lies in their very nature. They are defined on a large wavelength interval and display a relatively large range of asperity sizes. Each measurement method will introduce errors of different nature affecting the spectrum differently, and the derivatives will increase these relative errors. This is expected to have led to a deprecation of the small wavelength representations and to have affected the statistics of the surface as we applied derivatives. Importantly, however, the profilometry enabled us to verify the relative differences between the different surfaces, quantifying the preservation of the significant correlation between variations in H and the resulting roughness statistics.

3.3. PERCEPTUAL VALIDATION

We conducted a pilot study involving two observers to evaluate the utility of the database and to demonstrate the perceptual relevance of the stimuli. To gain comprehensive insights into the entire stimulus space, we employed an active learning paradigm called AEPsych [21]. This approach uses non-parametric Gaussian Process models to efficiently estimate psychometric fields by dynamically adjusting experimental conditions based on the responses from previous trials. It thereby optimizes the information gained per trial and increases threshold estimation efficiency across two or more stimulus dimensions (e.g., the Hurst exponent and elasticity).

The data presented are solely intended to illustrate the general discriminability of the stimulus space. Specifics of the procedure and the model's configuration are not detailed here.

In brief, data collection involved a two-alternative forced choice (2AFC) task for our 2D stimulus space, once for softness discrimination, using pressing with the index finger, and once for roughness discrimination, using lateral stroking. Each observer completed 50 trials for each task, during which they determined which one of two stimuli (as selected by the algorithm) felt rougher or softer, respectively. Visual and auditory cues were removed for each observer. Observers provided written informed consent prior to participation, and the study adhered to the ethical guidelines of Sorbonne University and the Helsinki Declaration.

Estimated psychometric fields are displayed in Figure 3.6 for each observer and task.

As can be seen in Figure 3.6, roughness and softness of the stimuli are distinctly discriminable within the stimulus space, where changes in the surface features coincide with changes in the perceived roughness of the surface while changes in the elasticity coincide with changes in the perceived softness of the stimuli. The perceptual space of both observers is highly similar. In addition, there are regions in the space, unique to each observer, where perceived roughness is influenced by both
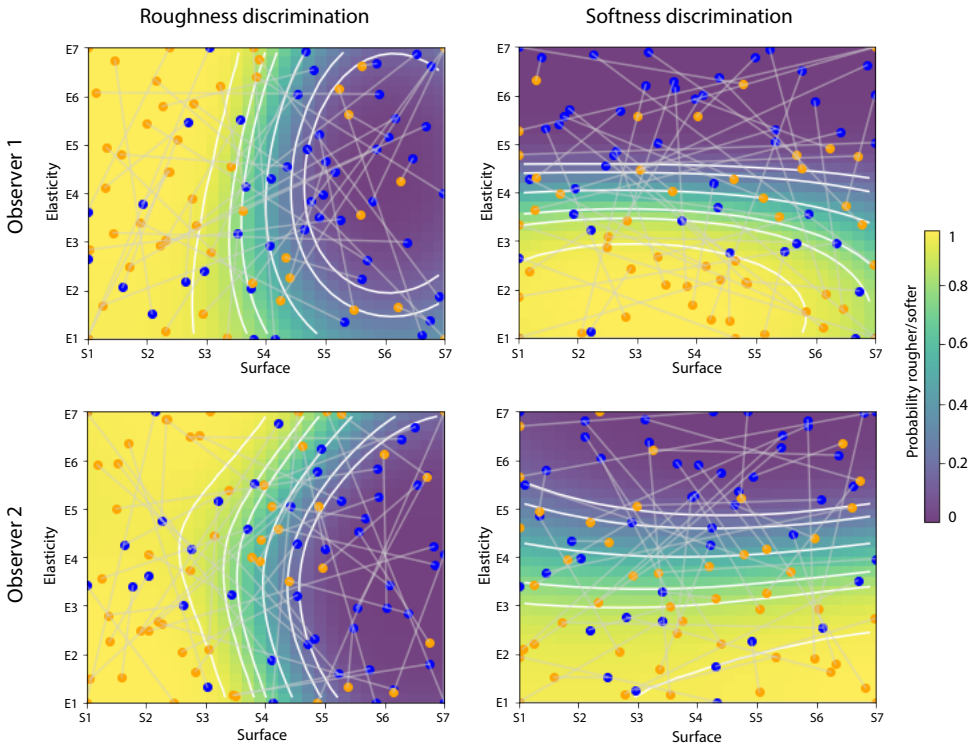
Figure 3.6. Estimated psychometric fields for two participants for roughness discrimination (left) and softness discrimination (right). These plots show the probability of any stimulus within the 2D stimulus space being perceived as rougher or softer compared to the midpoint of the stimulus space (S4, E4). Isocontours represent probability lines at 0.16, 0.25, 0.5, 0.75, 0.84, and 0.96 and can be interpreted in a similar manner as just-noticeable differences (JNDs). Each point pair linked by a gray line represents the actual stimulus pair chosen by the algorithm per trial, where the orange point corresponds to the stimulus chosen as rougher/softer by the observer.

surface cues and material elasticity. These confounded cue regions are indicated by the isocontours in Figure 3.6, left panel.

3.4. AVAILABILITY OF THE STIMULI DATABASE

The STL files for the stimuli described in this document can be requested from the authors. To replicate the dual-property stimuli database as detailed here, it is necessary to 3D print all seven files in seven different material compositions as specified in Section 3.2.2. We caution researchers that achieving highly precise

microscale features with variable elasticities must not be taken for granted. Deviations from the described printing procedures may lead to different outcomes.

3.5. CONCLUSION

In conclusion, the 3D-printed stimuli of our database represent a naturalistic and behaviorally relevant, yet controlled set of samples for haptic texture perception research. The stimuli exhibit systematic variations in both surface roughness (as defined by the Hurst exponent H) and material elasticity. The profilometry measurements demonstrate a strong correlation between H and the measured roughness parameters for both contact and optical profilometry. Pilot perceptual data confirm the perceptual relevance of the stimuli database, suggesting that our database can provide a useful tool for investigating the interplay between surface roughness, material elasticity, and haptic texture perception.

REFERENCES

[1] Driller, K. K., Fradet, C., Hayward, V., and Hartcher-O'Brien, J. "Conception and Design of a Dual-Property Haptic Stimuli Database Integrating Stochastic Roughness and Elasticity". In: Haptics: Understanding Touch; Technology and Systems; Applications and Interaction. Ed. by Kajimoto, H., Lopes, P., Pacchierotti, C., Basdogan, C., Gori, M., Lemaire-Semail, B., and Marchal, M. Springer Nature Switzerland, 2024, pp. 223–237. DOI: 10.1007/978-3-031-70061-3_19.

[2] Persson, B. N. J. On the fractal dimension of rough surfaces. *Tribology Letters* **54** (2014), 99–106. DOI: 10.1007/s11249-014-0313-4.

[3] Verrillo, R. T., Bolanowski, S. J., and McGlone, F. P. Subjective magnitude of tactile roughness. *Somatosensory & Motor Research* **16** (1999), 352–360. DOI: 10.1080/08990229970401.

[4] Hollins, M. and Risner, S. R. Evidence for the duplex theory of tactile texture perception. *Perception & Psychophysics* **62** (2000), 695–705. DOI: 10.3758/bf03206916.

[5] Libouton, X., Barbier, O., Plaghki, L., and Thonnard, J.-L. Tactile roughness discrimination threshold is unrelated to tactile spatial acuity. *Behavioural Brain Research* **208** (2010), 473–478. DOI: 10.1016/j.bbr.2009.12.017.

[6] Yoshioka, T., Gibb, B., Dorsch, A. K., Hsiao, S. S., and Johnson, K. O. Neural coding mechanisms underlying perceived roughness of finely textured surfaces. *The Journal of Neuroscience: The Official Journal of the Society for Neuroscience* **21** (2001), 6905–6916. DOI: 10.1523/JNEUROSCI.21-17-06905.2001.

[7] Bergmann Tiest, W. M. and Kappers, A. M. Analysis of haptic perception of materials by multidimensional scaling and physical measurements of roughness and compressibility. *Acta Psychologica* **121** (2006), 1–20. DOI: 10.1016/j.actpsy.2005.04.005.

[8] Hollins, M., Bensmaïa, S., Karlof, K., and Young, F. Individual differences in perceptual space for tactile textures: Evidence from multidimensional scaling. *Perception & Psychophysics* **62** (2000), 1534–1544. DOI: 10.3758/BF03212154.

[9] Okamoto, S., Nagano, H., and Yamada, Y. Psychophysical dimensions of tactile perception of textures. *IEEE Transactions on Haptics* **6** (2013), 81–93. DOI: 10.1109/TOH.2012.32.

[10] Ernst, M. O. and Bülthoff, H. H. Merging the senses into a robust percept. *Trends in Cognitive Sciences* **8** (2004), 162–169. DOI: 10.1016/j.tics.2004.02.002.

[11] Gedsun, A., Sahli, R., Meng, X., Hensel, R., and Bennewitz, R. Bending as key mechanism in the tactile perception of fibrillar surfaces. *Advanced Materials Interfaces* **9** (2022), 2101380. DOI: `10.1002/admi.202101380`.

[12] Muser, M. and Dapp, W. B. The contact mechanics challenge: Problem definition. *arXiv: Soft Condensed Matter* (2015).

[13] Müser, M. H., Dapp, W. B., Bugnicourt, R., Sainsot, P., Lesaffre, N., Lubrecht, T. A., Persson, B. N. J., Harris, K., Bennett, A., Schulze, K., Rohde, S., Ifju, P., Sawyer, W. G., Angelini, T., Ashtari Esfahani, H., Kadkhodaei, M., Akbarzadeh, S., Wu, J.-J., Vorlaufer, G., Vernes, A., Solhjoo, S., Vakis, A. I., Jackson, R. L., Xu, Y., Streator, J., Rostami, A., Dini, D., Medina, S., Carbone, G., Bottiglione, F., Afferrante, L., Monti, J., Pastewka, L., Robbins, M. O., and Greenwood, J. A. Meeting the contact-mechanics challenge. *Tribology Letters* **65** (2017), 118. DOI: `10.1007/s11249-017-0900-2`.

[14] Bensmaïa, S. J. and Hollins, M. The vibrations of texture. *Somatosensory & Motor Research* **20** (2003), 33–43. DOI: `10.1080/0899022031000083825`.

[15] Wiertlewski, M., Hudin, C., and Hayward, V. "On the 1/f noise and non-integer harmonic decay of the interaction of a finger sliding on flat and sinusoidal surfaces". In: 2011 IEEE World Haptics Conference. 2011, pp. 25–30. DOI: `10.1109/WHC.2011.5945456`.

[16] Kuroki, S., Sawayama, M., and Nishida, S. Haptic metameric textures. *bioRxiv* (2019), 653550. DOI: `10.1101/653550`.

[17] Kuroki, S., Sawayama, M., and Nishida, S. The roles of lower- and higher-order surface statistics in tactile texture perception. *Journal of Neurophysiology* **126** (2021), 95–111. DOI: `10.1152/jn.00577.2020`.

[18] Sahli, R., Prot, A., Wang, A., Müser, M. H., Piovarči, M., Didyk, P., and Bennewitz, R. Tactile perception of randomly rough surfaces. *Scientific Reports* **10** (2020), 15800. DOI: `10.1038/s41598-020-72890-y`.

[19] Gent, A. N. On the relation between indentation hardness and young's modulus. *Rubber Chemistry and Technology* **31** (1958), 896–906. DOI: `10.5254/1.3542351`.

[20] Röttger, M. C., Sanner, A., Thimons, L. A., Junge, T., Gujrati, A., Monti, J. M., Nöhring, W. G., Jacobs, T. D. B., and Pastewka, L. Contact.engineering—Create, analyze and publish digital surface twins from topography measurements across many scales. *Surface Topography: Metrology and Properties* **10** (2022), 035032. DOI: `10.1088/2051-672X/ac860a`.

[21] Owen, L., Browder, J., Letham, B., Stocek, G., Tymms, C., and Shvartsman, M. Adaptive nonparametric psychophysics. *arXiv* (2021). DOI: `10.48550/arXiv.2104.09549`.

4

PROPAGATION WAVES IN TEXTURE AND MATERIAL PERCEPTION

With a robust stimulus set established in Chapter 3, Chapter 4 utilizes this database in addressing the question: Do mechanical propagation waves provide a behaviorally relevant and sufficient cue to roughness and softness perception?

Authors: Karina Kirk Driller, Camille Fradet, Richard Goossens, Craig Sanders, Vincent Hayward and Jess Hartcher-O'Brien

Abstract: Recent research has highlighted the role of propagating vibrational waves through the human hand in resolving dynamic-touch-interaction properties relevant for perception. Using local anesthesia, it has been shown that propagation waves can provide a sufficient cue for roughness discrimination of simple stimulus material such as sandpapers and sinusoidal gratings. This study examines whether this invariance persists for the roughness discrimination of more naturalistic, complex surfaces, varying in statistical microscale roughness and material elasticity. We also explore whether propagation waves provide a sufficient cue to perceived softness (compliance) for the same surfaces and investigate mixed-cue effects of microscale surface roughness and material elasticity on perceived roughness and softness. Employing a two-alternative forced choice (2AFC) discrimination procedure and a non-parametric Bayesian inference framework, we show that the haptic perception of roughness of these surfaces remains considerably intact during temporary de-afferentation of the index finger via local anesthesia, although significant between-subject variability is observed. Perceived material softness, on the other hand, is highly distorted in the absence of local tactile feedback, even when free exploration is permitted. Notably, no mixed-cue effects of microscale surface roughness and material elasticity were observed on the perceived roughness or softness. Our results suggest that propagation waves may provide a key feature for resolving surface roughness across many length scales, but the large between-subject differences raise questions about the conditions under which this occurs. The results furthermore reaffirm the essential role of local cues in the perception of softness.

4.1. INTRODUCTION

During dynamic-touch interactions with the bare hand, vibratory signals arise and propagate through the fingers and hand. Traditional efforts to identify the key mechanical features of dynamic touch have often focused on "local" properties, that is, information collected close to the contact area between object and skin, typically the fingertip [1–4]). However, a recent line of research has turned its attention towards these vibratory signals. It has been demonstrated that these remote vibrations (i.e., measured at the dorsal side of the hand or at the wrist) contain rich mechanical information about the properties of manipulated objects and different gestures [5–9].

Using an array of accelerometers attached to the dorsal side of participant's hands, Shao et al. [10] showed how whole-hand interactions with objects elicit mechanical vibrations in the tactile-frequency range, whose spatial distribution can systematically be mapped to different interaction modes. In later work, the same authors [11] extended these findings by encoding a large database of naturally occurring tactile stimuli into spatiotemporal "primitives" with which they were able to classify touch interactions with high accuracy. These recent findings corroborate work suggesting that vibratory waves propagating through the hand effect an

efficient pre-neural compression of somatosensory information, facilitated by the biomechanical properties of the human hand [7, 12, 13]. Recent work has particularly highlighted the role of "surface" Rayleigh waves that travel cooperatively through both skin and bone in mediating such vibratory information [14].

However, while research into mechanical and neural response characteristics has demonstrated that these signals carry rich information about touched objects and their properties, to date, the question of whether these mechanical propagation waves are critical to perception has been addressed less. It thus remains unclear to which extent the somatosensory system collects information from afferents at more proximal locations than the immediate interaction area and how much it can rely on this information in given tasks.

Propagation waves are assumed to play a particular role in those tasks that involve dynamic exploration, such as the perception of textures. In fact, it has been argued that textures with a spatial period under approximately 100–200 μm require relative movement to be felt [15, 16]. This has prompted researchers to distinguish between spatial and temporal coding mechanisms relevant for the perception of coarse and fine textures respectively, in what has sometimes been called the duplex theory of texture perception [15, 17–20]. However, it is unlikely that different mechanoreceptor types function in isolation and this distinction may therefore best be looked at as the relative weight of contribution of tactile units in the perception of different textural features [21, 22]. Propagation waves are furthermore assumed to play a crucial role in texture constancy or invariance [5, 23], that is, the ability to perceive textures in a stable manner across changes in physical conditions, such as scanning velocity [24], although the exact mechanisms of this phenomenon remain poorly understood.

Importantly, one study showed how the tactile roughness discrimination of fine sandpapers remains intact when innervation of the finger is compromised, either due to a pathological condition or during ring-block anesthesia of the index finger in healthy subjects [25]. Following this finding, Delhaye et al. [5] showed how the intensity of vibrations (that is, the vibratory power) measured at the wrist of participants stroking sandpapers and periodic gratings could be well related to the roughness of these textures. However, it is unclear whether this sufficiency of vibratory information for roughness perception of sandpapers can be generalized to more natural surfaces, which are often statistically complex and may vary in more than just one dimension. Furthermore, the extent to which these remote vibrations are picked up by the human somatosensory system and used in the perception of other texture or material dimensions than roughness remains unexplored. One study did use local anesthesia of the index finger to investigate the relative role of kinaesthetic versus local tactile information in the haptic discrimination of softness and reported that kinaesthetic information alone was insufficient to discern softness via pressing/indentation [26]. However, vibratory cues were prevented in this study, allowing no conclusions about the potential role of propagation waves in this task. Notably, some evidence does suggest that vibrotaction can sometimes affect the perception of softness [27–30].

The present study was aimed at achieving a better understanding of the role of propagation waves in surface roughness and material softness (compliance) perception

of stimuli, exhibiting characteristics akin to those found in numerous natural surfaces. Most natural and engineered surfaces that we encounter during our everyday life are self-affine surfaces, exhibiting fractal properties over many different length scales [31]. Furthermore, changes in surface properties can covary with changes in material properties. To reflect this, we used a database of stochastically rough 3D-printed stimuli, varying systematically in their micro-scale surface roughness and material elasticity (cf. Chapter 3). We sought to uncover some of the perceptual mechanisms that remain intact during the free exploration and discrimination of these surfaces, while local information was temporarily inhibited using local anesthesia of the index finger.

It was hypothesized that propagation waves that arise during these haptic interactions contain behaviorally relevant information used for the discrimination of roughness. It was furthermore hypothesized that softness might be discernible via propagating vibration too, when unconstrained and dynamic exploration are permitted [30, 32].

A secondary aim was to determine potential mixed-cue effects of surface microscale roughness and material elasticity on roughness and softness perception. If both cues influence the perceptual outcome (roughness or softness), we hypothesized that regions of cue fusion should be found where different combinations of the two cues provide confounding percepts (metamers). Figure 4.1 displays different example scenarios illustrating these predictions.

4.2. Methods

4.2.1. Participants

16 adult volunteers with no reported psychiatric or neurological disorders and no history of finger/upper limb trauma or a disease affecting normal motor functioning were recruited for the study. One participant had to be excluded because a full ring block could not be reached (cf. Section 4.2.4 for the administration and assessment of the local anesthetic). This resulted in a final sample of 15 participants (9 women, 6 men; mean age: 26.93, SD: 8.94). Out of these, one participant was left-handed, and another participant was mixed-handed, while the remaining thirteen participants were right-handed, as assessed using the Edinburgh Handedness Inventory [33]. The mixed-handed participant reported being right-handed and thus performed the experiment with the right index finger.

The study was approved by the Dutch Medical Ethics Review Committee METC-LDD. Data were collected at the Reinier Haga Orthopaedic Centre, and the study was approved by the local ethics committee. The study is also registered on the website of ClinicalTrials.gov with the identifier NCT05253508 (date of first registration 23/02/2022). The methods of this study were performed in accordance with the relevant guidelines and regulations and in accordance with the Declaration of Helsinki. All participants gave written informed consent prior to the experiment and preparation.
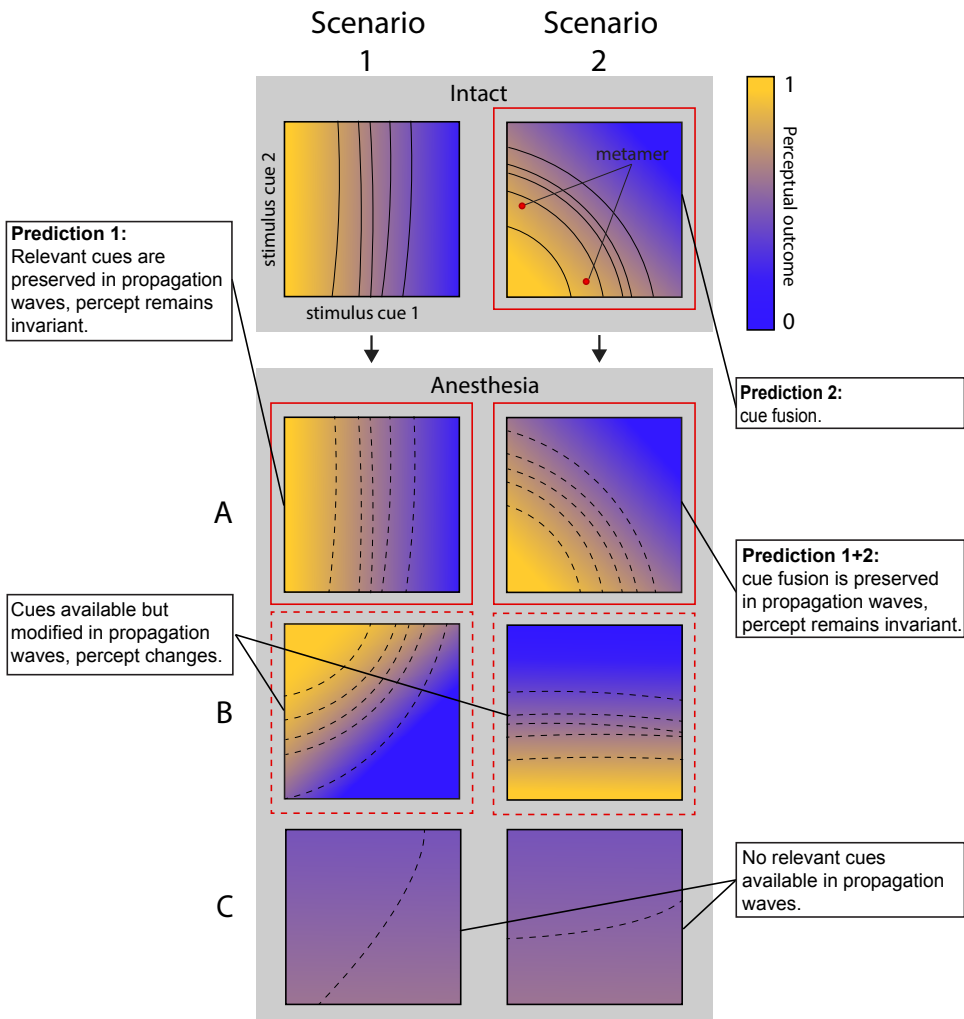
Figure 4.1. Predictions and example scenarios illustrating a differing cue influence and preservation of a perceptual outcome under local anesthesia. The plots represent a two-dimensional cue space (e.g., cue 1 = surface roughness and cue 2 = elasticity). Colors indicate the magnitude of a perceptual outcome (e.g., perceived roughness or softness) on a 0–1 scale where yellow corresponds to the highest magnitude (e.g., roughest/softest) while blue corresponds the lowest magnitude within the stimulus space. **Scenario 1:** Cue 2 is irrelevant to the perceptual outcome. **Scenario 2:** both cues determine the perceptual outcome. **A:** The perceptual outcome is preserved under local anesthesia. **B:** The perceptual outcome is modified under anesthesia. **C:** No task-relevant cues remain under anesthesia.

4.2.2. APPARATUS

Participants were seated on a chair at a desk in front of a computer screen. During the experiment, they wore noise-canceling headphones (Sony WH-1000XM3) playing pink noise at approximately 40 dB, to ensure that the feedback they received was purely haptic in nature. The light in the experimental room was dimmed so that differences between the stimuli could not be seen, while the outline of the stimuli could still be made out for targeted interactions. Stimuli were placed in front of the participant's dominant hand for semi-controlled exploration with the index finger, as illustrated in Figure 4.2. A numpad was provided for responses via keypress at the side of the participant's non-dominant hand.
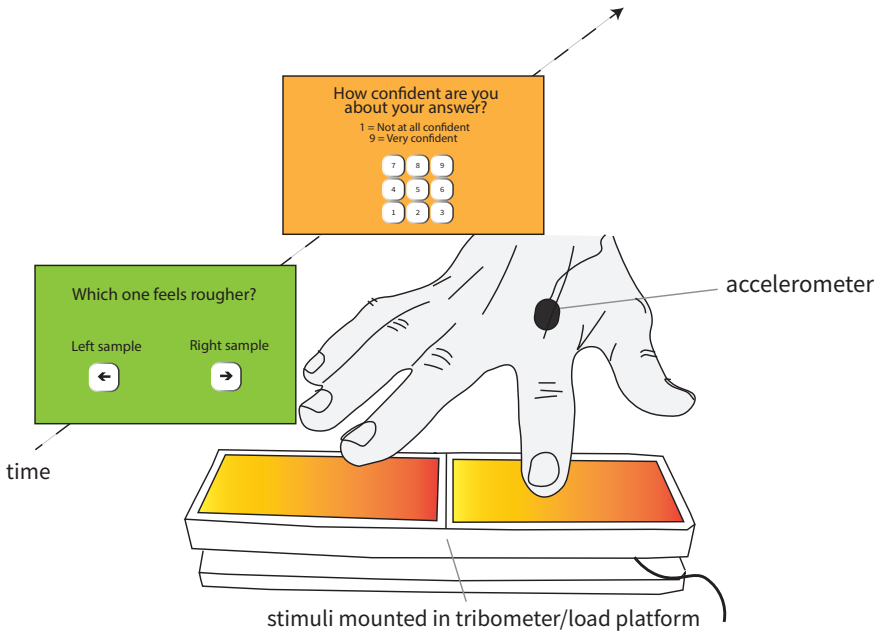
Figure 4.2. Setup and procedure.

Aspects of the participant's interactions with samples were recorded using custom-made sensor platforms, one for each perceptual dimension studied, developed by Vincent Hayward. In both cases, the signals from the sensors went through a pre-amplification phase before being collected by the acquisition interface.

For roughness discrimination, the stimuli were mounted in a tribometer. The tribometer consisted of two unidirectional force sensors oriented upwards to measure the load applied by the participant's finger as well as a bidirectional force sensor positioned horizontally to record the tangential forces of the finger-surface interactions. The two unidirectional force sensors saturated at 2.5 N and had a sensitivity of 0.625 N/V. The bidirectional force sensor saturated at 2.5 Newton in both directions, with a sensitivity of 2.5 N/V. This tribometer allowed for an accurate identification of the variations in the coefficient of friction up to about 100 Hz (cf. Figure 4.3, left side).

Figure 4.3. Left side: Dynamics tribometer used for roughness discrimination. Right side: Load sensor used for softness discrimination. Each containing two stimuli as used in the experiment.

4

For softness discrimination, the stimuli were mounted in a load sensor to accommodate higher loads (viz. 70 N) applied with the index finger and to guarantee a precise measurement despite variations of the region of contact. The load cell consisted of a unique unidirectional force sensor directed upwards to measure the load applied. The sensitivity of this sensor was 17.4 N/V (cf. Figure 4.3, right side).

Finally, a 3-axis accelerometer (KXTC9-2050, Kionix) was placed on the participant's dorsal side of the dominant hand on the first metacarpal behind the major knuckle (cf. Figure 4.2).

We used a BELA board and a National Instruments DAQ X 6343 to gather the signals from all our sources via analogue inputs (cf. Appendix G for details), connected to the computer via USB and controlled using MATLAB (version 2021b).

Note: the present work includes only a basic analysis of platform data while accelerometer data was excluded due to data integrity issues. A detailed account of the challenges that led to this decision is provided in Appendix G.

Because nerve blocks with lidocaine or ropivacaine inhibit a wide range of nerve fibers [34], which may as a result inhibit sweating [35], the hydration level of the fingertip skin was measured regularly using a corneometer (Corneometer® CM 825). Similarly, the temperature of the finger pad was measured regularly using an infrared thermometer (Tacklife IT-T09).

4.2.3. STIMULI

We used a database of 49 stochastically rough 3D-printed stimuli, varying systematically in their microscale roughness and elasticity (see Chapter 3). All stimuli were sized 50x31x10 mm. The database consists of seven different surface topographies that were generated using an algorithm that produces stochastically rough surfaces with well-defined spectral distributions [36]. The microscale roughness of these surfaces was varied by changing the Hurst exponent, which has been shown to be a perceptually relevant parameter for subjective roughness using the same surface algorithm [37, 38], albeit on much larger length scales. A smaller Hurst exponent H leads to a slower decay towards small length scales and thus results in a

higher microscale roughness. The stimuli used here spanned an H from 0.3 to 0.9. Each of these samples was available in seven elasticities. Table 4.1 and Table 4.2 summarize the parameters of the stimuli.

Table 4.1. Elasticity parameters of the stimulus database taken from Chapter 3.

Elasticity Nr.	E1	E2	E3	E4	E5	E6	E7
Shore A value	23.6	24.83	25.83	28.67	34	44.2	65.8
Y. Modulus (MPa)	0.121	0.122	0.128	0.144	0.179	0.264	0.611

Table 4.2. Roughness parameters of the stimulus database taken from Chapter 3.

Surface Nr.	S1	S2	S3	S4	S5	S6	S7
Hurst exponent	0.3	0.4	0.5	0.6	0.7	0.8	0.9
Rq[$\times 10^{-2}$ mm]	5.68	5.16	4.79	4.51	4.3	4.14	4.01

4.2.4. PREPARATION

Before the beginning of the experiment, participants were asked to fill out and sign the consent form, and the procedure was explained in detail. Then their hand size was measured[1]. Next, the anesthetic ring-block was applied (in the anesthesia condition only) via an injection of 1–2 ml lidocaine 2% or ropivacaine 0.2% at each side of the palmar root of the dominant index finger [39]. After ten to fifteen minutes, the effect of the ring-block was tested using the Semmes Weinstein monofilaments exam [40–42]. Anesthesia was considered complete when no sensation was reported to remain in the second and third phalanx. If anesthesia was still incomplete after 25 minutes, an additional dose was given (maximum of four injections and total volume of 4 ml). Where complete anesthesia could not be achieved, no experimental data were collected. Given that the muscles that move the index finger are located solely in the hand and forearm, we could infer that the local anesthesia would not influence the participants' motor behavior, except for motor control directly linked to afference from the finger itself [2, 43, 44].

4.2.5. EXPERIMENTAL DESIGN AND PROCEDURE

A 2AFC task was used within a nonparametric Bayesian inference framework called AEPsych [45, 46]. This procedure uses active sampling and Gaussian-Process classifications to efficiently estimate psychometric fields, without imposing any prior expectations on the relationship between stimulus parameters and the perceptual outcome. It enabled us to model a single latent function (F):

$$P(\text{"A rougher/softer than B"}) = \Psi(F(A) - F(B)) \tag{4.1}$$

---

[1]Hand length: distance from wrist crease to tip of the middle finger; Index finger length: distance from tip to palmar digital crease; Hand width: distance from radial to the ulnar side of the hand, measured at the metacarpals.

determining the probability of the perceptual judgment (rougher or softer) between any two stimuli in our stimulus space with the parameters "Hurst" and "Shore". The precise configuration of the model is specified in Appendix F. We used a repeated measures design. All participants received both conditions (anesthesia/intact) in different sessions and carried out both tasks (roughness/softness discrimination) during the two sessions. The two experimental sessions (anesthesia/intact) were separated by one to three days for each participant. This minimum 24-hour period was maintained because the effect of ropivacaine can last up to 23 hours. The order of conditions and tasks was balanced across participants.

Before each experimental session and task, participants were given at least four test trials (for each task and each condition), or more until they reported feeling acquainted with the task before starting the experiment proper. For the test trials, a pre-defined set of four sample pairs was used in a randomized order for all participants. This was done in order to make sure that the samples were reasonably distributed in our sample space and to ensure that all participants received the same prior information about what the stimulus space could be like. Where participants requested more than four test trials, the same four sample pairs would be used in a randomized order. Participants were given no feedback on their performance. When participants indicated they were ready and had understood the task, the experiment began.

In each trial of the experiment, a window appeared on the participant's screen asking them which one of the two surfaces felt rougher (in the roughness condition) or softer (in the softness condition), the left or the right one. Participants were instructed to explore the left sample first and then move to the right sample. They were allowed to explore the surfaces freely, using any interaction methods they wanted, but only with their dominant index finger. They were also asked not to explore the edges and corners of the samples and to avoid using their fingernails. Exploring the first sample again was not permitted after participants had started exploring the second sample, and participants were encouraged to give quick and intuitive answers. After they provided their answer, participants were asked to rate how confident they were about the answer given on a Likert scale from 1–9 (cf. Figure 4.2). All answers were given by keypress with the non-dominant hand. After each trial, the experimenter placed a new pair of samples in the tribometer/load platform, whereafter the task window reappeared on participant's screen, indicating that they could begin with the next trial. A note about the chosen exploration strategies was made by the experimenters for each participant, task, and condition.

One experimental session consisted of two blocks (one for each task) of 50 trials each. A 5–10-minute break was provided between the blocks, and a shorter 2–3-minute break was provided after 25 trials of each block, respectively. The duration of each block was approximately 30 minutes. Just before and after the experiment, as well as within the three breaks, the hydration level and temperature of participants index finger pads were measured, taking the average of three consecutive measurements with a skin hydration measurement instrument (Corneometer® CM 825) and thermometer (Tacklife IT-T09).

4.2.6. STATISTICAL ANALYSES

For continuous data from the finger-pad temperature and hydration level measurements, paired sample t-tests were carried out to compare the differences between conditions.

Basic behavioral interaction data, including normal peak loads applied during softness discrimination and the average normal load, velocity, and coefficient of friction for roughness discrimination, were analyzed using Wilcoxon signed-rank tests. This test was chosen due to the non-parametric nature of the data to assess overall differences between the intact and anesthesia conditions at a group level.

For the discrimination data, a multitask binary classification Gaussian Process (GP) model was fitted to capture the responses across different conditions and tasks. The model incorporated Houlsby's pairwise kernel with a latent Matern 5/2 kernel and an index kernel for condition and participant. Variational inference, a Bayesian method with hyperparameters fitted using maximum likelihood estimations, was used for fitting the model and approximating probability distribution. Model performance was evaluated using the area under the receiver operator characteristic curve (ROC AUC). Hypothesis testing was conducted using Bayesian methods, specifically comparing the posterior highest-density intervals (HDIs) against regions of practical equivalence (ROPE). This approach was employed to determine the overall differences between the anesthesia and intact conditions as well as comparisons to chance levels. The precise steps are described in more detail in Section 4.3.4.

Finally, for confidence ratings and response times, repeated measures ANOVAs were conducted to examine the main effects of condition (intact vs. anesthesia) and task (softness vs. roughness), as well as their interaction. Post-hoc pairwise comparisons with Bonferroni correction were performed to further investigate significant effects. While Likert-scale data are technically considered ordinal, they can in some cases be considered approximately continuous. This is particularly meaningful in the context of a larger numerical range. We here report means, rather than medians or modes, as they have the advantage of being easy to locate on the original scale. Furthermore, parametric tests are here considered a valid and useful tool for determining any differences between groups [47].

Exclusion criteria were predetermined. One participant was excluded from the entire study due to incomplete anesthesia. Additionally, two participants were excluded from the data analysis related to the softness discrimination task because they misunderstood the task instructions and discriminated smoothness instead. These two participants were retained for the roughness discrimination task and the analyses of finger pad temperature and hydration levels. For coherent within-group comparisons between tasks, these participants were also excluded from the analyses concerning confidence ratings and response times.

Statistical analyses on finger-pad temperature and hydration level, as well as the response times and confidence ratings, were performed using R (version 4.3.1, R Core Team, 2021).

Data processing and analysis of behavioral (interaction) data were performed in MatLAB (version R2023b).

All data analysis of the discrimination data was performed in Python (Anaconda Navigator, Spyder version 5.4.3) and using AEPsych [45, 46].

4.3. ANALYSIS AND RESULTS

4.3.1. ANESTHESIA

A complete digital nerve block was achieved for fifteen participants. Of these fifteen participants, one received only two injections of lidocaine. Another participant was given an additional lidocaine dose due to early signs of recovery after the first experimental block, resulting in a total of four injections. The remaining participants were given two ropivacaine injections each. For seven of these fifteen participants, all sensation was abolished on all three phalanges. This group reported a mild effect of the anesthetic on the adjacent side of the middle finger. For the remaining eight participants, some sensation was reported left on the upper part of the dorsal side of the proximal phalanx while no anesthetic effect was reported on the middle finger. This was consistent throughout the data collection for each participant. Such variation is normal given the cutaneous innervation of this region [48, 49]. All participants were treated equally in the analyses. Swelling of the base of the finger from the injection of the anesthetic solution was observed for all participants. This swelling was greatest immediately after the injection and did not restrict participant's movement except for during full flexion, which was not required for the task.

4.3.2. FINGER-PAD TEMPERATURE AND HYDRATION LEVELS

Paired sample t-tests revealed a significant difference between the index finger-pad moisture content of the intact condition ($M = 66.75$, $SD = 27.24$) and the anesthesia condition ($M = 25.98$, $SD = 7.54$), $t(14) = -6.42$, $p = 0.00002$, but no significant difference was found between the index finger-pad temperature of the intact condition ($M = 29.63$, $SD = 2.88$) and the anesthesia condition ($M = 28.39$, $SD = 3.31$), $t(14) = 1.71$, $p = 0.11$ (cf. Figure 4.4).

4.3.3. BEHAVIORAL (INTERACTION) DATA

Observation by the experimenters during data collection revealed that all participants used lateral motion (stroking or rubbing) for the roughness discrimination in both conditions. Furthermore, all participants used pressing for the softness discrimination task in the intact condition. This exploration strategy was retained by most participants during softness discrimination with the anesthetized finger. Only two participants (5 and 8) included dynamic lateral motion (stroking or rubbing) in their exploration strategies for softness discrimination under anesthesia.

We here only include initial insights from the data recorded with the load cell and tribometer during interactions with the samples. A more comprehensive analysis is subject to future work. Detailed reasons for this decision are provided in Appendix G.

Figure 4.5 shows the average normal peak load applied during interactions with the stimuli in the softness discrimination task for each condition (intact and

4
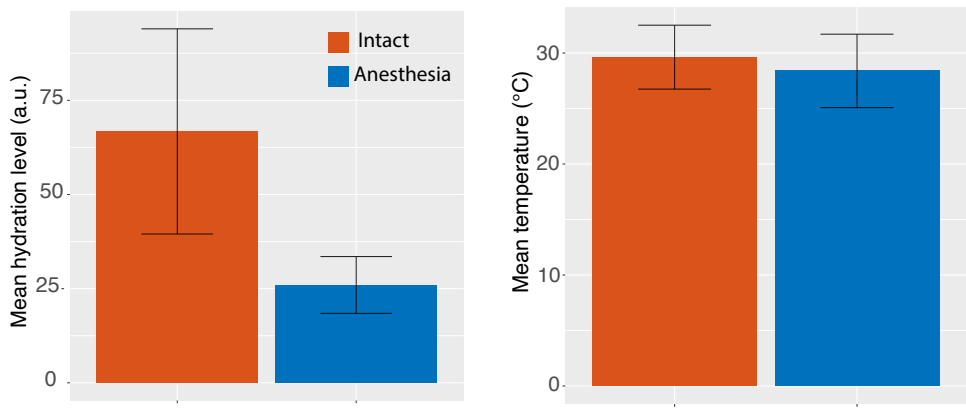
Figure 4.4. Mean index finger-pad moisture levels (left) and temperature (right) for the intact and anesthesia conditions. Error bars indicate the standard deviation from the mean.

anesthesia). Information about data processing, filtering, and exclusion is detailed in the Appendix G. From Figure 4.5 it is apparent how participants overall applied lower loads in the anesthesia condition compared to the intact condition. A Wilcoxon signed-rank test confirmed that this difference was significant ($V = 81415$, $p < .001$).
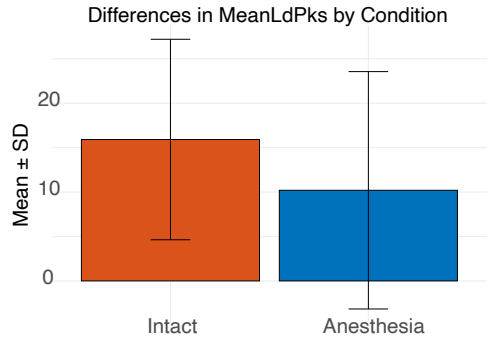
Figure 4.5. Average peak load applied during interactions with the stimuli for softness discrimination under both intact and anesthesia conditions. Error bars represent the standard deviation from the mean. Note that the error bars extending below zero are due to significant variations in peak load applied by different participants in the anesthesia condition (see Appendix I).

Figure 4.6 depicts the average normal load, velocity, and coefficient of friction for the interactions carried out during the roughness discrimination task for each condition (intact and anesthesia). Again, data exclusion and processing are detailed in Appendix G.
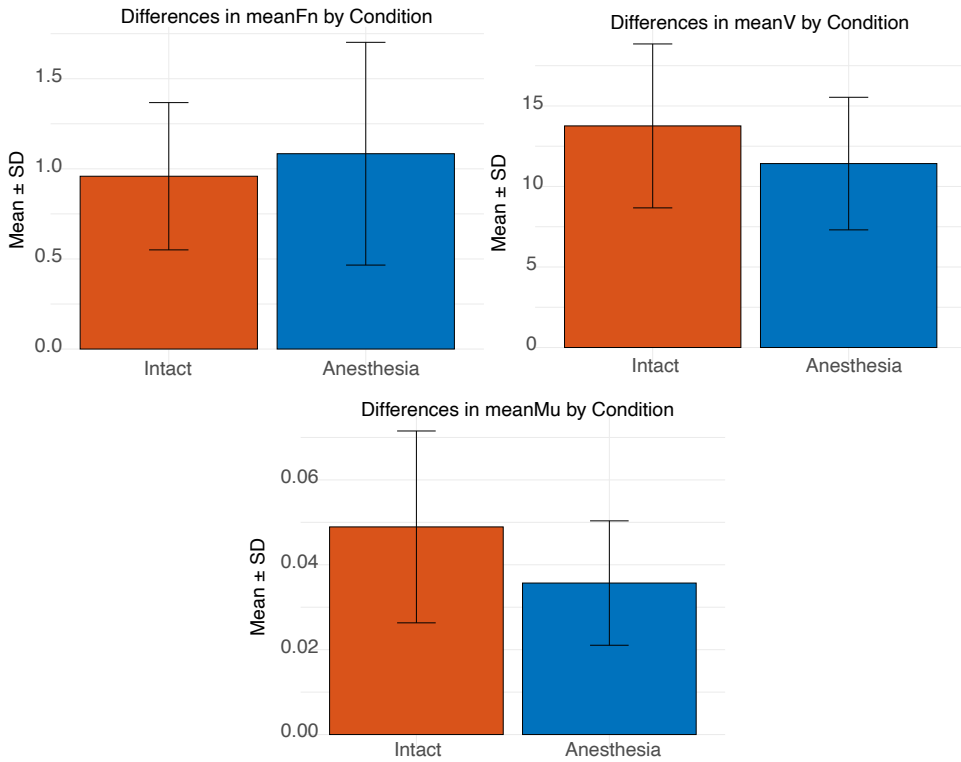
Figure 4.6. Mean normal force (left), velocity (center), and coefficient of friction (right) for interactions with the stimuli during roughness discrimination for the Intact and Anesthesia conditions.

Figure 4.6 shows that, on average, participants applied higher normal forces, used lower velocities, and achieved a lower coefficient of friction in the anesthesia condition compared to the intact condition. Wilcoxon signed-rank tests confirmed that these differences were significant ($V = 56944$, $p < .001$ for the average normal force, $V = 109363$, $p < .001$ for the average velocity, and $V = 114048$, $p < .001$ for the average coefficient of friction).

Individual-level plots illustrating differences in interactions between conditions, as well as variations between participants, are provided in Appendix I. The scatter plots in Figure I.2 demonstrate large variations in individual exploration behavior between the two experimental conditions.

4.3.4. DISCRIMINATION DATA

A multitask binary classification Gaussian Process (GP) model [50] was fitted across all participants and both conditions (anesthesia/intact) for each of the two tasks. GP models are non-parametric models characterized by a mean and covariance function. The model used Houlsby's [51] pairwise kernel[2] with a latent Matérn 5/2 kernel[3] for the two stimulus dimensions (Hurst and Shore values) and an index kernel for condition and participant. This model simultaneously models all participants across both conditions, treating different participants and conditions as separate yet interrelated, because correlations between conditions and participants are learned. For fitting the model's posterior and approximating the probability distributions, variational inference was used as outlined by Blei et al. [52].

The Hurst and Shore values (cf. Table 4.1 and Table 4.2) were min-max scaled to the range [0, 1]. Formally, due to the binary nature of the outcome, we assume each roughness or softness judgment, y, to be drawn from a Bernoulli distribution with probability $\Phi(f(u, v, c, p))$, where Φ is the Gaussian Cumulative Distribution Function (CDF), and $f(u, v, c, p)$ is a latent function over the model inputs: the left and right stimuli (given by their Hurst and Shore values, u and v), condition index (c), and participant index (p).

$$y|f, u, v, c, p \sim Bernoulli(\Phi(f(u, v, c, p))) \tag{4.2}$$

We placed a GP prior on f. As is typical in GP regression, we used a constant mean function of 0 and a covariance function that is the product of three different functions, k_{stim}, k_{cond}, and k_{part}:

$$f \sim GP(0, k_{stim} \cdot k_{cond} \cdot k_{part}) \tag{4.3}$$

The covariance function k_{stim} models the covariance between pairs of stimuli. Given pairs $[a, b]$ and $[c, d]$, the covariance is given by:

---

[2]Houlsby's pairwise kernel is designed for Gaussian Process models to effectively handle the interactions between pairs of data points. This kernel facilitates the modeling of complex dependencies between tasks, enhancing its ability to capture correlations across different data points or groups.

[3]Matérn kernels are covariance functions used in statistics to specify the covariance between any two points in an input space [50].

$$k_{stim}([a,b],[c,d]) = k(a,c) + k(b,d) - k(b,c) - k(a,d) \tag{4.4}$$

where k is the Matern 5/2 kernel. The derivation for this expression is provided by [51].

The index kernels, k_{cond} and k_{part}, model the covariance across conditions and across participants, respectively. These kernels capture the notion that different participants and conditions are related, allowing the model to learn correlations between these factors.

To assess the model fit, we used the area under the receiver operator characteristic curve (ROC AUC; [53, 54]), a measure interpreted as the likelihood of the model correctly predicting which stimulus in a random pair is chosen (i.e., as 'rougher' or 'softer'). In this context, a higher ROC AUC score indicates a better model fit. Given the Bayesian nature of Gaussian Processes (GPs), our model provided a distribution of predictions rather than a single outcome. This distribution was estimated by taking 10,000 samples from the model's predictions and computing the ROC AUC for each sample. We calculated the mean of this distribution and identified the limits of the 99% highest-density interval (HDI), an interval capturing 99% of the posterior mass, suggesting a 99% probability that the actual ROC AUC value falls within this range. HDIs are analogous to, but not equivalent to, frequentist confidence intervals. These results are represented as histograms in Figure 4.7.

(a) Softness Discrimination   **(b)** Roughness Discrimination
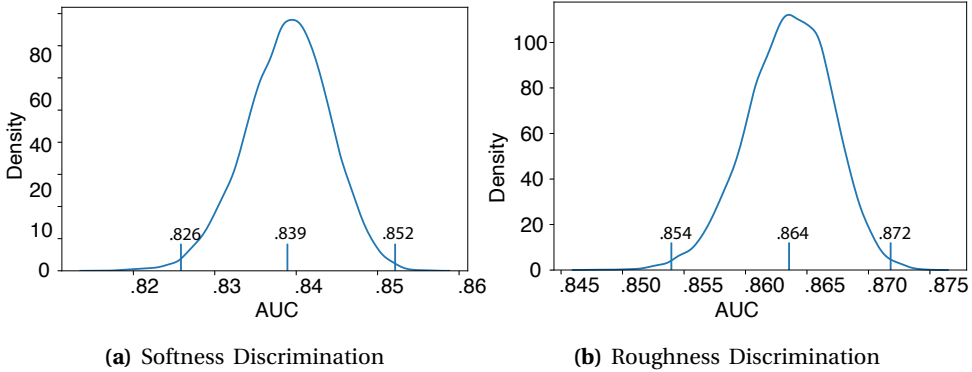
Figure 4.7. Area under the receiver operator characteristic curve (ROC AUC) displaying the model fit for (a) softness and (b) roughness discrimination. Calculated using 10,000 samples of the model's predictions. Mean of the distribution (84% and 86%) and the limits of the 99% highest-density interval (HDI; 83%–85% for a and 85%–87% for b) are labeled.

As can be seen in Figure 4.7, our analysis revealed that the model's ROC AUC ranged between 83% and 85% for softness discrimination, and 85% and 87% for roughness discrimination, both indicating a generally "good" model fit according to convention [55]. We opted for the 99% highest-density interval (HDI) over the conventional 95% HDI due to the tendency of variational inference to underestimate the variance in the model's posterior.

We then created model prediction plots for each participant and each condition on a dense grid of Hurst and Shore values for both tasks. Model predictions were visualized using contour plots to display the probability of stimuli being rated as rougher across the Hurst and Shore value space. Individual model predictions as well as delta plots illustrating the difference between the two conditions are available in Figure H.1 and Figure H.2 in Appendix H, while Figure 4.8 shows the mean probability across all participants for each task and condition as well as the mean difference between conditions. Generally, these data plots display the probability of any given sample being chosen (as rougher/softer) compared to the midpoint of our sample space (S4, E4, cf. Table 4.1 and Table 4.2) in a 0–1 probability space. Iso-contour lines are plotted at 16%, 25%, 50%, 75%, 84%, and 96%, representing levels of equal probability density in the 2-dimensional cue space. They can be interpreted in a similar manner as just-noticeable differences (JNDs). The total number as well as the distance between isocontours in the space is expressive of how finely participants were able to discriminate the space.

In Figure 4.8a as well as the individual model predictions (Figure H.1) in Appendix H, it is visible how **softness discrimination** in the intact condition was primarily determined by the Shore value and not the Hurst exponent, since changes in probability primarily occur on the *horizontal axis*. Although minor variations on the vertical axis corresponding to the Hurst exponent can be observed on an individual level (cf. Figure H.1), this is not systematic and averaged out on the mean model predictions (Figure 4.8a). Conversely, intact **roughness discrimination** was primarily determined by the Hurst exponent with a minor influence of the Shore value (cf. Figure 4.8b and Figure H.2), displaying changes in probability on the *vertical axis*. This was confirmed by examining the best-fitting length-scale values derived from the GP model. These values represent the distance along the stimulus parameter for which responses were highly correlated and indicate the model's sensitivity to change. While these values have to be viewed upon in relative terms within a model, a smaller value indicates higher sensitivity. For softness discrimination, these values were 0.7428 for the Hurst exponent and 0.1867 for the Shore value, testifying to a comparatively higher model sensitivity to changes in the Shore value than the Hurst exponent. For roughness discrimination, on the other hand, they were 0.3819 for the Hurst exponent and 1.3183 for the Shore value, suggesting a comparatively minor influence of the Shore value on roughness discrimination.

Figure 4.8 and the individual model predictions in Appendix H furthermore show how the probability of choosing a stimulus (as rougher or softer) changed under anesthesia compared to the intact condition. On average, a severe loss of discrimination ability can be observed for the softness task with many fewer isocontours above chance level (cf. Figure 4.8a). This is largely corroborated by the individual model predictions presented in Figure H.1, although certain participants did achieve probability levels of 75% or more, indicating that softness discrimination was not entirely impaired under anesthesia for these individuals. As a reminder to the reader, two participants (5 and 8) included lateral movement in their softness exploration under anesthesia while the remaining participants maintained pressing.
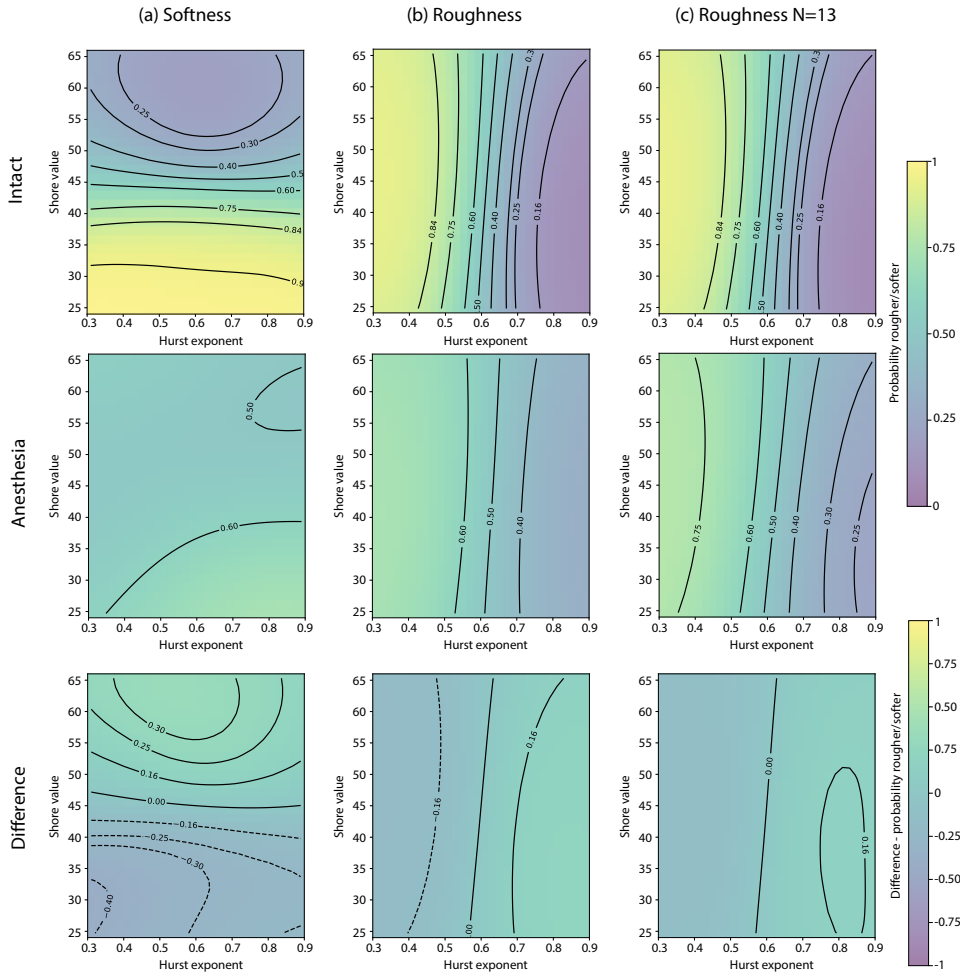
Figure 4.8. Mean psychometric fields across all participants for Intact, Anesthesia, and the difference between the two for (a) softness discrimination, (b) roughness discrimination, and (c) roughness discrimination excluding the two participants that displayed an inverse discrimination pattern. Predictions were made on a dense grid of Hurst and Shore values. These plots display the mean of the individual model predictions presented in Appendix H. The background color indicates the probability that a stimulus would be chosen as softer than a stimulus with the median Hurst/Shore values. Isocontours are plotted at 16%, 25%, 50%, 75%, 84%, and 96%.

Mean discrimination of roughness, on the other hand, remained partially intact under anesthesia, displaying a similar pattern as in the intact condition but with fewer isocontours. A closer look at the individual model predictions in Figure H.2 and Figure H.4 in Appendix H reveals large individual differences in the ability to discriminate roughness under anesthesia. While some participants displayed highly similar roughness discrimination between both conditions, roughness discrimination appeared partially or substantially disrupted for other participants.

Notably, two participants (1 and 4) displayed a seemingly *inverse* pattern of roughness discrimination under anesthesia, wherein lower-microscale roughness samples were consistently discriminated as rougher. Roughness discrimination of these two participants under anesthesia additionally displayed a clear influence of the Shore value, where stimuli with a lower Shore value exhibited a higher probability of being perceived as rougher. Due to these two participants, the mean model predictions for this condition in Figure 4.8b must be approached with some caution, as these opposing patterns may neutralize each other's effects. Figure 4.8c show mean model predictions without these two participants to illustrate this point. While mean model predictions remain qualitatively similar with and without these participants, higher average probability levels are reached in the anesthesia condition upon removing these two "inverse" datasets from the mean.

Following Kruschke [56], we then performed hypothesis testing by comparing the posterior HDI against a region of practical equivalence (ROPE). The ROPE represents the set of values that, for practical purposes, are equivalent to a null value.

Unlike in a frequentist framework where one can only reject a null hypothesis, in this Bayesian framework, it is possible to accept a null hypothesis or reject an alternative hypothesis according to the following rules:

- If the posterior Highest Density Interval (HDI) lies entirely within the Region of Practical Equivalence (ROPE), accept the null hypothesis and reject the alternative.
- If the posterior HDI lies entirely outside the ROPE, reject the null hypothesis and accept the alternative.
- If some of the HDI lies within the ROPE and some outside of it, fail to accept or reject either hypothesis.

While posing research questions in this hypothesis-testing framework can help make decisions, it is important to avoid dichotomous thinking and instead examine the full distributions given by the posterior and appreciate all the nuances therein.

We here set all ROPEs to a 5% width, akin to similar conventions like p < .05, meaning that values below 5% difference are considered equivalent to the null hypothesis of no difference. To assess whether there was an overall difference between the anesthesia and intact condition, we first tested the null hypothesis that there is no difference. This was done by taking 10,000 samples from the model's posterior for each possible stimulus pair (49 * 48/2 total pairs) and calculating the predicted probability of one stimulus being chosen over the other (as rougher/softer) for each of these, for each condition. We then calculated the difference in these predicted probabilities for each pair and averaged these differences across all participants.

Under the null hypothesis, which posits no difference between the anesthesia and intact conditions, the expected average difference would be zero. Figure 4.9 shows the posterior distribution of the mean difference in perceived roughness between anesthesia and intact conditions, overlaid with a ROPE of [-2.5%, 2.5%], for both tasks.

(a) Softness Discrimination   **(b)** Roughness Discrimination
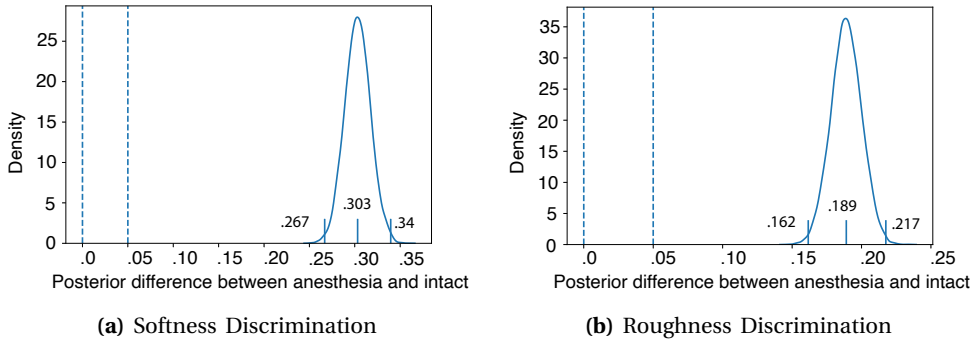
Figure 4.9. Posterior difference between anesthesia and intact conditions with a ROPE of [-2.5%, 2.5%]. (a) Softness discrimination and (b) roughness discrimination.

The fact that the 99%-HDI falls outside the designated ROPE suggests that we can reject the null hypothesis of no difference between the two distributions for both tasks, with a mean posterior difference of 30% for softness and and 19% for roughness discrimination. For both tasks, the HDIs are far enough from the ROPEs that we would still reject the null hypothesis for any reasonable ROPE values.

We also tested the hypothesis that there is no difference between each condition and chance by looking at the average absolute distance between the model predictions and chance (50%). Because the absolute distance cannot be less than 0% we set a ROPE of [0%, 5%]. Figure 4.10 and Figure 4.11 show that the HDIs lie outside the ROPE, indicating that we can accept the alternative hypothesis that performance was different from chance in both conditions for both tasks.
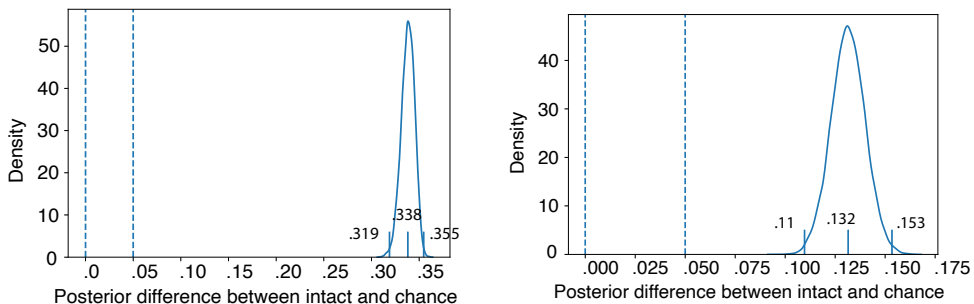
Figure 4.10. Softness Discrimination–Posterior Difference between Intact and chance (left) and Anesthesia and chance (right) with a ROPE of [0%, 5%].
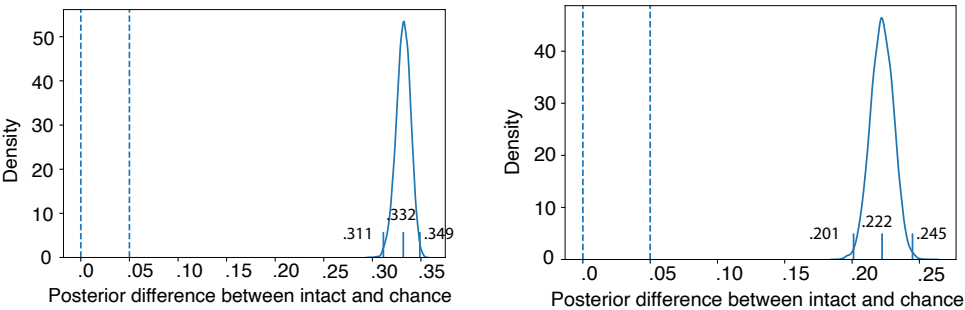
Figure 4.11. Roughness discrimination–posterior difference between intact and chance (left) and anesthesia and chance (right) with a ROPE of [0%, 5%].

Finally, we repeated the same analyses for each participant individually and plotted the posterior difference between the two conditions (anesthesia and intact) as well as each condition and chance for both tasks. The plots can be seen in Figure 4.12 and Figure 4.13.

(a)

(b)

(c)
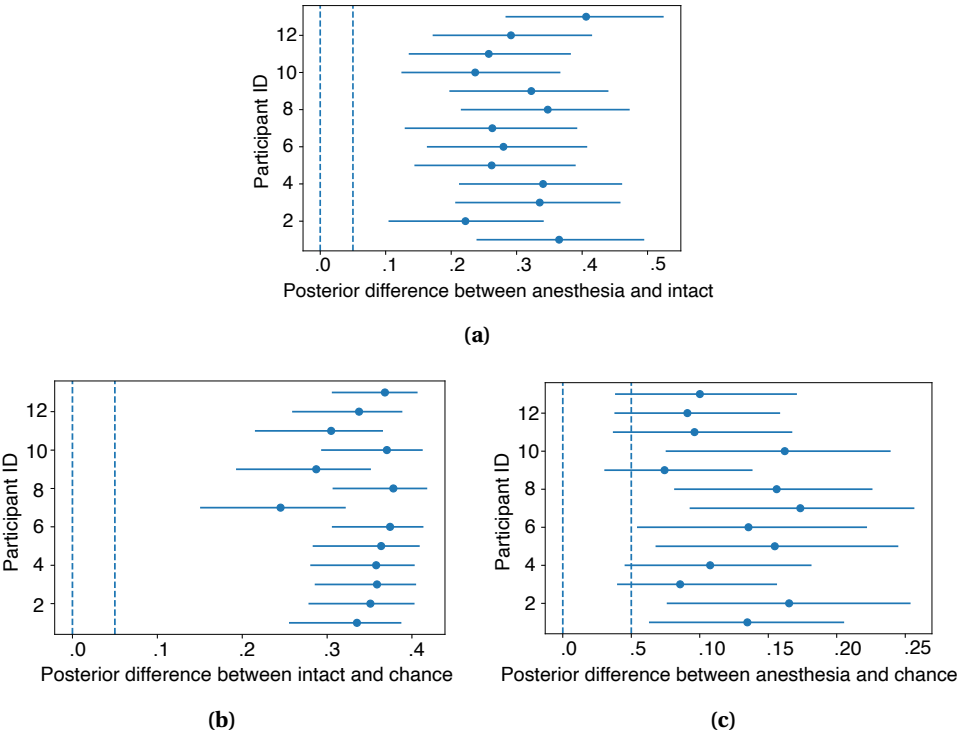
Figure 4.12. Softness discrimination–Posterior difference between (a) intact and anesthesia, (b) intact and chance, and (c) anesthesia and chance.

(a)

(b)

(c)
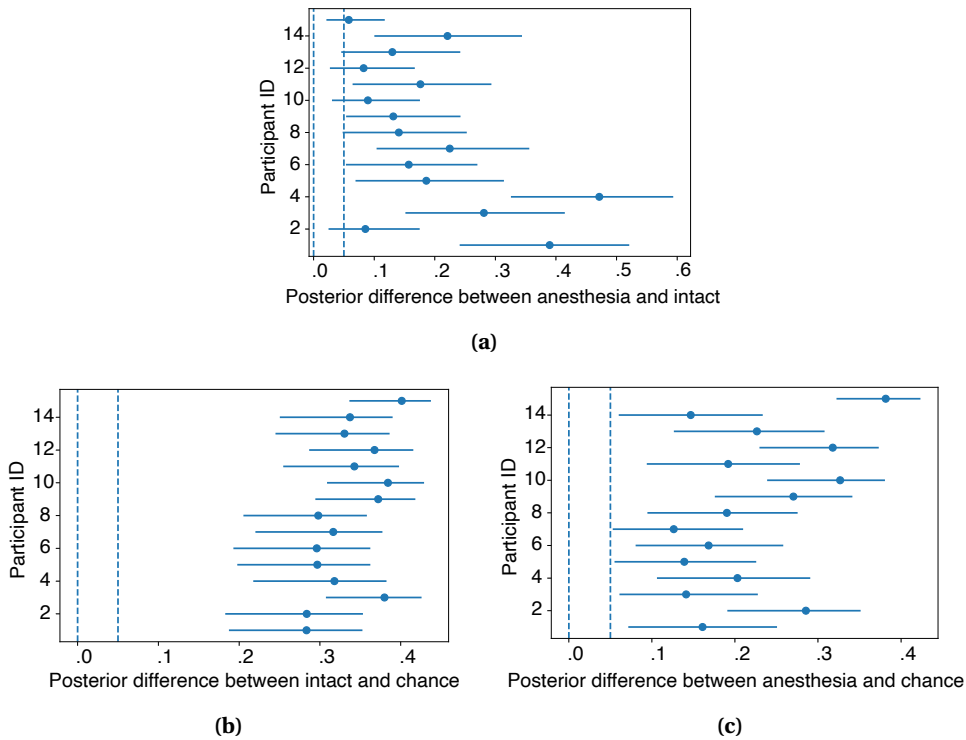
Figure 4.13. Roughness discrimination–Posterior difference between (a) intact and anesthesia, (b) intact and chance, and (c) anesthesia and chance.

Figure 4.12 and Figure 4.13 show how the uncertainty of each individual participant's data is much greater than the aggregate data, resulting in wider HDIs. For softness discrimination, all individual HDIs lie entirely outside the ROPE when comparing the two conditions. Therefore, we can conclude that the conditions differ for each individual participant (Figure 4.12a). Similarly, we can conclude that softness discrimination differed significantly from chance for each individual in the intact condition (Figure 4.12b). However, in the anesthesia condition, 6 out of 13 HDIs do not entirely lie outside the ROPE when comparing the model's predictions to chance. For these individuals, we therefore cannot conclude whether their discrimination was different from chance. For roughness discrimination, on the other hand, discrimination was above chance level for all individuals in both conditions (Figure 4.13b and Figure 4.13c). Because the HDIs of 6 participants do not lie completely outside the ROPE in the posterior difference between the conditions, however (cf. Figure 4.13a), we cannot conclude whether discrimination was different or not between the two conditions for these individuals. As did the individual model predictions, Figure 4.13a testifies to a large between-subject variability in the difference between the two conditions for roughness discrimination.

In summary, the analysis revealed a significant difference between anesthesia and intact conditions for both tasks. This difference was very large for softness discrimination, showing an overall difference of 30% between conditions and only minor variation from chance for some participants. For roughness discrimination, on the other hand, the difference between conditions was 19% on average but varied largely between participants, with some participants showing highly similar roughness judgments under both conditions while other participants showed substantially disrupted roughness discrimination under anesthesia. Finally, two participants showed a stable but highly modified (inverse) roughness discrimination under anesthesia.

4.3.5. CONFIDENCE RATINGS AND RESPONSE TIMES

Mean confidence ratings were calculated after the exclusion of the two participants who had erroneously discriminated smoothness rather than softness.

A 2×2 repeated measures ANOVA for the confidence ratings revealed a significant main effect of condition $F(1, 12) = 27.63, p = 0.00020, \eta^2 = 0.245$ with higher confidence ratings for the intact condition $M = 5.58, SD = 1.26$ than for the anesthesia condition $M = 4.17, SD = 1.23$, and a main effect of task $F(1, 12) = 39.02, p = 0.0000428, \eta^2 = 0.049$ with higher ratings for the roughness task $M = 5.16, SD = 1.19$ than for the softness task $M = 4.60, SD = 1.12$ overall. A significant interaction effect of condition and task was also found $F(1, 12) = 8.30, p = 0.014, \eta^2 = 0.034$. Bonferroni-corrected post-hoc pairwise comparisons indicated that the effect of task was specific to the anesthesia condition, where all $p < 0.05$ except for the difference between the two intact conditions ($p = 1$; cf. Figure 4.14).
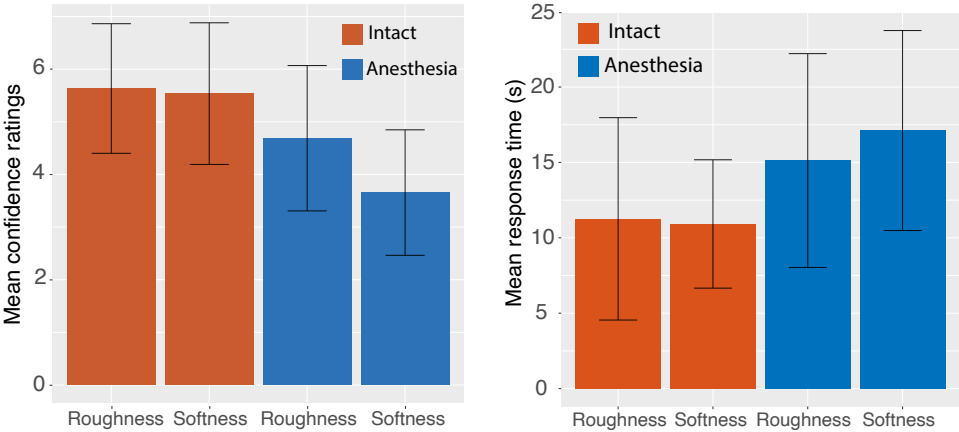

Figure 4.14. Mean confidence ratings (left), provided on a Likert scale from 1 to 9, and response times (right) per task and condition. Error bars indicate the standard deviation from the mean. Plots showing individual-level confidence ratings are available in Figure H.5 in Appendix H.

Mean response time (measured from the start of the trial until response given) for the intact condition was 11.26 ($SD = 6.71$) for the roughness estimates and 10.92 ($SD = 4.26$) for the softness estimates. For the anesthesia condition, these values rose to 15.13 ($SD = 7.09$) and 17.11 ($SD = 6.63$) respectively.

A 2×2 repeated measures ANOVA for response time revealed a significant main effect of condition $F(1, 12) = 29.77$, $p = 0.00015$, $\eta^2 = 0.15$, with longer response times for the anesthesia condition $M = 16.12$, $SD = 5.42$ than for the intact condition $M = 11.09$, $SD = 5.42$. No other significant main effects or interactions were found (all $p > 0.05$; cf. Figure 4.14).

4.4. DISCUSSION

We investigated the contribution of propagating vibratory cues to the perception of roughness and softness of surfaces, varying in their statistical microscale roughness and elasticity. Participants carried out a roughness and softness discrimination task, once with intact sensation and once under local anesthesia of their index finger. Our analysis supported a model of a significant difference between the intact and anesthesia conditions on a group level for both tasks. However, while softness discrimination was largely disrupted under local anesthesia, with all participants showing either a large drop or complete loss of discriminability in this condition, all participants were able to carry out the roughness task well above chance level in the anesthesia condition. However, a large between-subject variability was observed for roughness discrimination under local anesthesia.

The above observations were in accordance with the changes observed in the confidence ratings. Confidence ratings were significantly higher in the intact condition than in the anesthesia condition for both tasks and approximately similar for the two tasks in the intact condition. Under anesthesia, however, confidence ratings were significantly lower for the softness task than for the roughness task, demonstrating that discriminating softness was in general perceived as more challenging than roughness under anesthesia.

Finally, and contrary to our second hypothesis, we did not observe any joint influence of the two stimulus parameters on the perceptual outcome beyond individual differences. Roughness discrimination was thus primarily dominated by changes in the surface topography (Hurst exponent), while softness discrimination was dominated by changes in the material properties (Shore value). The results are discussed in detail below.

4.4.1. SOFTNESS DISCRIMINATION UNDER LOCAL ANESTHESIA

A significant drop or complete loss of the discrimination ability was found for all participants in the softness task. Considering that softness cues tend to be extracted using pressing/indentation [57], it seems unsurprising at first that participants' discrimination ability of softness suffered markedly when local tactile cues were removed, as these interaction modes do not result in extensive vibratory cues. This is furthermore in line with the findings reported by Srinivasan and LaMotte [26], who

found that participants were unable to extract the softness of flat deformable surfaces under local anesthesia. However, Srinivasan and LaMotte [26] were interested in addressing the role of kinaesthetic information alone for the task. They therefore explicitly instructed participants *not* to use lateral force and implemented measures to avoid vibratory cues. In the present study, participants were encouraged to explore the samples using their most intuitive and natural interactions to perform the task, as we were interested in seeing whether they would naturally adapt their strategy and find alternative ways of extracting the relevant information under local anesthesia. Furthermore, as opposed to the stimuli used in previous work, our stimuli did not only vary in their elasticity but were textured surfaces, potentially allowing for additional cues during dynamic exploration. However, although two participants did adapt their exploration strategies from pressing in the intact condition to rubbing/stroking under local anesthesia, the remaining participants maintained their original strategy, verifying this as the preferred exploration strategy for extracting softness information [57], even when relevant cues might have been accessible using other exploration modes. The two participants who employed lateral motion in the anesthesia condition did seem to achieve a higher discriminability of the space than most other participants (cf. participants 5 and 8 in Figure H.1 in Appendix H). This suggests that propagating waves generated by stroking in the absence of local skin information may provide a relevant, albeit disempowered, cue to softness discrimination. However, no firm conclusions can be drawn from solely two participants, and discrimination was considerably constrained for even these participants.

A conceivable conclusion of these results would therefore be that information about the softness of compliant surfaces does not transmit well via propagating vibration in the hand. However, it is possible to discriminate the softness of compliant surfaces using a tool, particularly using dynamic exploration modes like tapping [58], but also using pressing (albeit with a reduced sensitivity) [29]. In fact, discrimination of softness is even possible 'passively', when a compliant object is tapped against a handheld stylus [58]. These findings suggest that information about the softness of objects is well-transmittable via vibration under the right conditions (although the influence of local-skin deformations caused by the handheld stylus cannot be ruled out completely). It is therefore possible that participants were either unable to generate these cues with their bare finger and with the stimulus range provided in the present study, or unable to attribute the cues generated in a task-relevant manner.

It must be noted here that the stimuli used in the present study were considerably stiffer than the human finger pad itself. While pilot studies (and the intact condition in the present study) had confirmed that differences in elasticity were well-discriminable using direct interactions, participants used relatively high forces to carry out the task (cf. Figure 4.5). Furthermore, it has been argued that materials tend to be perceived as soft when the compliance is greater than the human finger during direct interactions [59]. Consequently, most studies investigating the perception of softness have used more elastic stimulus material (e.g., [26, 58, 60]).

Moreover, in comparing the direct interactions carried out under local anesthesia in the present study with indirect interactions using a tool, most everyday tools, including the stylus referenced by LaMotte [26], exhibit significantly greater rigidity

compared to the human finger. This characteristic not only enhances the ability to manipulate various objects in our surroundings but can also improve the transmission of vibratory signals to the hand. As a result, the vibratory feedback experienced through direct versus indirect touch can be markedly different, even during otherwise identical interactions [10, 61]. Tapping with a stylus compared to a finger does, for instance, not only result in very different peak frequencies, but the vibrations produced by indirect touch also tend to propagate further, to digits that are not in contact with the stylus [10]). It has thus been argued that the human somatosensory system is exquisitely tuned to the sensing with uniformly rigid rods by decoding vibratory patterns as they come into contact with objects [62–65]. Even if the right interactions may have been carried out in the present study by some participants, producing vibration cues that were pertinent to the task using only the finger proved inadequate. It is therefore possible that the finger's mechanical properties did not preserve or transform vibratory information about the softness of the stimuli as effectively as a tool might have done before these signals reached the hand.

In addition to the potential challenge of transmitting vibratory information about the softness of compliant stimuli through the human finger, it is possible that observers lacked the necessary training to effectively utilize this information, even when it was available. This could be due to the irrelevance of this cue in everyday life contexts, where more accessible cues such as skin deformation are available. The fact that a subset of participants was able to still pick up some softness cues under local anesthesia (reached a probability of at least 75%), supports this hypothesis. For these participants, the task was not completely impossible but very difficult, even when the right interactions were carried out.

Further research using more elastic stimulus material or prompted dynamic interactions with the stimulus material will have to clarify these questions.

4.4.2. ROUGHNESS DISCRIMINATION UNDER LOCAL ANESTHESIA

For roughness discrimination, most participants either maintained a comparable discrimination ability or displayed a reduced but still reliable discrimination under local anesthesia. However, for three participants, discrimination was largely disrupted (no probability levels of 75% or more), while for two subjects, discrimination was stable but strongly modified, with the model predictions displaying a seemingly inverse pattern (cf. participants 1 and 4 in Figure H.2). Potential reasons for this large between-subject variability are discussed below.

BETWEEN-SUBJECT VARIABILITY IN DISCRIMINATING ROUGHNESS UNDER LOCAL ANESTHESIA

The fact that some participants displayed a highly similar roughness discrimination in both conditions suggests that sufficient task-relevant cues must have been available remotely, provided that the right interactions were carried out. However, the large between-subject variability in the anesthesia condition indicates differences in participants' ability to create or extract task-relevant cues based solely on propagating

information (cf. Figure H.2 & Figure 4.13). We believe that this variability may have been caused by multiple factors.

First, a certain increase in noise in the anesthesia condition is unsurprising due to the novel experience of having an anesthetized finger as well as the biomechanical changes that inevitably followed the nerve block. The swelling of the finger from the injection will likely have influenced the propagation of vibratory information due to changes in both geometrical and mechanical properties of the finger. Furthermore, the significantly decreased hydration level of the finger pad in the anesthesia condition (cf. Figure 4.4) will have affected the friction dynamics during exploration of the surfaces. Decreased sweat-gland activity has previously been associated with a decreased coefficient of friction [66–68]. Normally, fingertip moisture levels are modulated actively during interactions with objects to optimize friction dynamics [69]. Hindering this function via the nerve block will inevitably have induced some changes in the skin-object dynamics during the interactions. More specifically, the decreased sweating of the finger in the anesthesia condition will have resulted in less adhesion, which consequently may also have impacted ploughing events. Some of these differences are apparent from the tribometer data, which revealed a significant increase in normal load and decrease in velocity, and, importantly, the coefficient of friction of interactions in the anesthesia condition compared to the intact condition. Although our sense of touch is remarkably good at adapting to changes in sensing conditions and humans readily optimize their behavior to generate the most relevant cues under changing conditions, it is possible that some participants adjusted more efficiently to the novel state in our study than others. However, a closer analysis of individual differences in the mechanical cues generated during the interactions would have to verify this.

A further possibility is that, albeit task-relevant cues may have been equally available to all participants, not all participants were able to discern and attribute them equally well. Given the likely redundancy of vibratory cues in many (but not all!) everyday-life haptic interactions, individual differences may be present in the weight these cues are normally given. This could result in some participants being more acquainted than others with the use of vibratory cues for certain perceptual judgments such as discerning textural properties. One observation endorsing this latter hypothesis is the two participants that displayed a seemingly inverse pattern of roughness discrimination in the anesthesia condition compared to the intact condition. These two participants consistently perceived samples with a lower microscale roughness (larger Hurst exponent) as rougher, albeit with diminished discriminability (cf. participants 1 and 4 in Figure H.1). In addition, these two participants also displayed a shift in the weight of the cues used for the task, where softer samples (with lower Shore values) were perceived as rougher than harder samples. While stimulus-dependent cues were therefore clearly present and discernible for these participants, they were not linked to the perceptual attribute (i.e., roughness) in the same manner as in the intact condition. Both participants showed no visible difference in their confidence ratings between the two conditions (cf. participants 1 and 4 in Figure H.5), indicating that they felt confident about their percept. In fact, one of these participants, unprompted, described how they

experienced the task to be simpler under local anesthesia than in the intact condition, "*as if the anesthesia acted as a filter leaving only one type of information to attend to*".

However, despite these individual differences, we can conclude that complex roughness information from several length scales can propagate well through the human finger and constitute a sufficient and invariant cue to roughness perception under certain conditions.

PROPAGATION WAVES AS INVARIANT ROUGHNESS CUE

A key aspect of the present study is that the stimuli used were more complex than the fine sandpapers used in a previous study that showed intact discrimination of roughness under local anesthesia of a finger [25]. The roughness of sandpapers is determined solely by it's grit size, and even under intact conditions, discrimination of such fine surfaces is often said to rely solely on vibratory information, or on what has been termed temporal coding mechanisms (e.g., [15, 16]). Therefore, observers are likely to be accustomed to using this information for perceptual judgments of such stimuli. In contrast, the roughness of the stimuli used in the present study varied on different length scales in a similar manner as many natural surfaces, with variations ranging from 0.03 mm to 5 mm, and the stimuli additionally co-varied in their elasticity. In the intact condition, it is therefore highly likely that spatial and temporal coding mechanisms worked together in creating the tactile representations of surface roughness. When interacting with the stimuli under local anesthesia, however, all features were inevitably reduced to vibration. It is therefore remarkable that roughness discrimination remained intact for some participants under these conditions.

While there has long been an agreement that "temporal" (i.e., vibration) coding is necessary and sufficient for roughness discrimination of fine surfaces, recent research has cast doubt on this consensus. The replaying of recordings of skin vibrations is, for instance, insufficient to reliably induce the percept of natural textures or their roughness [70, 71]. Additionally, the invariance of haptic texture perception to conditions such as speed and pressure [8, 24], which highly affect the spectra of the skin vibrations created, has reopened the question as to whether some type of spatial encoding may be involved in the perception of fine textures after all. Most recently, a study by Grigorii et al. [72] demonstrated that, next to temporal factors (i.e., the frequency of vibration), local skin deformations down to 9μm can mediate roughness perception, underscoring the potential role of spatially distributed skin stretch in the perception of even very fine surface features. However, while our results do not call the influence of local skin cues under intact conditions into question, they do provide strong evidence that propagating vibratory information alone can provide a sufficient and invariant cue for the roughness discrimination of more naturalistic and complex stimuli than has previously been shown. While spatial variations within the finger pad can thus play a role when available, they are not a necessary cue for roughness discrimination of non-periodic surfaces involving variations on both smaller and larger length scales during free explorations with the finger. Our findings are thus in line with previous research indicating that the biomechanical properties of the human hand effectively compress tactile information, facilitating subsequent perceptual processes [7, 11, 14].

It has previously been suggested that propagation waves may play a fundamental role in roughness- or general texture constancy/invariance, that is, the ability to perceive textures in a stable manner across changes in physical conditions, such as the scanning velocity or force [5, 23, 24, 73, 74]. Delhaye et al [5] have operationalized this as "*the brain's ability to access specific attributes of the invariant surface descriptor through the temporal gradient*" (p.3). Our findings corroborate these results. In conjunction with the studies showing that vibration alone is insufficient to reliably reproduce the roughness of textures [70, 71], our results further indicate that some type of information about the scanning velocity might be crucial for invariant, time-free (spatiotopic) representations of surfaces or their roughness. This could be through local tactile cues in studies that have used passive scanning (e.g., [24]) or via self-generated voluntary movements (c.f., [75]); the latter of which should be available even in a context where local information is diminished, as in the present study. However, future research would have to verify this.

4.4.3. NO EVIDENCE OF CUE FUSION

A secondary aim of the present study was to explore any interactions between the two stimulus cues – the microscale surface topography determined by the Hurst exponent and the material elasticity – in shaping the perceptual outcome (roughness and softness discrimination). We hypothesized that in combining these two cues, we might reveal regions where different cue combinations yield identical perceptual outcomes (i.e., metamers, cf. Figure 4.1). More specifically, we had hypothesized that variations in the sample elasticity might interact with variations in the Hurst exponent in determining roughness discrimination. No specific hypothesis was made about the influence of the Hurst exponent on the perceived softness of the surfaces, although effects of surface texture on the perceived softness of hard materials have been suggested [76] and it is known that the shape of a surface can sometimes affect softness perception [77]. A preliminary ranking task had confirmed that different surfaces of the same elasticity could be discriminated by pressing, while different elasticities with the same surface statistics could be discriminated via stroking. However, our analysis found no evidence to support such mixed-cue effects in the present data. While softness discrimination was primarily governed by changes in the Shore value, roughness discrimination was governed by changes in the Hurst exponent. Solely minor influences of "the other cue" were visible for individual participants in a non-systematic manner.

One possible interpretation of these findings would therefore be that microscale surface roughness does not constitute a relevant cue for tactile softness discrimination, just as material elasticity does not constitute a relevant cue for tactile roughness discrimination. Such a conclusion would suggest that individuals are able to disregard these "irrelevant" cues when making perceptual judgments about softness and roughness. However, our conclusions are confined to the specific stimulus range investigated in this study. It therefore remains conceivable that cue confounds could emerge within a different stimulus range, such as a different range of material elasticity or a different scale of surface features than the ones used here. It must

in this context specifically be repeated that the stimuli used in the present study were significantly more rigid than the human finger, which may have impacted these results. Despite each stimulus parameter being distinguishable through both stroking and pressing, as our pilot study indicated, the *salience* of the other cue may have rendered these differences negligible. Future research should address this further by probing different stimulus ranges before concluding that no mixed-cue effects exist between microscale surface roughness and material elasticity in determining roughness and softness perception.

4.4.4. LIMITATIONS OF THE PRESENT STUDY

The variability observed between subjects in this study remained unexplained, highlighting a significant limitation of the study. This variability emphasized the need for more controlled interaction conditions, potentially at the expense of ecological validity, or a detailed characterization of the proximal stimulus during free explorations to address individual differences effectively. An initial objective of this study was to collect vibration data at multiple sites on the hand using an array of accelerometers during interactions with these textures. However, the COVID-19 pandemic introduced unexpected material shortages, preventing our grant partners from supplying the planned equipment for these measurements. In response, our research team developed an alternative strategy to gather mechanical data from two critical sites: at an early interaction stage using a custom-made load platform and tribometer and at a distal location on the hand, using a single accelerometer. This method focused on quantifying the vibrations that propagated to intact areas of the hand during local anesthesia. Nevertheless, we encountered technical issues, including equipment failure and compromised data integrity, which presented further challenges in the processing of these data. The majority of these data are therefore left out in the presented work, constituting the main limitation of this study. This experience emphasizes the importance of developing well-characterized, robust, and standardized research equipment available to haptic perceptual scientists.

4.5. CONCLUSIONS AND FUTURE WORK

This study has demonstrated that roughness discrimination of complex, naturalistic surfaces can remain intact even when local tactile feedback is compromised due to local anesthesia for *some* participants. Propagation waves can therefore convey complex, non-periodic, roughness information from different length scales, and the somatosensory system is able to collect this information from sources other than afferents located in the finger itself. Conversely, the ability to discern softness was more generally impaired under the same conditions, despite some participants retaining a modicum of this capability, likely through dynamic explorations.

However, a large between-subject variability in the ability to discriminate roughness under local anesthesia raised questions about the specific circumstances enabling this roughness invariance. While these differences might be attributable to variability arising at the level of the proximal stimulus or an early biomechanical level, indicating

differing access to task-relevant cues, some evidence in the present data suggests variability at a perceptual level, indicating differing interpretations of available cues. However, future research should aim to elucidate the conditions under which this textural invariance is conserved in propagation waves and when it breaks down. A first step in doing so could be to employ constrained interaction modes with similarly complex stimuli under local anesthesia. While compromising on ecological validity, this would allow for a direct investigation of the role of different interaction modes (such as stroking, tapping, or pressing) in eliciting task-relevant cues and provide increased control over the possible input features created during these interactions. A further crucial step would be a more detailed account of the proximal stimulus, that is, the mechanical input features generated during interactions with the stimuli. While the present study provided initial insights from the platforms in which the stimuli were mounted during the interactions, we were not able to characterize any mechanical input characteristics propagating to intact sites of the hand as initially planned. A more detailed account would entail combining perceptual validation like in the present study with a precise characterization of the propagation waves created during these interactions. Not only at the stimulus level but also at remote locations on participants, such as areas in the hand unaffected by the local anesthesia of the finger. Ultimately, a better understanding of these mechanisms could have significant implications for enhancing feedback on material properties in sensorimotor control applications, particularly for individuals using prosthetic limbs.

Finally, the present study did not reveal any joint influence of elasticity on roughness perception or microscale surface features on softness perception. To definitively determine whether such areas of joint influence exist, it would be essential to explore a broader range of the two stimulus parameters.

REFERENCES

[1] Johansson, R. S. and Flanagan, J. R. Coding and use of tactile signals from the fingertips in object manipulation tasks. *Nature Reviews. Neuroscience* **10** (2009), 345–359. DOI: 10.1038/nrn2621.

[2] Moscatelli, A., Bianchi, M., Serio, A., Terekhov, A., Hayward, V., Ernst, M. O., and Bicchi, A. The change in fingertip contact area as a novel proprioceptive cue. *Current Biology* **26** (2016), 1159–1163. DOI: 10.1016/j.cub.2016.02.052.

[3] Delhaye, B., Lefèvre, P., and Thonnard, J.-L. Dynamics of fingertip contact during the onset of tangential slip. *Journal of the Royal Society, Interface* **11** (2014), 20140698. DOI: 10.1098/rsif.2014.0698.

[4] Saal, H., Birznieks, I., and Johansson, R. How viscoelasticity affects tactile neuron signaling. *eLife* **12** (2023), RP89616. DOI: 10.1101/2023.05.15.540820.

[5] Delhaye, B., Hayward, V., Lefèvre, P., and Thonnard, J.-L. Texture-induced vibrations in the forearm during tactile exploration. *Frontiers in Behavioral Neuroscience* **6** (2012). DOI: 10.3389/fnbeh.2012.00037.

[6] Kirsch, L. P., Job, X. E., Auvray, M., and Hayward, V. Harnessing tactile waves to measure skin-to-skin interactions. *bioRxiv* (2020), 2020.05.20.105817. DOI: 10.1101/2020.05.20.105817.

[7] Manfredi, L. R., Baker, A. T., Elias, D. O., Iii, J. F. D., Zielinski, M. C., Polashock, V. S., and Bensmaia, S. J. The effect of surface wave propagation on neural responses to vibration in primate glabrous skin. *PLOS ONE* **7** (2012), e31203. DOI: 10.1371/journal.pone.0031203.

[8] Manfredi, L. R., Saal, H. P., Brown, K. J., Zielinski, M. C., Dammann, J. F., Polashock, V. S., and Bensmaia, S. J. Natural scenes in tactile texture. *Journal of Neurophysiology* **111** (2014), 1792–1802. DOI: 10.1152/jn.00680.2013.

[9] Tanaka, Y., Horita, Y., and Sano, A. "Finger-Mounted Skin Vibration Sensor for Active Touch". In: Haptics: Perception, Devices, Mobility, and Communication. Ed. by Hutchison, D., Kanade, T., Kittler, J., Kleinberg, J. M., Mattern, F., Mitchell, J. C., Naor, M., Nierstrasz, O., Pandu Rangan, C., Steffen, B., Sudan, M., Terzopoulos, D., Tygar, D., Vardi, M. Y., Weikum, G., Isokoski, P., and Springare, J. Vol. 7283. Berlin, Heidelberg: Springer Berlin Heidelberg, 2012, pp. 169–174. DOI: 10.1007/978-3-642-31404-9_29.

[10] Shao, Y., Hayward, V., and Visell, Y. Spatial patterns of cutaneous vibration during whole-hand haptic interactions. *Proceedings of the National Academy of Sciences* **113** (2016), 4188–4193. DOI: 10.1073/pnas.1520866113.

[11] Shao, Y., Hayward, V., and Visell, Y. Compression of dynamic tactile information in the human hand. *Science Advances* **6** (2020), eaaz1158. DOI: `10.1126/sciadv.aaz1158`.

[12] Mackevicius, E. L., Best, M. D., Saal, H. P., and Bensmaia, S. J. Millisecond precision spike timing shapes tactile perception. *Journal of Neuroscience* **32** (2012), 15309–15317. DOI: `10.1523/JNEUROSCI.2161-12.2012`.

[13] Pubols, B. H. Effect of mechanical stimulus spread across glabrous skin of raccoon and squirrel monkey hand on tactile primary afferent fiber discharge. *Somatosensory Research* **4** (1987), 273–308. DOI: `10.3109/07367228709144611`.

[14] Andrews, J. W., Adams, M. J., and Montenegro-Johnson, T. D. A universal scaling law of mammalian touch. *Science Advances* **6** (2020), eabb6912. DOI: `10.1126/sciadv.abb6912`.

[15] Hollins, M. and Risner, S. R. Evidence for the duplex theory of tactile texture perception. *Perception & Psychophysics* **62** (2000), 695–705. DOI: `10.3758/bf03206916`.

[16] Hollins, M. and Bensmaïa, S. J. The coding of roughness. *Canadian Journal of Experimental Psychology = Revue Canadienne De Psychologie Experimentale* **61** (2007), 184–195. DOI: `10.1037/cjep2007020`.

[17] Blake, D., Hsiao, S., and Johnson, K. Neural coding mechanisms in tactile pattern recognition: the relative contributions of slowly and rapidly adapting mechanoreceptors to perceived roughness. *The Journal of Neuroscience* **17** (1997), 7480–9. DOI: `10.1523/JNEUROSCI.17-19-07480.1997`.

[18] Gescheider, G. A. Evidence in support of the duplex theory of mechanoreception. *Sensory Processes* **1** (1976), 68–76.

[19] Hollins, M., Bensmaïa, S. J., and Washburn, S. Vibrotactile adaptation impairs discrimination of fine, but not coarse, textures. *Somatosensory & Motor Research* **18** (2001), 253–262. DOI: `10.1080/01421590120089640`.

[20] Katz, D., Krueger, L. E., and Krueger, L. E. *The World of Touch.* New York: Psychology Press, 1989. DOI: `10.4324/9780203771976`.

[21] Saal, H. P. and Bensmaia, S. J. Touch is a team effort: interplay of submodalities in cutaneous sensibility. *Trends in Neurosciences* **37** (2014), 689–697. DOI: `10.1016/j.tins.2014.08.012`.

[22] Weber, A. I., Saal, H. P., Lieber, J. D., Cheng, J.-W., Manfredi, L. R., Dammann, J. F., and Bensmaia, S. J. Spatial and temporal codes mediate the tactile perception of natural textures. *Proceedings of the National Academy of Sciences of the United States of America* **110** (2013), 17107–17112. DOI: `10.1073/pnas.1305509110`.

[23] Yoshioka, T., Craig, J. C., Beck, G. C., and Hsiao, S. S. Perceptual constancy of texture roughness in the tactile system. *The Journal of Neuroscience: The Official Journal of the Society for Neuroscience* **31** (2011), 17603–17611. DOI: `10.1523/JNEUROSCI.3907-11.2011`.

4

[24] Boundy-Singer, Z. M., Saal, H. P., and Bensmaia, S. J. Speed invariance of tactile texture perception. *Journal of Neurophysiology* **118** (2017), 2371–2377. DOI: `10.1152/jn.00161.2017`.

[25] Libouton, X., Barbier, O., Berger, Y., Plaghki, L., and Thonnard, J.-L. Tactile roughness discrimination of the finger pad relies primarily on vibration sensitive afferents not necessarily located in the hand. *Behavioural Brain Research* **229** (2012), 273–279. DOI: `10.1016/j.bbr.2012.01.018`.

[26] Srinivasan, M. A. and LaMotte, R. H. Tactual discrimination of softness. *Journal of Neurophysiology* **73** (1995), 88–101. DOI: `10.1152/jn.1995.73.1.88`.

[27] Ikeda, A., Suzuki, T., Takamatsu, J., and Ogasawara, T. "Producing Method of Softness Sensation by Device Vibration". In: 2013 IEEE International Conference on Systems, Man, and Cybernetics. 2013, pp. 3384–3389. DOI: `10.1109/SMC.2013.577`.

[28] Kildal, J. "3D-press: haptic illusion of compliance when pressing on a rigid surface". In: International Conference on Multimodal Interfaces and the Workshop on Machine Learning for Multimodal Interaction. ICMI-MLMI '10. New York, NY, USA: Association for Computing Machinery, 2010, pp. 1–8. DOI: `10.1145/1891903.1891931`.

[29] Visell, Y., Giordano, B. L., Millet, G., and Cooperstock, J. R. Vibration influences haptic perception of surface compliance during walking. *PloS One* **6** (2011), e17697. DOI: `10.1371/journal.pone.0017697`.

[30] Visell, Y. and Okamoto, S. "Vibrotactile Sensation and Softness Perception". In: Multisensory Softness: Perceived Compliance from Multiple Sources of Information. Ed. by Di Luca, M. Springer Series on Touch and Haptic Systems. London: Springer, 2014, pp. 31–47. DOI: `10.1007/978-1-4471-6533-0_3`.

[31] Persson, B. N. J. On the fractal dimension of rough surfaces. *Tribology Letters* **54** (2014), 99–106. DOI: `10.1007/s11249-014-0313-4`.

[32] Callier, T., Saal, H. P., Davis-Berg, E. C., and Bensmaia, S. J. Kinematics of unconstrained tactile texture exploration. *Journal of Neurophysiology* **113** (2015), 3013–3020. DOI: `10.1152/jn.00703.2014`.

[33] Oldfield, R. C. The assessment and analysis of handedness: The Edinburgh inventory. *Neuropsychologia* **9** (1971), 97–113. DOI: `10.1016/0028-3932(71)90067-4`.

[34] Taylor, A. and McLeod, G. Basic pharmacology of local anaesthetics. *BJA Education* **20** (2020), 34–41. DOI: `10.1016/j.bjae.2019.10.002`.

[35] Shibasaki, M. and Crandall, C. G. Mechanisms and controllers of eccrine sweating in humans. *Frontiers in bioscience (Scholar edition)* **2** (2010), 685–696.

4

[36] Müser, M. H., Dapp, W. B., Bugnicourt, R., Sainsot, P., Lesaffre, N., Lubrecht, T. A., Persson, B. N. J., Harris, K., Bennett, A., Schulze, K., Rohde, S., Ifju, P., Sawyer, W. G., Angelini, T., Ashtari Esfahani, H., Kadkhodaei, M., Akbarzadeh, S., Wu, J.-J., Vorlaufer, G., Vernes, A., Solhjoo, S., Vakis, A. I., Jackson, R. L., Xu, Y., Streator, J., Rostami, A., Dini, D., Medina, S., Carbone, G., Bottiglione, F., Afferrante, L., Monti, J., Pastewka, L., Robbins, M. O., and Greenwood, J. A. Meeting the contact-mechanics challenge. *Tribology Letters* **65** (2017), 118. DOI: 10.1007/s11249-017-0900-2.

[37] Chen, S., Li, K., Qiao, X., Ru, W., and Xu, L. Tactile perception of fractal surfaces: An EEG-fNIRS study. *Tribology International* **180** (2023), 108266. DOI: 10.1016/j.triboint.2023.108266.

[38] Sahli, R., Prot, A., Wang, A., Müser, M. H., Piovarči, M., Didyk, P., and Bennewitz, R. Tactile perception of randomly rough surfaces. *Scientific Reports* **10** (2020), 15800. DOI: 10.1038/s41598-020-72890-y.

[39] Wolfe, S. W., Pederson, W. C., Kozin, S. H., and Cohen, M. S. *Green's Operative Hand Surgery*. Elsevier Health Sciences, 2021.

[40] Shaffer, S., Harrison, A., Brown, K., and Brennan, K. Reliability and validity of semmes-weinstein monofilament testing in older community-dwelling adults. *Journal of Geriatric Physical Therapy* **28** (2005), 112.

[41] Olaleye, D., Perkins, B. A., and Bril, V. Evaluation of three screening tests and a risk assessment model for diagnosing peripheral neuropathy in the diabetes clinic. *Diabetes Research and Clinical Practice* **54** (2001), 115–128. DOI: 10.1016/s0168-8227(01)00278-9.

[42] Park, J. H. and Kim, D. S. The necessity of the simple tests for diabetic peripheral neuropathy in type 2 diabetes mellitus patients without neuropathic symptoms in clinical practice. *Diabetes & Metabolism Journal* **42** (2018), 442–446. DOI: 10.4093/dmj.2017.0090.

[43] Edin, B. B. and Abbs, J. H. Finger movement responses of cutaneous mechanoreceptors in the dorsal skin of the human hand. *Journal of Neurophysiology* **65** (1991), 657–670. DOI: 10.1152/jn.1991.65.3.657.

[44] Terekhov, A. V. and Hayward, V. The brain uses extrasomatic information to estimate limb displacement. *Proceedings of the Royal Society B: Biological Sciences* **282** (2015), 20151661. DOI: 10.1098/rspb.2015.1661.

[45] Browder, J., Bochereau, S., van Beek, F., and King, R. "Stiffness in Virtual Contact Events: A Non-Parametric Bayesian Approach". In: 2019 IEEE World Haptics Conference (WHC). Tokyo, Japan: IEEE, 2019, pp. 515–520. DOI: 10.1109/WHC.2019.8816102.

[46] Owen, L., Browder, J., Letham, B., Stocek, G., Tymms, C., and Shvartsman, M. Adaptive nonparametric psychophysics. *arXiv* (2021). DOI: 10.48550/arXiv.2104.09549.

[47] Fagerland, M. W., Sandvik, L., and Mowinckel, P. Parametric methods outperformed non-parametric methods in comparisons of discrete numerical variables. *BMC Medical Research Methodology* **11** (2011), 44. DOI: `10.1186/1471-2288-11-44`.

[48] Hadzic, A., ed. *NYSORA textbook of regional anesthesia and acute pain management.* New York, N.Y.: McGraw-Hill Education LLC., 2007.

[49] Li, H., Hu, X., and Yang, S. The overall distribution pattern of the hand's cutaneous nerves and its clinical implications in sensory reconstruction. *International Journal of Morphology* **39** (2021), 447–454. DOI: `10.4067/S0717-95022021000200447`.

[50] Rasmussen, C. E. and Williams, C. K. I. *Gaussian processes for machine learning.* Adaptive computation and machine learning. Cambridge, Mass: MIT Press, 2006.

[51] Houlsby, N., Huszár, F., Ghahramani, Z., and Lengyel, M. Bayesian active learning for classification and preference learning. *ArXiv* (2011). DOI: `10.48550/arXiv.1112.5745`.

[52] Blei, D. M., Kucukelbir, A., and McAuliffe, J. D. Variational inference: A review for statisticians. *Journal of the American Statistical Association* **112** (2017), 859–877. DOI: `10.1080/01621459.2017.1285773`.

[53] Fawcett, T. An introduction to ROC analysis. *Pattern Recognition Letters.* ROC Analysis in Pattern Recognition **27** (2006), 861–874. DOI: `10.1016/j.patrec.2005.10.010`.

[54] Nahm, F. S. Receiver operating characteristic curve: overview and practical use for clinicians. *Korean Journal of Anesthesiology* **75** (2022), 25–36. DOI: `10.4097/kja.21209`.

[55] Jr, D. W. H., Lemeshow, S., and Sturdivant, R. X. *Applied Logistic Regression.* John Wiley & Sons, 2013.

[56] Kruschke, J. *Doing Bayesian data analysis: A tutorial with R, JAGS, and Stan, second edition.* 2014. DOI: `10.1016/B978-0-12-405888-0.09999-2`.

[57] Lederman, S. J. and Klatzky, R. L. Hand movements: A window into haptic object recognition. *Cognitive Psychology* **19** (1987), 342–368. DOI: `10.1016/0010-0285(87)90008-9`.

[58] LaMotte, R. H. Softness discrimination with a tool. *Journal of Neurophysiology* **83** (2000), 1777–1786. DOI: `10.1152/jn.2000.83.4.1777`.

[59] Friedman, R. M., Hester, K. D., Green, B. G., and LaMotte, R. H. Magnitude estimation of softness. *Experimental Brain Research* **191** (2008), 133–142. DOI: `10.1007/s00221-008-1507-5`.

[60] Zoeller, A. C. and Drewing, K. A systematic comparison of perceptual performance in softness discrimination with different fingers. *Attention, Perception, & Psychophysics* (2020). DOI: `10.3758/s13414-020-02100-4`.

[61] Klatzky, R. L., Lederman, S. J., Hamilton, C., Grindley, M., and Swendsen, R. H. Feeling textures through a probe: Effects of probe and surface geometry and exploratory factors. *Perception & Psychophysics* **65** (2003), 613–631. DOI: 10.3758/BF03194587.

[62] Imamizu, H., Miyauchi, S., Tamada, T., Sasaki, Y., Takino, R., and Kawato, M. Human cerebellar activity reflecting an acquired internal model of a new tool. *Nature* **403** (2000), 192–5.

[63] Kilteni, K. and Ehrsson, H. H. Sensorimotor predictions and tool use: Hand-held tools attenuate self-touch. *Cognition* **165** (2017), 1–9. DOI: 10.1016/j.cognition.2017.04.005.

[64] Miller, L. E., Montroni, L., Koun, E., Salemme, R., Hayward, V., and Farnè, A. Sensing with tools extends somatosensory processing beyond the body. *Nature* **561** (2018), 239–242. DOI: 10.1038/s41586-018-0460-0.

[65] Miller, L. E., Fabio, C., Ravenda, V., Bahmad, S., Koun, E., Salemme, R., Luauté, J., Bolognini, N., Hayward, V., and Farnè, A. Somatosensory cortex efficiently processes touch located beyond the body. *Current Biology* **29** (2019), 4276–4283.e5. DOI: 10.1016/j.cub.2019.10.043.

[66] Smith, A. M., Cadoret, G., and St-Amour, D. Scopolamine increases prehensile force during object manipulation by reducing palmar sweating and decreasing skin friction. *Experimental Brain Research* **114** (1997), 578–583. DOI: 10.1007/pl00005666.

[67] Buchholz, B., Frederick, L. J., and Armstrong, T. J. An investigation of human palmar skin friction and the effects of materials, pinch force and moisture. *Ergonomics* **31** (1988), 317–325. DOI: 10.1080/00140138808966676.

[68] Pasumarty, S. M., Johnson, S. A., Watson, S. A., and Adams, M. J. Friction of the human finger pad: Influence of moisture, occlusion and velocity. *Tribology Letters* **44** (2011), 117. DOI: 10.1007/s11249-011-9828-0.

[69] André, T., Lefèvre, P., and Thonnard, J.-L. Fingertip moisture is optimally modulated during object manipulation. *Journal of Neurophysiology* **103** (2010), 402–408. DOI: 10.1152/jn.00901.2009.

[70] Grigorii, R. V., Klatzky, R. L., and Colgate, J. E. Data-driven playback of natural tactile texture via broadband friction modulation. *IEEE transactions on haptics* **15** (2022), 429–440. DOI: 10.1109/TOH.2021.3130091.

[71] Wiertlewski, M., Lozada, J., and Hayward, V. The spatial spectrum of tangential skin displacement can encode tactual texture. *IEEE Transactions on Robotics* **27** (2011), 461–472. DOI: 10.1109/TRO.2011.2132830.

[72] Grigorii, R. V., Colgate, J. E., and Klatzky, R. The spatial profile of skin indentation shapes tactile perception across stimulus frequencies. *Scientific Reports* **12** (2022), 13185. DOI: 10.1038/s41598-022-17324-7.

[73] Lederman, S. J. and Taylor, M. M. Fingertip force, surface geometry, and the perception of roughness by active touch. *Perception & Psychophysics* **12** (1972), 401–408. DOI: 10.3758/BF03205850.

[74] Lieber, J. D. and Bensmaia, S. J. Emergence of an invariant representation of texture in primate somatosensory cortex. *Cerebral Cortex* **30** (2020), 3228–3239. DOI: `10.1093/cercor/bhz305`.

[75] Dione, M. and Wessberg, J. Human 8- to 10-Hz pulsatile motor output during active exploration of textured surfaces reflects the textures' frictional properties. *Journal of Neurophysiology* **122** (2019), 922–932. DOI: `10.1152/jn.00756.2018`.

[76] Sun, Q., Guo, J., and Okamoto, S. "Effects of surface textures and shapes on perceived softness of hard materials". In: International Symposium on Affective Science and Engineering ISASE2022. Japan Society of Kansei Engineering, 2022, pp. 1–4.

[77] Hartcher-O'Brien, J., Edin, B., and Hayward, V. "Shape-elasticity tactile confound". In: Hand, Brain and Technology: The Somatosensory System CSF Conferenc. 2018, p. 1.

4

5

MATERIAL-TEXTURE CONFOUNDS IN HAPTIC ROUGHNESS PERCEPTION DURING DIRECT AND INDIRECT TOUCH

Continuing the investigation into haptic texture and material perception in Chapter 3 and Chapter 4, Chapter 5 examines the combined effects of surface roughness and material elasticity in detail by addressing the questions: Does surface roughness provide a relevant cue to softness perception, and does material elasticity provide a relevant cue to roughness perception? And to what extent are these mechanisms local to the contact and invariant to contact conditions?

Authors: Karina Kirk Driller, Camille Fradet, Vincent Hayward and Jess Hartcher-O'Brien.

Abstract: In everyday interactions with objects, surface features rarely occur independently of other material properties, such as elasticity. Despite this, the combined influence of surface and material parameters on haptic surface and material perception has been little investigated. In this study, we explored the interdependent effects of surface roughness and material elasticity on the perceived roughness and softness (compliance) of stochastically rough, elastic surfaces. We used a two-alternative forced choice (2AFC) discrimination procedure within a non-parametric Bayesian inference framework across several discrimination experiments. These experiments spanned two stimulus sets (high and low elasticity), two interaction conditions (direct touch and indirect touch), and two discrimination tasks (softness and roughness). Our results reveal that variations in surface roughness and material elasticity can lead to perceptual roughness metamers, where different physical configurations of surface roughness and material compliance yield identical roughness perceptions. These metamers occur during both direct and indirect touch but depend on the relative stiffness of stimuli and probe. This phenomenon is not observed for the perception of softness. These findings underscore the multidimensional nature of roughness perception and highlight the importance of considering the combined effects of surface and material characteristics in haptic research and applications.

5.1. INTRODUCTION

Texture and material perception have been a matter of great interest in research on haptic perception. The perceptual dimensions *roughness/smoothness* and *hardness/softness* (also referred to as compliance) have often been argued to be the most salient dimensions for the discrimination of textures – sometimes alongside the dimensions *coldness/warmness* and *stickiness/slipperiness* – as revealed by research using multidimensional scaling methods (e.g., [1–4]). Consequently, the haptic perceptions of roughness and softness have been studied extensively.

Haptic roughness perception is generally considered a complex multidimensional process that can be influenced by various factors and cues [5–8]. In manufactured surfaces, the groove width, ridge height, particle diameter, and the spacing of raised dots, have, for instance, all been related to perceived surface roughness [9–12]. Perceived roughness has furthermore been suggested to correlate with various physical properties that arise during dynamic interactions with rough surfaces. These include friction [5, 13], the amplitude of vibration weighted with the frequency response of the Pacinian receptors [14, 15], as well as the average rate of change of the tangential force [16]. While one-dimensional roughness parameters such as the arithmetic average (Rα) and root mean square average (Rq or rms) of the profile height deviations from the mean line exist and are frequently used, no singular definition or predictive roughness feature has been identified to date. Yet, there is general agreement that roughness perception is largely influenced by vibratory information [14, 15, 17, 18], see also Chapter 4. While the so-called duplex theory

has highlighted the role of both static and dynamic exploration modes in mediating roughness information [19], dynamic exploration and the generation of vibration become increasingly essential for the discrimination of fine textures [17, 20]. This is also evidenced by the fact that roughness perception through a probe and with the bare finger tends to be highly correlated [21, 22].

The haptic perception of softness (or compliance) has been studied extensively as well. Physically, a material's softness is often expressed in terms of its stiffness (the ratio between applied force and displacement), elasticity (the ratio between stress and strain), or indentation hardness (resistance to indentation) [23–25]. The perceived softness of a material tends to be extracted using pressing or squeezing, but is sometimes available during other interactions, such as tapping or stroking, too [26–29]. It can furthermore be extracted both via direct and indirect touch (i.e., tool use [22, 26, 30]). While materials tend to be perceived as soft when the compliance is greater than the human finger during direct interactions, stimuli in the harder range are perceived as softer with a rigid tool [26]. The importance of cutaneous cues for softness perception has been stressed to a great extent [24, 26, 31], although a few studies have demonstrated that softness perception can sometimes be modulated by vibrotactile feedback too [29, 32–34].

While the haptic perceptions of roughness and softness have thus each been studied extensively, in controlled experimental contexts they have most frequently been investigated in isolation—that is, by manipulating surface features to evaluate their role in roughness perception and by manipulating material features to evaluate their role in softness perception. Furthermore, experimental research has often relied on either simplified materials, like sandpapers and periodic gratings, to maintain experimental control, or on natural textures and materials that vary in so many dimensions, making it hard to link perception to specific physical properties. However, in the real world, changes in microscale surface features co-exist with changes in material properties (such as elasticity). Natural materials like tree bark, animal hides, or certain food products may, for instance, exhibit rougher textures when older, drier, or more weathered, which may be accompanied by an increased stiffness. As we navigate the world, we rarely encounter individual attributes in isolation, and prior experiences and beliefs can shape our perception [35–37]. Therefore, examining how attributes interact and conflict with one another becomes critical when predicting or rendering perception from a reduced cue space [38–41].

Beyond their co-occurrence, there are additional reasons why one might expect both surface and material cues to determine the perception of a surface interaction. It has already been shown for simple stimulus material (i.e., fibrillar surfaces) that variations in the material stiffness and surface features can interact in shaping the final percept of the surface [42]. It is furthermore known that the elasticity of a material affects its measured and perceived friction [43], although the relationship between friction and perceived roughness is complex [2, 5, 16]. Additionally, changing a textured body's elasticity will likely entail changes in the vibratory pattern created during lateral exploration because the sliding dynamics may be directly shaped by bulk material properties and thus physically relate compliance to surface property perception [29]. During direct pressing with the finger, on the other hand, the texture

of a surface might affect the way both the surface itself and the skin deform locally and, as a consequence, affect the perceived softness of the material.

The aim of the present study was to investigate whether microscale surface topography and material elasticity jointly influence roughness and softness perceptions during direct and indirect haptic explorations. To this end, we carried out a line of roughness and softness discrimination experiments, using naturalistic stimuli, systematically varying in their statistical microscale roughness and elasticity. In a previous experiment (cf. Chapter 4), we did not find such mixed-cue effects in shaping the perceptual outcome (roughness or softness) during direct-touch interactions, potentially due to a mismatch between the elasticity range of the samples and the human finger as a probe. In the current study, we aimed to investigate whether adjusting the elasticity parameters to more closely match the human finger pad's elasticity range would change this relationship during direct interactions. Because we were also interested in dissociating the potential role of local cutaneous cues from propagating vibratory information during roughness discrimination, we furthermore employed an indirect-touch (rigid probe) condition, both for the original sample set (cf. Chapter 3 and Chapter 4) and the more elastic sample set created here. Confidence ratings were used to assess whether differences in each of the stimulus cues were linked to changes in participants' confidence levels and to evaluate the effect of potential cue fusion on their confidence.

We hypothesized that a joint influence of microscale surface roughness and material elasticity on roughness or softness perception should lead to perceptual regions of cue fusion in which different combinations of these cues would elicit indistinguishable roughness or softness percepts (metamers). Such "metameric relationships", where different physical stimulus combinations converge on identical perceptual experiences, can offer valuable insights into how the brain integrates different sensory inputs to form a coherent percept [44–47]. We furthermore hypothesized that, if such a relationship exists for roughness discrimination during direct, dynamic touch, it might persist in indirect touch scenarios.

5.2. METHODS

5.2.1. PARTICIPANTS

Five healthy adult volunteers (2 female, 3 male), average age of 32.2 (SD 2.05) participated in the study. Small sample studies like this are customary in sensory psychophysical research where the focus is on measurement reliability and repetitions within subjects, and the experimental power is concentrated at the individual participant level [48, 49]. All participants reported being right-handed and carried out the experiment with their right hand. All participants gave written informed consent prior to the study. The methods of this study were performed in accordance with relevant guidelines at Sorbonne University and the Declaration of Helsinki.

5.2.2. APPARATUS

Participants were seated in a chair at a desk in front of a computer screen. During the experiment, they wore noise protection headphones to ensure that the feedback they received was purely haptic in nature. The light in the experimental room was dimmed so that differences between the stimuli could not be seen, while the outline of the stimuli could still be made out for targeted interactions. Stimuli were placed in front of the participant's dominant hand for semi-controlled exploration with the index finger or a rigid tool (the rounded backside of a wooden paintbrush). A numpad was provided for responses via keypress at the side of the participant's non-dominant hand.

5.2.3. STIMULI

Two stimulus sets were used in the present study. First, we made use of the 3D-printed database of 49 stochastically rough, self-affine stimuli, systematically varying in their microscale surface roughness (Hurst exponent) and material elasticity as reported in detail in Chapter 3. This stimulus set was also used in a previous experiment for direct-touch interactions (cf. Chapter 4). Elasticity and roughness parameters of this database are summarized in Table 5.1 A and B, while a precise characterization of it can be found in Chapter 3.

Table 5.1. Roughness parameters (A) of both stimulus databases and elasticity parameters of the original low-elasticity stimulus database (B) and the new high-elasticity database (C). Note the different Shore scales in tables B and C.

A: Surface roughness parameters of both stimulus sets						
Surface Nr.	S1	S2	S3	S4	S5	S6	S7
Hurst exponent	0.3	0.4	0.5	0.6	0.7	0.8	0.9
$Rq[\times 10^{-2}$ mm]	5.68	5.16	4.79	4.51	4.30	4.14	4.01

B: Elasticity parameters of the low-elasticity sample set taken from Chapter 3						
Elasticity Nr.	E1	E2	E3	E4	E5	E6	E7
Shore-A value	24	25	26	29	34	44	66
Y. Modulus (MPa)	0.121	0.122	0.128	0.144	0.179	0.264	0.611

C: Material elasticity parameters of the high-elasticity stimulus set created here						
Elasticity Nr.	E1	E2	E3	E4	E5	E6	E7
Shore-00 value	9	18	25	32	39	43	47
Y. Modulus (MPa)	0.017	0.029	0.041	0.055	0.072	0.084	0.097

In addition, we created a new stimulus set with the same surface parameters as the original database, but with an updated elasticity range close to the elasticity of a human finger pad. This was done by creating negative molds using Ecoflex™ 00-30 silicone. While resulting in an inversion of peaks and valleys, the statistical roughness of these stimuli could be considered the same as that of the previous stimulus set.

Since most commercially available stereolithography (SLA) resins inhibit the curing of polydimethylsiloxane (PDMS), we first printed an additional set of 7 rigid surface

samples suitable to be used as molds for the final silicone specimens. To avoid curing inhibition, we followed the steps outlined by Venzac et al. [50] in the fabrication of these surfaces. The rigid surface samples were printed using a Formlabs Form 3 Printer and grey resin, which has a similar resolution to the Polyjet 735 used for the printing of the original stimulus database. After printing, the samples were washed in IPA for thirty minutes in a Formlabs Form Wash station and carefully rinsed manually with isopropanol using a soft paint brush. The samples were then cured for twenty-four hours at 60°C.

Each of these seven rigid surfaces was then mounted into 3D-printed frames, together creating molds for the uncured silicone mass. These frames were printed in PETG and covered in Kapton tape to further prevent potential curing inhibition at the sides of the molds. Upon mixing the two parts of the silicone, a total mass of 18 g was carefully poured into each of the molds and then removed again after curing. To achieve different elasticities, we adjusted the mixing ratio of the two-part elastomer Ecoflex™ 00-30. The above procedure was therefore repeated seven times, with an adjusted mixing ratio for all the 7 surfaces. This resulted in a final database of 49 silicone rubber samples sized 50x31x13 mm. Their Shore hardness was subsequently measured using a Shore-00 durometer (ASTM 2240) and the Young's modulus was calculated using Gent's equation [25]. Table 5.1C summarizes the achieved elasticity values for this stimulus database. Detailed information about the precise mixing ratios used to achieve the different elasticities can be found in Appendix J.

After fabrication and before every data collection, all specimens were coated in talcum powder to reduce differences in adhesion associated with different elasticities, as softer samples are universally more adhesive [51]. A pilot study had ensured that elasticity and surface cues were discernible within the cue space using both stroking and pressing in the absence of the other cue.

5.2.4. Experimental Design and Procedure

The overall task and procedure were the same as the ones used in Chapter 4 and are therefore presented in less detail here.

We used the non-parametric Bayesian inference framework Aepsych [52, 53]) to model a single latent function F:

$$P(\text{"A rougher/softer than B"}) = \Psi(F(A) - F(B))$$

determining the probability of the perceptual judgment (as rougher or softer) between any two stimuli in the stimulus space. The precise configuration of the model is specified in Appendix F.

Participants carried out a 2AFC-discrimination task, in which they had to indicate which one of two stimuli felt rougher (in the roughness condition) or softer (in the softness condition). Each trial began with a window appearing on the participant screen indicating for example "Which stimulus feels rougher?". Participants were instructed to use free natural explorations of the surfaces, using any interaction methods they wanted [54], but only using their dominant index finger in the direct-touch condition or the provided tool in the indirect-touch condition. They were

asked to explore the left stimulus first and then move to the right stimulus. They were also asked not to explore the edges and corners of the samples and to avoid using their fingernails. Participants were encouraged to give quick and intuitive answers. After their response, participants were asked to rate how confident they were about the answer given on a 1–9-Likert scale. All answers were given by keypress with the non-dominant hand. After each trial, the experimenter placed a new pair of samples in front of the participant, whereafter the task window reappeared on the participant's screen, indicating that they could begin with the next trial.
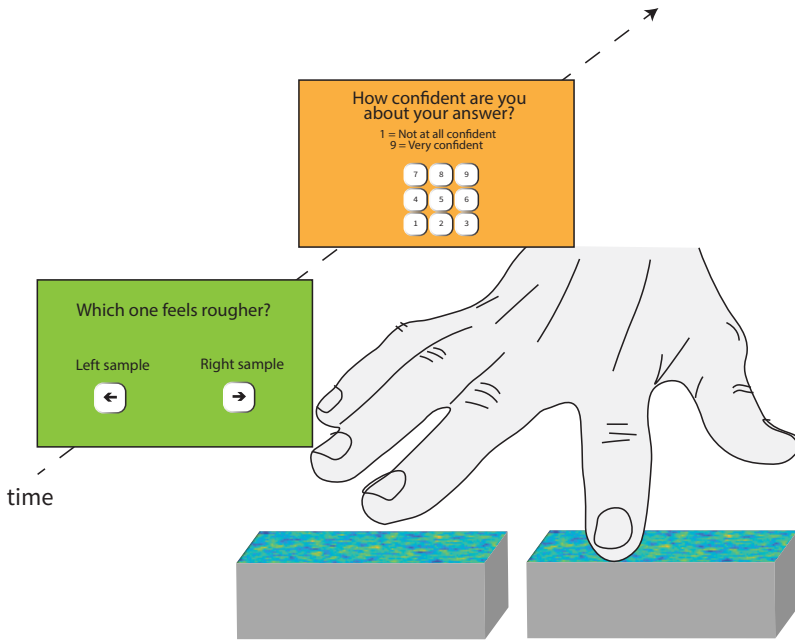

Figure 5.1. Procedure.

The experiment consisted of four conditions, each constituting a block comprising 50 trials. Each block was interspersed with a 5–10-minute break. The approximate duration for each block was 30 minutes. The blocks were designed to cover the four different combinations of *discrimination task* (roughness/softness), *exploration mode* (direct/tool), and *stimulus set* (high-/low-elasticity) included in this study. Table 5.2 summarizes these four conditions.

Softness discrimination using indirect touch was not included, since our previous study (cf. Chapter 4) indicated that propagating information alone is insufficient for this task, while local skin cues are unavailable through tool use.

5.2.5. STATISTICAL ANALYSES

For the discrimination data, a Gaussian Process (GP) model was fitted to each of the four experimental conditions, utilizing Houlsby's pairwise kernel for the Hurst and

Table 5.2. The four conditions included in this study, each constituting one experimental block.

Condition	Task	Mode	Stimulus set
A	Roughness	Direct	High-elast. set
B	Roughness	Tool	High-elast. set
C	Roughness	Tool	Low-elast. set
D	Softness	Direct	High-elast. set

Shore values and an index kernel for participants. Model posterior estimation was carried out using variational inference with hyperparameters fitted through maximum likelihood estimation. Model performance was assessed using the area under the receiver operating characteristic curve (ROC AUC). Further details are provided in the Analysis and Results section.

Confidence ratings were compared using means and standard deviations and then visually assessed using scatter plots. Likert-scale data are technically considered ordinal, but they can in some cases be considered approximately continuous (especially in the context of a larger numerical range) [55]. We therefore report means, rather than medians or modes, as they have the advantage of being easy to locate on the original scale. However, Generalized Linear Mixed Models (ordinal package, "clmm" function in R [56]) were used to evaluate the effects and interactions of changes in Hurst and Shore values on the confidence ratings.

Statistical analyses of the discrimination data were conducted using Python (Anaconda Navigator, Spyder version 5.4.3) and using AEPsych [52, 53]. Analyses of the confidence ratings were performed using R (version 4.3.1, R Core Team, 2021).

5.3. ANALYSIS AND RESULTS

5.3.1. OBSERVATIONS ON EXPLORATION STRATEGY

While free exploration was permitted in the present study, observations by the experimenters confirmed that all participants used lateral movement (stroking) in all conditions involving roughness discrimination, while pressing was used for softness discrimination.

5.3.2. DISCRIMINATION DATA

A Gaussian Process (GP) model [57] was fitted to each of the four conditions individually for all participants. The model used Houlsby's [58] pairwise kernel for the Hurst and Shore values and an index kernel for participants. The model posterior was estimated using variational inference [59], with hyperparameters fitted using maximum likelihood estimation. The Hurst and Shore values (cf. the corresponding

values in Table 5.1) were min-max scaled to the range [0, 1]. Formally, given the binary nature of the outcome, we assume each roughness or softness judgment, y, to be drawn from a Bernoulli distribution with probability $\Phi(f(u, v, p))$, where Φ is the Gaussian Cumulative Distribution Function (CDF), and $f(u, v, p)$ is a latent function over the model inputs: the left and right stimuli (given by their Hurst and Shore values) and participant index.

$$y|f, u, v, p \sim Bernoulli(\Phi(f(u, v, p)))$$ (5.1)

We placed a Gaussian Process (GP) prior on f. As is typical in GP regression, we used a constant mean function of zero, and we used a covariance function that is the product of two different covariance functions, k_{stim} and k_{part}.

$$f \sim GP(0, k_{\text{stim}} \cdot k_{\text{part}})$$ (5.2)

The function k_{stim} models the covariance between pairs of stimuli. Given pairs $[a, b]$ and $[c, d]$, the covariance is given by

$$k_{\text{stim}}([a, b], [c, d]) = k(a, c) + k(b, d) - k(b, c) - k(a, d)$$ (5.3)

where k is the Matérn 5/2 kernel (the derivation for this expression is provided by Houlsby et al. [58]). The function k_{part} is an index kernel, which models the covariance across participants. Except for the additional index kernel modeling the covariance between conditions in Chapter 4, the analysis carried out in the present study was precisely the same.

Model fits were subsequently assessed using the area under the receiver operator characteristic curve (ROC AUC) [60]. To estimate the distribution of predictions, 10,000 samples were drawn and the ROC AUC was calculated for each of those samples for each model. Figure 5.2 shows a histogram of those scores for each of the four conditions/blocks.

The 99% highest-density interval (HDI) is the shortest interval in which 99% of the posterior mass lies, meaning that the "true" ROC AUC lies within the bounds of the HDI with 99% certainty. As can be seen in Figure 5.2, all HDIs lie above 85%, which is generally considered to be a "good" model fit.

We then created plots of model predictions for each participant for each of the four conditions. The predictions were made on a dense grid corresponding to our two stimulus parameters (Hurst and Shore) and can be seen in Figure 5.3.

The individual probability plots in Figure 5.3 illustrate the probability of any stimulus within our stimulus space being identified as rougher/softer compared to a central reference for each subject and condition. The black iso-contour lines symbolize the corresponding 16%, 25%, 50%, 75%, 84%, and 96% probability lines. Similar to just-noticeable-differences (JNDs), the overall quantity of and the spacing between the isocontours in the space provide a picture of how precisely participants were capable of differentiating within the stimulus space.
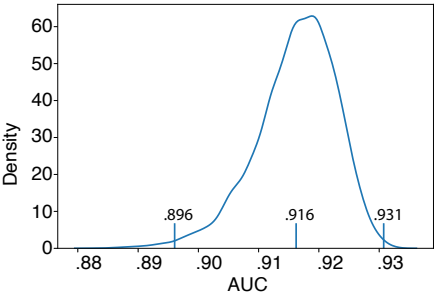
In the individual psychometric fields (Figure 5.3), it is visible how roughness judgments using direct touch of the high-elasticity stimulus set were highly influenced
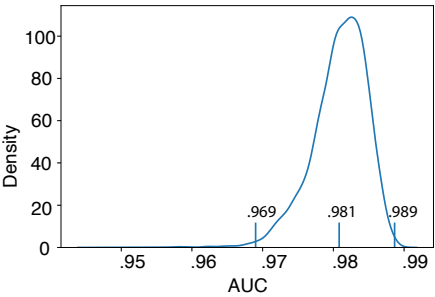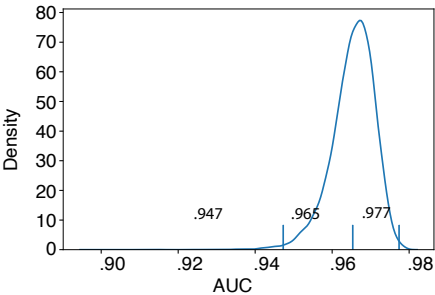
(A) Roughness, Direct, High elasticity
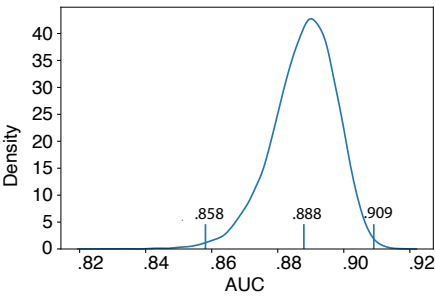
(B) Roughness, Tool, High elasticity

(D) Roughness, Tool, Low elasticity

(C) Softness, Direct, High elasticity

Figure 5.2. The area under the receiver operator characteristic curve (ROC AUC) of each of the four models. The mean of the distributions, as well as the limits of the 99% highest-density interval (HDI), are labeled.

by the Shore value and to a lesser degree by the Hurst exponent (cf. column A). This pattern was somewhat retained in roughness discrimination of the same stimulus set using a tool (cf. column B) but with an even larger influence of the Shore value, leaving the influence of the Hurst exponent almost negligible. Roughness discrimination of the low-elasticity sample set using a tool, on the other hand, was strongly predicted by both stimulus parameters with a slightly larger influence of the Hurst exponent (cf. column C). Finally, softness discrimination using direct touch (cf. column D) was primarily determined by the Shore value. This was confirmed by examining the best-fitting length-scale values derived from the GP model. These values, which represent the distance along the parameter for which responses are highly correlated and thus indicate the model's sensitivity to change in the respective parameter, are displayed in Table 5.3. The values have to be viewed in relative terms within each model, where a smaller value indicates a higher sensitivity.
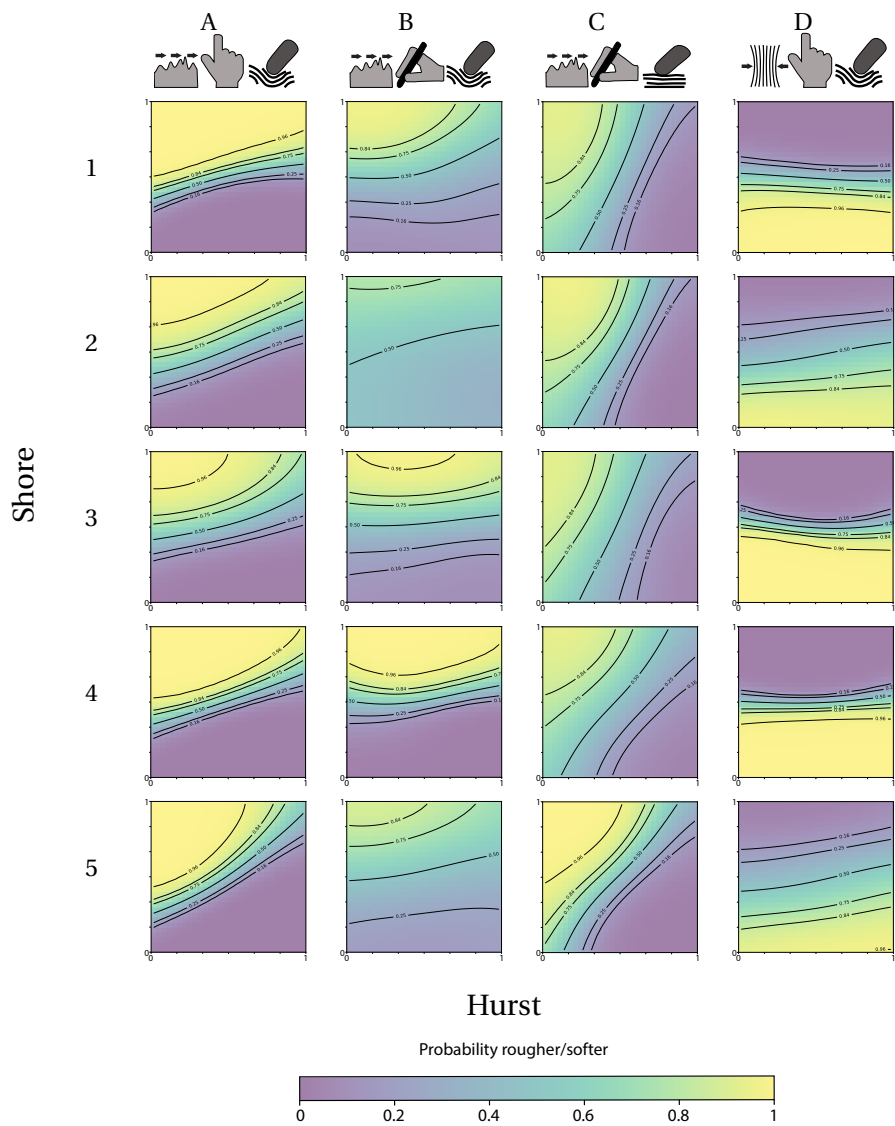
Figure 5.3. Individual probability plots as a function of Hurst and Shore values. Columns indicate conditions (cf. Table 5.2), rows indicate participants. The background color indicates the probability of a stimulus being chosen (as rougher/softer) compared to a stimulus with the medium Hurst and Shore values. Isocontours are plotted at 16%, 25%, 50%, 75%, 84%, and 96%. Note: because Shore values differ between stimulus sets and are measured on different Shore scales, the plots here correspond to the rescaled [0.1] stimulus space. Min and max values thus correspond to the values indicated in Table 5.1 for the respective stimulus sets.

Table 5.3. Summary of best-fitting lengthscales for Hurst and Shore across the four conditions. Smaller values indicate a greater sensitivity.

Condition	A	B	C	D
Task	Roughness	Roughness	Roughness	Softness
Mode	Direct	Tool	Tool	Direct
Stimulus Set	High-elast.	High-elast.	Low-elast.	High-elast.
Lengthscale Hurst	1.2047	0.7083	0.1541	1.4682
Lengthscale Shore	0.4655	0.0653	0.7466	0.0651

5.3.3. CONFIDENCE RATINGS

Mean confidence ratings were 6.1 (SD = 2.5) for direct roughness discrimination of the high-elasticity sample set (Condition A), 4.69 (SD = 2.56) for roughness discrimination with a tool of the same stimulus set (Condition B), while they were 6.15 (SD = 2.69) for roughness discrimination with a tool of the low-elasticity sample set (Condition C). Mean confidence ratings for direct softness discrimination of the high-elasticity sample set (Condition D) were 6.06 (SD = 2.87). These results are shown in Figure 5.4.
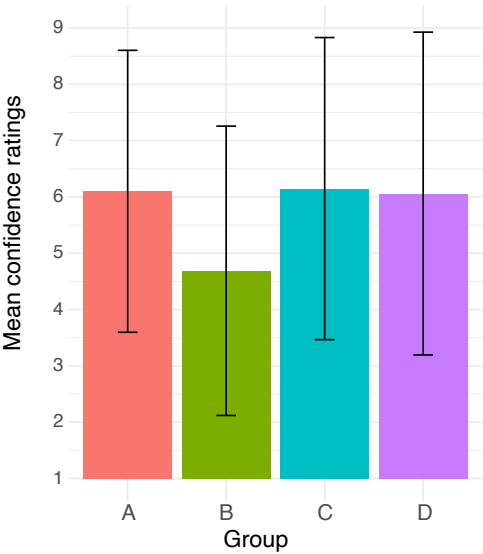
Figure 5.4. Mean confidence ratings of each of the four conditions, with error bars showing the standard deviations around the means.

In order to evaluate the relationship between participant's confidence ratings and changes in the stimulus parameters within a trial, we first created scatter plots displaying mean confidence ratings as a function of ΔHurst and ΔShore values. ΔHurst and ΔShore values were calculated by first standardizing each parameter range

to values ranging from 1 to 7 and then calculating the absolute difference between the values of each stimulus pair within a trial. This was done for each task and condition. Figure 5.5 shows these scatter plots.
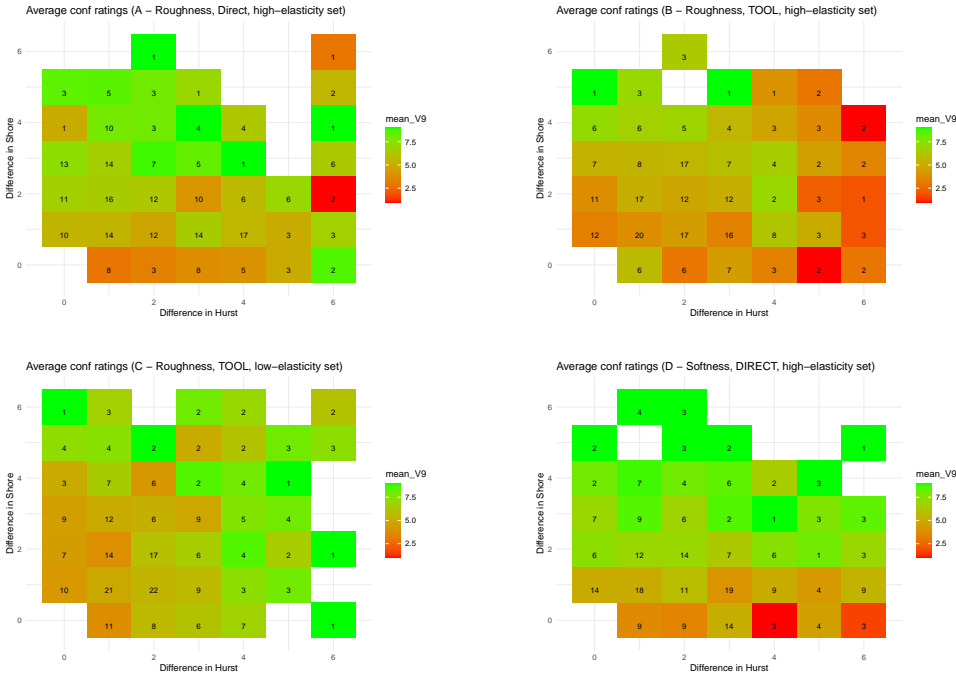

Figure 5.5. Scatter plots displaying mean confidence ratings as a function of ΔShore and ΔHurst for each of the four experimental conditions. Numbers in each cell indicate the number of observations. Note: these plots do not represent the absolute 2D stimulus space but show confidence ratings as a function of differences within it.

An unbalanced number of observations in each cell lies in the nature of the experimentation framework used, which concentrated its trials around areas of high uncertainty. Furthermore, a concentration of data points in cells with lower ΔHurst and ΔShore values is a natural consequence of these instances being more frequent within the stimulus space. However, qualitative visual assessments of Figure 5.5 show that confidence ratings for all roughness discrimination conditions appear to vary along differences in both stimulus dimensions, although differences in the Shore value (ΔShore) appear to be dominant in roughness discrimination of the high-elasticity stimulus (conditions A and B), while differences in the Hurst value (ΔHurst) appear dominant for the low-elasticity sample set (condition C). Confidence ratings during softness discrimination, on the other hand, appear to mainly vary as a function of ΔShore (condition D). Figure 5.4 and Figure 5.5 also show how roughness

discrimination of the high-elasticity stimulus set using a tool overall resulted in the lowest confidence ratings across the stimulus space (condition B).

To better assess the relationship between ΔHurst and ΔShore and changes in confidence ratings, Cumulative Link Mixed Models (CLMMs) were fitted to the data for each condition using ordinal logistic regression. The models included ΔHurst, ΔShore, and their interaction as fixed effects, with a random intercept for participants to account for individual variability. Model fitting was performed using the Laplace approximation. Table 5.4 summarizes the results.

Table 5.4. Results of Cumulative Link Mixed Models for each condition.

Condition	Parameter	b	SE	z	p
A: Roughness, Direct, High-elast. set	ΔHurst	0.266	0.122	2.173	0.030
	ΔShore	1.148	0.164	6.980	<0.001
	ΔHurst:ΔShore	-0.145	0.051	-2.855	0.004
B: Roughness, Tool, High-elast. set	ΔHurst	-0.138	0.135	-1.022	0.307
	ΔShore	0.662	0.160	4.149	<0.001
	ΔHurst:ΔShore	-0.020	0.055	-0.354	0.723
C: Roughness, Tool, Low-elast. set	ΔHurst	0.748	0.154	4.849	<0.001
	ΔShore	0.372	0.130	2.850	0.004
	ΔHurst:ΔShore	-0.092	0.050	-1.858	0.063
D: Softness, Direct, High-elast. set	ΔHurst	-0.085	0.117	-0.721	0.471
	ΔShore	1.129	0.194	5.825	<0.001
	ΔHurst:ΔShore	0.057	0.066	0.864	0.388

From Table 5.4 it is evident how ΔShore consistently had a significant positive effect on the confidence ratings for all conditions. ΔHurst, on the other, hand, had a significant positive effect on confidence ratings in conditions A and C. The interaction between ΔHurst and ΔShore was significant in Dataset A, trending towards significance in Dataset C , and not significant in Datasets B and D. These findings suggest that Shore values played a significant role in determining participant's confidence ratings in all conditions, whereas the influence of Hurst values varied depending on the specific task, interaction condition, and stimulus set.

5.4. DISCUSSION

We conducted a series of experiments to explore the interplay between microscale surface features and material elasticity in shaping the perceptions of roughness and softness during both direct and indirect touch interactions. The data provided

evidence supporting a model where both microscale surface features and material elasticity contribute to the perceived roughness within the parameter range tested. This held true for both interaction conditions (direct and indirect touch), but the relationship appeared dependent on, and thus variant to, the range of elasticities of the stimuli (high vs low) as well as that of the probe (finger vs tool). Combined effects of microscale surface features and material elasticity were also observable in the corresponding confidence ratings during roughness discrimination, where differences in each of the two stimulus parameters could predict differences in the confidence ratings in varying degrees (except for condition B, roughness discrimination with a tool of the high-elasticity sample set, where confidence ratings were primarily predicted by differences in stimulus elasticity). Conversely, when it comes to perceived softness, the evidence supported a model where only material elasticity plays a role, with no discernible influence from microscale surface features on subjective softness. These data were consistent with the analysis performed on the confidence ratings, where only the stimulus elasticity was identified as a significant predictor. The findings are discussed in detail below.

5.4.1. ROUGHNESS DISCRIMINATION

We observed an interdependent relationship between surface roughness and material elasticity in determining perceived roughness. Across all participants and conditions, roughness discrimination was governed by both microscale features and elasticity, albeit to a different degree for different conditions. Our data identified metameric regions where differing combinations of both cues resulted in indistinguishable perceptions. The example individual observer plot (Figure 5.6) illustrates these concepts.

As illustrated in Figure 5.6, a texture with a higher microscale roughness (lower Hurst exponent) in a more elastic material (lower Shore value) can therefore be experienced as similarly rough as a stiffer texture with a lower microscale roughness. This holds true for both direct and indirect dynamic touch interactions, but is dependent on the relative stiffness of the probe and stimulus (see Section 5.4.1).

VIBRATION AS A ROUGHNESS CUE—A PROPAGATING METAMER

Roughness perception has long been acknowledged as a complex and multidimensional process, involving the integration of a multitude of cues [5–8, 12]. Yet, the direct effects of changes in the elasticity of a textured surface on the perceived roughness are to the best of our knowledge previously unreported.

One physical property related to the perceived roughness that tends to change with alterations in both elasticity and surface microscale features is friction. Since friction between the fingertip or probe and a rough surface is related to the real contact area between them (e.g., [61, 62]), it is likely that variations in both elasticity and surface features will have had an influence on the friction dynamics in the present study. However, the relationship between friction and both perceived and physical surface roughness is complex [2, 16]. At a small scale, friction often decreases as the surface roughness increases, but this pattern inverts with higher degrees of roughness [5, 63,
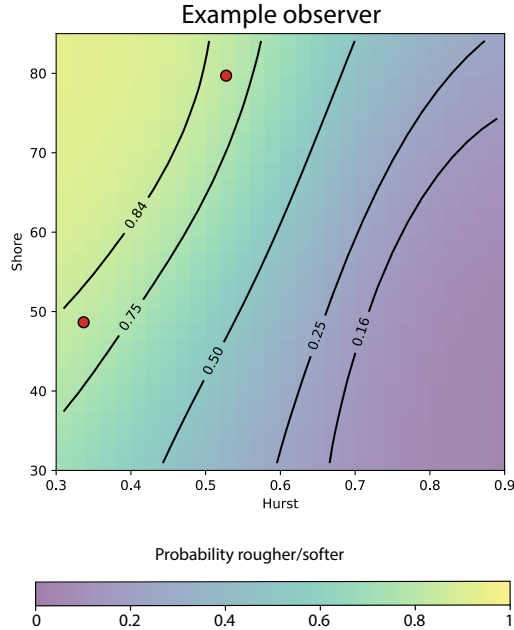
Figure 5.6. Example observer (i.e., for roughness discrimination of the low-elasticity sample set using a tool) illustrating the concept of a perceptual roughness metamer. The two red points illustrate just one example of a roughness metamer, where two stimuli markedly differing in their Hurst and Shore values become indiscernible in their subjective roughness. Within the stimulus space, any two points substantially far apart on both stimulus dimensions along the isocontours as well as in the area between them will qualify as such metamers. Regions along or between isocontours displaying the same probability levels are referred to as metameric regions.

64]. However, greater friction is often associated with greater perceived roughness [1, 5, 65]. Consequently, exceptionally smooth or flat surfaces can sometimes be perceived as rougher than textured ones, due to their heightened resistance to sliding and the potential for increased large-scale stick-slip [5]. A higher elasticity, on the other hand, is sometimes associated with increased friction [43, 61, 64]. A study by Fehlberg et al. [43], for instance, reported how both friction and perceived friction *increase* as the stiffness of micro-structured rubber samples *decreases*. However, we did not observe that more elastic surfaces were perceived as rougher in the present study for any of the interaction types, but the reverse. While friction may therefore have played a role in the perceived roughness of the samples in the present study, it is unlikely to have been the direct mediating factor in the metameric relationship observed between elasticity and surface roughness on the perceived roughness.

It is generally well-known that surface roughness estimates rely heavily on vibratory information (e.g., [19, 66, 67]) and that subjects can discriminate complex textures on the basis of vibration alone [68] (cf. Chapter 4). This raises pertinent questions about the vibratory cues as participants interacted with the surfaces in the present study. Changing a textured body's elasticity will likely affect tribological events such as ploughing, adhesion, and the frequency response of impact events during lateral exploration of the body's surface [69, 70]. A mechanistic interpretation may thus posit that more elastic samples deform more upon dynamic touch (i.e., ploughing events), resulting in decreased impact and indentation on the finger/probe during lateral exploration. Magnitude and frequency of the resulting vibrations during sliding may consequently directly depend on the bulk elasticity of the material [29].

The impact of vibratory cues on the final perceptual outcome of a roughness judgment becomes particularly evident in the tool interactions. During indirect touch with a tool, vibrations propagate along the tool to the hand [67, 71, 72]. In the present study, vibratory information was conserved yet transformed by the tool's mechanical properties before it reached the participant's hand. Notably, roughness discrimination of the more elastic stimulus set was remarkably similar for direct and indirect touch, although a transformation could be seen towards a stronger influence of the Shore value during indirect touch, probably due to the large difference in stiffness between the tool and the sample (see Section 5.4.1). However, the fact that this metameric relationship was evident in both exploration conditions – when local skin information was available and when it was not – underscores the primacy of vibratory information in roughness perception. It suggests that participants did not selectively subtract or compensate for the elasticity cues in their roughness judgments, even when local tactile information was directly available through finger contact. Instead, the cue confound was conserved across both probes (finger and tool) for the elastic stimulus set, despite the transformation imposed on the frequency and magnitude of the vibration response.

THE SIGNIFICANCE OF THE PARAMETER RANGE

In the present study, we were able to demonstrate clear instances of mixed cue effects on roughness perception for both direct and indirect touch interactions with the elastic sample set. We furthermore demonstrated the same relationship for indirect touch interactions with the less elastic sample set. However, in our prior experiment, focusing on direct touch interactions with the less elastic sample set, no evidence was found for mixed-cue effects related to the perceived roughness of the samples (cf. Chapter 4). During direct touch, the perceived roughness of these samples was predominantly governed by changes in microscale surface features (Hurst exponent). The absence of a metameric relationship in the previous study was hypothesized to be due to multiple potential factors. One hypothesis was that the salience of the changes in the surface features was simply greater than that of the changes in the elasticity, thus overruling any effect the elasticity could have had on roughness perception. Another hypothesis was that the elasticity range tested was not relevant to direct interactions with the human finger (i.e., orders of magnitude stiffer than the human finger itself). The results of the present study specifically highlight the

significance of the latter factor. Here, we did not only observe a mixed influence of both parameters but, in fact, a comparatively larger influence of the Shore value than the Hurst exponent on the final roughness percept for the high-elasticity sample set (cf. Figure 5.3 and Table 5.3), an effect that was present in the corresponding confidence ratings as well (cf. Table 5.4 and Figure 5.5). A significant contribution of material elasticity on the final roughness percept may therefore only occur in cases where the stiffness of the probe (i.e., finger or tool) is either close to or significantly higher than that of the samples explored. When probe and sample exhibit a similar resistance to movement and deformation, the two surfaces can be said to be matched in their impedance [73–75]. This is related to the equivalent modulus of two elastic bodies in contact [76, 77]. The specific contact mechanics between the two bodies were not characterized in the present study, preventing us from making any precise claims about the mechanical interactions that occurred. However, the present data still suggest that the relative (not absolute) stiffness/elasticity of the probe and the sample appear to be decisive for mixed-cue effects on roughness perception to occur during sliding. Figure 5.7 illustrates this point.
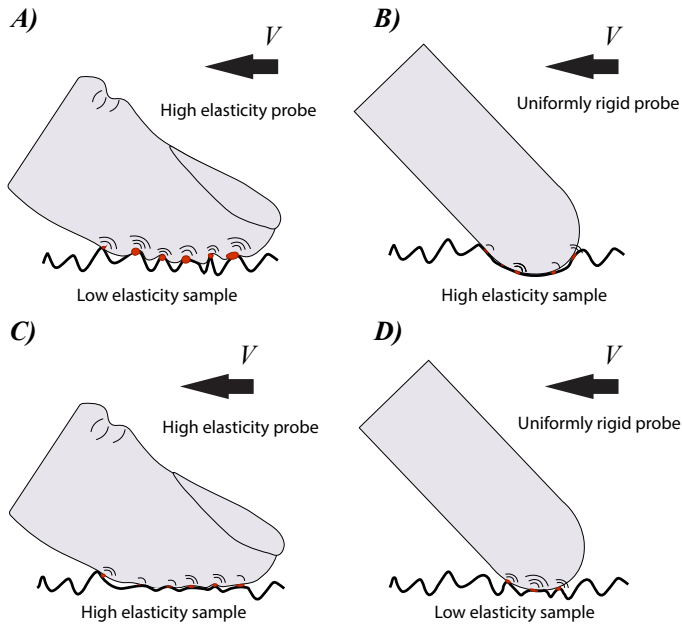

Figure 5.7. Four scenarios illustrating the effect of the relative elasticity of a textured sample and the probe used during sliding in the present study.

If a textured surface and its asperities are significantly more rigid than the probe, little or no deformation of the sample should take place during dynamic interactions, and impact events will be absorbed by the probe's material elasticity which deforms around the sample (Figure 5.7, scenario A). Since the real-contact area is unlikely to change with changes in the elasticity of the sample, no significant changes in

adhesion should be present either. Within this range, the resulting vibration and roughness percept should be predominantly defined by surface features. Conversely, if the probe is significantly more rigid than the sample, sample asperities will be significantly deformed and oppose little to no resistance to the probe. Here, the actual shape of the asperities may thus have little impact on the frequency response and the resulting roughness percept (Figure 5.7, scenario B). However, within a given range of relative sample elasticity to the probe, changes in the elasticity of the sample should significantly alter the frequency response of dynamic impacts during lateral exploration. In Figure 5.7, scenario C, the probe and sample deform against each other. Changes in the material elasticity within this range should change both the dynamics of adhesion, ploughing, and the resulting frequency response of impacts. Finally, in the scenario of a uniformly rigid probe and a sample low in elasticity (Figure 5.7 D), sample asperities will be deformed but still oppose a significant resistance to the probe. Changes in the elasticity of the sample within this range should result in changes in ploughing, adhesion, as well as the resulting frequency response of impact events propagating through the probe.

Together, the relative elasticity of the sample and the probe thus shapes the frequency response of the vibrations that arise during dynamic impact, which, as we show in this study, can result in cue confusion for roughness perception.

5.4.2. SOFTNESS DISCRIMINATION

The results of the softness discrimination task yielded no evidence of a notable influence of changes in microscale roughness (Hurst exponent) on the perceived softness in the direct-touch condition of the elastic stimulus set. Perceptual judgments were largely dominated by the elasticity of the samples and so were the corresponding confidence ratings. These results are in line with our previous study in which we used the less elastic sample set for direct interactions (cf. Chapter 4). As a reminder to the reader: pilot testing on both the high- and low-elasticity sample sets had ensured that changes in surface features were discriminable by mere pressing. Our results therefore suggest that changes in microscale surface features (as operationalized here, covering feature changes between 30 and 500 μm) do not affect softness perception of elastic surfaces within the two ranges of elasticity tested. This finding is interesting for several reasons.

First, it is known that the perceived softness of a material is largely defined by local skin deformation and displacement [31, 78–80]. When examining the relative weight of information for hardness discrimination, Bergmann Tiest and Kappers [24] showed that approximately 90% of the information is drawn from surface deformation cues and 10% from force/displacement cues. Similarly, stretching the skin of the fingertip immediately increases the perceived stiffness of materials [81]. The importance of local cutaneous cues has become particularly evident in studies using local anesthesia. Without local cutaneous information from the finger, it is impossible for participants to discriminate between samples with a significant difference in stiffness, using pressing only [31] or when dynamic explorations are permitted (Chapter 4). Therefore, although softness discrimination can be influenced by kinaesthetic information [26,

82], it does not rely on it, nor is it sufficient for softness discrimination, considering kinaesthetic information remains intact during local anesthesia [31]. In the present study, changes in the microscale topography of the samples will likely have modified local skin deformation cues during bare-finger interactions. Therefore, one might have expected them to consequently modify the softness percept. It has, for instance, previously been shown that the shape of a surface can affect the perceived compliance of it [83, 84], such that interactions with a convex surface yield a perceptual outcome equivalent to a harder sample whereas interactions with a concave surface yield a percept equivalent to a softer sample [83]. It is furthermore known that the evolution of the gross contact area provides information about the softness of a material [85] as well as the finger displacement relative to a surface [86], which in some instances can lead to confounding percepts of compliance and displacement [80]. In the present study, a larger evolution in the overall contact surface will likely have taken place from initial contact to maximal force applied on a rougher (smaller Hurst exponent) compared to a smoother or more flat (larger Hurst exponent) surface of the same elasticity. One could therefore have reasoned that, within a given range of elasticity, finer surface features (approaching a flat surface) might bias toward a harder percept, since the lack of prominent surface features (larger Hurst exponent) might provide less information about the deformability of the surface. However, this is not what we found. Our findings therefore suggest that participants were able to dissociate the perceived differences in surface features from their final softness judgments during pressing; thus avoiding a confounding influence of surface roughness on softness discrimination.

An important observation of the present study concerns participants' choice of exploration mode for the softness discrimination. Okamoto and Visell [29] have highlighted humans' ability to extract weak softness information from vibratory cues, and a line of further studies has demonstrated that vibrotactile information can affect the perceived object softness in certain contexts [29, 32–34]. This especially becomes relevant during dynamic explorations of surfaces such as tapping or stroking of textured surfaces. It has, for instance, been shown that a lower surface friction leads to skin or skin-like materials feeling softer during stroking but not pressing [87]. However, like in our previous study, participants consistently used pressing rather than stroking, verifying this as a preferred exploration strategy for extracting softness information [28], even when relevant cues might have been accessible during other exploration modes. The present research therefore makes no claims about the potential influence of microscale surface features on softness perception during instructed dynamic explorations. Future research will have to investigate this, although the present study once more verifies the power of preferred exploration procedures to extract certain material qualities [28].

5.4.3. METAMERIC CUE FUSION AND CONFIDENCE

While not the primary aim of this study, an observation from the analysis of the confidence ratings indicates that the presence of a metameric relationship did *not* appear to result in an altered confidence about the perceptual judgments. Confidence

ratings were generally stable across conditions A (Roughness, Direct, High-elast. set), C (Roughness, Tool, Low-elast. set), and D (Softness, Direct, High-elast. set). Conditions A and C were subject to mandatory cue fusion, resulting in a metameric relationship for perceived roughness, while condition D was not. Notably, only condition B (Roughness, Tool, Low-elast. set) exhibited significantly lower confidence ratings on average (cf. Figure 5.4). We believe this to be a likely effect of the reduced availability of behaviorally relevant cues for roughness perception in this condition, attributed to the high elasticity difference between the tool used and the samples probed (cf. Section 5.4.1 and Figure 5.7).

This observation suggests that a true metamer, involving the joint influence of two behaviorally relevant cues, may entail no alterations in the perceived confidence about perceptual judgments compared to scenarios where only one cue determines the perceptual outcome. However, future research should directly investigate this by comparing multi-cue scenarios with and without cue fusion (as done here) with single-cue scenarios.

5.5. CONCLUSION

We investigated the combined influence of microscale surface features and material elasticity in shaping perceived roughness and softness during both direct and indirect (tool) touch. We demonstrated how material elasticity can provide a behaviorally relevant cue to roughness perception depending on the relative elasticity of the stimuli and a rigid probe. Herein, we uncovered a perceptual roughness metamer, where different combinations of material elasticity and microscale surface roughness can result in the same subjective roughness. While this mechanism was present for both contact conditions, we showed how the weight of each of these stimulus cues is dependent on the relative stiffness of the stimuli compared to the probe (i.e., rigid probe or finger). Conversely, no effects of microscale surface features were observed on softness perception during direct touch. A critical implication of this finding is an increased flexibility in conveying roughness information in haptic applications. Roughness can thus be communicated via both surface and material cues as well as via alterations to not only stimulus characteristics but also the probe itself. The material composition and stiffness of an artificial limb will thus, for instance, dictate the way materials and textures are perceived through it.

REFERENCES

[1] Bergmann Tiest, W. M. and Kappers, A. M. Analysis of haptic perception of materials by multidimensional scaling and physical measurements of roughness and compressibility. *Acta Psychologica* **121** (2006), 1–20. DOI: `10.1016/j.actpsy.2005.04.005`.

[2] Holliins, M., Faldowski, R., Rao, S., and Young, F. Perceptual dimensions of tactile surface texture: A multidimensional scaling analysis. *Perception & Psychophysics* **54** (1993), 697–705. DOI: `10.3758/BF03211795`.

[3] Hollins, M., Bensmaïa, S., Karlof, K., and Young, F. Individual differences in perceptual space for tactile textures: Evidence from multidimensional scaling. *Perception & Psychophysics* **62** (2000), 1534–1544. DOI: `10.3758/BF03212154`.

[4] Okamoto, S., Nagano, H., and Yamada, Y. Psychophysical dimensions of tactile perception of textures. *IEEE Transactions on Haptics* **6** (2013), 81–93. DOI: `10.1109/TOH.2012.32`.

[5] Arvidsson, M., Ringstad, L., Skedung, L., Duvefelt, K., and Rutland, M. W. Feeling fine - the effect of topography and friction on perceived roughness and slipperiness. *Biotribology*. Special issue on the 3rd International Conference on Biotribology. **11** (2017), 92–101. DOI: `10.1016/j.biotri.2017.01.002`.

[6] Connor, C. E., Hsiao, S. S., Phillips, J. R., and Johnson, K. O. Tactile roughness: neural codes that account for psychophysical magnitude estimates. *The Journal of Neuroscience: The Official Journal of the Society for Neuroscience* **10** (1990), 3823–3836. DOI: `10.1523/JNEUROSCI.10-12-03823.1990`.

[7] Di Stefano, N. and Spence, C. Roughness perception: A multisensory/crossmodal perspective. *Attention, Perception & Psychophysics* **84** (2022), 2087–2114. DOI: `10.3758/s13414-022-02550-y`.

[8] Kahrimanovic, M., Bergmann Tiest, W. M., and Kappers, A. M. L. Context effects in haptic perception of roughness. *Experimental Brain Research* **194** (2009), 287–297. DOI: `10.1007/s00221-008-1697-x`.

[9] Lamb, G. D. Tactile discrimination of textured surfaces: psychophysical performance measurements in humans. *The Journal of Physiology* **338** (1983), 551–565. DOI: `10.1113/jphysiol.1983.sp014689`.

[10] Lederman, S. J. and Taylor, M. M. Fingertip force, surface geometry, and the perception of roughness by active touch. *Perception & Psychophysics* **12** (1972), 401–408. DOI: `10.3758/BF03205850`.

[11] Miyaoka, T., Mano, T., and Ohka, M. Mechanisms of fine-surface-texture discrimination in human tactile sensation. *The Journal of the Acoustical Society of America* **105** (1999), 2485–2492. DOI: 10.1121/1.426852.

[12] Tymms, C., Zorin, D., and Gardner, E. P. Tactile perception of the roughness of 3D-printed textures. *Journal of Neurophysiology* **119** (2018), 862–876. DOI: 10.1152/jn.00564.2017.

[13] Ekman, G., Hosman, J., and Lindstrom, B. Roughness, smoothness, and preference: A study of quantitative relations in individual subjects. *Journal of Experimental Psychology* **70** (1965), 18–26. DOI: 10.1037/h0021985.

[14] Bensmaïa, S., Hollins, M., and Yau, J. Vibrotactile intensity and frequency information in the pacinian system: a psychophysical model. *Perception & Psychophysics* **67** (2005), 828–841. DOI: 10.3758/bf03193536.

[15] Bensmaïa, S. J. and Hollins, M. The vibrations of texture. *Somatosensory & Motor Research* **20** (2003), 33–43. DOI: 10.1080/0899022031000083825.

[16] Smith, A. M., Chapman, C. E., Deslandes, M., Langlais, J.-S., and Thibodeau, M.-P. Role of friction and tangential force variation in the subjective scaling of tactile roughness. *Experimental Brain Research* **144** (2002), 211–223. DOI: 10.1007/s00221-002-1015-y.

[17] Roberts, R. D., Loomes, A. R., Allen, H. A., Di Luca, M., and Wing, A. M. Contact forces in roughness discrimination. *Scientific Reports* **10** (2020), 5108. DOI: 10.1038/s41598-020-61943-x.

[18] Weber, A. I., Saal, H. P., Lieber, J. D., Cheng, J.-W., Manfredi, L. R., Dammann, J. F., and Bensmaia, S. J. Spatial and temporal codes mediate the tactile perception of natural textures. *Proceedings of the National Academy of Sciences of the United States of America* **110** (2013), 17107–17112. DOI: 10.1073/pnas.1305509110.

[19] Hollins, M. and Risner, S. R. Evidence for the duplex theory of tactile texture perception. *Perception & Psychophysics* **62** (2000), 695–705. DOI: 10.3758/bf03206916.

[20] Hollins, M., Bensmaïa, S. J., and Washburn, S. Vibrotactile adaptation impairs discrimination of fine, but not coarse, textures. *Somatosensory & Motor Research* **18** (2001), 253–262. DOI: 10.1080/01421590120089640.

[21] Klatzky, R. L., Lederman, S. J., Hamilton, C., Grindley, M., and Swendsen, R. H. Feeling textures through a probe: Effects of probe and surface geometry and exploratory factors. *Perception & Psychophysics* **65** (2003), 613–631. DOI: 10.3758/BF03194587.

[22] Yoshioka, T., Bensmaïa, S. J., Craig, J. C., and Hsiao, S. S. Texture perception through direct and indirect touch: An analysis of perceptual space for tactile textures in two modes of exploration. *Somatosensory & Motor Research* **24** (2007), 53–70. DOI: 10.1080/08890220701318163.

[23] Bergmann Tiest, W. M. Tactual perception of material properties. *Vision Research*. Perception and Action: Part I **50** (2010), 2775–2782. DOI: 10.1016/j.visres.2010.10.005.

[24] Bergmann Tiest, W. and Kappers, A. Cues for Haptic Perception of Compliance. *IEEE Transactions on Haptics* **2** (2009), 189–199. DOI: 10.1109/TOH.2009.16.

[25] Gent, A. N. On the relation between indentation hardness and young's modulus. *Rubber Chemistry and Technology* **31** (1958), 896–906. DOI: 10.5254/1.3542351.

[26] Friedman, R. M., Hester, K. D., Green, B. G., and LaMotte, R. H. Magnitude estimation of softness. *Experimental Brain Research* **191** (2008), 133–142. DOI: 10.1007/s00221-008-1507-5.

[27] Higashi, K., Okamoto, S., Yamada, Y., Nagano, H., and Konyo, M. Hardness perception based on dynamic stiffness in tapping. *Frontiers in Psychology* **9** (2019), 2654. DOI: 10.3389/fpsyg.2018.02654.

[28] Lederman, S. J. and Klatzky, R. L. Hand movements: A window into haptic object recognition. *Cognitive Psychology* **19** (1987), 342–368. DOI: 10.1016/0010-0285(87)90008-9.

[29] Visell, Y. and Okamoto, S. "Vibrotactile Sensation and Softness Perception". In: Multisensory Softness: Perceived Compliance from Multiple Sources of Information. Ed. by Di Luca, M. Springer Series on Touch and Haptic Systems. London: Springer, 2014, pp. 31–47. DOI: 10.1007/978-1-4471-6533-0_3.

[30] LaMotte, R. H. Softness discrimination with a tool. *Journal of Neurophysiology* **83** (2000), 1777–1786. DOI: 10.1152/jn.2000.83.4.1777.

[31] Srinivasan, M. A. and LaMotte, R. H. Tactual discrimination of softness. *Journal of Neurophysiology* **73** (1995), 88–101. DOI: 10.1152/jn.1995.73.1.88.

[32] Ikeda, A., Suzuki, T., Takamatsu, J., and Ogasawara, T. "Producing Method of Softness Sensation by Device Vibration". In: 2013 IEEE International Conference on Systems, Man, and Cybernetics. 2013, pp. 3384–3389. DOI: 10.1109/SMC.2013.577.

[33] Kildal, J. "3D-press: haptic illusion of compliance when pressing on a rigid surface". In: International Conference on Multimodal Interfaces and the Workshop on Machine Learning for Multimodal Interaction. ICMI-MLMI '10. New York, NY, USA: Association for Computing Machinery, 2010, pp. 1–8. DOI: 10.1145/1891903.1891931.

[34] Visell, Y., Giordano, B. L., Millet, G., and Cooperstock, J. R. Vibration influences haptic perception of surface compliance during walking. *PloS One* **6** (2011), e17697. DOI: 10.1371/journal.pone.0017697.

[35] De Lange, F. P., Heilbron, M., and Kok, P. How do expectations shape perception? *Trends in Cognitive Sciences* **22** (2018), 764–779. DOI: 10.1016/j.tics.2018.06.002.

[36] Hohwy, J. *The Predictive Mind*. Oxford, GB: Oxford University Press UK, 2013.

5

[37] Trommershauser, J., Kording, K., and Landy, M. S. *Sensory Cue Integration*. Oxford University Press, 2011.

[38] Drewing, K. and Ernst, M. O. Integration of force and position cues for shape perception through active touch. *Brain Research* **1078** (2006), 92–100. DOI: `10.1016/j.brainres.2005.12.026`.

[39] Ernst, M. O. and Bülthoff, H. H. Merging the senses into a robust percept. *Trends in Cognitive Sciences* **8** (2004), 162–169. DOI: `10.1016/j.tics.2004.02.002`.

[40] Frisoli, A., Solazzi, M., Reiner, M., and Bergamasco, M. The contribution of cutaneous and kinesthetic sensory modalities in haptic perception of orientation. *Brain Research Bulletin*. Presence: Brian, Virtual Reality and Robots **85** (2011), 260–266. DOI: `10.1016/j.brainresbull.2010.11.011`.

[41] Metzger, A., Lezkan, A., and Drewing, K. Integration of serial sensory information in haptic perception of softness. *Journal of Experimental Psychology: Human Perception and Performance* **44** (2018), 551–565. DOI: `10.1037/xhp0000466`.

[42] Gedsun, A., Sahli, R., Meng, X., Hensel, R., and Bennewitz, R. Bending as key mechanism in the tactile perception of fibrillar surfaces. *Advanced Materials Interfaces* **9** (2022), 2101380. DOI: `10.1002/admi.202101380`.

[43] Fehlberg, M., Kim, K.-S., Drewing, K., Hensel, R., and Bennewitz, R. "Perception of Friction in Tactile Exploration of Micro-structured Rubber Samples". In: Haptics: Science, Technology, Applications. Ed. by Seifi, H., Kappers, A. M. L., Schneider, O., Drewing, K., Pacchierotti, C., Abbasimoshaei, A., Huisman, G., and Kern, T. A. Lecture Notes in Computer Science. Cham: Springer International Publishing, 2022, pp. 21–29. DOI: `10.1007/978-3-031-06249-0_3`.

[44] Loftus, G. R. and Ruthruff, E. A theory of visual information acquisition and visual memory with special application to intensity-duration trade-offs. *Journal of Experimental Psychology. Human Perception and Performance* **20** (1994), 33–49. DOI: `10.1037//0096-1523.20.1.33`.

[45] Shockley, K., Carello, C., and Turvey, M. T. Metamers in the haptic perception of heaviness and moveableness. *Perception & Psychophysics* **66** (2004), 731–742. DOI: `10.3758/BF03194968`.

[46] Sekuler, R. and Blake, R. *Perception*. McGraw-Hill, 1994.

[47] Kuroki, S., Sawayama, M., and Nishida, S. Haptic metameric textures. *bioRxiv* (2019), 653550. DOI: `10.1101/653550`.

[48] Smith, P. L. and Little, D. R. Small is beautiful: In defense of the small-N design. *Psychonomic Bulletin & Review* **25** (2018), 2083–2101. DOI: `10.3758/s13423-018-1451-8`.

[49] Schwarzkopf, D. S. and Huang, Z. *A simple statistical framework for small sample studies*. preprint. Neuroscience, 2023. DOI: `10.1101/2023.09.19.558509`.

5

[50] Venzac, B., Deng, S., Mahmoud, Z., Lenferink, A., Costa, A., Bray, F., Otto, C., Rolando, C., and Le Gac, S. PDMS curing inhibition on 3D-printed molds: why? Also, how to avoid It? *Analytical Chemistry* **93** (2021), 7180–7187. DOI: 10.1021/acs.analchem.0c04944.

[51] Darby, D. R., Cai, Z., Mason, C. R., and Pham, J. T. Modulus and adhesion of Sylgard 184, Solaris, and Ecoflex 00-30 silicone elastomers with varied mixing ratios. *Journal of Applied Polymer Science* **139** (2022). DOI: 10.1002/app.52412.

[52] Browder, J., Bochereau, S., van Beek, F., and King, R. "Stiffness in Virtual Contact Events: A Non-Parametric Bayesian Approach". In: 2019 IEEE World Haptics Conference (WHC). Tokyo, Japan: IEEE, 2019, pp. 515–520. DOI: 10.1109/WHC.2019.8816102.

[53] Owen, L., Browder, J., Letham, B., Stocek, G., Tymms, C., and Shvartsman, M. Adaptive nonparametric psychophysics. *arXiv* (2021). DOI: 10.48550/arXiv.2104.09549.

[54] Callier, T., Saal, H. P., Davis-Berg, E. C., and Bensmaia, S. J. Kinematics of unconstrained tactile texture exploration. *Journal of Neurophysiology* **113** (2015), 3013–3020. DOI: 10.1152/jn.00703.2014.

[55] Fagerland, M. W., Sandvik, L., and Mowinckel, P. Parametric methods outperformed non-parametric methods in comparisons of discrete numerical variables. *BMC Medical Research Methodology* **11** (2011), 44. DOI: 10.1186/1471-2288-11-44.

[56] Christensen, R. H. B. *ordinal: Regression Models for Ordinal Data. https://cran.r-project.org/web/packages/ordinal/index.html.* 2023.

[57] Rasmussen, C. E. and Williams, C. K. I. *Gaussian processes for machine learning.* Adaptive computation and machine learning. Cambridge, Mass: MIT Press, 2006.

[58] Houlsby, N., Huszár, F., Ghahramani, Z., and Lengyel, M. Bayesian active learning for classification and preference learning. *ArXiv* (2011). DOI: 10.48550/arXiv.1112.5745.

[59] Blei, D. M., Kucukelbir, A., and McAuliffe, J. D. Variational inference: A review for statisticians. *Journal of the American Statistical Association* **112** (2017), 859–877. DOI: 10.1080/01621459.2017.1285773.

[60] Fawcett, T. An introduction to ROC analysis. *Pattern Recognition Letters*. ROC Analysis in Pattern Recognition **27** (2006), 861–874. DOI: 10.1016/j.patrec.2005.10.010.

[61] Adams, M. J., Johnson, S. A., Lefèvre, P., Lévesque, V., Hayward, V., André, T., and Thonnard, J.-L. Finger pad friction and its role in grip and touch. *Journal of The Royal Society Interface* **10** (2013), 20120467. DOI: 10.1098/rsif.2012.0467.

5

[62] Sahli, R., Pallares, G., Ducottet, C., Ben Ali, I. E., Al Akhrass, S., Guibert, M., and Scheibert, J. Evolution of real contact area under shear and the value of static friction of soft materials. *Proceedings of the National Academy of Sciences* **115** (2018), 471–476. DOI: 10.1073/pnas.1706434115.

[63] Tomlinson, S. E., Lewis, R., and Carré, M. J. The effect of normal force and roughness on friction in human finger contact. *Wear*. 17th International Conference on Wear of Materials **267** (2009), 1311–1318. DOI: 10.1016/j.wear.2008.12.084.

[64] Van Kuilenburg, J., Masen, M. A., and van der Heide, E. A review of fingerpad contact mechanics and friction and how this affects tactile perception. *Proceedings of the Institution of Mechanical Engineers, Part J: Journal of Engineering Tribology* **229** (2015), 243–258. DOI: 10.1177/1350650113504908.

[65] Gwosdow, A., Stevens, J., Berglund, L., and Stolwijk, J. Skin friction and fabric sensations in neutral and warm environments. *Textile Research Journal* **56** (1986), 574–580. DOI: 10.1177/004051758605600909.

[66] Hollins, M., Bensmaïa, S. J., and Roy, E. A. Vibrotaction and texture perception. *Behavioural Brain Research* **135** (2002), 51–56. DOI: 10.1016/S0166-4328(02)00154-7.

[67] Yoshioka, T., Craig, J. C., Beck, G. C., and Hsiao, S. S. Perceptual constancy of texture roughness in the tactile system. *The Journal of Neuroscience: The Official Journal of the Society for Neuroscience* **31** (2011), 17603–17611. DOI: 10.1523/JNEUROSCI.3907-11.2011.

[68] Wiertlewski, M., Lozada, J., and Hayward, V. The spatial spectrum of tangential skin displacement can encode tactual texture. *IEEE Transactions on Robotics* **27** (2011), 461–472. DOI: 10.1109/TRO.2011.2132830.

[69] Spurr, R. T. The "ploughing" contribution to friction. *British Journal of Applied Physics* **7** (1956), 260. DOI: 10.1088/0508-3443/7/7/305.

[70] Persson, B. N. J. *Sliding Friction*. Ed. by Von Klitzing, K. and Wiesendanger, R. NanoScience and Technology. Berlin, Heidelberg: Springer Berlin Heidelberg, 2000. DOI: 10.1007/978-3-662-04283-0.

[71] Klatzky, R. L. and Lederman, S. J. Tactile roughness perception with a rigid link interposed between skin and surface. *Perception & Psychophysics* **61** (1999), 591–607. DOI: 10.3758/bf03205532.

[72] Miller, L. E., Montroni, L., Koun, E., Salemme, R., Hayward, V., and Farnè, A. Sensing with tools extends somatosensory processing beyond the body. *Nature* **561** (2018), 239–242. DOI: 10.1038/s41586-018-0460-0.

[73] McMahon, T. Mechanics of locomotion. *The International Journal of Robotics Research* **3** (1984), 4–28. DOI: 10.1177/027836498400300202.

[74] Suzuki, S. and Furuta, K. Adaptive impedance control to enhance human skill on a haptic interface system. *Journal of Control Science and Engineering* **2012** (2012), e365067. DOI: 10.1155/2012/365067.

[75] Choi, J., Gu, Z., Lee, J., and Lee, I. Impedance matching control between a human arm and a haptic joystick for long-term. *Robotica* **40** (2022), 1880–1893. DOI: 10.1017/S0263574721001430.

[76] Hertz, H. Ueber die Berührung fester elastischer Körper. **1882** (1882), 156–171. DOI: 10.1515/crll.1882.92.156.

[77] Persson, B. N. J. Theory of rubber friction and contact mechanics. *The Journal of Chemical Physics* **115** (2001), 3840–3861. DOI: 10.1063/1.1388626.

[78] Dhong, C., Miller, R., Root, N. B., Gupta, S., Kayser, L. V., Carpenter, C. W., Loh, K. J., Ramachandran, V. S., and Lipomi, D. J. Role of indentation depth and contact area on human perception of softness for haptic interfaces. *Science Advances* **5** (2019), eaaw8845. DOI: 10.1126/sciadv.aaw8845.

[79] Hauser, S. C. and Gerling, G. J. Force-rate cues reduce object deformation necessary to discriminate compliances harder than the skin. *IEEE Transactions on Haptics* **11** (2018), 232–240. DOI: 10.1109/TOH.2017.2715845.

[80] Moscatelli, A., Bianchi, M., Serio, A., Terekhov, A., Hayward, V., Ernst, M. O., and Bicchi, A. The change in fingertip contact area as a novel proprioceptive cue. *Current Biology* **26** (2016), 1159–1163. DOI: 10.1016/j.cub.2016.02.052.

[81] Farajian, M., Leib, R., Kossowsky, H., Zaidenberg, T., Mussa-Ivaldi, F. A., and Nisky, I. Stretching the skin immediately enhances perceived stiffness and gradually enhances the predictive control of grip force. *eLife* **9** (2020). DOI: 10.7554/eLife.52653.

[82] Bergmann Tiest, W. M. and Kappers, A. M. L. "Kinaesthetic and Cutaneous Contributions to the Perception of Compressibility". In: Haptics: Perception, Devices and Scenarios. Ed. by Ferre, M. Vol. 5024. Berlin, Heidelberg: Springer Berlin Heidelberg, 2008, pp. 255–264. DOI: 10.1007/978-3-540-69057-3_30.

[83] Hartcher-O'Brien, J., Edin, B., and Hayward, V. "Shape-elasticity tactile confound". In: Hand, Brain and Technology: The Somatosensory System CSF Conferenc. 2018, p. 1.

[84] Xu, C., Wang, Y., and Gerling, G. J. An elasticity-curvature illusion decouples cutaneous and proprioceptive cues in active exploration of soft objects. *PLOS Computational Biology* **17** (2021), e1008848. DOI: 10.1371/journal.pcbi.1008848.

[85] Bicchi, A., Scilingo, E., and De Rossi, D. Haptic discrimination of softness in teleoperation: the role of the contact area spread rate. *IEEE Transactions on Robotics and Automation* **16** (2000), 496–504. DOI: 10.1109/70.880800.

[86] Serina, E. R., Mockensturm, E., Mote, C. D., and Rempel, D. A structural model of the forced compression of the fingertip pulp. *Journal of Biomechanics* **31** (1998), 639–646. DOI: 10.1016/s0021-9290(98)00067-0.

[87] Arakawa, N., Saito, N., and Okamoto, S. Less frictional skin feels softer in a tribologically paradoxical manner. *IEEE Access* **10** (2022), 55279–55287. DOI: 10.1109/ACCESS.2022.3175875.

5

6

INCREASED TEMPORAL BINDING DURING VOLUNTARY MOTOR TASK UNDER LOCAL ANESTHESIA

Chapters 3 through 5 investigated the haptic perception of texture and material properties. Concluding the empirical studies of this dissertation, Chapter 6 shifts focus to investigating time perception during haptic object interactions. The chapter ties back to the overall research question by exploring how the sensory system detects change and maintains stability when relevant information is missing. It addresses the specific question: How does the absence of local tactile feedback during a behaviorally relevant motor interaction affect the perception of the timing of contact and its outcomes?

Abstract: Temporal binding refers to a systemic bias in the perceived time interval between two related events, most frequently voluntary motor actions and a subsequent sensory effect. An inevitable component of most instrumental motor actions is tactile feedback. Yet, the role of tactile feedback within this phenomenon remains largely unexplored. Here, we used local anesthesia of the index finger to temporarily inhibit incoming sensory input from the finger itself, while participants performed an interval-estimation task in which they estimated the delay between a voluntary motor action (button press) and a second sensory event (click sound). Results were compared to a control condition with intact sensation. While clear binding was present in both conditions, the effect was significantly enhanced when tactile feedback was temporarily removed via local anesthesia. The results are discussed in light of current debates surrounding the underlying mechanisms and function of this temporal bias.

6.1. INTRODUCTION

Temporal binding can be described as a perceptual illusion in the temporal domain characterized by a compression of the perceived time interval between two causally related events [1, 2]. In the context of voluntary actions and their external sensory outcome, this phenomenon is also widely known as *intentional binding*. It is often considered to be an implicit marker of agency, that is, the conscious experience of bringing about changes in the external world through voluntary actions [3, 4]. This link has, however, recently been questioned [5, 6]. Temporal binding has been shown to be altered in certain psychiatric disorders, most notably schizophrenia [7, 8], and has been linked to personality traits in non-clinical individuals too [9–11]. Extensive research has been conducted to uncover the factors that influence this phenomenon.

Previous research has highlighted the importance of intentionality and volition, such as free choice of action and outcome pursued as well as motor control over the action and outcome prediction for achieving robust binding [3, 12–18]. While voluntary motor actions produce binding, involuntary motor actions (i.e., via TMS of motor cortex) tend to produce reverse binding [3]. Similarly, sensory events exogenous to the agent (e.g., tactile sensations and auditory signals) in the absence of motor movements lead to repulsion rather than a binding effect [12, 13]. Furthermore, self-associated stimuli have been shown to produce stronger binding than stimuli associated with others [19], although there are inconsistencies among the findings [20]. Finally, researchers have emphasized the importance of a causal or contingent relationship between action and outcome for temporal binding [21–25]. Consequently, while intentional movement is necessary, it may not be sufficient to induce binding if the outcome is not perceived to be action contingent. These studies stress the favorability of an overall naturalistic experimental setup since naturalistic events tend to be associated with inherently plausible event links [26].

An inherent aspect of instrumental, voluntary motor actions such as pressing a button or snapping a twig, is immediate tactile feedback that, alongside proprioceptive

signals, contributes to an awareness of having changed the state of the world. To date, only limited research has examined the role of tactile information in temporal binding during a voluntary motor task, and the results have been contentious. While some research has indirectly suggested the importance of tactile sensations in temporal binding [26–30], only a few studies have attempted to directly manipulate tactile signals. This latter research, which has utilized mid-air, contactless gesture-based tactile interactions, has led to incongruent findings, reporting either no binding for contactless interactions [31] or no difference between contactless interactions and physical keypress control conditions [32]. Contactless interactions fundamentally differ from mechanical interactions, leading to limited mechanistic insights and potential confounds. Despite the steady development and expanding applications of mid-air contactless interfaces, mechanical button presses constitute a more common interaction condition encountered by most people on a daily basis.

To address the role of tactile feedback in temporal binding, the current study took the approach of directly abolishing local tactile information during a voluntary motor task, while leaving the long-range consequences of the action intact. Using local anesthesia of participants' index finger, we measured the perceived temporal attraction between an action (button press) and a sensory outcome (click sound), while preserving all other aspects of a mechanical button press. The 'anesthesia' condition was compared to an 'intact' control condition. Since the muscles that move an index finger are located entirely in the hand and forearm, we could assume that the participants' motor behavior would be unaffected by the local anesthesia, except for motor control directly linked to afference from the finger itself [33–35]. Because local anesthesia can result in a perceived enlargement of the anesthetized body part [36], participants also estimated their perceived finger length in the two conditions.

Recent research has cast doubt on the link between temporal binding and agency or intention-related aspects of behavior. This research has emphasized the role of causal inferences and processes of multisensory integration, arguing that substantial evidence ought to be provided when claiming effects to be more than multisensory causal binding [5, 6]. In the present study, no preliminary assumptions were made about such a relationship. Following this reasoning we therefore adhere to the term "temporal binding" instead of the more commonly used term "intentional binding" when referring to the mere effect of a perceived compression of the time interval between a voluntary motor action and sensory outcome.

6.2. METHODS

6.2.1. PARTICIPANTS

Fifteen participants were recruited for the study. None of the participants reported psychiatric or neurological disorders, a history of finger/hand/upper limb trauma, or any condition affecting normal sensorimotor function. One participant was excluded due to incomplete local anesthesia, resulting in a final sample of fourteen participants (8 female, 6 male). The mean age of this remaining cohort was 26.72 (SD 9.24). As assessed by the Edinburgh Handedness Inventory [37], one participant was

left-handed, one participant was mixed-handed, and the remaining twelve participants were right-handed. The mixed-handed participant reported being right-handed and therefore performed the experiment with the right index finger.

The study was approved by the Dutch Medical Ethics Review Committee METC-LDD. Data were collected at the Reinier Haga Orthopaedic Centre and the study was approved by the local ethics committee. The study is also registered on the website of ClinicalTrials.gov with the identifier NCT05253508 (date of first registration 23/02/2022). The methods of this study were performed in accordance with the relevant guidelines and regulations and in accordance with the Declaration of Helsinki. All participants gave written informed consent prior to the start of the experiment and preparation.

6.2.2. APPARATUS

Participants were seated in front of a computer screen, and a snap action switch button was placed in front of their dominant hand, as shown in Figure 6.1. When pressed and released, the button responded with a sharp audible click and a clear tactile detent. The switch button was connected to a digital signal processor (Bela, Augmented Instruments Ltd, Mile End Road, London, England) that sensed its state at a rate of 44,100 samples per second. Upon release, a second auditory click was produced through a loudspeaker with delays of 100, 300, 500, or 700 ms. A Matlab ® (MathWorks, Natick, Massachusetts, USA, Version R2021b) application, communicating with the digital signal processor through a User Datagram Protocol (UDP), specified the delay between the button press and the auditory click, and collected the responses. Once this parameter was transmitted, the trial started and only the digital signal processor was involved, whose inner latency is systematically less than 1 ms. Participants were able to see their hands throughout the experiment.
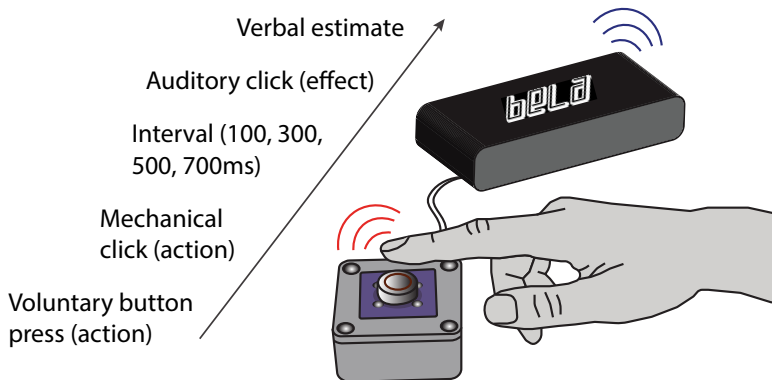

Figure 6.1. Setup and trial structure. Upon pressing the button, an instant mechanical "click" (action) with audible and tactile detent was emitted and then followed by a delayed auditory "click" sound (effect) either 100, 300, 500, or 700 ms after the action. Participants then estimated the interval between their own action and the effect in milliseconds.

6.2.3. PREPARATION

Local anesthesia was induced via a two-sided subcutaneous digital nerve block resulting from an injection of 1–2 ml of ropivacaine 0.2% or lidocaine 2% at either side of the palmar root of the dominant index finger [38]. The effect of the digital nerve-block was assessed using Semmes-Weinstein monofilaments examination. Anesthesia was considered complete when no sensation was reported to remain in the second and third phalanx. One participant had to be excluded because a complete digital nerve block could not be achieved. A complete digital nerve-block was achieved for the remaining fourteen participants. On one of these fourteen participants, the nerve block was done with two injections of lidocaine only. A second participant received a second dose of lidocaine (4 injections in total), when showing early recovery during the data collection of the preceding experiment. The remaining twelve participants received two injections of ropivacaine each. For seven of these participants, sensation was completely abolished on three phalanges. This group reported a mild effect of the anesthetic on the adjacent side of the middle finger. For the remaining seven participants, some sensation was reported on the dorsal side of the proximal phalanx, close to the knuckle. This variation is considered normal due to the cutaneous innervation of this specific region. Small, dorsal branches of the radial nerve may depart from primary branches located proximal to the injection site and will thus eventually not be blocked by the palmar approach of the digital nerve-block [39, 40]. No distinction between these groups was made in the analysis.

6.2.4. EXPERIMENTAL DESIGN AND PROCEDURE

We used a verbal interval estimation paradigm which has been validated in prior studies on temporal binding [41–44]. At the beginning of each trial, a green window appeared on the screen placed in front of participants to indicate that testing could start. Participants then pressed the button to initiate a trial whenever they liked. The button responded with an immediate audible and palpable actionclick when successfully pressed, which was necessary as an objective marker for the start of the interval for both conditions. A second effect-click sound was then emitted with a delay of 100, 300, 500, or 700 ms. Participants' task was to estimate the interval between the button press and the resulting effect-click in milliseconds. They were asked to provide estimates that were as accurate as possible. Estimates were provided verbally and recorded by the experimenter. The setup and trial structure are illustrated in Figure 6.1.

Participants were told that the time interval between the button press and the effect-click could be any random value between 10 and 1000 ms. Prior to testing, all participants were given examples of real time intervals of 10, 500, and 1000 ms. To familiarize themselves with the delay space, they pressed the button and heard the response for each of these intervals as many times as they felt it necessary.

The experiment adopted a repeated-measures design in which all participants took part in two conditions, 'anesthetized' and 'intact'. The order of these conditions was balanced across participants. The experiment comprised two separate blocks of sixty trials encompassing all delays. Each delay was repeated fifteen times in a randomized

order. The blocks were administered on different days, separated by one to three days. This minimum 24-h period was maintained because the effect of ropivacaine can last up to 23 h. Due to practical constraints, two participants completed only forty trials per block. Prior to testing, the participants' index finger length was measured. Then the temperature of their index finger pad was recorded with an infrared thermometer (Tacklife IT-T09) and its hydration level was measured with a skin hydration measurement instrument (Corneometer® CM 825). Participants also assessed the perceived length of their index finger by adjusting the arm of a caliper with both their hands and the display concealed. Temperature, hydration level, and perceived finger length were recorded three times per condition and per participant.

The present experiment was conducted after a material-property discrimination experiment reported elsewhere and approximately 1 ½ hours after the application of the digital nerve block. This other experiment involved exploring surfaces with the index finger, meaning that all participants had the chance to become familiar with the novel experience of an anesthetized finger ahead of the data-collection. The Semmes-Weinstein monofilament examination and all finger-pad temperature and moisture measurements reported here were taken just prior to data collection of the present experiment.

6.2.5. STATISTICAL ANALYSES

Differences in finger temperature, hydration level, and perceived finger length between the two conditions (anesthesia/intact) were assessed using paired-sample t-tests. A linear-trend analysis with an exclusion criterion of $R^2 > 0.5$ was carried out for each participant and condition to ensure that there was a significant trend of gradual increase in the estimates of the 100, 300, 500, and 700 ms intervals. Furthermore, interval estimates that were three or more standard deviations from the mean were excluded. The remaining estimates were subjected to an ANOVA with repeated measures on factors *condition* (anesthesia/intact) and *delay* (100, 300, 500, 700 ms). A second ANOVA with repeated measures on *order* (first block/second block) and *delay* (100, 300, 500, 700 ms) was performed to control for any order effects, although the condition order was balanced. The significance level was set at $p < 0.05$. Sphericity was assessed using Mauchly's test, and adjustments were made using Greenhouse-Geisser corrections. Post-hoc Bonferroni-corrected pairwise comparisons were used to determine which conditions differ from one another for significant effects of factors with more than two levels.

All statistical analyses were performed in R (version 4.2.0, R Core Team, 2021).

6.3. ANALYSIS AND RESULTS

The mean duration of trials from the button release to response logging was 6.33 s (SD 1.46) for the intact condition and 6.69 s (SD 1.08) for the anesthesia condition. The duration of the entire experiment was approximately six minutes for each condition recorded on separate days.

Mean hydration values were 65.96 (SD 28.09) for the intact condition and 25.28 (SD 7.30) for the anesthesia condition. Mean finger pad temperatures were 28.63 (SD 3.10) for the intact condition and 29.81 (SD 2.90) for the anesthesia condition. Paired-samples t-tests revealed a significant difference between the hydration measurements ($t(13) = 5.96, p < 0.01$) but not the temperature measurements ($t(13) = -1.51, p = 0.15$) for the two conditions. On average, the index finger length was estimated to be 3.18 mm longer than the actual finger length for the intact condition (SD 14.31) and 3.20 mm longer for the anesthesia condition (SD 11.63). A paired-sample t-test revealed no significant difference between the two conditions ($t(13) < 0.01, p = 1.00$).

To ensure that there was a significant trend of gradual increase in the estimates of the 100, 300, 500, and 700 ms intervals, a linear trend analysis was performed for each participant and for each condition. No participant had to be excluded based on the criterion of R2 > 0.5. Next, interval estimates that differed by more than three standard deviations from the mean were excluded. A total of four responses were excluded on the basis of this criterion. A fifth response was excluded from the analysis due to an undesired disturbance during the data collection.

The remaining interval estimates were subjected to a two-way repeated-measures Analysis of Variance (ANOVA) with factors *condition* (anesthesia/intact) and *delay* (100, 300, 500, 700 ms). The ANOVA yielded a main effect of condition ($F(1, 13) = 5.37, p = 0.04, \eta^2 = 0.05$), indicating shorter interval estimates in the anesthesia condition (mean 213.41, SD 95.14) than in the intact condition (mean 282.96, SD 147.51). The analysis revealed a significant main effect of delay, indicating that longer delays were estimated as longer intervals. This effect did not pass Mauchly's test for sphericity but remained significant after Greenhouse-Geisser corrections ($F(1, 14) = 49.20, p_{GG} < 0.01, \eta^2 = 0.52$). For the anesthesia condition, the mean estimates were 59.53 (SD 48.19) at 100 ms, 118.15 (SD 76.26) at 300 ms, 259.14 (SD 123.99) at 500 ms, and 417.22 (SD 209.53) at 700 ms. For the intact condition, the mean estimates were 87.05 (SD 87.51) at 100 ms, 167.62 (SD 125.79) at 300 ms, 352.22 (SD 195.13) at 500 ms, and 524.79 (SD 249.07) at 700 ms. Bonferroni-corrected post-hoc pairwise comparisons for the main effect of delay revealed significant differences between all levels of delay (all $p < 0.01$). However, the interaction between *condition* and *delay* was not significant ($F(1, 20) = 2.16, p_{GG} = 0.15, \eta^2 = 0.01$), indicating that the difference in binding between the two conditions was not specific to any delay. A second ANOVA with the factors *order* (first block/second block) and *delays* (100, 300, 500, 700 ms) was carried out to control for any order effects, although the order of the conditions was balanced. The analysis revealed no significant main effect of order ($F(1, 13) = 0.13, p = 0.72, \eta^2 < 0.01$). Figure 6.2 shows the mean estimated intervals for each condition and delay.

6.4. DISCUSSION

The analysis revealed a significantly *increased* effect of temporal binding in the anesthesia condition as compared to the intact condition. This difference was not
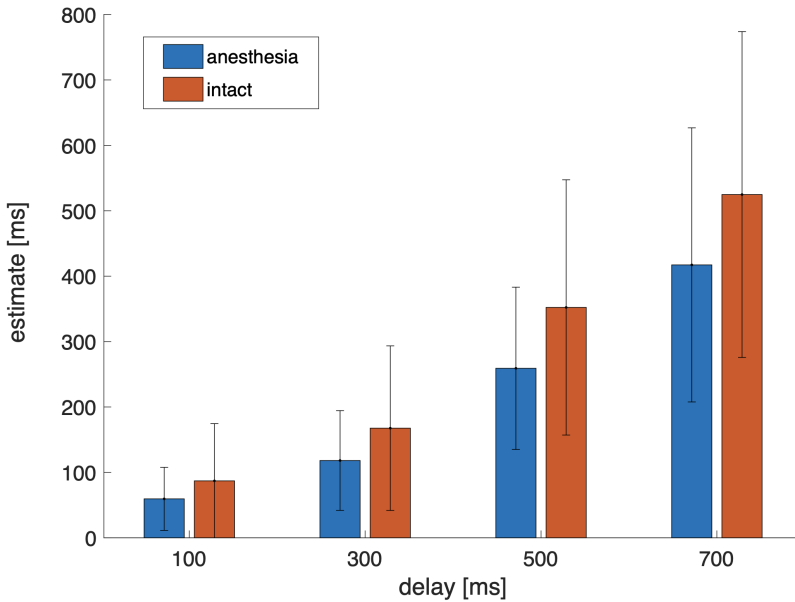
Figure 6.2. Figure 2. Mean estimated intervals per delay for the anesthesia (blue) and intact (orange) condition. Error bars indicate the standard deviation of the mean.

specific to any of the delays. Possible mechanisms and implications of these results are discussed below.

Some studies have indirectly suggested the importance of tactile sensory feedback in temporal binding. Increased temporal binding is for instance observed when the voluntary action involves touching skin rather than a button [27, 29]. Furthermore, a temporal compression effect can be observed for tactile stimuli delivered to the hand during hand movements [30]. However, few studies have directly manipulated this variable in a temporal binding paradigm. One study used a laser-beam paradigm in which participants could cause a visual stimulus to instantly disappear via mid-air button-press gestures, which then led to the appearance of a second visual target stimulus after a specified delay [31]. In contrast to a control condition which involved pressing a physical key, the contactless key-press gesture did not result in a significant binding effect, leading the authors to conclude that "both intentionality and tactile sensory feedback are necessary to induce the binding effect". However, another study investigating temporal binding using contactless key-press gestures, reported no statistical difference between this condition and a control condition involving a physical key press action—provided that the outcome stimulus was auditory or haptic in nature [32]. When the actions were followed by a visual outcome, the binding was diminished for either of these conditions. The lack of efficiency of visual targets in

producing binding as compared to auditory targets has been reported previously [45, 46], although visual targets have successfully been used elsewhere to induce temporal binding [42, 47]. Further differences between the two studies include that Cornelio Martinez et al. [32] did not provide any initial, action-related, feedback to indicate that the mid-air button-press gesture had successfully been carried out, which may have introduced some inaccuracy for the participants to judge the exact onset of the intervals and higher temporal uncertainty in their motor production estimation [48].

While we cannot assert what caused these incongruent results, 'contactless' gesture-based actions are not directly comparable to mechanical keypress actions. Observers come with a prediction of the consequences of their own actions based on the physics of their everyday environment. In contactless gesture interactions, observers may not apply the same physics and may anticipate different consequences of their actions. In the present study we believe to have mitigated this shortcoming by introducing an endogenous modification in the participant, resulting in sensationless rather than contactless interactions. Here, we did not only observe a significant binding-effect for both experimental conditions, but an increased effect after temporary deafferentation via local anesthesia. While this finding may seem counter-intuitive, considering previous research highlighting the significance of tactile feedback for temporal binding, it is important to bear the differences between those previous studies and the present study in mind. These previous studies either added additional tactile stimulation to a normal somatosensory condition [27, 29, 30] or avoided tactile feedback by eliminating physical contact altogether [31, 32]. Adding tactile stimulations or feedback in some of the previous studies may for instance have increased the perceived contingency or simply relevance of the interaction in question, leading to a comparatively stronger effect of temporal compression. Similarly, preventing contact entirely may have strained participants sense of control over the event, affected its perceived plausibility, or challenged the inherent cause-effect link between the action and outcome. However, it is unlikely that endogenously suppressing tactile feedback in the present study would have weakened such links. Furthermore, we have no reason to believe that participants' experience of control or 'ownership' over their anesthetized finger was impaired. We readily observed that participants were able to move their anesthetized finger freely, with the exception of mild restrictions due to the swelling of the finger from the anesthetic solution injected at the base. This swelling was however greatest immediately after the injection of the anesthetic and mainly affected full flexion of the finger, which was not required during the task. Moreover, while disproving that tactile sensory feedback is necessary to induce a temporal binding effect, this finding still provides evidence that tactile feedback is functional in determining temporal binding, since diminishing it significantly alters the outcome.

The finding that tactile sensory feedback is not a prerequisite for a stable temporal-binding effect to occur, is furthermore consistent with observations reported in studies of body ownership. Body ownership refers to the experience of one's body and body parts belonging to oneself [49], and the phenomenon has frequently, but not always, been argued to be related to agency and temporal binding [50–52]. Whilst it is known that cutaneous stimulation can induce a sense of ownership of an artificial

6

limb in the so-called rubber-hand illusion [53–56], two studies have shown that tactile sensations do not seem to be essential for an ownership illusion to take place, provided that proprioceptive cues from muscle receptors are present [57, 58]. By exciting muscle receptors during movement, the researchers showed how ownership over a plastic finger could reliably be induced, while cutaneous and joint receptors of participants real finger had been blocked using local anesthesia. The present results show how a similar non-conditional relationship seems to exist between tactile sensations and temporal binding. However, while these arguments support our finding that tactile sensory feedback is not strictly necessary for temporal binding to occur, they do not address potential reasons for why the effect is exaggerated under local anesthesia. In the following section, we discuss potential mechanisms that may have contributed to such an effect.

Human body representations are malleable [36, 54, 57, 59], and perceptual changes associated with local anesthesia have been described previously, some of which may be worth considering here. For example, perceptual distortions of the body image are a commonly reported consequence of local anesthesia. Most notably, it is known that local anesthesia can lead to an increase in the perceived size and shape of the anesthetized body part, as well as changes in its perceived posture [36, 59–63]. Gandevia and Phegan [36], for instance, used a drawing task as well as the selecting of drawings of thumbs to demonstrate that perceived thumb size increases by 60–70% under local anesthesia (using a digital nerve block as in the present study).

In the present study we did not find an effect of the digital nerve block on perceived finger length. However, a study performed by Walsh et al. [63], in which the perceived enlargement of a finger during a digital nerve block was compared to a saline injection control, reported a significant perceptual enlargement of the finger width but not length, suggesting nonuniform changes in the perceived size of the finger following digital anesthesia.

The exact causes and mechanisms behind these perceptual changes are still unclear, although perceptual enlargements may be a consequence of acute changes in cortical representations [36, 63–65]. Walsh et al. [63] further proposed that when sensory information is lost during local anesthesia, the brain might infer injury and increase the body's perceptual perimeter to protect it from further injury, since body parts that feel larger may be kept further away from hazardous objects. This is in line with findings showing that partial anesthesia [63], as well as an elevation of peripheral input through painful cooling and innocuous stimulation of the digital nerve [36], also result in a perceptual enlargement of the affected digit, albeit smaller than the effect observed under local anesthesia.

While perceived *spatial* distortions resulting from acute deafferentation (e.g., local anesthesia) have been reported regularly, no research yet, to the best of our knowledge, has provided insights into perceived *temporal* distortions resulting from voluntary actions with a temporarily deafferented body part. Our results provide initial insights into such a phenomenon. It is known from research on temporal recalibration that our sensory system is able to rapidly adapt to small inter-sensory asynchronies in order to maintain coherence during multisensory interactions [66–69]. Moreover, recent mechanistic approaches to temporal binding itself have highlighted the role of

multisensory cue integration and cross-modal grouping as the driving mechanism behind the phenomenon [2, 6, 28, 70]. A redundant cue from a different modality (here auditory) provided at both action and outcome in a delay detection task, can for instance reduce both the perceptual grouping of the action and outcome event as well as explicit ratings of agency over the outcome event [71]. This occurs because the additional cue, rather than the outcome event, is integrated with the action event. While this does not occur when the additional auditory cue coincides with only one of the events (action or outcome), it is still plausible that the lack of tactile feedback during the action in the anesthesia condition of the present study somehow facilitated the linking of action and outcome, resulting in an even stronger binding than in the intact condition. Furthermore, a recent study demonstrated how *lighter* key presses lead to *stronger* action binding (that is, the degree to which the perceived time of an action is shifted forward in the so-called Libet-clock paradigm), when followed by an auditory cue [28]. Such results are in line with the findings reported here, suggesting that somatosensory or tactile feedback is negatively correlated with temporal binding. Whether the increased binding reported by Cao et al. [28] or in the present study coincided with an exaggerated sense of agency, remains to be tested but could be expected if one adopts a view of the sense of agency as being the general product of causality determination between action and outcome [21, 71, 72].

It could finally be reasoned, that increased temporal binding when interacting with objects in the environment with a sensorily affected body part plays a functional role in avoiding perceptual conflicts or in preventing injury. An exaggerated temporal link between one's actions and the outcome could consequently be useful in confirming that an action has been performed successfully with the deafferented or injured body part, in the absence of tactile feedback. In this view, increased temporal binding during local anesthesia could be seen as a compensatory mechanism to ensure that significant events are linked together when confirmation from one sensory modality is either specifically missing or more generally modulated. If the latter hypothesis holds true, then other somatosensory modulations (such as for example increased tactile stimulation or pain) might also lead to a change in temporal binding. In fact, Faivre et al. [73] demonstrated how sensorimotor conflicts induced by asynchronous (as opposed to synchronous) tactile stimulation of the trunk or hand while tapping with the finger, led to an increase in temporal binding similar to that observed under local anesthesia. Together with the present results, this may point to a more general account in which the temporal-binding effect is sensitive to sensory modulations. Findings showing that arousal itself can enhance temporal binding [74] would be in line with such a hypothesis. However, further research would be needed to verify this hypothesis. Research on pain and temporal binding could for instance shed further light on this question. While no research has yet been reported investigating the effect of painful sensations on temporal binding, effects of increased analgesia through an increased sense of agency or control is a well-known phenomenon [75–78].

It remains to be tested whether the temporal perceptual distortions described in the current study are a direct consequence of the temporary deafferentation (e.g., a protective mechanism) or a more indirect effect, such as a consequence of the better-documented spatial distortions (perceived enlargement of the finger leads to

increased temporal binding). De Vignemont et al. [79] demonstrated how spatial distances are perceived to be larger when touched with a body part that is perceived to be larger. In other words, if we believe to have caused an event further away or closer to our body, spatial separation may alter our perceived timing of this event too. In the present study, we must furthermore bear in mind that participants had the opportunity to become familiar with the sensation and the use of their anesthetized finger during a preceding experiment. This prompts the question of the phenomenon's sensitivity to learning and time. While the effect observed here could be an acute and immediate response to the temporary deafferentation itself, it might also be an effect ascribable to learning and adapting to the new biomechanical constraints and changes in feedback from the anesthetized finger. Future studies will need to investigate the time course of such perceptual changes. Research on temporal binding using tools or prosthetic limbs, as well as research including individuals who have lived with deafferented limbs over a longer period of time, could potentially shed light on some of these questions.

6.4.1. CLINICAL CONSIDERATIONS

Temporal binding has been reported to be altered in certain psychiatric disorders. Most clinical research has focused on schizophrenia, which has been associated with increased temporal binding [80–82]. However, other clinical populations, such as individuals with apraxia and alien limb [83, 84], Parkinson's disease [85, 86], autism spectrum disorder [87, 88], Gilles de la Tourette [89], and individuals with borderline personality disorder traits [90] and obsessive-compulsive tendencies [91] have been associated with altered temporal binding effects. Altered temporal binding effects in clinical populations have most frequently been viewed upon in the light of an altered sense of agency. However, our findings once again highlight the importance of not taking this link for given [5, 6, 21, 22, 46]. Temporal binding appears to be sensitive to a multitude of factors that may not be directly linked to agency-related modulations. Here, we have shown that it is sensitive to a specific type of sensory alterations. Although we can only speculate, alterations in sensory processing, which is a commonly described symptom in many of the above-mentioned conditions, could for instance be one of several mediating factors in the altered temporal-binding effects observed in certain clinical populations. It would be important for future research to try to uncover such mediating factors where they exist.

6.4.2. LIMITATIONS OF THE CURRENT STUDY AND FUTURE DIRECTIONS

The present study comprises several limitations. While the interval estimation procedure used in this study has the advantage of being less visually demanding and less sensitive to precise instructions and certain changes in the setup as compared to the Libet Clock paradigm [92, 93], a clear drawback of the interval-estimation procedure is, that it does not allow distinguishing between so-called action-binding from effect-binding. Consequently, we cannot know whether the effect observed in the present study was due to participants experiencing their action as occurring later, the effect as occurring earlier, or a combination of both. Another limitation is, that

we did not measure changes in the perceived finger-width, only length, as this would have required a saline control in the intact condition. However, knowledge of this might have facilitated a potential linking of well-known spatial distortions during local anesthesia with the temporal distortions observed here. Finally, it is important to bear in mind that the removal of tactile cues using local anesthesia in the current study did not eliminate all haptic cues. Proprioceptive cues in the hand and forearm, as well as vibratory cues propagating to remote sites, may still have been available [94–97]. Recording of such propagating cues at remote intact sites (such as the back of the hand) could have provided a way to assess their potential role in the observed effect.

6.5. CONCLUSION

The present study revealed an enhanced effect of temporal binding for motor actions carried out with an anesthetized finger as compared to an intact finger. While this supports the conclusion that tactile sensory feedback is not a prerequisite for temporal binding to occur, it also emphasizes the importance of this parameter in modulating temporal binding. The precise mechanism by which the effect is enhanced when tactile feedback is temporarily removed, remains to be understood. Whether the effect observed in the current study was a mere effect of changes in multisensory causal binding or was in any way linked to changes in action-intentionality or agency (increased sense of "I did that"), remains to be tested. Similarly, future research will need to investigate whether the temporal distortions observed here are related to previously reported spatial distortions under regional anesthesia, or whether these are two independent effects.

6

REFERENCES

[1] Hoerl, C., Lorimer, S., McCormack, T., Lagnado, D. A., Blakey, E., Tecwyn, E. C., and Buehner, M. J. Temporal binding, causation, and agency: developing a new theoretical framework. *Cognitive Science* **44** (2020), e12843. DOI: `10.1111/cogs.12843`.

[2] Klaffehn, A. L., Sellmann, F. B., Kirsch, W., Kunde, W., and Pfister, R. Temporal binding as multisensory integration: Manipulating perceptual certainty of actions and their effects. *Attention, Perception, & Psychophysics* **83** (2021), 3135–3145. DOI: `10.3758/s13414-021-02314-0`.

[3] Haggard, P., Clark, S., and Kalogeras, J. Voluntary action and conscious awareness. *Nature Neuroscience* **5** (2002), 382–385. DOI: `10.1038/nn827`.

[4] Moore, J. W. and Obhi, S. S. Intentional binding and the sense of agency: A review. *Consciousness and Cognition*. Beyond the Comparator Model **21** (2012), 546–561. DOI: `10.1016/j.concog.2011.12.002`.

[5] Suzuki, K., Lush, P., Seth, A. K., and Roseboom, W. Intentional binding without intentional action. *Psychological Science* **30** (2019), 842–853. DOI: `10.1177/0956797619842191`.

[6] Kirsch, W., Kunde, W., and Herbort, O. Intentional binding is unrelated to action intention. *Journal of Experimental Psychology. Human Perception and Performance* **45** (2019), 378–385. DOI: `10.1037/xhp0000612`.

[7] Haggard, P., Martin, F., Taylor-Clarke, M., Jeannerod, M., and Franck, N. Awareness of action in schizophrenia. *Neuroreport* **14** (2003), 1081–1085. DOI: `10.1097/01.wnr.0000073684.00308.c0`.

[8] Voss, M., Moore, J., Hauser, M., Gallinat, J., Heinz, A., and Haggard, P. Altered awareness of action in schizophrenia: a specific deficit in predicting action consequences. *Brain: A Journal of Neurology* **133** (2010), 3104–3112. DOI: `10.1093/brain/awq152`.

[9] Di Plinio, S., Arnò, S., Perrucci, M. G., and Ebisch, S. J. H. Environmental control and psychosis-relevant traits modulate the prospective sense of agency in non-clinical individuals. *Consciousness and Cognition* **73** (2019), 102776. DOI: `10.1016/j.concog.2019.102776`.

[10] Hascalovitz, A. C. and Obhi, S. S. Personality and intentional binding: an exploratory study using the narcissistic personality inventory. *Frontiers in Human Neuroscience* **9** (2015). DOI: `10.3389/fnhum.2015.00013`.

[11] Moore, J. W., Dickinson, A., and Fletcher, P. C. Sense of agency, associative learning, and schizotypy. *Consciousness and Cognition* **20** (2011), 792–800. DOI: `10.1016/j.concog.2011.01.002`.

[12] Antusch, S., Custers, R., Marien, H., and Aarts, H. Studying the sense of agency in the absence of motor movement: an investigation into temporal binding of tactile sensations and auditory effects. *Experimental Brain Research* **239** (2021), 1795–1806. DOI: `10.1007/s00221-021-06087-8`.

[13] Antusch, S., Custers, R., Marien, H., and Aarts, H. Intentionality and temporal binding: Do causality beliefs increase the perceived temporal attraction between events? *Consciousness and Cognition* **77** (2020), 102835. DOI: `10.1016/j.concog.2019.102835`.

[14] Borhani, K., Beck, B., and Haggard, P. Choosing, doing, and controlling: Implicit sense of agency over somatosensory events. *Psychological Science* **28** (2017), 882–893. DOI: `10.1177/0956797617697693`.

[15] Hayashida, K., Nishi, Y., Masuike, A., and Morioka, S. Intentional binding effects in the experience of noticing the regularity of a perceptual-motor task. *Brain Sciences* **10** (2020), E659. DOI: `10.3390/brainsci10090659`.

[16] Moore, J. and Haggard, P. Awareness of action: Inference and prediction. *Consciousness and Cognition* **17** (2008), 136–144. DOI: `10.1016/j.concog.2006.12.004`.

[17] Morioka, S., Hayashida, K., Nishi, Y., Negi, S., Nishi, Y., Osumi, M., and Nobusako, S. Changes in intentional binding effect during a novel perceptual-motor task. *PeerJ* **6** (2018), e6066. DOI: `10.7717/peerj.6066`.

[18] Soral, W., Kofta, M., and Bukowski, M. Helplessness experience and intentional (un-)binding: Control deprivation disrupts the implicit sense of agency. *Journal of Experimental Psychology. General* **150** (2021), 289–305. DOI: `10.1037/xge0000791`.

[19] Makwana, M. and Srinivasan, N. Self-associated stimuli produce stronger intentional binding. *Journal of Experimental Psychology: Human Perception and Performance* **45** (2019), 1436. DOI: `10.1037/xhp0000687`.

[20] Poonian, S. K. and Cunnington, R. Intentional binding in self-made and observed actions. *Experimental Brain Research* **229** (2013), 419–427. DOI: `10.1007/s00221-013-3505-5`.

[21] Buehner, M. J. and Humphreys, G. R. Causal binding of actions to their effects. *Psychological Science* **20** (2009), 1221–1228. DOI: `10.1111/j.1467-9280.2009.02435.x`.

[22] Buehner, M. J. Understanding the past, predicting the future: causation, not intentional action, is the root of temporal binding. *Psychological Science* **23** (2012), 1490–1497. DOI: `10.1177/0956797612444612`.

[23] Cravo, A. M., Claessens, P. M. E., and Baldo, M. V. C. Voluntary action and causality in temporal binding. *Experimental Brain Research* **199** (2009), 95–99. DOI: `10.1007/s00221-009-1969-0`.

6

[24] Moore, J. W., Lagnado, D., Deal, D. C., and Haggard, P. Feelings of control: contingency determines experience of action. *Cognition* **110** (2009), 279–283. DOI: 10.1016/j.cognition.2008.11.006.

[25] Ruess, M., Thomaschke, R., and Kiesel, A. Intentional binding for unintended effects. *Timing & Time Perception* **8** (2020), 341–349. DOI: 10.1163/22134468-bja10005.

[26] Thanopoulos, V., Psarou, E., and Vatakis, A. Robust intentional binding for causally-linked sequences of naturalistic events but not for abstract event sequences. *Acta Psychologica* **190** (2018), 159–173. DOI: 10.1016/j.actpsy.2018.08.001.

[27] Bergström, J., Coyle, D., Knibbe, J., and Hornbæk, K. "I Really did That: Sense of Agency with Touchpad, Keyboard, and On-skin Interaction". In: 2018, pp. 1–8. DOI: 10.1145/3173574.3173952.

[28] Cao, L., Steinborn, M., Kunde, W., and Haendel, B. Action force modulates action binding: evidence for a multisensory information integration explanation. *Experimental Brain Research* **238** (2020), 2019–2029. DOI: 10.1007/s00221-020-05861-4.

[29] Coyle, D., Moore, J., Kristensson, P. O., Fletcher, P., and Blackwell, A. "I did that! Measuring users' experience of agency in their own actions". In: Proceedings of the SIGCHI Conference on Human Factors in Computing Systems. CHI '12. New York, NY, USA: Association for Computing Machinery, 2012, pp. 2025–2034. DOI: 10.1145/2207676.2208350.

[30] Tomassini, A., Gori, M., Baud-Bovy, G., Sandini, G., and Morrone, M. C. Motor commands induce time compression for tactile stimuli. *Procedia - Social and Behavioral Sciences* **126** (2014), 100–101. DOI: 10.1016/j.sbspro.2014.02.327.

[31] Zhao, K., Hu, L., Qu, F., Cui, Q., Piao, Q., Xu, H., Li, Y., Wang, L., and Fu, X. Voluntary action and tactile sensory feedback in the intentional binding effect. *Experimental Brain Research* **234** (2016), 2283–2292. DOI: 10.1007/s00221-016-4633-5.

[32] Cornelio Martinez, P. I., De Pirro, S., Vi, C. T., and Subramanian, S. "Agency in Mid-air Interfaces". In: Proceedings of the 2017 CHI Conference on Human Factors in Computing Systems. CHI '17. New York, NY, USA: Association for Computing Machinery, 2017, pp. 2426–2439. DOI: 10.1145/3025453.3025457.

[33] Edin, B. B. and Abbs, J. H. Finger movement responses of cutaneous mechanoreceptors in the dorsal skin of the human hand. *Journal of Neurophysiology* **65** (1991), 657–670. DOI: 10.1152/jn.1991.65.3.657.

[34] Moscatelli, A., Bianchi, M., Serio, A., Terekhov, A., Hayward, V., Ernst, M. O., and Bicchi, A. The change in fingertip contact area as a novel proprioceptive cue. *Current Biology* **26** (2016), 1159–1163. DOI: 10.1016/j.cub.2016.02.052.

6

[35] Terekhov, A. V. and Hayward, V. The brain uses extrasomatic information to estimate limb displacement. *Proceedings of the Royal Society B: Biological Sciences* **282** (2015), 20151661. DOI: `10.1098/rspb.2015.1661`.

[36] Gandevia, S. C. and Phegan, C. M. L. Perceptual distortions of the human body image produced by local anaesthesia, pain and cutaneous stimulation. *The Journal of Physiology* **514** (1999), 609–616. DOI: `10.1111/j.1469-7793.1999.609ae.x`.

[37] Oldfield, R. C. The assessment and analysis of handedness: The Edinburgh inventory. *Neuropsychologia* **9** (1971), 97–113. DOI: `10.1016/0028-3932(71)90067-4`.

[38] Wolfe, S. W., Pederson, W. C., Kozin, S. H., and Cohen, M. S. *Green's Operative Hand Surgery*. Elsevier Health Sciences, 2021.

[39] Hadzic, A., ed. *NYSORA textbook of regional anesthesia and acute pain management*. New York, N.Y.: McGraw-Hill Education LLC., 2007.

[40] Li, H., Hu, X., and Yang, S. The overall distribution pattern of the hand's cutaneous nerves and its clinical implications in sensory reconstruction. *International Journal of Morphology* **39** (2021), 447–454. DOI: `10.4067/S0717-95022021000200447`.

[41] Engbert, K., Wohlschläger, A., Thomas, R., and Haggard, P. Agency, subjective time, and other minds. *Journal of Experimental Psychology: Human Perception and Performance* **33** (2007), 1261–1268. DOI: `10.1037/0096-1523.33.6.1261`.

[42] Engbert, K., Wohlschläger, A., and Haggard, P. Who is causing what? The sense of agency is relational and efferent-triggered. *Cognition* **107** (2008), 693–704. DOI: `10.1016/j.cognition.2007.07.021`.

[43] Fereday, R. and Buehner, M. J. Temporal binding and internal clocks: No evidence for general pacemaker slowing. *Journal of Experimental Psychology. Human Perception and Performance* **43** (2017), 971–985. DOI: `10.1037/xhp0000370`.

[44] Humphreys, G. R. and Buehner, M. J. Magnitude estimation reveals temporal binding at super-second intervals. *Journal of Experimental Psychology. Human Perception and Performance* **35** (2009), 1542–1549. DOI: `10.1037/a0014492`.

[45] Imaizumi, S. and Tanno, Y. Intentional binding coincides with explicit sense of agency. *Consciousness and Cognition* **67** (2019), 1–15. DOI: `10.1016/j.concog.2018.11.005`.

[46] Ruess, M., Thomaschke, R., and Kiesel, A. Intentional binding of visual effects. *Attention, Perception, & Psychophysics* **80** (2018), 713–722. DOI: `10.3758/s13414-017-1479-2`.

[47] Ebert, J. P. and Wegner, D. M. Time warp: Authorship shapes the perceived timing of actions and events. *Consciousness and Cognition* **19** (2010), 481–489. DOI: `10.1016/j.concog.2009.10.002`.

[48] Jazayeri, M. and Shadlen, M. N. Temporal context calibrates interval timing. *Nature Neuroscience* **13** (2010), 1020–1026. DOI: `10.1038/nn.2590`.

6

[49] Gallagher, S. Philosophical conceptions of the self: implications for cognitive science. *Trends in Cognitive Sciences* **4** (2000), 14–21. DOI: 10.1016/S1364-6613(99)01417-5.

[50] Braun, N., Thorne, J. D., Hildebrandt, H., and Debener, S. Interplay of agency and ownership: the intentional binding and rubber hand illusion paradigm combined. *PloS One* **9** (2014), e111967. DOI: 10.1371/journal.pone.0111967.

[51] Pyasik, M., Burin, D., and Pia, L. On the relation between body ownership and sense of agency: A link at the level of sensory-related signals. *Acta Psychologica* **185** (2018), 219–228. DOI: 10.1016/j.actpsy.2018.03.001.

[52] Zopf, R., Polito, V., and Moore, J. Revisiting the link between body and agency: visual movement congruency enhances intentional binding but is not body-specific. *Scientific Reports* **8** (2018), 196. DOI: 10.1038/s41598-017-18492-7.

[53] Cataldo, A., Di Luca, M., Deroy, O., and Hayward, V. Touching with the eyes: Oculomotor self-touch induces illusory body ownership. *iScience* **26** (2023), 106180. DOI: 10.1016/j.isci.2023.106180.

[54] Botvinick, M. and Cohen, J. Rubber hands 'feel' touch that eyes see. *Nature* **391** (1998), 756. DOI: 10.1038/35784.

[55] Costantini, M. and Haggard, P. The rubber hand illusion: Sensitivity and reference frame for body ownership. *Consciousness and Cognition* **16** (2007), 229–240. DOI: 10.1016/j.concog.2007.01.001.

[56] Ehrsson, H. H., Spence, C., and Passingham, R. E. That's my hand! Activity in premotor cortex reflects feeling of ownership of a limb. *Science* **305** (2004), 875–877. DOI: 10.1126/science.1097011.

[57] Héroux, M. E., Walsh, L. D., Butler, A. A., and Gandevia, S. C. Is this my finger? Proprioceptive illusions of body ownership and representation. *The Journal of Physiology* **591** (2013), 5661–5670. DOI: 10.1113/jphysiol.2013.261461.

[58] Walsh, L. D., Moseley, G. L., Taylor, J. L., and Gandevia, S. C. Proprioceptive signals contribute to the sense of body ownership. *The Journal of Physiology* **589** (2011), 3009–3021. DOI: 10.1113/jphysiol.2011.204941.

[59] Inui, N., Walsh, L. D., Taylor, J. L., and Gandevia, S. C. Dynamic changes in the perceived posture of the hand during ischaemic anaesthesia of the arm. *The Journal of Physiology* **589** (2011), 5775–5784. DOI: 10.1113/jphysiol.2011.219949.

[60] Paqueron, X., Leguen, M., Rosenthal, D., Coriat, P., Willer, J. C., and Danziger, N. The phenomenology of body image distortions induced by regional anaesthesia. *Brain* **126** (2003), 702–712. DOI: 10.1093/brain/awg063.

[61] Paqueron, X., Gentili, M. E., Willer, J. C., Coriat, P., and Riou, B. Time sequence of sensory changes after upper extremity block: swelling sensation is an early and accurate predictor of success. *Anesthesiology* **101** (2004), 162–168. DOI: 10.1097/00000542-200407000-00025.

6

[62] Silva, S., Bataille, B., Jucla, M., Minville, V., Samii, K., Fourcade, O., Démonet, J.-F., and Loubinoux, I. Temporal analysis of regional anaesthesia-induced sensorimotor dysfunction: a model for understanding phantom limb. *British Journal of Anaesthesia* **105** (2010), 208–213. DOI: 10.1093/bja/aeq144.

[63] Walsh, L. D., Hoad, D., Rothwell, J. C., Gandevia, S. C., and Haggard, P. Anaesthesia changes perceived finger width but not finger length. *Experimental Brain Research* **233** (2015), 1761–1771. DOI: 10.1007/s00221-015-4249-1.

[64] Giurgola, S., Pisoni, A., Maravita, A., Vallar, G., and Bolognini, N. Somatosensory cortical representation of the body size. *Human Brain Mapping* **40** (2019), 3534–3547. DOI: 10.1002/hbm.24614.

[65] Medina, J. and Coslett, H. B. What can errors tell us about body representations? *Cognitive Neuropsychology* **33** (2016), 5–25. DOI: 10.1080/02643294.2016.1188065.

[66] Fujisaki, W., Shimojo, S., Kashino, M., and Nishida, S. Recalibration of audiovisual simultaneity. *Nature Neuroscience* **7** (2004), 773–778. DOI: 10.1038/nn1268.

[67] Navarra, J., Vatakis, A., Zampini, M., Soto-Faraco, S., Humphreys, W., and Spence, C. Exposure to asynchronous audiovisual speech extends the temporal window for audiovisual integration. *Brain Research. Cognitive Brain Research* **25** (2005), 499–507. DOI: 10.1016/j.cogbrainres.2005.07.009.

[68] Navarra, J., Soto-Faraco, S., and Spence, C. Adaptation to audiotactile asynchrony. *Neuroscience Letters* **413** (2007), 72–76. DOI: 10.1016/j.neulet.2006.11.027.

[69] Vroomen, J., Keetels, M., de Gelder, B., and Bertelson, P. Recalibration of temporal order perception by exposure to audio-visual asynchrony. *Brain Research. Cognitive Brain Research* **22** (2004), 32–35. DOI: 10.1016/j.cogbrainres.2004.07.003.

[70] Wolpe, N., Haggard, P., Siebner, H. R., and Rowe, J. B. Cue integration and the perception of action in intentional binding. *Experimental Brain Research* **229** (2013), 467–474. DOI: 10.1007/s00221-013-3419-2.

[71] Kawabe, T., Roseboom, W., and Nishida, S. The sense of agency is action–effect causality perception based on cross-modal grouping. *Proceedings of the Royal Society B: Biological Sciences* **280** (2013), 20130991. DOI: 10.1098/rspb.2013.0991.

[72] Wegner, D. M. Précis of the illusion of conscious will. *The Behavioral and Brain Sciences* **27** (2004), 649–659, discussion 659–692. DOI: 10.1017/s0140525x04000159.

[73] Faivre, N., Vuillaume, L., Bernasconi, F., Salomon, R., Blanke, O., and Cleeremans, A. Sensorimotor conflicts alter metacognitive and action monitoring. *Cortex; a Journal Devoted to the Study of the Nervous System and Behavior* **124** (2020), 224–234. DOI: 10.1016/j.cortex.2019.12.001.

6

[74] Wen, W., Yamashita, A., and Asama, H. The influence of action-outcome delay and arousal on sense of agency and the intentional binding effect. *Consciousness and Cognition* **36** (2015), 87–95. DOI: `10.1016/j.concog.2015.06.004`.

[75] Beck, B. and Haggard, P. "Pain, voluntary action, and the sense of agency". In: The Routledge Handbook of Philosophy of Pain. Routledge, 2017.

[76] Mohr, C., Binkofski, F., Erdmann, C., Büchel, C., and Helmchen, C. The anterior cingulate cortex contains distinct areas dissociating external from self-administered painful stimulation: a parametric fMRI study. *Pain* **114** (2005), 347–357. DOI: `10.1016/j.pain.2004.12.036`.

[77] Salomons, T. V., Johnstone, T., Backonja, M.-M., and Davidson, R. J. Perceived controllability modulates the neural response to pain. *The Journal of Neuroscience: The Official Journal of the Society for Neuroscience* **24** (2004), 7199–7203. DOI: `10.1523/JNEUROSCI.1315-04.2004`.

[78] Wiech, K., Kalisch, R., Weiskopf, N., Pleger, B., Stephan, K. E., and Dolan, R. J. Anterolateral prefrontal cortex mediates the analgesic effect of expected and perceived control over pain. *The Journal of Neuroscience: The Official Journal of the Society for Neuroscience* **26** (2006), 11501–11509. DOI: `10.1523/JNEUROSCI.2568-06.2006`.

[79] De Vignemont, F., Ehrsson, H. H., and Haggard, P. Bodily illusions modulate tactile perception. *Current Biology* **15** (2005), 1286–1290. DOI: `10.1016/j.cub.2005.06.067`.

[80] Frith, C. The self in action: Lessons from delusions of control. *Consciousness and Cognition.* The Brain and Its Self **14** (2005), 752–770. DOI: `10.1016/j.concog.2005.04.002`.

[81] Graham-Schmidt, K. T., Martin-Iverson, M. T., and Waters, F. A. V. Self- and other-agency in people with passivity (first rank) symptoms in schizophrenia. *Schizophrenia Research* **192** (2018), 75–81. DOI: `10.1016/j.schres.2017.04.024`.

[82] Moore, J. W., Cambridge, V. C., Morgan, H., Giorlando, F., Adapa, R., and Fletcher, P. C. Time, action and psychosis: Using subjective time to investigate the effects of ketamine on sense of agency. *Neuropsychologia.* Special Issue: How Does the Brain Process Time? **51** (2013), 377–384. DOI: `10.1016/j.neuropsychologia.2012.07.005`.

[83] Pazzaglia, M. and Galli, G. Loss of agency in apraxia. *Frontiers in Human Neuroscience* **8** (2014), 751. DOI: `10.3389/fnhum.2014.00751`.

[84] Wolpe, N., Moore, J. W., Rae, C. L., Rittman, T., Altena, E., Haggard, P., and Rowe, J. B. The medial frontal-prefrontal network for altered awareness and control of action in corticobasal syndrome. *Brain: A Journal of Neurology* **137** (2014), 208–220. DOI: `10.1093/brain/awt302`.

6

[85] Moore, J. W., Schneider, S. A., Schwingenschuh, P., Moretto, G., Bhatia, K. P., and Haggard, P. Dopaminergic medication boosts action-effect binding in Parkinson's disease. *Neuropsychologia* **48** (2010), 1125–1132. DOI: 10.1016/j.neuropsychologia.2009.12.014.

[86] Saito, N., Takahata, K., Yamakado, H., Sawamoto, N., Saito, S., Takahashi, R., Murai, T., and Takahashi, H. Altered awareness of action in Parkinson's disease: evaluations by explicit and implicit measures. *Scientific Reports* **7** (2017), 8019. DOI: 10.1038/s41598-017-08482-0.

[87] Sperduti, M., Pieron, M., Leboyer, M., and Zalla, T. Altered pre-reflective sense of agency in autism spectrum disorders as revealed by reduced intentional binding. *Journal of Autism and Developmental Disorders* **44** (2014), 343–352. DOI: 10.1007/s10803-013-1891-y.

[88] Vogel, D. H. V., Jording, M., Esser, C., Conrad, A., Weiss, P. H., and Vogeley, K. Temporal binding of social events less pronounced in individuals with Autism Spectrum Disorder. *Scientific Reports* **12** (2022), 14853. DOI: 10.1038/s41598-022-19309-y.

[89] Zapparoli, L., Seghezzi, S., Devoto, F., Mariano, M., Banfi, G., Porta, M., and Paulesu, E. Altered sense of agency in Gilles de la Tourette syndrome: behavioural, clinical and functional magnetic resonance imaging findings. *Brain Communications* **2** (2020), fcaa204. DOI: 10.1093/braincomms/fcaa204.

[90] Moore, J. W. The relationship between sense of agency and borderline personality disorder traits in the general population. *Current Psychology* (2022). DOI: 10.1007/s12144-022-03517-w.

[91] Oren, E., Eitam, B., and Dar, R. Intentional binding and obsessive-compulsive tendencies: A dissociation between indirect and direct measures of the sense of agency. *Journal of Obsessive-Compulsive and Related Disorders*. Experimental studies of cognitive processes in OCD – new insights and challenges **20** (2019), 59–65. DOI: 10.1016/j.jocrd.2017.11.002.

[92] Ivanof, B. E., Terhune, D. B., Coyle, D., and Moore, J. W. Manipulations of Libet clock parameters affect intention timing awareness. *Scientific Reports* **12** (2022), 20249. DOI: 10.1038/s41598-022-23513-1.

[93] Pockett, S. and Miller, A. The rotating spot method of timing subjective events. *Consciousness and Cognition* **16** (2007), 241–254. DOI: 10.1016/j.concog.2006.09.002.

[94] Delhaye, B., Hayward, V., Lefèvre, P., and Thonnard, J.-L. Texture-induced vibrations in the forearm during tactile exploration. *Frontiers in Behavioral Neuroscience* **6** (2012). DOI: 10.3389/fnbeh.2012.00037.

[95] Kirsch, L. P., Job, X. E., Auvray, M., and Hayward, V. Harnessing tactile waves to measure skin-to-skin interactions. *Behavior Research Methods* **53** (2021), 1469–1477. DOI: 10.3758/s13428-020-01492-3.

6

[96] Manfredi, L. R., Baker, A. T., Elias, D. O., Iii, J. F. D., Zielinski, M. C., Polashock, V. S., and Bensmaia, S. J. The effect of surface wave propagation on neural responses to vibration in primate glabrous skin. *PLOS ONE* **7** (2012), e31203. DOI: 10.1371/journal.pone.0031203.

[97] Shao, Y., Hayward, V., and Visell, Y. Spatial patterns of cutaneous vibration during whole-hand haptic interactions. *Proceedings of the National Academy of Sciences* **113** (2016), 4188–4193. DOI: 10.1073/pnas.1520866113.

6

7

GENERAL DISCUSSION AND CONCLUSION

This final chapter summarizes the thesis's main findings and contributions, addressing the research questions introduced in Chapter 1. It also reflects on limitations of the research and suggests avenues for future work.

Author: Karina Kirk Driller

7.1. MAIN FINDINGS AND CONTRIBUTIONS

This dissertation has addressed the questions of how the human sensory system detects and processes changes in behaviorally relevant haptic events. It also examined how it can ensure stable haptic percepts that inform us about the state of relevant haptic affairs under changing conditions. The two main research questions were formulated as follows:

A. Which cues and mechanisms does the human somatosensory system use to robustly detect relevant changes in the mechanical state of the body and the world during dynamic touch events?

and

B. How does our sensory system ensure stable haptic percepts that inform us about the state of these events under changing conditions and cues?

Over the course of the chapters, I have addressed these questions by characterizing, combining, and reducing information and assessing the perceptual outcomes and mechanisms triggered for encoding dynamic touch events. I have done so in three overall contexts, as summarized below.

7.1.1. DETECTION OF CONTACT (CHAPTER 2)

Chapter 2 addressed these questions at a fundamental level via sub-question 1: ***Can we identify metamers of duration and intensity in the detection of transient contact events? And if so, can they be associated with invariant states of mechanical energy transfer?***

Human touch has often been analyzed through a frequency-specific lens using non-transient sinusoidal stimuli. In contrast, this chapter investigated the somatosensory system's responsiveness to very short, broadband impulses and their mechanical energy. We demonstrated a basic intensity metamer, a mechanism that may support perceptual stability, in which different combinations of signal amplitude and duration render consistent detection responses. An evaluation of these thresholds in light of the mechanical work produced by different combinations of our stimulus parameters highlighted energy as an important feature driving the detection of brief contact events. However, the data did not completely testify to a state of constant mechanical work at threshold level. Instead, a degree of differing energy content at threshold for certain signal durations was observed, suggesting the involvement of mechanisms beyond simple energy summation, such as a potential preferential encoding of certain temporal cues.

7.1.2. MATERIAL AND TEXTURE PERCEPTION (CHAPTERS 3–5)

Chapters 3–5 addressed the main research questions in the specific case of haptic material and texture perception. **Chapter 3** addressed sub-question 2: ***Can we determine behaviorally relevant and naturalistic cues to texture perception that are realizable in manufactured stimuli?***

This chapter highlighted the need for well-characterized physical stimulus material to bridge the gap between behaviorally relevant touch interactions and well-controlled

experimentation. It then detailed the conception, design, and verification of such a stimulus set and provided initial evidence for its behavioral relevance. The resulting stimulus set provided the opportunity to investigate the perceptual correlates of complex and naturalistic, yet well-characterized, surface texture and material features. It furthermore allowed for the investigation of the combined influence of two important cues for texture perception, namely statistical microscale roughness and material elasticity, constituting a practical contribution in answering the overall research questions of this dissertation. The stimuli were subsequently used in Chapter 4 and Chapter 5.

In **Chapter 4**, sub-question 3 was addressed: ***Do mechanical propagation waves provide a behaviorally relevant and sufficient cue to roughness and softness perception?***

In order to disentangle the contribution of "propagating" versus "local" touch cues in communicating roughness and softness information during dynamic explorations of these surfaces, we used local anesthesia of the index finger. The work showed how propagation waves provide a behaviorally relevant cue to surface roughness. However, a large between-subject variability in roughness discrimination under local anesthesia raised questions about the specific conditions under which propagation waves can be described not only as a *relevant* but *sufficient* cue to an invariant roughness percept. Softness perception, on the other hand, was more generally disrupted under the same conditions. A secondary aim was to uncover any combined effects of microscale surface features and material elasticity in determining roughness and softness judgments. However, no such effects were found beyond minor individual-level variations.

Motivated by the lack of clear mixed-cue effects in Chapter 4, **Chapter 5** subsequently addressed this question in more detail via sub-question 4: ***Does surface roughness provide a relevant cue to softness perception, and does material elasticity provide a relevant cue to roughness perception? And to what extent are these mechanisms local to the contact and invariant to contact conditions?***

In this chapter, we explored a wider elasticity range as well as both direct and indirect (rigid probe) interactions to uncover potential mixed-cue effects of surface roughness and material elasticity on roughness and softness perception. The results revealed clear areas of cue fusion or *perceptual metamers* of subjective roughness, in which different combinations of material elasticity and microscale surface features resulted in indistinguishable percepts. This held true for both direct and indirect touch interactions but was largely dependent on the relative elasticity of the probe and stimulus. No such metamers were found for the perceived softness of the stimuli, suggesting that microscale surface features do not provide a behaviorally relevant cue to subjective softness.

7.1.3. TIME PERCEPTION DURING HAPTIC INTERACTIONS (CHAPTER 6)

The final part of this dissertation explored the sensory system's response when a behaviorally relevant haptic cue is removed. **Chapter 6** addressed sub-question 5: ***How does***

the absence of local tactile feedback during a behaviorally relevant motor interaction affect the perception of the timing of contact and its outcomes?

Here we again explored dynamic touch interactions in the absence of a very salient cue to contact (i.e., "local" cutaneous feedback) using local anesthesia this, time for the motor action of a mechanical button press. We used the well-known temporal-binding paradigm to uncover how the sensory system may compensate for the absence of this information in determining the timing between a voluntary action (a button press) and its sensory outcome (a click sound). The work showed how removing local tactile information exaggerates this temporal distortion, leading to a more pronounced compression in the perceived time between action and outcome under local anesthesia. Whether being a mere effect of altered multisensory binding or reflecting changes in action intentionality or agency remained unclear, but the effect could be a potential mechanism to increase the detectability of behaviorally relevant touch events when important information is missing or at conflict.

Together, the work of this dissertation has uncovered behaviorally relevant cues and mechanisms on the physical (distal stimulus), mechanical (proximal stimulus), and pre-neural or neural (transduction and neural processing) levels used by the somatosensory system in reconstructing dynamic skin-object interactions. In exploring such cues and mechanisms, the work has highlighted the importance of distinguishing among them and determining at which level in the perceptual pathway they shape perceptual phenomena. In referring back to the initial Figure 1.3 from the Introduction (Chapter 1), it is now possible to visualize at which level within the haptic perceptual pathway the manipulation of the cue space took place in each chapter and to evaluate at which level the findings suggest that perception and stability (if achieved) were determined. Table 7.1 summarizes these insights.

The research of this dissertation has furthermore highlighted the somatosensory system's mechanisms for ensuring constancy of behaviorally relevant perceptual representations amidst drastic changes in contact conditions or the available cue space. Perception is inference-based and often far from veridical, yet remarkably stable. Both change and stability are thus essential for meaningful perceptual representations. The work has revealed some of the extensive measures the perceptual system employs to maintain a stable representation of our world of touch: from disregarding available cues, through merging cues, to substituting or compensating when relevant cues are missing. Notably, perceptual metamers constitute one such mechanism. Additionally, a highly sensitive yet flexible sense of subjective time may sometimes act as a crucial mechanism for ensuring perceptual stability and coherence. The work showed the somatosensory system's adaptability in utilizing available cues when others are removed, although stability can falter when the available information becomes overly ambiguous or sparse, highlighting the interdependence of change and stability in creating perceptual sense. As is the case for visual and auditory perception, perceptual constancy thus represents an indispensable mechanism in the haptic domain as well.

Table 7.1. Summary of experimental chapters: Levels of cue manipulation and measurement. **Manipulation Levels:** 1: Manipulating distal stimuli; 2: Shaping proximal stimuli; 3: Shaping transduction and neural processing. **Measurement Levels:** 1: Characterizing distal stimuli; 2: Characterizing proximal stimuli; 3: Measuring or modeling transduction; 4: Measuring neural processes; 5: Measuring perception; 6: Measuring metacognition.

Chapter	Perceptual Dimension	Cues Manipulated	Manipulation Level	Bh-Relevant Cue Determined	Measurement Level
2	• Contact magnitude (detection)	• Amplitude and frequency (duration) of impulses	2	• Amplitude and duration of impulses • Mechanical work	5
3	• (Subjective roughness and softness)	• Elasticity and microscale surface roughness of samples	1	• Elasticity and microscale surface roughness of samples	1, (5)
4	• Subjective roughness and softness	• Elasticity and microscale surface roughness of samples • Inhibition of action potentials via local anesthesia	1, 3	• Elasticity and microscale surface roughness of samples • Propagation waves	2, 5, 6
5	• Subjective roughness and softness	• Elasticity and microscale surface roughness of samples • Contact condition (direct/tool)	1, 2	• Elasticity and microscale surface roughness of samples	5, 6
6	• Subjective time	• Time interval between events • Inhibition of action potentials via local anesthesia	1, 3	• Local tactile information	5

7

Finally, the work presented in this dissertation once again confirms that single physical descriptors of the real world rarely constitute the sole determinants of a "corresponding" perceptual outcome or dimension. In this way, the perceived magnitude of an impact and its detectability involve more than just its amplitude; subjective roughness encompasses more than just surface features; and subjective time is about more than physical time. A critical implication that can be derived from these insights is an increased flexibility in conveying information in haptic applications: intensity cues can be communicated through changes in duration (frequency) or amplitude, and roughness cues through modifications of surface or material properties, as well as alterations to not only stimulus characteristics but also the probe. The material composition and stiffness of an artificial limb will thus dictate the way materials and textures are perceived with it. Additionally, the observation that certain cues are well-preserved within propagating information and therewith accessible from locations beyond the skin-object interface holds promising applications in the design of prosthetic devices.

7.2. A NOTE ON THE APPENDICES OF THIS DISSERTATION

Included in the appendices of this dissertation are two further studies, together delving into the spatial and temporal constraints of the perception of a rather novel haptic stimulus, namely ultrasonic mid-air haptic (UMH) stimuli. In the first study (Appendix A), we demonstrated the presence of a duration-intensity metamer somewhat akin to the one reported in Chapter 2 for UMH stimuli. In the second study (Appendix B), we explored one of the most basic components of haptic shape perception using UMH stimuli, namely the sensations of continuity versus gaps in the arrangement of two points in space. However, the general sensation produced by UMH stimuli is relatively weak and diffuse, suggesting a minimal behavioral relevance for haptic tasks demanding high spatial and temporal precision, typical of most skin-object interactions. Additionally, the inherent complexity of this technology introduces a multitude of factors affecting the stimulus, rendering it ambiguous and challenging to control in an experimental setting. In both studies, this was evidenced by a large within- and between-subject variability and by the observation that stimulus parameters (i.e., the point-spacing or stimulus duration) must be significantly amplified to induce any perceivable difference, indicating a low sensitivity to these cues and, consequently, limited behavioral relevance. These two studies thus underscore the importance of interface transparency in the study of haptic perception. Therefore, the contributions of these studies can more accurately be framed as perception-based rendering guidelines rather than direct insights into haptic perceptual mechanisms. This additional work contributes towards understanding the perceptually achievable temporal and spatial resolution of UMH interfaces, thereby improving our ability to harness UMH technologies effectively for precise and meaningful haptic feedback in various applications.

7.3. LIMITATIONS AND FUTURE WORK

As the studies in the appendices highlight, interface transparency remains a significant challenge in research on haptic perception. Moreover, effectively harnessing the multi-

dimensional input signals generated during natural skin-object interactions — that is, the proximal stimulus — continues to pose difficulties. Some limitations of the work presented in Chapter 2 thus relate to final aspects of the characterization of the stimulus when in contact with a finger and its inherent material properties (i.e., the modeling of the skin as a viscoelastic material). Similarly, in Chapters 3, 4, and 5, significant efforts were made to characterize the properties of the distal stimulus (here texture and material properties). However, the lack of, or only rudimentary, characterization of the proximal stimulus, that is, the input features generated during interactions with these textures, constitutes a clear shortcoming of this work. Consequently, in Chapter 4 we demonstrated that crucial information arising from mechanical skin-object interactions is present and processed well beyond the immediate contact area of these interactions. Nonetheless, the variability observed between subjects remained unexplained, prompting further research into the conditions under which propagating vibrations can facilitate invariant haptic perception. Even in the final Chapter 6, insights into the potential propagation of mechanical cues to remote, intact sites of the hand during the interactions of a bottom press would have been valuable in determining mechanisms behind the increased temporal illusion. Ultimately, deeper insights into the characteristics of the proximal stimulus at local as well as remote sites would have provided valuable contributions to our understanding of these mechanisms.

While the trade-off between ecological validity and experimental control is a familiar topic in the study of perception and other psychological phenomena, the inevitable proximity between the distal and proximal stimulus in haptic research exacerbates the challenge. This challenge becomes particularly evident when aiming at characterizing a perceptual system using either a poorly characterized interface or an interface of low behavioral relevance. A transparent haptic interface as well as a precise characterization of the proximal stimulus in haptic interaction become key in mitigating this challenge and closing the gap.

Still today, finding the golden mean between testing behaviorally relevant haptic phenomena in ecologically valid settings and maintaining rigorous experimental control thus remains a delicate balance. However, the research field of haptics, still in its relative infancy, has experienced rapid advancements in recent years. Steep progress in the characterization of the mechanical response characteristics during haptic interactions alongside the development of innovative and adaptive behavioral testing paradigms signals a promising trajectory for the field. It is a lively time for haptic research, where interdisciplinary advancements hold great promise to unlock further fundamental questions about behaviorally relevant cues and mechanisms of haptic perception during real-world, natural skin-object interactions.

7

APPENDICES

A

TEMPORAL SUMMATION AT SUPRA-THRESHOLD-LEVEL IN THE TACTILE PERCEPTION OF AIR-BORNE ULTRASOUND

Abstract: It is known that the duration of a short stimulus affects the perceived intensity of both visual, auditory, and vibrotactile events, a phenomenon sometimes referred to as temporal summation. However, it remains unclear whether such a relationship also exists for ultrasound mid-air haptic (UMH) inputs to the hand, which on a mechanical level differ significantly from contact-vibrotactile stimulation. Here we investigate this issue for three different modulation frequencies and show how the perceived intensity of focused ultrasonic stimulations of the palm is indeed systematically related to the stimulus duration—a relationship that is, however, independent of the modulation frequency. This finding sheds light on the universal yet bounded nature of the phenomenon's underlying mechanisms and constitutes an important step towards the overall goal of providing perceptually stronger inputs and enlarging the repertoire of mid-air haptic experiences. However, the study also raises questions about the behavioral relevance of ultrasound UMH stimuli in simulating skin-contact interactions and emphasizes the constraints that they impose on investigating haptic perceptual phenomena.

A

A.1. INTRODUCTION

In many sensory systems, the perceived magnitude of a brief stimulus increases as its duration is increased, a phenomenon often referred to as "temporal summation" or "temporal integration" in psychophysics (not to be confused with neural summation). In vision, this reciprocal relationship between perceived intensity (e.g., brightness) and stimulus duration is sometimes referred to as Bunsen-Roscoe law or Bloch's law, and has been reported for a variety of cases [2–6]. In audition, a similar relationship can be observed between the perceived loudness and stimulus duration for stimuli shorter than a critical duration of about 150 ms [7–9]. In the same line, thermal perception [10] as well as perceived pain elicited by electrical stimulation [11, 12], or heat [13, 14] have all been shown to grow as an approximate power function of the stimulus duration. This suggests an amodal perceptual metamer in which stimulus duration and intensity can be interchanged for the same perceptual outcome. The robustness and ubiquity of this phenomenon as well as its apparent independence of sensory-modalities has hence led researchers to suggest that it might constitute a general principle of perception [10, 15].

In the tactile domain, a substantial number of studies have investigated temporal summation for vibrotactile stimuli on the liminal level (i.e., detection thresholds [16–18]). Here, detection thresholds have been shown to decrease as a function of stimulus duration, but only for high-frequency vibration (e.g., [16, 18]). Somewhat fewer studies have investigated the phenomenon on a supra-liminal level (i.e., as discrimination thresholds). Among these, Berglund et al. [19] observed a logarithmic growth of the perceived intensity as a function of stimulus duration for up to 1 second for 250 Hz sinusoidal vibrations delivered to a fingertip. Gescheider [16] and Verrillo and Smith [20] later reported similar findings for 250 Hz sinusoidal stimuli delivered to the thenar eminence, albeit with some disagreements about the precise function describing this relationship. When investigating the same phenomenon for low-frequency (25 Hz and 40 Hz) sinusoidal vibration, however, no evidence of supra-threshold temporal summation was found by Gescheider [16] nor Gescheider and Joelson [21]. This frequency-dependent nature of the phenomenon has since been interpreted as evidence for the existence of distinct receptor systems or tactile channels (i.e., the Pacinian channel, referring to Pacinian corpuscles and their peripheral and central connections, and the non-Pacinian channels) [16, 22–24]. Tempotal and spatial summation (a closely-related phenomenon where the perceived intensity of a stimulus increases as the area over which a stimulus is applied is increased, e.g., [2, 25–27]) has thus been argued to be a distinct feature of the Pacinian channel (See [28] for a review).

More recently, Bochereau et al. [15] investigated the phenomenon for pink noise Gabor wavelets delivered to the fingertip via a metal plate. Using a two-alternative forced-choice staircase procedure, discrimination thresholds were estimated for stimuli varying in their duration (100–700 ms) and amplitude. The results showed "a negative power law relationship with a regression coefficient of −0.23" (p. 98), thus extending the findings from sinusoidal vibrations to more complex tactile signals, although a high-pass filter with a 70 Hz cut-off frequency ensured the removal of low frequencies. Finally, a study by Guemann et al. [29] recently reported the effect

for vibratory stimuli on the upper arm, while a translational study by Fassihi et al. [30] reported the phenomenon for "noisy" (stochastic) vibratory stimuli in not only humans but also rodents. These findings highlight the phenomenon's applicability and contribute to the understanding that it may reflect a more universal aspect of sensory perception, applicable across not only different modalities but also species. Together, these later reports of temporal-summation effects for more complex signals than sinusoidal contact-induced sinusoidal vibrations furthermore raise the question of whether this phenomenon is indeed as frequency-specific as previously reported.

The present study was aimed at investigating temporal summation for a relatively novel, vibrotactile stimulus, namely Ultrasound Mid-air Haptic (UMH) vibration. UMH technology typically involves directing focused airborne ultrasound waves to create contactless vibrotactile sensations on human skin (e.g.[31–33]). Although the device transducers emit frequencies in the ultrasonic range imperceptible by human touch [22], they are able to create oscillatory skin indentations or "focal points" once modulated to frequencies relevant for tactile rendering [31, 33]. The resulting sensation is often described as "blowing" or "pulsing" [34]. The technology furthermore provides a unique approach to investigate vibration perception without direct skin contact. Our first aim was therefore to develop a deeper understanding of the fundamental mechanisms underlying temporal summation, particularly in the context of haptic perception without direct skin contact. We furthermore wished to achieve a better understanding of the reported frequency-specific nature of this phenomenon. In fact, it has been argued that the mechanoreceptors primarily responsible for the sensations induced by UMH devices are Pacinian corpuscles, which is based on the observation of a maximum sensitivity to the stimulus at a modulation frequency around 200–250 Hz [35, 36]. If true, this therefore positions UMH stimuli as an ideal subject for investigating temporal summation and its supposed distinctness to higher frequencies. Finally, while this technology finds a growing number of applications [36], the comparatively low forces generated on the user's skin remain a common issue, limiting the repertoire of haptic experiences using this technology [37–39]. If the perceived intensity of such stimuli could therefore be enhanced via changes in stimulus duration, this could help widen the range of applications for this technology.

We hypothesized that UMH stimulations of the hand would result in perceptual temporal summation effects similar to those observed for other vibrotactile stimulations. If the phenomenon is indeed as frequency-specific as previously reported, the magnitude of temporal summation effects should furthermore vary with modulation frequency. Specifically, higher frequencies (e.g., 200 Hz) should exhibit greater temporal summation than lower frequencies (e.g., 50 Hz).

A.2. MATERIALS AND METHODS

PARTICIPANTS

Six healthy participants (1 female, 5 male; mean age = 27,83, SD = 1.72) were recruited from Delft University of Technology. All participants were right-handed, as assessed using Edinburgh's handedness inventory [40]. Participants reported no neurological

A

disorders or issues with somatosensory functioning. All participants gave written informed consent to participate in line with the Human Ethics Committee at the Delft University of Technology and the Helsinki Declaration and received 25 Euro for participating in the study.

A.2.1. STIMULI AND SETUP

The setup comprised a generic desktop computer with an audio channel driving the UMH interface (STRATOS^{TM} Explore development kit) developed by Ultrahaptics (now Ultraleap) Ltd. The interface was located in a sound-attenuated box equipped with an arm rest such that the ventral area of the participants' hand could be centered over the midpoint of the transducer array (see Figure A.1). The stimulus was a focal point set to 20 cm above the array for all conditions reported here.
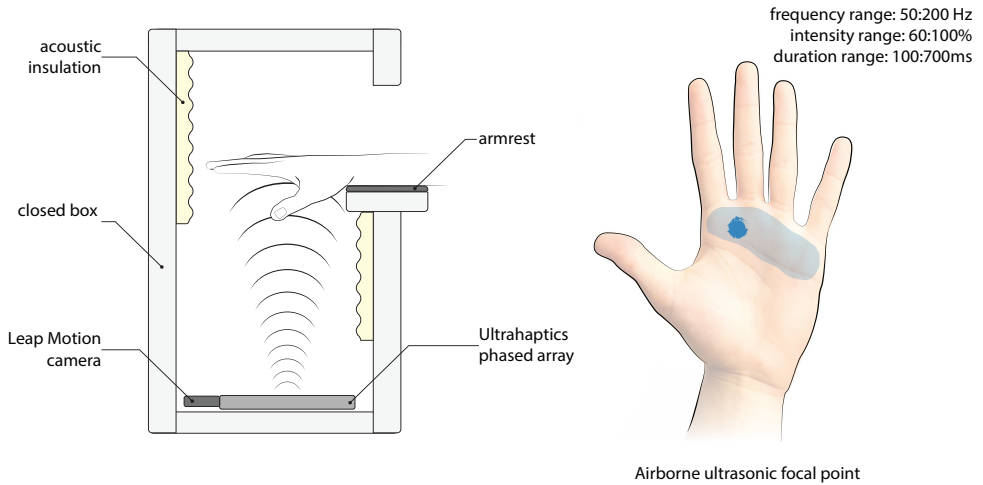
Stimulus and setup

Figure A.1. Stimulus and setup. The UMH array was placed in a sound-attenuated box. Participants rested their arm on an armrest. The stimulus, a fixed UMH focal point, was directed towards a point within the upper ventral part of the palm (shaded light blue area).

The stimulus, a focused square-windowed sinusoidal wave, was generated at a sampling rate of 40000 Hz, using the spatiotemporal modulation method (cf. [37, 41], and Appendix B for an introduction to different modulation methods). The stimulus was directed to the upper ventral area of the participant's palm at a location where the participant indicated to be able to feel the stimulus clearly (cf. Figure A.1). We manipulated the the duration (100–700 ms), the intensity (60–100% of the maximum device output), and the modulation frequency (50, 125, and 200 Hz) of the stimuli used in the experiment. During interactions with the array, participants wore

noise-canceling headphones playing pink noise at approximately 40 dB to ensure that the feedback they received was purely haptic in nature.

A.2.2. PROCEDURE

Prior to the experiment proper, detection thresholds were obtained for the minimum stimulus duration (100 ms) for all frequencies to ensure that the stimuli were in the supra-threshold range for all participants. This was done using an adaptive Quest+ interleaved staircase procedure.

After positioning the participant's hand, five test trials were given. The participant was asked to hold their hand still during the experiment. We used a two-alternatives-forced-choice (2AFC) task and the method of constant-stimuli. Each trial consisted of a sequence of two stimuli, one being the reference and the other the comparison (see Figure A.2).
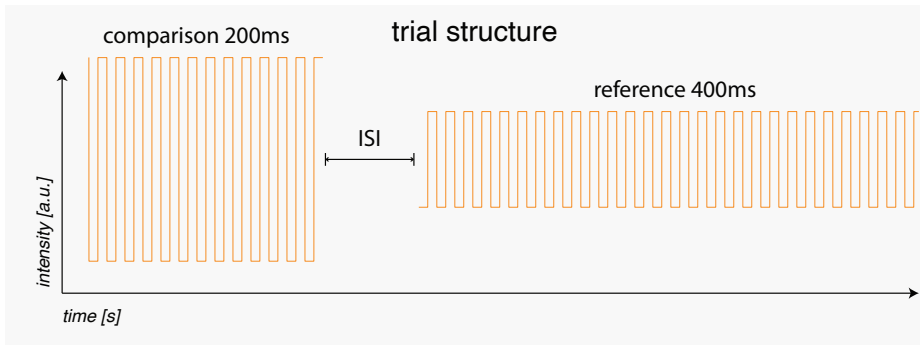

Figure A.2. Example trial. A 2AFC task and a method of constant stimuli was used to determine discrimination thresholds for focal points varying in their duration and intensity. Stimuli ranged in intensity from 0.6 to 1 of the scalar power output [a.u] and durations ranged from 100 ms to 700 ms. Three modulation frequencies (50 Hz, 125 Hz, and 200 Hz) were tested.

The reference stimulus had a duration of 400 ms and an intensity of 80% of the maximum intensity of the interface. Comparison stimuli varied in 7 steps of duration from 100 to 700 ms and 5 steps of intensity from 60% to 100% of the maximum of the device output. The stimuli were separated by an interstimulus interval (ISI) of 350 ms and the order of both stimuli and trials was randomized. After each stimulus pair, participants were asked to indicate by keypress "which stimulus felt strongest, the first or the second". After the response, the next trial began automatically after 500 ms. The whole experiment consisted of 1050 total trials (350 for each modulation frequency). It was divided into five blocks of 210 trials, each consisting of 70 trials with each modulation frequency in a randomized order. Modulation frequency never varied within but only across trials. Breaks, in which the participant could move their hand freely, were provided after each block but could be requested at any time during

the experiment. The whole experiment lasted approximately one hour. Figure A.2 represents a schematic of a single trial and example stimuli.

A.2.3. ANALYSIS AND RESULTS

Mean detection thresholds across all participants from the Quest+ procedure were calculated for each of the three modulation frequencies and can be seen in Figure A.3.
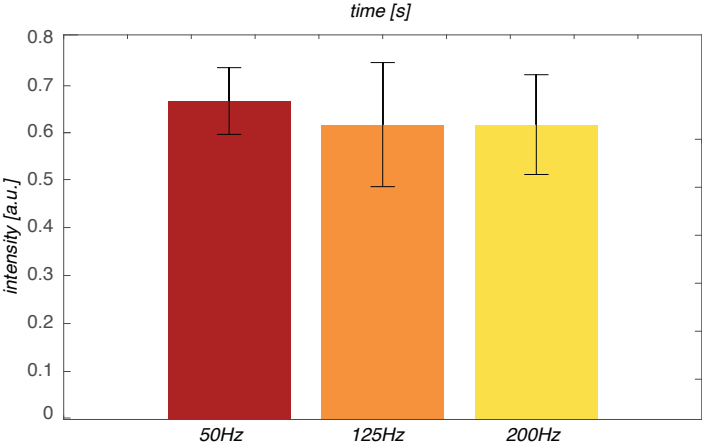

Figure A.3. Detection thresholds for a 100 ms stimulus, three frequencies, and 6 participants. Determined using an adaptive Quest+ interleaved staircase procedure. Error bars represent standard deviations of the mean values.

For the discrimination data, the proportion of 'comparison stronger' responses, varying with the comparison stimulus duration and intensity, were individually analyzed for each participant and stimulus frequency. This analysis involved fitting a logistic function to the data using the Psignifit tool in MATLAB. The fitting process estimated the Point of Subjective Equality (PSE) and Just Noticeable Difference (JND) for each condition. Function fits for an example participant are presented in Figure A.4, with each panel representing the results for different stimulus modulation frequencies.

Figure A.4 demonstrates how a higher stimulus intensity was required for the stimulus to be felt as equally strong as the reference stimulus, as the comparison duration decreased, while a lower intensity was required for stimuli of longer durations. The PSE, derived from the psychometric function fits, represents the comparison intensity at which the participant was equally likely to perceive the comparison stimulus as stronger or weaker than the reference. Our analysis revealed that for shorter durations, the PSE shifts to higher intensities, suggesting that participants require a more intense comparison stimulus to perceive it as equivalent to the reference stimulus. This pattern was consistently observed across all modulation frequencies and for all participants.
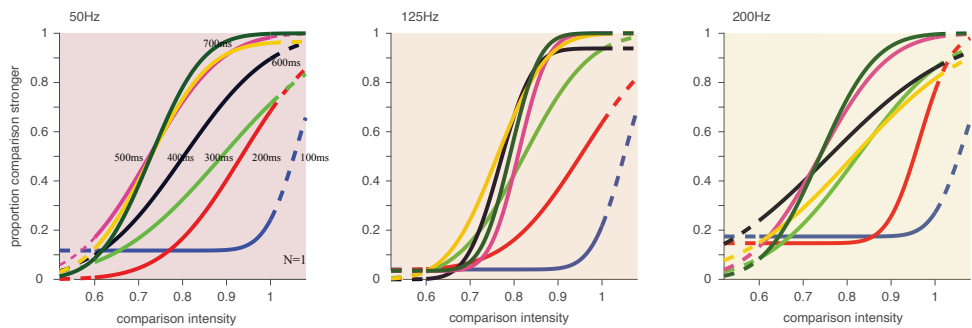
Figure A.4. Psychometric functions for an example participant and the three modulation frequencies used in this study (50 Hz, 125 Hz, and 200 Hz. Dashed lines represent predicted values outside the tested stimulus space.
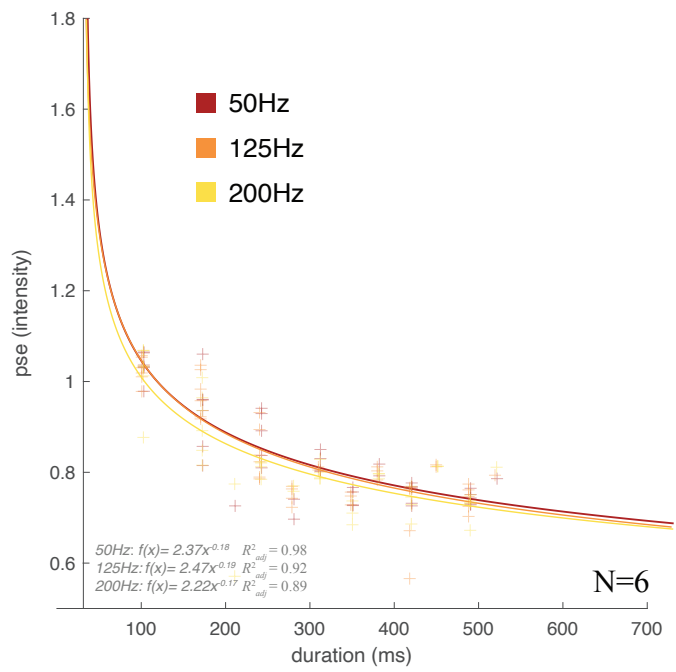

Figure A.5. PSE for all six participants as a function of stimulus duration, estimated for the 400 ms-long and 80-% strong reference. The fits show a negative power-law relationship with a regression coefficient of -0.18, -0.19, and -0.17 respectively. Red = 50 Hz, orange = 125 Hz, yellow = 200 Hz.

Figure A.5 shows the PSE for all six participants as a function of stimulus duration, estimated for the 400-ms long and 80% strong reference stimulus and the three

A

different modulation frequencies used. The observed effect was best described by a negative power law with a regression coefficient of -0.18, -0.19, and -0.17 for 50 Hz, 125 Hz, and 200 Hz respectively. The best fit was observed for the 50 Hz stimulation with highest adjusted R-squared value of 0.98.

A.3. Discussion

We used a 2AFC-task and a constant-stimuli procedure to explore the phenomenon of temporal summation for airborne ultrasonic stimuli of the palm for three different modulation frequencies. Our results showed a robust effect of stimulus duration on the perceived stimulus intensity, such that longer duration stimuli felt more intense than shorter duration stimuli. We observed no significant difference in this metameric relationship between the different modulation frequencies tested.

Our observation that the relationship between perceived stimulus intensity and stimulus duration follows a power law with a negative exponent, aligns with prior findings in various sensory modalities [3, 5, 8–10, 12, 13] as well as for contact-vibrotactile stimuli within the haptic domain [15, 19, 20]. Temporal summation is a well-established phenomenon across different sensory systems, but its demonstration in the haptic domain at a supra-liminal level using signals beyond simple contact-vibrotactile sinusoidal waves, is a relatively recent development [15, 30]. Our finding contributes to this research, underscoring the robustness of temporal summation in haptic perception. It further reinforces the hypothesis that temporal summation may be a fundamental and universal characteristic of sensory processing [15, 30].

In fact, it could be reasoned that temporal summation might be an important mechanism of perceptual constancy, such as when stroking across a single asperity with changing velocity [42], or possibly even in more complex scenarios like the invariant perception of textures across changes in exploratory movements. When exploring a surface or material, minor changes in exploratory movements such as the scanning speed [43, 44], or force [43, 45] can lead to significant changes in signals at the sensory periphery. Yet, texture perception tends to remain remarkably consistent across these changes [46–48], and the mechanisms of this ability remain far from understood. However, intensity summation could be one such mechanism.

However, contrary to previous reports of this phenomenon for *contact*-vibrotactile stimulation, we observed no significant difference in this metameric relationship between the different modulation frequencies tested in the present study. Our results therefore did not reveal any evidence supporting frequency-selectivity in this phenomenon. If the phenomenon were specific to the Pacinian Corpuscle (PC) channel [19, 21], and this channel were tuned to specific frequencies, one should have expected the phenomenon to be markedly reduced or diminished for the lowest modulation frequency used in this study (50 Hz), which falls outside the optimal frequency range for Pacinian corpuscles, commonly reported as approximately 80–450 Hz [49–51]. Similarly, the strongest effect of temporal summation should have been observed for the 200 Hz stimulus, a frequency at which peak sensitivity has been

reported for UMH stimuli [35, 36]. However, the present findings speak against such a frequency tuning in the specific case of temporal summation and UMH stimuli.

A.3.1. LIMITATIONS AND FUTURE WORK

First, as addressed in the introduction, the overall sensation of UMH stimuli is extraordinarily light, which significantly restricts the available stimulus space. It thus necessitated the use of comparatively long stimuli overall, while the phenomenon is known to be strongest for shorter durations for vibrotactile stimuli [19]. This limitation is also evident from the detection thresholds measured prior to the discrimination experiment in this study, which were close to the intensity of the weakest stimulus used (cf. Figure A.3). As a result, there may have been an increase in overall noise, potentially obscuring any frequency-specific effects. Second, and related to the former, we used a sinusoidal wave in a square envelope to achieve maximum energy within each signal duration. However, such signals are not akin to the complex tactile signals created when interacting with objects or materials in everyday life that our somatosensory system is accustomed to [52–54]. Not only does the lack of tuning to this input result in a weak sensation and the need for a longer time scale to achieve equivalent energy transmission. But the sharp onset and offset of the signal may additionally have resulted in participants particularly detecting the salient beginning and end of the stimulation event, rather than the total event, considering that the human somatosensory system is strongly tuned to detecting change [55].

In an attempt to determine whether the observed frequency independence was a result of the square pulse used, we compared the results to those obtained with a Gaussian envelope signal for the three frequencies for two participants. Additionally, detection thresholds for this stimulus were acquired for the same 6 participants as the ones that took part in the initial experiment. The data are shown in Figure A.6.

However, as can be seen in Figure A.6, no significant difference was observed (Figure 3C), but deviations at shorter durations were noticeable. However, a problem with these ramped up signals is that they result in spectral leakage above detection thresholds, smearing out the modulation frequency and thus making them unfit for testing frequency-specific effects.

A.4. CONCLUSION

We conducted an experiment aimed at identifying whether perceptual discrimination thresholds of Ultrasound Mid-air Haptic (UMH) stimuli are governed by signal amplitude, duration, or a combination of the two across different modulation frequencies. We observed a duration-intensity metamer, an effect of temporal summation, in our study, similar to those observed across vision, audition, and vibro-tactile inputs to the skin. A negative power-law governed the relationship between perceived intensity and stimulus duration of ultrasonic inputs to the palm. Thus, skin responses to ultrasonic inputs obey a temporal energy summation model. However, this mechanism appeared invariant to modulation frequency. The results not only confirm the robustness and ubiquity of the temporal summation phenomenon
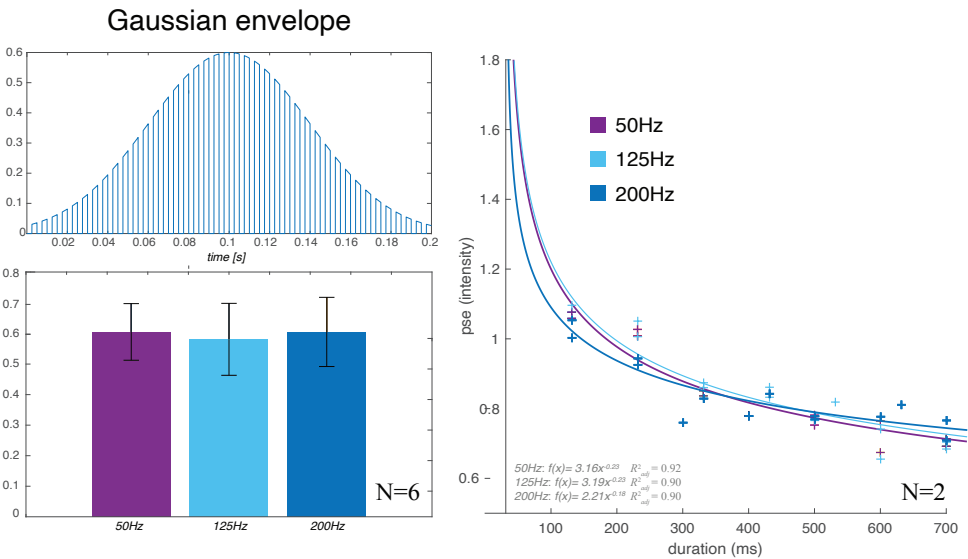
A

Figure A.6. Left: Detection thresholds for a 100 ms stimulus, three frequencies, two envelope types, and 6 participants. Determined using an adaptive Quest+ interleaved staircase procedure. Right: PSE for 2 participants as a function of stimulus duration, estimated for the 400-ms long and 80-% strong reference. The fits show a negative power-law relationship with a regression coefficient of -0.23, -0.23, and -0.18 respectively. Purple = 50 Hz, light blue = 125 Hz, dark blue = 200 Hz.

in sensory processing but also offer practical guidelines for modifying the perceptual thresholds of UMH devices. Nevertheless, our findings also underscore the unique challenges encountered in investigating perceptual phenomena through a medium that is not inherently aligned with behavioral assumptions or one to which the somatosensory system is not naturally attuned.

REFERENCES

[1] Driller, K., Frier, W., Pont, S., and Hartcher-O'Brien, J. Mid-Air Ultrasonic Stimulations of the Palm - The Influence of Frequency and Stimulus Duration on Perceived Intensity: WHC 2019 : IEEE World Haptics Conference. *World Haptics Conference, Tokyo, Japan* (2019). Ed. by Shinoda, H. and Kajimoto, H.

[2] Barlow, H. B. Temporal and spatial summation in human vision at different background intensities. *The Journal of Physiology* **141** (1958), 337–350.

[3] Baumgardt, E. and Hillmann, B. duration and size as determinants of peripheral retinal response. *Journal of the Optical Society of America* **51** (1961), 340. DOI: 10.1364/JOSA.51.000340.

[4] Ekman, G. Temporal integration of brightness. *Vision Research* **6** (1966), 683–688. DOI: 10.1016/0042-6989(66)90079-4.

[5] Kahneman, D. and Norman, J. G. The time-intensity relation in visual perception as a function of observer's task. *Journal of experimental psychology* **68** (1964), 215–220. DOI: 10.1037/h0046097.

[6] Niven, J. I. and Brown, R. H. Visual resolution as a function of intensity and exposure time in the human fovea. *Journal of the Optical Society of America* **34** (1944), 738. DOI: 10.1364/JOSA.34.000738.

[7] Kryter, K. D. and Pearsons, K. S. Some effects of spectral content and duration on perceived noise level. *The Journal of the Acoustical Society of America* **35** (1963), 866–883. DOI: 10.1121/1.1918620.

[8] Stévens, J. C. and Hall, J. W. Brightness and loudness as functions of stimulus duration. *Perception & Psychophysics* **1** (1966), 319–327. DOI: 10.3758/BF03215796.

[9] Zwislocki, J. J. Temporal summation of loudness: An analysis. *The Journal of the Acoustical Society of America* **46** (1969), 431–441. DOI: 10.1121/1.1911708.

[10] Dufour, A., Després, O., Pebayle, T., and Lithfous, S. Thermal sensitivity in humans at the depth of thermal receptor endings beneath the skin: validation of a heat transfer model of the skin using high-temporal resolution stimuli. *European Journal of Applied Physiology* **120** (2020), 1509–1518. DOI: 10.1007/s00421-020-04372-y.

[11] Shimizu, T. Tooth pre-pain sensation elicited by electrical stimulation. *Journal of Dental Research* **43** (1964), 467–475. DOI: 10.1177/00220345640430040201.

[12] Ekman, G., Frankenhaeuser, M., Berglund, B., and Waszak, M. Apparent duration as a function of intensity of vibrotactile stimulation. *Perceptual and Motor Skills* **28** (1969), 151–156. DOI: 10.2466/pms.1969.28.1.151.

[13] Koyama, Y., Koyama, T., Kroncke, A. P., and Coghill, R. C. Effects of stimulus duration on heat induced pain: the relationship between real-time and post-stimulus pain ratings. *Pain* **107** (2004), 256–266. DOI: 10.1016/j.pain.2003.11.007.

[14] Tran, T. D., Wang, H., Tandon, A., Hernandez-Garica, L., and Casey, K. L. Temporal summation of heat pain in humans: Evidence supporting thalamocortical modulation. *Pain* **150** (2010), 93–102. DOI: 10.1016/j.pain.2010.04.001.

[15] Bochereau, S., Terekhov, A., and Hayward, V. "Amplitude and Duration Interdependence in the Perceived Intensity of Complex Tactile Signals". In: Haptics: Neuroscience, Devices, Modeling, and Applications. Ed. by Auvray, M. and Duriez, C. Lecture Notes in Computer Science. Springer Berlin Heidelberg, 2014, pp. 93–100.

[16] Gescheider, G. A. Evidence in support of the duplex theory of mechanoreception. *Sensory Processes* **1** (1976), 68–76.

[17] Gescheider, G. A., Berryhill, M. E., Verrillo, R. T., and Bolanowski, S. J. Vibrotactile temporal summation: probability summation or neural integration? *Somatosensory & motor research* **16** (1999), 229–242. DOI: 10.1080/08990229970483.

[18] Verrillo, R. T. Temporal summation in vibrotactile sensitivity. *The Journal of the Acoustical Society of America* **37** (1965), 843–846. DOI: 10.1121/1.1909458.

[19] Berglund, B., Berglund, U., and Ekman, G. Temporal integration of vibrotactile stimulation. *Perceptual and Motor Skills* **25** (1967), 549–560. DOI: 10.2466/pms.1967.25.2.549.

[20] Verrillo, R. T. and Smith, R. L. Effect of stimulus duration on vibrotactile sensation magnitude. *Bulletin of the Psychonomic Society* **8** (1976), 112–114. DOI: 10.3758/BF03335097.

[21] Gescheider, G. A. and Joelson, J. M. Vibrotactile temporal summation for threshold and suprathreshold levels of stimulation. *Perception & Psychophysics* **33** (1983), 156–162. DOI: 10.3758/BF03202833.

[22] Bolanowski, S. J., Gescheider, G. A., Verrillo, R. T., and Checkosky, C. M. Four channels mediate the mechanical aspects of touch. *The Journal of the Acoustical Society of America* **84** (1988), 1680–1694. DOI: 10.1121/1.397184.

[23] Gescheider, G., Bolanowski, S., and Verrillo, R. Some characteristics of tactile channels. *Behavioural Brain Research* **148** (2004), 35–40. DOI: 10.1016/S0166-4328(03)00177-3.

[24] Verrillo, R. T. A duplex mechanism of mechanoreception. *Proc. First International Symposium on the Skin Sense, Thomas, Springfield, Illinois, 1968* (1968), 139–159.

[25] Gescheider, G. A., Güçlü, B., Sexton, J. L., Karalunas, S., and Fontana, A. Spatial summation in the tactile sensory system: Probability summation and neural integration. *Somatosensory & Motor Research* **22** (2005), 255–268. DOI: 10.1080/08990220500420236.

[26] Franzén, O. On spatial summatin in the tactual sense. A psychophysical and neurophysiological study. *Scandinavian Journal of Psychology* **10** (1969), 193–208. DOI: 10.1111/j.1467-9450.1969.tb00027.x.

[27] Stevens, J. C. and Marks, L. E. Spatial summation and the dynamics of warmth sensation. *Perception & Psychophysics* **9** (1971), 391–398. DOI: 10.3758/BF03210236.

[28] Gescheider, G. A., Wright, J. H., and Verrillo, R. T. *Information-Processing Channels in the Tactile Sensory System*. 1st ed. Psychology Press, 2010. DOI: 10.4324/9780203890004.

[29] Guemann, M., Bouvier, S., Halgand, C., Paclet, F., Borrini, L., Ricard, D., Lapeyre, E., Cattaert, D., and Rugy, A. d. Effect of vibration characteristics and vibror arrangement on the tactile perception of the upper arm in healthy subjects and upper limb amputees. *Journal of Neuroengineering and Rehabilitation* **16** (2019), 138. DOI: 10.1186/s12984-019-0597-6.

[30] Fassihi, A., Akrami, A., Pulecchi, F., Schönfelder, V., and Diamond, M. E. Transformation of perception from sensory to motor cortex. *Current Biology* **27** (2017), 1585–1596.e6. DOI: 10.1016/j.cub.2017.05.011.

[31] Carter, T., Seah, S. A., Long, B., Drinkwater, B., and Subramanian, S. "UltraHaptics: Multi-point Mid-air Haptic Feedback for Touch Surfaces". In: Proceedings of the 26th Annual ACM Symposium on User Interface Software and Technology. UIST '13. New York, NY, USA: ACM, 2013, pp. 505–514. DOI: 10.1145/2501988.2502018.

[32] Georgiou, O., Frier, W., Freeman, E., Pacchierotti, C., and Hoshi, T., eds. *Ultrasound Mid-Air Haptics for Touchless Interfaces*. Human–Computer Interaction Series. Cham: Springer International Publishing, 2022. DOI: 10.1007/978-3-031-04043-6.

[33] Hoshi, T., Takahashi, M., Iwamoto, T., and Shinoda, H. Noncontact tactile display based on radiation pressure of airborne ultrasound. *IEEE Transactions on Haptics* **3** (2010), 155–165. DOI: 10.1109/TOH.2010.4.

[34] Obrist, M., Ann Seah, S., and Subramanian, S. "Talking about Tactile Experiences". In: CHI '13: Proceedings of the SIGCHI Conference on Human Factors in Computing Systems. 2013. DOI: 10.1145/2470654.2466220.

[35] Hasegawa, K. and Shinoda, H. Aerial vibrotactile display based on multiUnit ultrasound phased array. *IEEE transactions on haptics* (2018). DOI: 10.1109/TOH.2018.2799220.

[36] Rakkolainen, I., Freeman, E., Sand, A., Raisamo, R., and Brewster, S. A survey of mid-air ultrasound haptics and its applications. *IEEE Transactions on Haptics* **14** (2021), 2–19. DOI: 10.1109/TOH.2020.3018754.

A

[37] Frier, W., Ablart, D., Chilles, J., Long, B., Giordano, M., Obrist, M., and Subramanian, S. "Using Spatiotemporal Modulation to Draw Tactile Patterns in Mid-Air". In: Haptics: Science, Technology, and Applications. Ed. by Prattichizzo, D., Shinoda, H., Tan, H. Z., Ruffaldi, E., and Frisoli, A. Lecture Notes in Computer Science. Cham: Springer International Publishing, 2018, pp. 270–281. DOI: 10.1007/978-3-319-93445-7_24.

[38] Frier, W., Abdouni, A., Pittera, D., Georgiou, O., and Malkin, R. Simulating airborne ultrasound vibrations in human skin for haptic applications. *IEEE Access* **10** (2022), 15443–15456. DOI: 10.1109/ACCESS.2022.3147725.

[39] Korres, G., Aujeszky, T., and Eid, M. "Characterizing tactile rendering parameters for ultrasound based stimulation". In: 2017 IEEE World Haptics Conference (WHC). 2017, pp. 293–298. DOI: 10.1109/WHC.2017.7989917.

[40] Oldfield, R. C. The assessment and analysis of handedness: The Edinburgh inventory. *Neuropsychologia* **9** (1971), 97–113. DOI: 10.1016/0028-3932(71)90067-4.

[41] Hasegawa, K. and Shinoda, H. "Modulation Methods for Ultrasound Midair Haptics". In: Ultrasound Mid-Air Haptics for Touchless Interfaces. Ed. by Georgiou, O., Frier, W., Freeman, E., Pacchierotti, C., and Hoshi, T. Human–Computer Interaction Series. Cham: Springer International Publishing, 2022, pp. 225–240. DOI: 10.1007/978-3-031-04043-6_9.

[42] Bochereau, S., Sinclair, S., and Hayward, V. "Looking for physical invariants in the mechanical response of a tactually scanned Braille dot". In: 2015 IEEE World Haptics Conference (WHC). 2015, pp. 119–124. DOI: 10.1109/WHC.2015.7177701.

[43] Phillips, J. R., Johansson, R. S., and Johnson, K. O. Responses of human mechanoreceptive afferents to embossed dot arrays scanned across fingerpad skin. *The Journal of Neuroscience: The Official Journal of the Society for Neuroscience* **12** (1992), 827–839. DOI: 10.1523/JNEUROSCI.12-03-00827.1992.

[44] Goodwin, A. W. and Morley, J. W. Sinusoidal movement of a grating across the monkey's fingerpad: representation of grating and movement features in afferent fiber responses. *The Journal of Neuroscience: The Official Journal of the Society for Neuroscience* **7** (1987), 2168–2180. DOI: 10.1523/JNEUROSCI.07-07-02168.1987.

[45] Saal, H. P., Suresh, A. K., Solorzano, L. E., Weber, A. I., and Bensmaia, S. J. The effect of contact force on the responses of tactile nerve fibers to scanned textures. *Neuroscience.* Sensory Sequence Processing in the Brain **389** (2018), 99–103. DOI: 10.1016/j.neuroscience.2017.08.024.

[46] Boundy-Singer, Z. M., Saal, H. P., and Bensmaia, S. J. Speed invariance of tactile texture perception. *Journal of Neurophysiology* **118** (2017), 2371–2377. DOI: 10.1152/jn.00161.2017.

[47]   Lederman, S. J. and Taylor, M. M. Fingertip force, surface geometry, and the perception of roughness by active touch. *Perception & Psychophysics* **12** (1972), 401–408. DOI: 10.3758/BF03205850.

[48]   Lieber, J. D. and Bensmaia, S. J. Emergence of an invariant representation of texture in primate somatosensory cortex. *Cerebral Cortex* **30** (2020), 3228–3239. DOI: 10.1093/cercor/bhz305.

[49]   LaMotte, R. H. and Mountcastle, V. B. Capacities of humans and monkeys to discriminate vibratory stimuli of different frequency and amplitude: a correlation between neural events and psychological measurements. *Journal of Neurophysiology* **38** (1975), 539–559. DOI: 10.1152/jn.1975.38.3.539.

[50]   Sato, M. Response of Pacinian corpuscles to sinusoidal vibration. *The Journal of Physiology* **159** (1961), 391–409. DOI: 10.1113/jphysiol.1961.sp006817.

[51]   Talbot, W. H., Darian-Smith, I., Kornhuber, H. H., and Mountcastle, V. B. The sense of flutter-vibration: comparison of the human capacity with response patterns of mechanoreceptive afferents from the monkey hand. *Journal of Neurophysiology* **31** (1968), 301–334. DOI: 10.1152/jn.1968.31.2.301.

[52]   Andrews, J. W., Adams, M. J., and Montenegro-Johnson, T. D. A universal scaling law of mammalian touch. *Science Advances* **6** (2020), eabb6912. DOI: 10.1126/sciadv.abb6912.

[53]   Bensmaïa, S. and Hollins, M. Pacinian representations of fine surface texture. *Perception & Psychophysics* **67** (2005), 842–854. DOI: 10.3758/BF03193537.

[54]   Yau, J. M., Hollins, M., and Bensmaia, S. J. Textural timbre: The perception of surface microtexture depends in part on multimodal spectral cues. *Communicative & Integrative Biology* **2** (2009), 344–346. DOI: 10.4161/cib.2.4.8551.

[55]   Johnson, K. O. The roles and functions of cutaneous mechanoreceptors. *Current Opinion in Neurobiology* **11** (2001), 455–461. DOI: 10.1016/s0959-4388(00)00234-8.

B

GAP DETECTION IN PAIRS OF ULTRASOUND MID-AIR VIBROTACTILE STIMULI

Abstract: Ultrasound mid-air haptic (UMH) devices are a novel tool for haptic feedback, capable of providing localized vibrotactile stimuli to users at a distance. UMH applications largely rely on generating tactile shape outlines on the users' skin. Here we investigate how to achieve sensations of continuity or gaps within such two-dimensional curves by studying the perception of pairs of amplitude-modulated focused ultrasound stimuli. On the one hand, we aim to investigate perceptual effects that may arise from providing simultaneous UMH stimuli. On the other hand, we wish to provide perception-based rendering guidelines for generating continuous or discontinuous sensations of tactile shapes. Finally, we hope to contribute toward a measure of the perceptually achievable resolution of UMH interfaces. We performed a user study to identify how far apart two focal points need to be to elicit a perceptual experience of two distinct stimuli separated by a gap. Mean gap detection thresholds were found at 32.3-mm spacing between focal points, but a high within- and between-subject variability was observed. Pairs spaced below 15 mm were consistently (>95%) perceived as a single stimulus, while pairs spaced 45 mm apart were consistently (84%) perceived as two separate stimuli. To investigate the observed variability, we resort to acoustic simulations of the resulting pressure fields. These show a non-linear evolution of actual peak pressure spacing as a function of nominal focal point spacing. Beyond an initial threshold in spacing (between 15 and 18 mm), which we

believe to be related to the perceived size of a focal point, the probability of detecting a gap between focal points appears to linearly increase with spacing. Our work highlights physical interactions and perceptual effects to consider when designing or investigating the perception of UMH shapes.

B.1. Introduction

Ultrasound mid-air haptic (UMH) devices are a novel technology for tactile feedback requiring no direct physical contact between the device and user. Several detailed surveys of the technology, its functioning principle, and its applications have been published [2, 3].

These devices use an array of ultrasonic transducers to emit acoustic waves timed in such a way as to coincide at fixed positions in their workspace, called focal points. This generates a localized region where the air pressure oscillates, with pressure maxima high enough to indent the skin in an oscillatory motion. However, this motion occurs at a rate equal to the ultrasound transducers' operating frequency, usually between 40 [4] and 70 kHz [5], well outside the range of human tactile perception capabilities [6]. It is therefore necessary to apply some form of lower frequency amplitude modulation to the pressure generated at individual points on the user's skin to obtain a perceivable stimulus. There are several methods for achieving this required amplitude modulation. The most straightforward method is to attenuate the output of the transducers cyclically over time, i.e., amplitude-modulating the transducers' outputs [4, 7]. This method is commonly referred to as *amplitude modulation (AM)* (see Figure B.1(a)). A more versatile approach consists of rapidly moving an unmodulated focal point between neighboring positions, while controlling the frequency at which the focal point passes any given position, through techniques called lateral modulation [8] or spatio-temporal modulation [9] (see Figure B.1(a)). Effectively, these techniques also lead to an amplitude modulation of the pressure signal at any fixed position along the focal point's path (see, e.g., pressure curves for positions 1 through 4 in Figure B.1(a)).

UMH interfaces are capable of simultaneously generating multiple focal points [4] whose positions can be updated at rates up to the array's transducers' operating frequency and that can be either in or out of phase with one another. By moving focal points along a path, through sequential AM or *spatio-temporal modulation (STM)* (see Figure B.1), it is possible to generate the perception of continuous vibrotactile shapes [4, 10, 11], surfaces, or textures [12]. UMH interfaces are increasingly finding applications in human-computer interaction [13, 14] and mid-air gesture interfaces [15], yet there are still only relatively few studies on the perception of focused ultrasound haptic stimuli despite such information being crucial in informing stimulus design for haptic rendering with these interfaces (see Rakkolainen et al.'s review [3] and the related work section from Mulot et al.'s recent work [16] for an overview of existing work on ultrasound haptic stimulus perception).

We discuss related work relevant to this article in more detail in Appendix B.2. We then present a human participant experiment and simulation study investigating
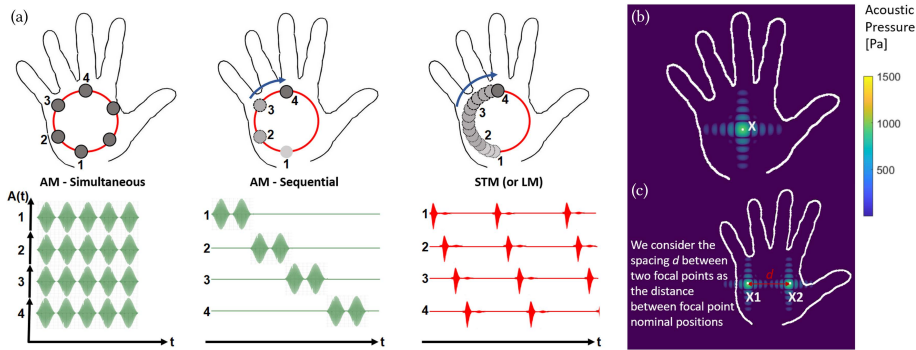
Figure B.1. (a) Tactile shapes with ultrasound mid-air haptics can be achieved through amplitude modulation of distinct points along the shape, either presented simultaneously [17] or sequentially [11, 18, 19]. Alternatively, a much finer step size can be used to sweep an unmodulated focal point across the shape in so-called spatio-temporal [20] or lateral modulation [8]. The plots schematically show the temporal evolution of acoustic pressure A(t) at four arbitrary points for each of the methods (time axes t are not at scale). (b) While ultrasound arrays usually enable users to command specific nominal coordinates for the focal point, the resulting pressure distribution affects a relatively large area of the skin. The acoustic pressure distribution in the plane for a single focal point at nominal position X is shown roughly at scale with the outline of a hand. (c) Here we define the spacing within pairs of focal points as the distance between both focal points' nominal positions.

the perception of neighboring simultaneous focal points (Appendix B.3). In this experiment, we record gap detection probabilities as a function of spacing between pairs of focal points (defined as per Figure B.1(c)), which can be explained both through perceptual phenomena as well as physical interactions between neighboring focal points. To help interpret the human participant experiment results, we run acoustic simulations of the pressure fields generated in the experiment, which we describe in Appendix B.4. Finally, we discuss limitations of our work, draw conclusions regarding the perception of UMH stimuli, and provide avenues for future work in Appendix B.5 and Appendix B.6.

Our contributions are as follows:

• A replication and extension of the preliminary human subject experiment presented by Carter et al. [4], aimed at understanding perceptual aspects of rendering continuous and discontinuous shapes with UMH.

• A detailed simulation study investigating the possible physical interactions between focal points that could explain the observed gap detection behavior.

With this work, we intend to provide guidelines for rendering continuous or discontinuous tactile shapes by determining how close two simultaneous focal points

need to be to produce a continuous sensation or, conversely, how far apart they need to be to produce the sensation of a gap between them. For rendering purposes, this can then serve as a basic building block for more complex continuous or discontinuous mid-air tactile geometries. Ultimately, our results may also contribute toward understanding the perceived size of focal points.

B.2. RELATED WORK

UMH stimuli are built around focal points. Despite their name and the fact that these are defined through nominal focal point coordinates, the generated vibrotactile stimulus is far from feeling like a point. When rendering a focal point at a nominal position X, UMH devices will generate a continuous pressure distribution in three-dimensional (3D) space with a maximum at X and a gradual decrease from this maximum as one moves away from X (see Figure B.1(b)). The shape of this pressure function is usually symmetrical around X but differs according to the direction considered [7, 18]. This pressure distribution gives rise to tactile stimuli that are described as localized areas of vibration on the skin [18] with fuzzy boundaries [21] which we refer to as the perceived focal point. The exact relationship between focal point pressure distribution and dimensions of the perceived focal point are not clearly understood. Early work on the topic often assumed this perceived focal point to have a diameter of roughly 8 mm based on the wavelength of the ultrasound in air for arrays operating at 40 kHz [4, 7]. To date, only one preliminary study has attempted to estimate the perceived diameter of a focal point, finding a mean value of 13.1 mm for a 70-kHz array [5]. However, these data are far from sufficient to understand the relationship between pressure and the perceived focal point size. Furthermore, knowing the perceived focal point's size by itself is still not sufficient to inform all aspects of rendering, as focal points are rarely used alone nor at static positions.

The ability for UMH devices to display multiple focal points at once [4] has been proposed as a means of displaying multiple tactile elements (e.g., in mid-air tactile user interfaces [22]). In this scenario, it is imperative to understand how close such tactile elements can be in different conditions while still allowing a user to easily discriminate between elements. A study by Carter et al. [4] investigated the ability of UMH devices to indicate different spatial regions or elements within a set. The authors performed a small-scale study on the discrimination of neighboring focal points at identical or different modulation frequencies. They found that participants were rarely capable of accurately distinguishing two focal points of same frequency below 50 mm apart, a performance that improved down to 20 mm apart for focal points of different modulation frequencies. Since the authors were not explicitly concerned with UMH shape rendering, they did not address the question of perceived continuity or gaps in shapes as a function of focal point spacing as we do here. Also because of its preliminary nature, their work did not provide a precise two-point threshold measure.

Multiple simultaneous focal points can also be used to draw shapes that either feel continuous or have holes or gaps within them (see "Simultaneous AM" in Figure B.1(a)). For example, Rutten et al. used a certain number of static sensations

made from four simultaneous AM focal points in a study on shape identification [17]. In this case, the approach remains limited to sensations using few distinct focal points, since the energy output of the device must be split between multiple focal points [4].

In addition, the ability to rapidly move the focal point in space makes UMH interfaces uniquely suited to drawing tactile geometric shapes (see "Sequential AM" and "STM" in Figure B.1(a)). Depending on the chosen method and focal point motion parameters, the resulting sensations are either static shapes [20] or the sensation of a stimulus moving along a shape [11]. Freeman et al. detail some of the relationships between these parameters in their work on focal point motion [23].

In early work on UMH, Hoshi et al. used sequential AM focal points to draw mid-air tactile shapes [18], a method that was later successfully applied to rendering the outline of larger shapes [16, 19]. Although no longer limited by achievable focal point intensity, this method requires a minimum amount of time to be spent at each spatial sampling position along the shape and can thus run into limitations for rendering shapes that must appear static. The most effective method in terms of achievable intensity and freedom in the design of shapes is STM [20, 23–25], which usually uses a very large number of closely spaced focal point positions which are rapidly scanned with an unmodulated focal point. While it affords great freedom in designing UMH shapes, STM is not as suitable as AM for displaying sets of static focal points, which may be detrimental to some applications. Sand et al. compared the effects of focal point motion speed, shape, and pattern repetitions on mid-air haptic shape identification for shapes drawn with sequential AM and STM [26].

The process of transforming an abstract geometric shape into a concrete geometric mid-air tactile pattern can be summed up under the notion of sampling strategy, introduced for STM by Frier et al. [24] and later formalized and extended to all modulation approaches by Mulot et al. [16]. Depending on the application, it may be desirable to adjust the sampling strategy to produce shapes that either feel continuous (i.e., that have no gaps in their contour) or discontinuous (i.e., that have perceivable gaps in their contour). This in turn requires understanding of the spacing limits beyond which focal points are perceived as distinct stimuli rather than merging into a single continuous shape sensation. Howard et al. [25] proposed an approach to simulate holes in an STM contour by overlaying a position-dependent intensity modulation onto a standard STM sampling strategy. The stimuli tested used 50-mm "holes" in 150-mm STM lines and yielded mixed results in terms of perceptual accuracy. Since the number of spatial sampling points that can be used is limited, in particular for simultaneous and sequential AM shape rendering, this information is even more critical for optimizing rendering. The present work aims to shed light on the basic building block of continuous or discontinuous UMH shapes, i.e., pairs of focal points at varying distances from one another.

B.3. GAP DETECTION EXPERIMENT

We conducted a user study to identify how far apart two focal points need to be to elicit a perceptual experience of two distinct stimuli separated by a gap. The experimental design is inspired by investigations into tactile two-point discrimination

thresholds, a well established procedure for measuring tactile acuity [27]. Our study, however, is notably different from conventional two-point discrimination threshold studies, first because it deals with vibrotactile stimuli rather than static skin indentation. Second, and more importantly, our study does not aim to provide any threshold measures relating to human physiology (contrary to studies on vibrotactile acuity, e.g., References [28–30]), since the stimulus used is not suitable for this. Vibrotactile stimuli generated by focal points are not localized enough for such a task, with skin indentation for a single focal point occurring over diameters that are of the same order of magnitude as vibrotactile two-point thresholds reported in the literature (see Figure B.1(b)).

B.3.1. MATERIALS AND METHODS

APPARATUS AND SETUP

Apparatus and Setup. The setup comprised a desktop computer that drove the Ultraleap Stratos Explore focused ultrasound array [31]. The device was placed in front of the dominant hand of the participant, inside an open wooden box resting on a tabletop. The box was equipped with an arm rest that positioned the participant's arm 20 cm above the transducer array while the hand could still be moved freely. Furthermore, four red wires were spun 18 cm above the device surface to act as a visual indication of the space in which stimuli could be expected (see Figure B.2 (left)). A keyboard was placed in front of the participant's non-dominant hand. Participants wore noise canceling headphones playing pink noise throughout the experiment to ensure that the feedback received was purely haptic in nature. No blindfolding was required given the invisibility of the stimuli to the user and absence of visual cues indicating device operation. The participants' hand was visible to them at all times.
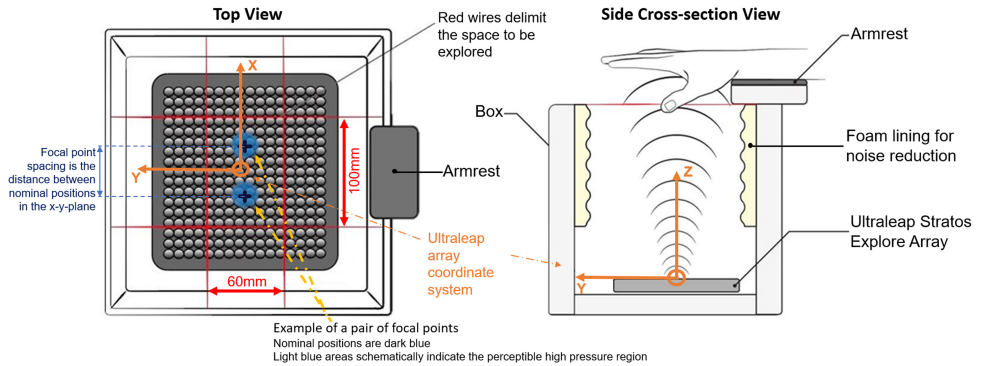

Figure B.2. Experimental setup. The exploration space (central rectangle, dimensions: 10x6 cm) is indicated to the participant using red wires. Focal point pairs are centered within this exploration space.

PROCEDURE

Focal point spacing was defined as per Figure B.1(c), as the distance between the nominal positions of both focal points in the emitted pair (see also Figure B.2). We used an interleaved staircase procedure varying the spacing between focal points following a two-down-one-up algorithm [32]. Bounds were set at 5 and 50 mm as starting values. Staircases were terminated after eight reversals or when boundaries were reached 5 times in a row. The average of the last six reversals was taken as an estimate of the gap detection threshold for a given condition. This gap detection threshold indicates the mean distance below which two simultaneous focal points are perceived as one single stimulus versus two separate stimuli at least 50% of the time.

We evaluated the threshold for three different focal point amplitude modulation frequencies (50, 125, and 200 Hz) to assess possible effects of frequency on gap detection. We chose the 200-Hz AM frequency, since this value is largely regarded as being optimal (e.g., Reference [33]) because of its proximity to peak Pacinian sensitivity in humans [6]. The 50-Hz AM frequency was chosen because it lies on the lower end of the Pacinian's response range [6]. Finally, 125 Hz was chosen as an intermediary value between both other frequencies. These modulation frequency choices are in line with other literature studies (e.g., References [8, 34]). A larger range of frequencies was not considered due to time constraints.

The experiment was split into nine blocks (three for each frequency condition). The order of blocks (i.e., frequencies) was balanced between participants as shown in Table B.1. The duration of each block was approximately 5 minutes. During the experiment, participants were instructed to keep their posture still but encouraged to explore the whole stimulus space with their palm (but not their fingers) while the stimulus was displayed. A pilot study on four participants had shown no difference in threshold values, measured via a two-down-one-up staircase procedure, for active versus passive exploration. In each trial, the stimulus was presented for 2 seconds, after which the question "Did you feel two points of stimulation?" appeared on the screen. Following a 2-alternative forced choice paradigm, a "Yes" or "No" response had to be given by pressing the corresponding key (left or right arrow, balanced across participants; see Table B.1). The next stimulus was then displayed with a response-stimulus interval of 300 ms.

Table B.1. Overview of the Experimental Design.

SUBJECT ID	FREQUENCY CONDITION ORDER	REPETITIONS	RESPONSE KEY ARRANGEMENT	SUBJECT ID	FREQUENCY CONDITION ORDER	REPETITIONS	RESPONSE KEY ARRANGEMENT
1			Y – N	4			N – Y
7	50 Hz - 125 Hz - 200 Hz		N – Y	10	50 Hz - 200 Hz - 125 Hz		Y – N
13			Y – N	16			N – Y
2			N – Y	5			Y – N
8	125 Hz - 50 Hz - 200 Hz	x3	Y – N	11	125 Hz - 200 Hz - 50 Hz	x3	N – Y
14			N – Y	17			Y – N
3			Y – N	6			N – Y
9	200 Hz - 50 Hz - 125 Hz		N – Y	12	200 Hz - 125 Hz - 50 Hz		Y – N
15			Y – N	18			N – Y

Participants were not explicitly trained on what constituted a focal point or a gap between focal points. However, since participants were mostly unfamiliar with UMH

devices, they performed a minimum of five test trials with stimuli in the modulation frequency of the first block before the experiment proper. Participants were not provided feedback on their performance during these test trials to avoid altering their experience of the stimulus. They were told that there was no right or wrong answer but that it was their perception that mattered. The test trials were halted when the participants indicated that they understood the task and could relate it to the novel sensation. Participants were carefully informed that they would be experiencing either one or two stimulation areas on their palm. If they experienced one area, then it could possibly vary in size, and if they experienced two areas, then these could vary in size and in spacing along the horizontal axis. Participants were told that focal points might partly overlap or touch each other but that a significant decrease in stimulus intensity had to be perceived in between two more intense points of stimulation to qualify as a gap.

B.3.2. PARTICIPANTS

Fifteen students (7 male, 8 female, ages 19 to 33 (mean 24.07, SD = 4.25)) with no reported neurological disorders or issues with somatosensory function took part in the study. All but three participants were right handed (M = 0.8, SD = 0.41) as assessed by the Edinburgh Handedness Inventory [35]). All participants gave written informed consent to participate in line with the Human Ethics Committee of Delft University of Technology and the Helsinki Declaration.

B.3.3. RESULTS

We recorded responses for all focal point pair spacing values at three amplitude modulation frequencies. We observed a strong within- and between-subject variability, possibly indicating a high task difficulty (see Figure B.3).

For each participant, we calculated the mean threshold for each of the repetitions and for each modulation frequency according to the procedure outlined in Appendix B.3.1 (see Figure B.4). Shapiro-Wilk tests on data grouped by modulation frequencies failed to reject the null hypothesis according to which data were normally distributed (W(50 Hz) = 0.92, p(50 Hz) = 0.17;W(125 Hz) = 0.95, p(125 Hz) = 0.48;W(200 Hz) = 0.97, p(200 Hz) = 0.83). Bartlett's test failed to reject the hypothesis according to which samples had unequal variances (B = 0.14, p = 0.93). We thus performed repeated-measures ANOVAs and found a significant difference between modulation frequencies (F (2,44) = 3.47, p = 0.056). However, the effect did not remain significant for any of the post hoc pairwise comparisons. No significant difference was observed in thresholds across repetitions, within a given AM frequency condition (see Figure B.4). Thus, there is no indication of either short-term learning or desensitizing effects for participants between repetitions of a given condition. No significant differences were found between participants across modulation frequencies and repetitions. In the 50-Hz AM frequency condition, participants' mean thresholds varied from 17.5 to 45.8 mm (IQR: 15.41 mm). For the 125-Hz AM frequency condition, participants' mean thresholds varied from 17 to 45 mm(IQR: 16.25 mm). For the 200-Hz AM frequency condition, participants' mean thresholds varied from
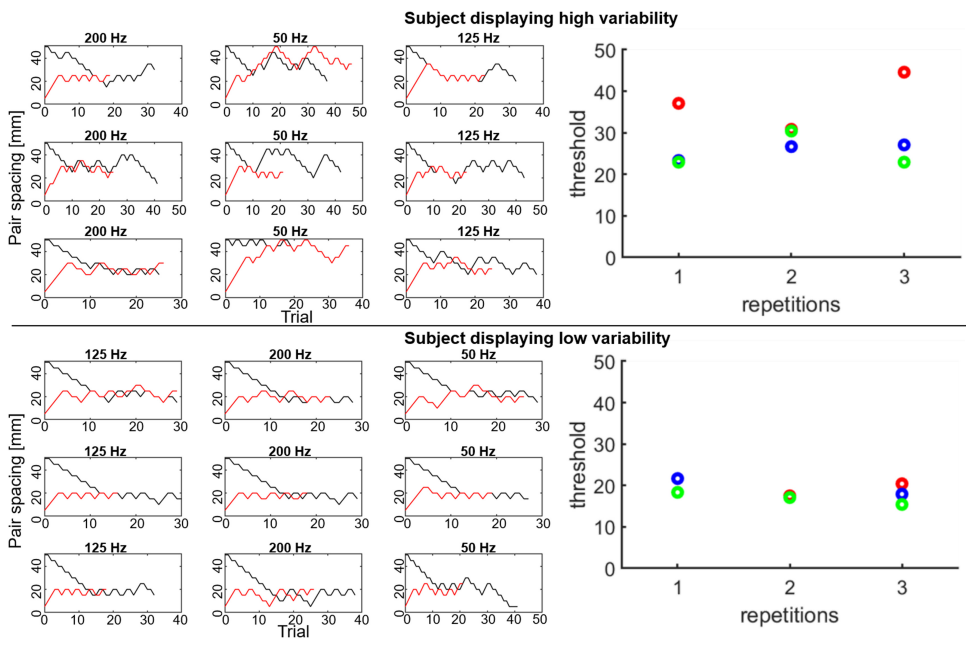
Figure B.3. Recorded responses for a participant exhibiting high variability between repetitions (top) and one exhibiting low variability between repetitions (bottom). The black lines show the progression of pair spacing for the descending staircase trials, the red lines show the progression of spacing for the ascending staircase trials. The plots on the right show the corresponding thresholds for the 50 Hz (red), 125 Hz (green), and 200 Hz (blue) trials across all repetitions. Similar plots were processed for each of the participants.

15.4 to 47 mm (IQR: 14.27 mm) (see Figure B.4). We estimate the mean thresholds for gap detection at 33.81 mm (SD = 8.66 mm), 32.36 mm (SD = 8.33 mm), and 30.78 mm (SD = 8.87 mm), respectively, for the 50-, 125-, and 200-Hz AM frequency conditions. Given the absence of significant differences between frequencies, repetitions or participants, we can estimate the overall mean gap detection threshold at 32.3 mm.

These results confirm prior findings from the literature [4], indicating that pairs of focal points under 15 mm apart are consistently perceived as a single stimulus while pairs spaced more than 45 mm apart are consistently perceived as two distinct stimuli. However, the large variability in thresholds across participants does not allow us to draw any stronger conclusions on the exact distance at which two focal points become distinct, nor to infer any estimate of the perceived size of an individual focal point.

We performed an additional analysis of the same data set, this time considering trials within the staircase procedures as independent observations of gap detection for a given spacing, for each participant. From this, we calculated the probability of
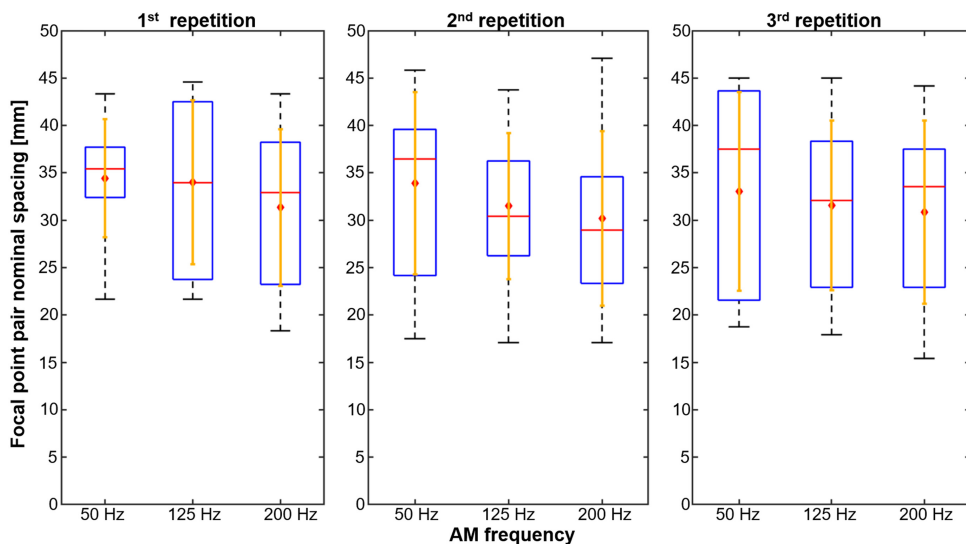
Figure B.4. Gap detection threshold (in mm) distributions plotted by AM frequency: 50 Hz (left), 125 Hz (center), 200 Hz (right) for each repetition. Solid red bars indicate the median threshold across participants, red diamonds show the mean and orange bars show the standard deviation.

gap detection at each nominal spacing, per participant. Conclusions drawn from this analysis must be regarded as tentative given the differences in sample sizes for each spacing value. However, all samples were sufficiently large to obtain small 95%-confidence intervals (CI) when estimating the gap detection probability for each spacing for each participant. The 95%-CI ranged from 0.017 (15 mm spacing) to 0.07 (35 mm spacing). Shapiro-Wilk tests failed to reject the hypothesis according to which data were normally distributed; however, Bartlett's test showed that the assumption of homogeneity of variances was likely violated (B = 317.02, p = 0). A Kruskall-Wallis ANOVA failed to reject the null hypothesis according to which some gap detection probabilities differ from the rest at the 5% significance level ($\chi^2 = 26.11, p = 0.073$). Figure B.5 shows the obtained mean probability of gap detection as a function of nominal focal point spacing.

Results once again show that participants tend to consistently detect no gap for focal points nominally spaced up to 15 mm, above which the mean probability of gap detection first steeply increases up to a nominal spacing of 25 mm and then linearly increases with a milder slope up to 45 mm nominal spacing. The observed mean probability of gap detection at 50 mm spacing then drops again (see Figure B.5).

However, two sources of bias may affect the gap detection probability value at this spacing. First, the relatively large spacing places the focal points closer to the edges of the hand. If some interplay of imperfect hand positioning and poorer tactile sensitivity on one side of the palm led subjects to feel only one of the focal points, then they may inaccurately report "no gap". Second, it is possible that residual uncertainty
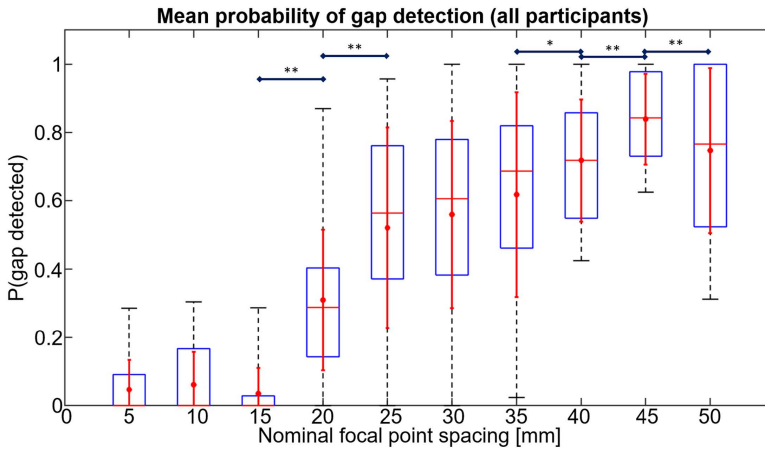
Figure B.5. Probability of detecting a gap between two stimuli as a function of nominal focal point spacing. Box plots show the distribution of probabilities across participants, with median values shown by a horizontal red bar. The mean and standard deviation are highlighted with a red diamond and vertical bar. Significant pairwise differences (Welch's t-test) between adjacent spacing values at respectively 5% (**) and 10% (*) significance levels are highlighted with black horizontal bars.

about what they were feeling biased subjects toward responding "No" at the start of a set of trials due to and the phrasing of our question. Investigations over a wider range of focal point spacing values would, however, be necessary to confirm this.

Before drawing any further conclusions, we performed an investigation into the pressure fields achieved when commanding the pairs of focal points, to determine whether any physical interactions played a role in the observed participant responses.

B.4. PHYSICAL SIMULATION OF FOCAL POINT PAIRS

An in-depth understanding of the behavior of the sound field around the generated pairs of focal points is required to accurately interpret participants' gap detection behavior. While it is possible to measure the generated sound field using one or several microphones, this option is impractical in the present case due to the high technical complexity and time required for such scanning measurements of the sound field. We therefore opted for a physical simulation of the sound fields generated by the stimuli from Appendix B.3 (see Appendix B.4.2 below).

We used a custom developed linear acoustic simulator for this. Transducers are represented as point source baffled pistons, and we apply Huygens' principle of superposition to construct the cross-sectional pressure profile of a focal point. The amplitude and directivity of each transducer are represented with a Bessel function, whose parameters have been adjusted to best match the real-world behavior of the Murata MA40S4S transducers built into our array [10]. The transducers assumed for

this ideal phased array have a phase that can be continuously varied between 0 and 2π.

Simulations are an effective way of quickly obtaining high-resolution data on the generated sound fields; however, it is still necessary to ensure their validity by comparing them to real-world measurements. We therefore began by performing preliminary validation measurements to verify the fit between actual acoustic pressures and our simulation results.

B.4.1. PRELIMINARY VALIDATION OF THE SIMULATION ACCURACY

To validate the accuracy of the simulated sound fields, we used a microphone (B&K 4138 1/8"microphone) to record the acoustic pressure at two positions of interest (see Figure B.6). Data were acquired digitally using a B&K Type 3161 single-channel input/output acquisition module operating at 204.8 kHz [36] and the *Pulse* software.
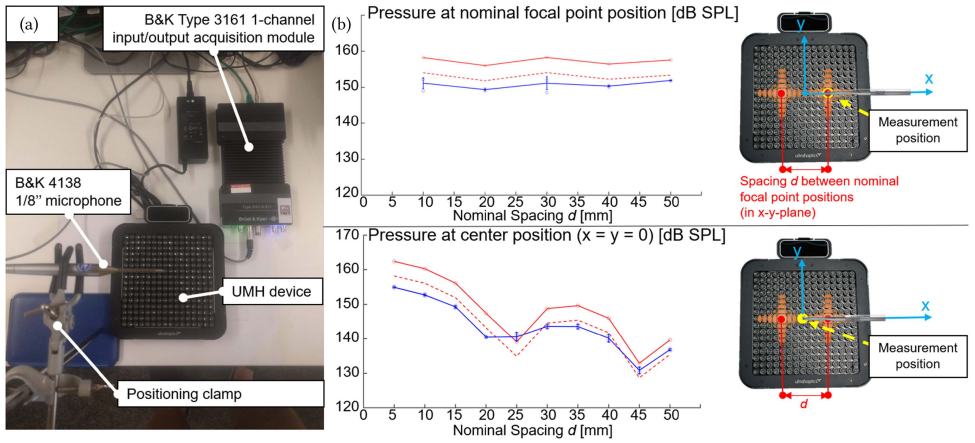

Figure B.6. (a) Microphone recording setup for validation measurements. (b) Plots showing the measured (blue) vs. simulated (red) pressure at the focal point nominal positions for five spacing values (top), as well as the mean pressure at the center position between both nominal positions (x = 0, y = 0 in the array coordinate system) (bottom). Circles indicate data points while lines show the mean and error bars show one standard deviation. The dashed red line shows the pressure expected for AM focal point pairs based on the simulation of unmodulated focal point pairs, i.e., with a –4.2-dB offset applied.

Pairs of focal points were generated with an equal-phase 200 Hz amplitude modulation applied to them, allowing easier alignment of the microphone with the focal point position.We recorded time-data of acoustic pressure levels for a few seconds at a time.We measured the acoustic pressure at the focal point nominal position for five pairs of focal points (spaced respectively by 10, 20, 30, 40 and 50 mm). We also measured the acoustic pressure at the midpoint between both focal

points (x = 0, y = 0 in the array coordinate system) for all 10 pairs of focal points from the previous experiment. Measurements were repeated 3 times for each of the three positions and for each focal point pair spacing. Analysing the time-recorded data, the peak-to-peak pressure was extracted using a lab-written python-script, and then converted to dB SPL (see Figure B.6(b)).

Overall measured values were found to be very repeatable with standard deviations below 1.7-dB SPL for measurements at the focal points and below 1.3-dB SPL for measurements at the center position. We observed a consistent approximate 6-dB offset between the measured and simulated values at the focal point nominal positions. This is to be expected, since the simulation assumed non-modulated focal points and measurement were performed with a 200-Hz sinusoidal amplitude modulation applied to the focal point. In theory this modulation should introduce a 4.2-dB difference between the modulated and non-modulated acoustic radiation pressure. The remaining 1.4-dB offset could be due to three factors. First, some deviation from the nominal transducer output pressure used in the simulation is to be expected as the simulation assumed an ideal phased array and was not specifically calibrated with respect to the transducers used. Second, small inaccuracies in the microphone placement and angle with respect to the focal point may also introduce a constant offset. Finally the linear acoustic model assumed in the simulation would not account for non-linear acoustic effects that can occur at these high pressures. Since the offset between measured and simulated values is almost constant and small, we can conclude to a good match between the simulated and actual peak focal point pressures, confirming the validity of our simulation.

Regarding the measurements at the center position (Figure B.1(b)), we also observe a strong correlation between simulated and measured values. Contrary to the measurements at the focal point nominal position, the pressure at the center position is highly dependent on focal point spacing as pressure at this point is a direct result of the interaction between the pressure fields generated for each of the two focal points. The offset measured at the focal point center position is not systematically observed in this case, although an approximately 5-dB offset is apparent for all spacing values except 25, 45, and 50 mm. This indicates some inaccuracy in the simulation of interference between focal points. However, for our purposes, the fact that the general trend in acoustic pressure is well predicted and that the actual acoustic pressure is either lower or equal to the simulated values in between focal points is sufficient.

B.4.2. SIMULATING STIMULI FROM THE HUMAN PARTICIPANT STUDY

With the reliability of the focal point pair simulations established, we proceeded to fully simulate the pressure fields in the plane of the participants' palm for all 10 pairs of focal points used in the experiment from Appendix B.3.

These simulations (see Figure B.7) show that for nominal spacing values of 5 and 10 mm, the focal points completely merge, forming a wider main pressure lobe centered on the (x = 0, y = 0) position. This is in line with the very low gap detection probability at these nominal spacing values. This phenomenon also highlights the fact that physical interactions may cause the actual positions of pressure maxima to
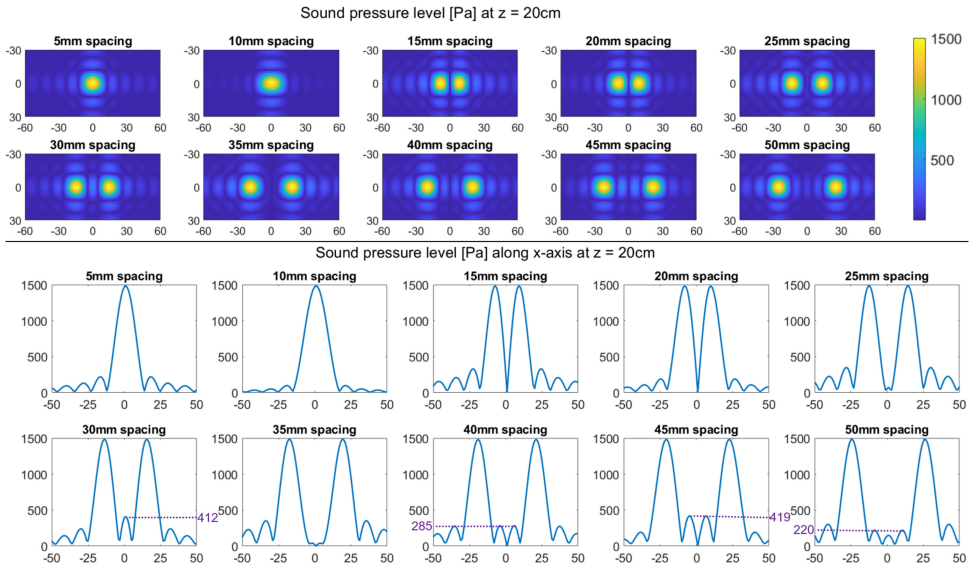
Figure B.7. (Top) Heat maps showing the sound pressure level in the plane at z = 20 cm above the array (in Pa). (Bottom) Sound pressure plots along the y = 0 axis in the same plane (in Pa). Notable pressure lobes occurring between the peaks around the focal points are annotated with their peak pressure value (in Pa) in purple.

deviate significantly from the nominal positions commanded in the software. To understand to what extent this is the case, we simulated focal point pairs in 1-mm spacing increments between 1- and 50-mm spacing and plotted the actual versus nominal spacing between pressure maxima (see Figure B.8(a)). Results show that at a height of z = 20 cm above the presently used array, it is physically impossible to achieve an actual focal point pair spacing below 15 mm. Furthermore, there is a non-linear relationship between actual spacing and nominal spacing, even above 15 mm, although the deviations are usually below 3 mm. It should be noted that these deviations are predicted by simulations based on an ideal phased array and thus are not the result of focusing inaccuracies of a real array. In light of these results, we corrected the plot of results initially shown in Figure B.5 to instead reflect the probability of gap detection as a function of actual focal point spacing (see Figure B.8(b)).

This correction confirms that overall, the probability of gap detection is not a linear function of spacing. Gap detection probability seems to follow a pattern where it stays constant and close to 0 up until a threshold in pressure peak spacing between 15 and 18 mm. After this a sharp increase occurs, followed by a more or less linear increase in probability of gap detection as the focal points get further apart (between 18 and 45 mm). The seemingly linear relationship between spacing and gap detection probability for spacing values above 26 mm appears to be unaffected by the presence
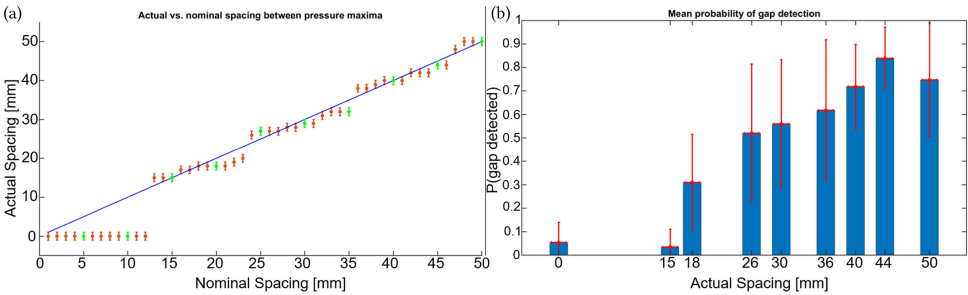
Figure B.8. (a) Plot of the actual distance between pressure maxima against the nominal focal point spacing compared to the y = x reference line (in blue). Green points highlight the actual spacing achieved for the stimuli in the human participant study, while additional simulation results for 1-mm increments in nominal spacing are shown in red. Error bars show the uncertainty in actual spacing estimation due to the simulation's resolution. (b) Adjusted graph of probability of gap detection (from Figure B.5) plotting the measured probabilities against the actual spacing between pressure maxima. Bar plots show the mean probability of gap detection (all participants). The standard deviation is shown with a red vertical bar, the red horizontal bar reflects the uncertainty in actual spacing estimation (corresponding to the vertical error bar in plot (a)).

or intensity of secondary pressure lobes, regardless of their intensity (see Figure B.7 (bottom) for spacing values of 30, 40, 45, and 50 mm).

B.5. DISCUSSION AND PERSPECTIVES

B.5.1. EFFECTS OF HAND SIZE, AGE, OR GENDER

We found no correlation between participant hand size and the mean or standard deviation of thresholds, be it by frequency condition or averaged across frequency conditions. Women appeared to have lower thresholds than men; however, this could not be shown statistically given the small sample size. Similarly, younger participants also tended to achieve lower thresholds, though this effect was not significant and the sample size and age distribution do not allow any firm conclusions. Studies on a larger and more diverse population would likely be required to detect any effect of the participants on gap detection ability and perceived focal point diameter.

B.5.2. LIMITATIONS OF THE PRESENT STUDY

One should keep in mind that because of the limited sample size and sample diversity, as well as the large uncertainty associated with the results of the human participant study (Appendix B.3) and some imperfections in the simulation (Appendix B.4.1), the conclusions presented here are tentative and require confirmation through additional

studies. A more suitable experimental protocol for additional perception studies would be a method of constant stimuli to determine the probability of gap detection at each considered spacing value. Such studies should also take into account discrepancies between nominal and actual peak pressure positions from the start.

Also, the present study restricted the exploration region to the center of the plane above the array, guaranteeing that only the desired focal points were potentially perceived. Because of their design, UMH arrays produce so-called grating lobes at a distance from the nominal focal point position. These are usually not problematic but could, in the case of larger shapes, introduce additional unwanted stimuli that in turn could affect perceived continuity or discontinuity of UMH shapes. This issue can, however, be mitigated by using, e.g., hardware approaches such as appropriate array design, as proposed by Price et al. [37].

Despite these limitations, some interesting hypotheses about perception of focal points as well as basic guidelines for rendering can be derived from the present work and are discussed below.

B.5.3. PERCEIVED FOCAL POINT DIAMETER

When only one focal point is presented, there is a minimum peak pressure value below which focal points are never detected, and thus their perceived diameter is zero. Above this pressure threshold value, the probability of detecting the focal point (and thus of perceiving it to have a non-zero diameter) gradually increases until a minimum pressure threshold value where focal points are systematically detected (with a non-zero diameter). For a given probability x of detecting the focal point, the associated peak pressure is referred to as the x%- detection threshold. The 50%-detection threshold, which is usually considered to characterize stimulus detection in psychophysics, was found to be 560 Pa [25].

Alone, data from this perception study are insufficient to conclude on the relationship between pressure profile and perceived focal point diameter. However, they can provide some insights and serve as a basis for laying out hypotheses on the subject, especially when considering our observations for the 15 and 18 mm actual spacing.

The probability of gap detection at 18 mm actual spacing, where the pressure profile shows both main lobes to be tangent at the base, was found to differ significantly from zero. From this, we can conclude that the perceived focal point diameter is likely less than the base diameter of the focal point main pressure lobe (in this case <18 mm). Following a similar reasoning, the fact that the probability of gap detection at 15 mm actual spacing is close to zero could be construed as showing that the perceived focal point diameter is greater than 15 mm in that case, and that the perceived focal points thus overlap. However this would contradict the conclusion drawn from the observation at 18 mm spacing as the perceived focal point diameter would in one case be smaller and in the other larger than the base diameter of the main lobe. The more likely explanation is thus that at 15 mm spacing, the perceived focal point diameter is also smaller than 15 mm (a value that is coherent with prior literature results [5]), and that some other effect is at play (see Appendix B.5.4).

If the diameter of the perceived focal point is less than that of the base diameter of the focal point main pressure lobe, then we may be able to model the perceived focal point diameter as the diameter of a cross section of said main pressure lobe, cut off at some pressure threshold that may relate to an x%-detection threshold discussed above.

This would suggest that secondary lobes have a negligible impact on the perceived focal point diameter, something that also matches observations from the present study. Indeed, above 30-mm nominal spacing, the different patterns of secondary lobes between the main lobes (see Figure B.7) do not seem to affect the linear trend observed in the mean probability of gap detection.

B.5.4. Perceptual Interactions With Focal Point Pairs

The probability of gap detection increases with spacing, albeit in a non-linear manner. For spacing values below 15 mm, focal point pairs are perceived mostly as a single continuous stimulus, even though the largest spacing in this range is larger than previous literature estimates of the perceived diameter of focal points [4, 5, 7]. This is possibly indicative of spatial summation effects. Such effects are common in vibrotactile perception, occurring when a larger surface area is stimulated, and leading to a lowering of detection thresholds around the stimulation area [38]. In the case of UMH, a large skin surface area is subjected to continuously decreasing pressure the further one gets from the nominal focal point position, with only a fraction of this area centered on the nominal focal point position being perceived as a vibrotactile stimulus. A local decrease in detection threshold would thus result in a larger perceived stimulus area. Therefore, it appears plausible that two focal points in close proximity may stimulate a sufficient area to cause spatial summation effects, increasing the perceived sizes of both focal points and thus lowering the probability of gap detection. These effects would, however, disappear beyond a threshold in spacing, which could help explain the gap detection probability between 15- and 18-mm spacing.

Prior results by Carter et al. [4] showed that pairs of focal points with different modulation frequencies are more readily discriminated than pairs with identical modulation frequencies. If spatial summation effects arise as suggested above, given the fact that the dimensions of focal point main pressure lobes are independent from the modulation frequency, then these would likely also depend upon frequency characteristics of the focal points.

Further investigation into the perceived size of focal points, alone and in pairs, are required to shed light the exact nature of perceptual interactions occurring within focal point pairs.

B.5.5. Influence of Array, Focal Point Height, Intensity, and Modulation Frequency on Gap Detection

Given our hypothesis according to which the perceived size of a focal point is directly linked to the dimensions of the focal point main pressure lobe, we propose an

approach that could enable future investigations by changing the main pressure lobe shape in a controlled manner.

The minimum width w of the focal point main lobe is a function of ultrasound wavelength λ, focal point height above the array h and array aperture A (all in $[m]$) [5]:

$$w = 1.22 \cdot \lambda \cdot \frac{\sqrt{h^2 + \left(\frac{A}{2}\right)^2}}{\frac{A}{2}}. \tag{B.1}$$

We therefore hypothesize that changing the focal point height while keeping the same array aperture and carrier frequency could possibly impact the minimum achievable actual spacing between pressure maxima. To verify this, we conducted an additional series of simulations in identical conditions to those described in Appendix B.4.2 for focal point pairs at z = 10 cm above the array (see Figure B.9).
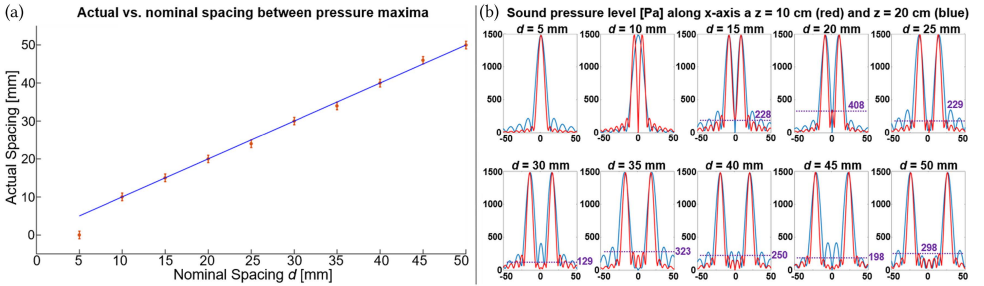

Figure B.9. Simulation of focal point pairs with identical spacing to those used in the human participant study, on the same array but at a height of z = 10 cm above the array. (a) The relationship between actual and nominal spacing. (b) Plots of the acoustic pressure along the x axis in red, overlaid on the plots from Figure B.7 (at z = 20 cm) in blue.

Results show that the achieved focal point main pressure lobes are indeed thinner by what appears to be a constant amount of 8 mm at the base. This also leads to focal point pairs merging at lower spacing values, in this case between 5 and 10 mm. On average the peak pressures of the secondary lobes in between the main pressure lobes also appear to be lower (mean of 257 Pa against a mean of 354 Pa for z = 20 cm). An unexpected side-effect is that the relationship between nominal and actual focal point spacing appears more linear with these rendering parameters. This hints to the fact that gap detection between focal points may be affected by array design and focal point height, although additional perceptual studies are required to validate this hypothesis.

In theory, scaling down the commanded focal point intensity (peak intensity) should scale down the pressures generated throughout the resulting pressure field by the same constant factor. Thus, assuming that the distance of some pressure threshold to the focal point center plays a role in the perceived focal point diameter, intensity could be used to vary said diameter. In turn, this could have an effect

on gap detection. However, gap detection ability may also be affected by the pressure gradient within a perceived focal point, which would also be scaled down, counteracting or reinforcing the effects of intensity on perceived focal point diameter. Further investigations into gap detection behavior between pairs of equal- and unequal-intensity focal points at intensities different from the maximum could shed light on this aspect.

In our present work, we did not observe any influence of modulation frequency on gap detection ability. However, a previous preliminary study by Carter et al. [4] suggests that two focal points with large differences in AM frequency are more easily distinguished from one another. In future work, it may therefore be interesting to investigate whether small differences in AM frequency between neighboring focal points can reduce the gap detection threshold without both points being interpreted as independent stimuli. This could have interesting applications in finer discontinuous shape rendering using simultaneous or sequential AM.

B.5.6. IMPLICATIONS FOR RENDERING

Our investigations allow some conclusions to be drawn with respect to the shape rendering methods presented in Figure B.1. STM provides greater freedom than AM in terms of geometric shape sizes and number of spatial sampling points, yet it poses constraints in terms of draw frequency that may alter the perceived tactile properties of the shape, making AM preferable in certain cases. For simultaneous AM shape rendering, our results show that perception of continuous shapes is almost guaranteed for spatial sampling points spaced up to 15 mm apart. For the Ultraleap Stratos Explore device used in our studies, which allows rendering of only up to approx. 4 perceivable simultaneous focal points [4, 31], this implies that lines up to 60 mm in length might reliably be perceived as continuous, and that a surface stimulus up to 30 mm2 may be achieved by arranging these points in a 15-mm-sided square pattern. These limits, however, vary depending on device design and could be increased by using devices with larger power output (e.g., Reference [33]). Larger continuous AM patterns may be achievable by using out-of-phase focal points that would allow better use of the device's full power output or by using more powerful arrays.

These findings also provide a starting point for further investigations into continuity of shapes for sequential AM shapes, although it remains to be seen to what extent these results hold true for this rendering scenario. Further investigations into the perception of gaps in sequential AM and STM shapes would be beneficial to better understand rendering requirements for mid-air haptic shapes.

B.6. CONCLUSION

We presented a human participant experiment investigating the perception of gaps or continuity between neighboring AM focal points generated by an UMH device. Gap detection thresholds were found to lie around 32.3 mm on average; however, a large within- and between-subject variability was observed during the task. Focal points spaced less than 15 mm apart were consistently perceived as a single continuous

stimulus (>95% of the time), and focal points spaced 45 mm apart were consistently (84% of the time) perceived as two distinct stimuli.

Subsequent simulations of the acoustic pressure distribution generated by pairs of focal points show that at a height of 20 cm above the array used, focal points spaced less than 13 mm apart merge into a single wider focal point. Furthermore, there is a non-linear relationship between nominal focal point spacing and actual pressure peak spacing. By correlating the results from the human participant study with the simulation data, we find that both merging focal points (nominal spacing below 13 mm) and close pairs (nominal spacing of 15 mm) are consistently perceived as a single continuous stimulus. For pairs of focal points yielding pressure peaks actually spaced 18mm apart or more, there appears to be a linear relationship between focal point spacing and probability of detecting a gap between the stimuli.

The present work provides initial guidelines for rendering continuous and discontinuous mid-air tactile shapes. It also provides insights into additional investigation required to draw strong conclusions about the perceived size of a focal point and the nature of perceptual interactions between neighboring focal points.

Our simulation study highlights the importance of validating the physical nature of the stimuli presented when running perception studies on ultrasound mid-air haptics, especially in situations involving complex shapes or multiple focal points. As we saw, significant deviations occur between the nominally commanded positions of pressure maxima and their actual positions, and interference between focal points can lead to unexpected interactions that may significantly modify the stimuli and bias results of perception experiments.

In the future, we plan to conduct investigations into the perceived diameters of focal points alone, in pairs and in complex patterns to gain further insight into perceptual interactions and to better predict perceived UMH shapes on the basis of physical pressure distributions. We hope this work will ultimately contribute toward a reliable model of mid-air haptic shape perception.

REFERENCES

[1] Howard, T., Driller, K., Frier, W., Pacchierotti, C., Marchal, M., and Hartcher-O'Brien, J. Gap detection in pairs of ultrasound mid-air vibrotactile stimuli. *ACM Transactions on Applied Perception* **20** (2023), 5:1–5:17. DOI: 10.1145/3570904.

[2] Georgiou, O., Frier, W., Freeman, E., Pacchierotti, C., and Hoshi, T., eds. *Ultrasound Mid-Air Haptics for Touchless Interfaces*. Human–Computer Interaction Series. Cham: Springer International Publishing, 2022. DOI: 10.1007/978-3-031-04043-6.

[3] Rakkolainen, I., Freeman, E., Sand, A., Raisamo, R., and Brewster, S. A survey of mid-air ultrasound haptics and its applications. *IEEE Transactions on Haptics* **14** (2021), 2–19. DOI: 10.1109/TOH.2020.3018754.

[4] Carter, T., Seah, S. A., Long, B., Drinkwater, B., and Subramanian, S. "UltraHaptics: Multi-point Mid-air Haptic Feedback for Touch Surfaces". In: Proceedings of the 26th Annual ACM Symposium on User Interface Software and Technology. UIST '13. New York, NY, USA: ACM, 2013, pp. 505–514. DOI: 10.1145/2501988.2502018.

[5] Ito, M., Wakuda, D., Inoue, S., Makino, Y., and Shinoda, H. "High Spatial Resolution Midair Tactile Display Using 70 kHz Ultrasound". In: ed. by Bello, F., Kajimoto, H., and Visell, Y. Vol. 9774. Cham: Springer International Publishing, 2016, pp. 57–67. DOI: 10.1007/978-3-319-42321-0_6.

[6] Bolanowski, S. J., Gescheider, G. A., Verrillo, R. T., and Checkosky, C. M. Four channels mediate the mechanical aspects of touch. *The Journal of the Acoustical Society of America* **84** (1988), 1680–1694. DOI: 10.1121/1.397184.

[7] Iwamoto, T., Tatezono, M., and Shinoda, H. "Non-contact Method for Producing Tactile Sensation Using Airborne Ultrasound". In: Haptics: Perception, Devices and Scenarios. Ed. by Ferre, M. Lecture Notes in Computer Science. Berlin, Heidelberg: Springer, 2008, pp. 504–513. DOI: 10.1007/978-3-540-69057-3_64.

[8] Takahashi, R., Hasegawa, K., and Shinoda, H. Lateral modulation of midair ultrasound focus for intensified vibrotactile stimuli. *Haptics: Science, Technology, and Applications* (2018), 276.

[9] Kappus, B. and Long, B. Spatiotemporal modulation for mid-air haptic feedback from an ultrasonic phased array. *Acoustical Society of America Journal* **143** (2018), 1836–1836. DOI: 10.1121/1.5036027.

[10] Frier, W., Abdouni, A., Pittera, D., Georgiou, O., and Malkin, R. Simulating airborne ultrasound vibrations in human skin for haptic applications. *IEEE Access* **10** (2022), 15443–15456. DOI: 10.1109/ACCESS.2022.3147725.

[11] Hajas, D., Pittera, D., Nasce, A., Georgiou, O., and Obrist, M. Mid-air haptic rendering of 2D geometric shapes with a dynamic tactile pointer. *IEEE transactions on haptics* **13** (2020), 806–817. DOI: 10.1109/TOH.2020.2966445.

[12] Beattie, D., Frier, W., Georgiou, O., Long, B., and Ablart, D. "Incorporating the Perception of Visual Roughness into the Design of Mid-Air Haptic Textures". In: ACM Symposium on Applied Perception 2020. SAP '20. New York, NY, USA: Association for Computing Machinery, 2020, pp. 1–10. DOI: 10.1145/3385955.3407927.

[13] Howard, T., Pacchierotti, C., and Marchal, M. "Ultrasound Mid-Air Tactile Feedback for Immersive Virtual Reality Interaction". In: Ultrasound Mid-Air Haptics for Touchless Interfaces. Human–Computer Interaction Series. Springer International Publishing, 2022, pp. 147–183. DOI: 10.1007/978-3-031-04043-6_6.

[14] Shakeri, G., Freeman, E., Frier, W., Iodice, M., Long, B., Georgiou, O., and Andersson, C. "Three-in-one: Levitation, Parametric Audio, and Mid-Air Haptic Feedback". In: 2019, pp. 1–4. DOI: 10.1145/3290607.3313264.

[15] Large, D. R., Harrington, K., Burnett, G., and Georgiou, O. Feel the noise: Mid-air ultrasound haptics as a novel human-vehicle interaction paradigm. *Applied Ergonomics* **81** (2019), 102909. DOI: 10.1016/j.apergo.2019.102909.

[16] Mulot, L., Gicquel, G., Zanini, Q., Frier, W., Marchal, M., Pacchierotti, C., and Howard, T. "Dolphin: A Framework for the Design and Perceptual Evaluation of Ultrasound Mid-Air Haptic Stimuli". In: ACM Symposium on Applied Perception 2021. Virtual Event France: ACM, 2021, pp. 1–10. DOI: 10.1145/3474451.3476232.

[17] Rutten, I., Frier, W., Van Den Bogaert, L., and Geerts, D. "Invisible Touch: How Identifiable are Mid-Air Haptic Shapes?" In: Extended Abstracts of the 2019 CHI Conference on Human Factors in Computing Systems. Glasgow Scotland Uk: ACM, 2019, pp. 1–6. DOI: 10.1145/3290607.3313004.

[18] Hoshi, T., Takahashi, M., Iwamoto, T., and Shinoda, H. Noncontact tactile display based on radiation pressure of airborne ultrasound. *IEEE Transactions on Haptics* **3** (2010), 155–165. DOI: 10.1109/TOH.2010.4.

[19] Korres, G., Aujeszky, T., and Eid, M. "Characterizing tactile rendering parameters for ultrasound based stimulation". In: 2017 IEEE World Haptics Conference (WHC). 2017, pp. 293–298. DOI: 10.1109/WHC.2017.7989917.

[20] Frier, W., Ablart, D., Chilles, J., Long, B., Giordano, M., Obrist, M., and Subramanian, S. "Using Spatiotemporal Modulation to Draw Tactile Patterns in Mid-Air". In: Haptics: Science, Technology, and Applications. Ed. by Prattichizzo, D., Shinoda, H., Tan, H. Z., Ruffaldi, E., and Frisoli, A. Lecture Notes in Computer Science. Cham: Springer International Publishing, 2018, pp. 270–281. DOI: 10.1007/978-3-319-93445-7_24.

[21] Obrist, M., Ann Seah, S., and Subramanian, S. "Talking about Tactile Experiences". In: CHI '13: Proceedings of the SIGCHI Conference on Human Factors in Computing Systems. 2013. DOI: 10.1145/2470654.2466220.

[22] Harrington, K., Large, D. R., Burnett, G., and Georgiou, O. "Exploring the Use of Mid-Air Ultrasonic Feedback to Enhance Automotive User Interfaces". In: Proceedings of the 10th International Conference on Automotive User Interfaces and Interactive Vehicular Applications. AutomotiveUI '18. New York, NY, USA: Association for Computing Machinery, 2018, pp. 11–20. DOI: 10.1145/3239060.3239089.

[23] Freeman, E. and Wilson, G. Perception of ultrasound haptic focal point motion: 23rd ACM International Conference on Multimodal Interaction. *ICMI '21.* ICMI 2021 - Proceedings of the 2021 International Conference on Multimodal Interaction (2021). Ed. by Hammal, Z., Busso, C., Pelachaud, C., Oviatt, S., Ali Salah, A., and Zhao, G., 697–701. DOI: 10.1145/3462244.3479950.

[24] Frier, W., Pittera, D., Ablart, D., Obrist, M., and Subramanian, S. "Sampling Strategy for Ultrasonic Mid-Air Haptics". In: Proceedings of the 2019 CHI Conference on Human Factors in Computing Systems. CHI '19. New York, NY, USA: Association for Computing Machinery, 2019, pp. 1–11. DOI: 10.1145/3290605.3300351.

[25] Howard, T., Gallagher, G., Lecuyer, A., Pacchierotti, C., and Marchal, M. "Investigating the Recognition of Local Shapes Using Mid-air Ultrasound Haptics". In: 2019 IEEE World Haptics Conference (WHC). Tokyo, Japan: IEEE, 2019, pp. 503–508. DOI: 10.1109/WHC.2019.8816127.

[26] Sand, A., Rakkolainen, I., Surakka, V., Raisamo, R., and Brewster, S. "Evaluating Ultrasonic Tactile Feedback Stimuli". In: Haptics: Science, Technology, Applications. Ed. by Nisky, I., Hartcher-O'Brien, J., Wiertlewski, M., and Smeets, J. Lecture Notes in Computer Science. Cham: Springer International Publishing, 2020, pp. 253–261. DOI: 10.1007/978-3-030-58147-3_28.

[27] Jones, L. A. The assessment of hand function: a critical review of techniques. *The Journal of Hand Surgery* **14** (1989), 221–228. DOI: 10.1016/0363-5023(89)90010-5.

[28] Kowalzik, R., Hermann, B., Biedermann, H., and Peiper, U. Two-point discrimination of vibratory perception on the sole of the human foot. *Foot & Ankle International* **17** (1996), 629–634. DOI: 10.1177/107110079601701008.

[29] Perez, C. A., Holzmann, C. A., and Jaeschke, H. E. Two-point vibrotactile discrimination related to parameters of pulse burst stimulus. *Medical and Biological Engineering and Computing* **38** (2000), 74–79. DOI: 10.1007/BF02344692.

[30] Perez, C., Holzmann, C., and Sandoval, E. "Two point vibrotactile spatial resolution as a function of pulse frequency and pulse width". In: Proceedings of the 20th Annual International Conference of the IEEE Engineering in Medicine and Biology Society. Vol.20 Biomedical Engineering Towards the Year

B

2000 and Beyond (Cat. No.98CH36286). Vol. 5. 1998, 2542–2545 vol.5. DOI: 10.1109/IEMBS.1998.744968.

[31] Ultraleap. *Ultraleap–Haptics. Retrieved from https://www.ultraleap.com/haptics/.*

[32] Levitt, H. Transformed up-down methods in psychoacoustics. *The Journal of the Acoustical Society of America* **49** (1971), 467–477.

[33] Hasegawa, K. and Shinoda, H. Aerial vibrotactile display based on multiUnit ultrasound phased array. *IEEE transactions on haptics* (2018). DOI: 10.1109/TOH.2018.2799220.

[34] Tsumoto, K., Morisaki, T., Fujiwara, M., Makino, Y., and Shinoda, H. "Presentation of Tactile Pleasantness Using Airborne Ultrasound". In: 2021, pp. 602–606. DOI: 10.1109/WHC49131.2021.9517249.

[35] Oldfield, R. C. The assessment and analysis of handedness: The Edinburgh inventory. *Neuropsychologia* **9** (1971), 97–113. DOI: 10.1016/0028-3932(71)90067-4.

[36] B&K. *Brüel & Kjaer Sound and Vibration Measurement Systems.*

[37] Price, D. D., McHaffie, J. G., and Larson, M. A. Spatial summation of heat-induced pain: influence of stimulus area and spatial separation of stimuli on perceived pain sensation intensity and unpleasantness. *Journal of Neurophysiology* **62** (1989), 1270–1279. DOI: 10.1152/jn.1989.62.6.1270.

[38] Gescheider, G. A., Güçlü, B., Sexton, J. L., Karalunas, S., and Fontana, A. Spatial summation in the tactile sensory system: Probability summation and neural integration. *Somatosensory & Motor Research* **22** (2005), 255–268. DOI: 10.1080/08990220500420236.

C

STIMULATOR CHARACTERIZATION FOR CHAPTER 2

A series of measurements was performed by Vincent Hayward using the apparatus described in Chapter 2. Figure C.1 shows the results.
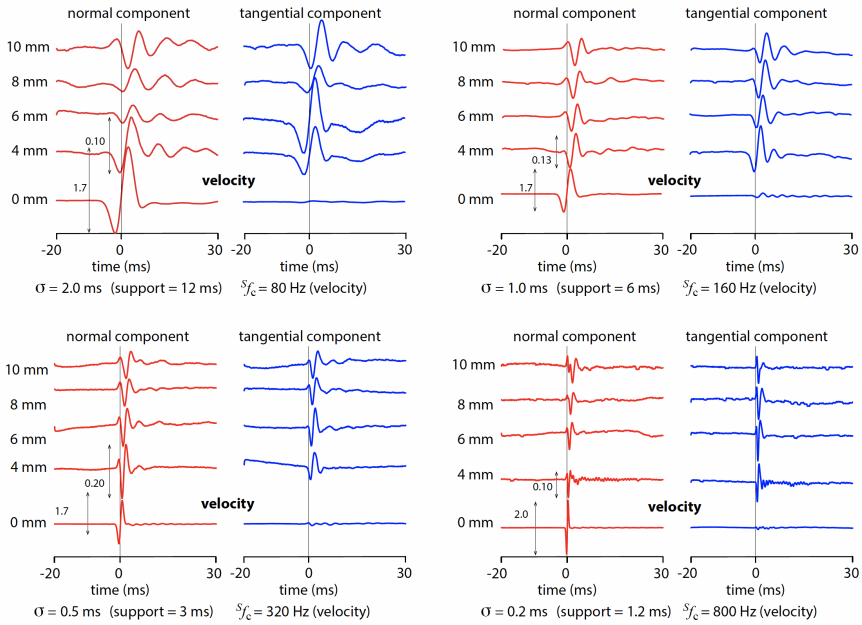

Author: Vincent Hayward

Figure C.1. Excitation and sensor measurements for 4 wavelets with a sigma (σ) of 2.0, 1.0, 0.5, and 0.2 respectively. Measurements at 0 mm were made by engaging the sensor stylus directly with the probe. Time 0 was set at the velocity zero crossing. The amplitude was just below the maximum admissible excitation which peaked at about 1.0 m/s, corresponding to 0.5 mm peak indentation in the vertical direction. A small asymmetry may be noted. However, given that the signal frequency region overlaps the resonance region of the exciter, the signal is remarkably correct. It may also be noted that despite the elastic guidance of the probe, residual movements in the horizontal direction are minimal. The remaining curves show the velocity measured on the skin, away from the locus of excitation, in the vertical and horizontal directions at distances of 4, 6, 8, and 10 mm.

D

CALCULATIONS OF THE VISCOUS WORK FOR CHAPTER 2

A short and local interaction between two solids, one much harder than the other, is assumed. Such interaction must be such that the deformation rate (velocity) approaches zero at the beginning and end of the event, and passes through a maximum. The evolution of the deflection through time can therefore be represented by a Gaussian function, g(t). If it can be assumed that the interaction causes a viscous force proportional to the rate of deflection by a factor b, the work lost is a function of the amplitude, α, and the duration, σ, of the event. The rate of deflection is thus the derivative of a Gaussian (3).

$$g(t) = \alpha\sigma^2 \exp\left(-\frac{t^2}{2\sigma^2}\right), \qquad\qquad G(\omega) = \alpha\sigma^3\sqrt{2\pi}\exp\left(-\frac{\sigma^2\omega^2}{2}\right), \quad \text{Gaussian} \quad \text{(D.1)}$$

$$s(t) = -\alpha\, t \exp\left(-\frac{t^2}{2\sigma^2}\right), \qquad\qquad S(\omega) = i\omega G(\omega), \qquad\qquad\qquad\qquad \text{(D.2)}$$

$$r(t) = \alpha\left(\frac{t^2}{\sigma^2}-1\right)\exp\left(-\frac{t^2}{2\sigma^2}\right), \qquad R(\omega) = -\omega^2 G(\omega), \qquad\qquad\quad \text{Ricker} \quad \text{(D.3)}$$

$$j(t) = \alpha\frac{1}{\sigma^2}\left(3\,t - \frac{t^3}{\sigma^2}\right)\exp\left(-\frac{t^2}{2\sigma^2}\right), \quad J(\omega) = -i\omega^3 G(\omega). \qquad\qquad\qquad \text{(D.4)}$$

Given the above wavelet formulations used to represent displacement, acceleration, velocity, and jitter, the calculation of the work done by the viscous force work goes as follows:

$$w = 2\int_0^d F(x)\,\mathrm{d}x$$

$$= \int_{-\infty}^{+\infty} F(t)\frac{\mathrm{d}x(t)}{\mathrm{d}t}\,\mathrm{d}t$$

Authors: Vincent Hayward, Camille Fradet, James Andrews

In the case of a viscous force F_{visc} generated by our gaussian wavelet $g(t)$:

$$w = 2\int_0^d F_{visc}(g(t))\,\mathrm{d}g(t)$$

$$= \int_{-\infty}^{+\infty} F_{visc}(t)\frac{\mathrm{d}g(t)}{\mathrm{d}t}\,\mathrm{d}t$$

$$F_{visc} = b\frac{\mathrm{d}g(t)}{\mathrm{d}t}$$

$$w = \int_{-\infty}^{+\infty} b\frac{\mathrm{d}g(t)}{\mathrm{d}t}\frac{\mathrm{d}g(t)}{\mathrm{d}t}\,\mathrm{d}t$$

$$s(t) = \frac{\mathrm{d}g(t)}{\mathrm{d}t}$$

$$\Rightarrow w = \int_{-\infty}^{+\infty} b\,s(t)^2\,\mathrm{d}t \tag{D.5}$$

From the wavelets formulations, eq. (D.2) is used in eq. (D.5):

$$s(t) = -\alpha\,t\exp\left(-\frac{t^2}{2\sigma^2}\right)$$

$$\Rightarrow w(\alpha,\sigma) = \int_{-\infty}^{+\infty} b\left(-\alpha\,t\exp\left(-\frac{t^2}{2\sigma^2}\right)\right)^2\,\mathrm{d}t$$

$$= b\,\alpha^2\int_{-\infty}^{+\infty} t^2\exp\left(-\frac{t^2}{\sigma^2}\right)\,\mathrm{d}t \tag{D.6}$$

The solution from Laplace on the gaussian integral gives :

$$\int_{-\infty}^{+\infty} x^2\exp\left(-ax^2\right)\,\mathrm{d}t = \frac{\pi^{1/2}}{2\,a^{3/2}} \tag{D.7}$$

Using $x = t$ and $a = \frac{1}{\sigma^2}$ in eq. (D.7) allows to compute the integral of the total work done through the gaussian wavelet deformation :

$$\Rightarrow w(\alpha,\sigma) = b\,\alpha^2\frac{\pi^{1/2}}{2\,(1/\sigma^2)^{3/2}}$$

$$= \frac{b\alpha^2\pi^{1/2}\sigma^3}{2}$$

$$\boxed{w(\alpha,\sigma) = \frac{\sqrt{\pi}}{2}b\alpha^2\sigma^3} \tag{D.8}$$

The dimensions of work $[w]$ are given as:

$$[w] = \mathrm{J} = \mathrm{N}\cdot\mathrm{m} = \mathrm{kg}\cdot\mathrm{m}^2\cdot\mathrm{s}^{-2}$$

For the viscous force, defined as $F_{visc} = b\dot{x}(t)$, where $\dot{x}(t)$ is the velocity in $\mathrm{m}\cdot\mathrm{s}^{-1}$, the parameter b has dimensions $[b] = \mathrm{kg}\cdot\mathrm{s}^{-1}$. When we normalize the viscous work w by b, the resulting normalized work $\tilde{w} = \frac{w}{b}$ has the dimensions:

$$[\tilde{w}] = \frac{[w]}{[b]} = \frac{\text{kg}\cdot\text{m}^2\cdot\text{s}^{-2}}{\text{kg}\cdot\text{s}^{-1}} = \text{m}^2\cdot\text{s}^{-1}$$

Now, when disregarding the constant b in the analysis, the normalized work $\tilde{w}$ can be expressed as:

$$\tilde{w} = \frac{w}{b} = \frac{\text{J}}{\text{kg}\cdot\text{s}^{-1}} = \text{J}\cdot\text{s}\cdot\text{kg}^{-1}$$

The unit $\text{J}\cdot\text{s}\cdot\text{kg}^{-1}$ therefore represents a normalized measure of viscous work where the effects of mass and time scaling, originally accounted for by b, are removed. It gives us a unit of work that reflects the energy dissipated over time per unit mass, providing a meaningful measure of work in scenarios where b is not explicitly provided.

Thus, the unit of viscous (normalized) work without considering b should be expressed as:

$$\text{J}\cdot\text{s}\cdot\text{kg}^{-1}$$

D

E

POST-EXPERIMENTAL STIMULATOR CHARACTERIZATION FOR CHAPTER 2

Let $R_{IO} = \alpha_{out}/\alpha_{in}$ denote the ratio between the peak acceleration amplitudes of the output displacement α_{out} and of the input signal α_{in}. This ratio enables conversion of the input signal peak amplitude to the output acceleration peak amplitude:

$$R_{IO}(\sigma) = \frac{\alpha_{out}(\sigma)}{\alpha_{in}} \tag{E.1}$$

$$\boxed{\alpha_{out}(\sigma) = R_{IO}(\sigma)\alpha_{in}} \tag{E.2}$$

Through measurements across different wavelet parameters, we found that the relationship between the ratio R_{IO} and the time parameter σ of the wavelet was nonlinear. We estimated this relationship using quadratic regression, allowing for the determination of the correct R_{IO} for any value of σ.

$$R_{IO}(\sigma) = c_2\,\sigma^2 + c_1\sigma + c_0 \tag{E.3}$$

$$\tag{E.4}$$

The regression coefficients, determined from measurements, are:

$$c_2 = 1.9403 \times 10^7$$
$$c_1 = -9.3989 \times 10^4$$
$$c_0 = 199.1421$$

Therefore, the complete transfer function is:

$$\boxed{R_{IO}(\sigma) = 1.9403 \times 10^7\,\sigma^2 - 9.3989 \times 10^4\sigma + 199.1421} \tag{E.5}$$

Authors: Camille Fradet, Karina Kirk Driller

For $s(t)$, the velocity profile (that is, the derivative of the Gaussian displacement wavelet, cf., Section 2.2.3) exhibits two peaks of equal absolute amplitude, one negative one positive. These peaks occur at t_m, where the Ricker wavelet, $r(t)$, crosses through zero. This occurs because the Ricker wavelet is the derivative of the velocity profile. Using the expression of the Ricker wavelet from eq. (2.3):

$$r(t_m) = \alpha \left(\frac{t_m^2}{\sigma^2} - 1 \right) \exp \left(-\frac{t_m^2}{2\sigma^2} \right) = 0$$

$$\forall t_m \; \exp \left(-\frac{t_m^2}{2\sigma^2} \right) > 0$$

$$\Rightarrow \left(\frac{t_m^2}{\sigma^2} - 1 \right) = 0$$

$$t_m = \pm \sigma \tag{E.6}$$

By substituting eq. (E.6) into the expression of $s(t)$ (eq. (2.2)), the two peak velocity values are obtained as: Using eq. (E.6) in the expression of $s(t)$ (eq. (2.2)), the two peak velocity values are:

$$s(t_{m+} = \sigma) = -\alpha \sigma \exp \left(-\frac{1}{2} \right) \tag{E.7}$$

$$s(t_{m-} = -\sigma) = \alpha \sigma \exp \left(-\frac{1}{2} \right) \tag{E.8}$$

The peak-to-peak velocity amplitude V_{p2p} can thus be used to determine the amplitude parameter α:

$$V_{p2p} = s(-\sigma) - s(\sigma)$$

$$= 2\alpha \sigma \exp \left(-\frac{1}{2} \right)$$

$$\boxed{\alpha = \frac{V_{p2p}}{2 \exp \left(-\frac{1}{2} \right)}} \tag{E.9}$$

From this value of α (in m/s^2) other physical quantities, such as the amplitude of displacement, can be derived.

F

AEPSYCH-MODEL CONFIGURATIONS FOR CHAPTERS 2, 3, 4, AND 5

AEpsych uses state of the art machine learning models but is designed to allow users to configure experiments using 'config files' without directly interacting with he underlying code. The config file used for the experiment in Chapter 2 is presented in listing F.1. The config file used in the experiments of Chapters 3, 4, and 5 is presented in Listing F.2.

Listing F.1 AEPsychconfig used in Chapter 2

```
[common]
parnames = [intensity, sigma]
lb = [0, 0]
ub = [1, 1]
stimuli_per_trial = 1
outcome_types = [binary]
strategy_names = [init_strat, opt_strat]
pregen_asks = True

[init_strat]
min_asks = Nsobol
generator = SobolGenerator

[opt_strat]
min_asks = Nmodel
refit_every = 5
generator = OptimizeAcqfGenerator
acqf = EAVC
model = GPClassificationModel
```

```
[GPClassificationModel]
inducing_size = 60
mean_covar_factory = default_mean_covar_factory

[OptimizeAcqfGenerator]
restarts = 10
samps = 1000
max_gen_time = 2.0

[EAVC]
target = 0.75
objective = ProbitObjective
```

For F.1 the number of initiation or sobol trials (Nsobol) was set to 20 and the number of model trials (Nmodel) was set to 30 in the experimental matlab code.

Listing F.2 AEPsychconfig used in Chapters 3, 4, and 5

F

```
[common]
parnames = [Hurst, Shore]
lb = [1, 1]
ub = [7, 7]
outcome_type = pairwise_probit
strategy_names = [init_strat, opt_strat]

[init_strat]
n_trials = 40
generator = PairwiseSobolGenerator

[opt_strat]
n_trials = n_trials_opt_strat
refit_every = 5
generator = PairwiseOptimizeAcqfGenerator
acqf = PairwiseMCPosteriorVariance
model = PairwiseProbitModel

[PairwiseMCPosteriorVariance]
objective = ProbitObjective

[PairwiseProbitModel]
inducing_size = 100
mean_covar_factory = default_mean_covar_factory
```

```
[PairwiseOptimizeAcqfGenerator]
restarts = 10
samps = 1000
```

While the sobol or initiation trials where thus set in the config, the total number of trials trials (50) was configured in the experimental matlab code. Furthermore, because the AEPsych server provided sampling parameters between 1 and 7 (a Hurst and a Shore value) that were continuous, these values were rounded up or down to the closest whole numbers, corresponding to the discrete number of stimuli (49) that were available in our 2D-stimulus space. In order to avoid that the the same physical stimulus would be selected twice, which would have required a duplicate of each stimulus, each point in the server space was matched to corresponding points in the sample space based on euclidean distances between the continuous space points and the discrete space points.

F

G

EXCLUSION AND PROCESSING OF MECHANICAL DATA FROM CHAPTER 4

G.1. INTEGRITY ISSUES AND DATA EXCLUSION

An initial aim of the study described in Chapter 4 was to collect vibration data from various points on the hand using an array of accelerometers during interactions with the textures. However, unforeseen material shortages caused by the COVID-19 pandemic prevented our grant partners from providing the necessary equipment for these measurements. In response, we developed an alternate approach to collect mechanical data from two key sites: using a custom-built load platform and tribometer at an initial interaction stage, and a single accelerometer behind the major knuckle, an early location on the hand that remained intact during local anesthesia. However, due to several data integrity issues encountered with the data collected with this equipment, the decision was made to exclude mechanical data except for rudimentary insights from the platforms. These issues are detailed below to clarify the rationale behind this decision.

BELA SYSTEM

The initial data collection used a digital signal processor (Bela, Augmented Instruments Ltd, Mile End Road, London, England), which was configured to write data at a rate of 44 kHz. Unfortunately, this rate occasionally exceeded the system's memory write speed, resulting in skipped entries and significant data loss. To address the deficiencies of the BELA system, we switched to using a Data Acquisition System (DAQ X 6343) after collection of data for the first three participants. However, further challenges were encountered as outlines below.

Authors: Camille Fradet and Karina Kirk Driller

A Drift Problem in the DAQ

For a significant proportion of the data (accelerometer and platforms), an upward trend was present, likely of electronic origin. The trials for which this drift was extreme have been excluded.

Malfunctioning Accelerometer

Because accelerometer data would have provided insights into the vibratory information available at intact hand sites, this was the most crucial element of the mechanical data collection. However, a large subset of the data was lost due to a faulty solder joint. This was first signified by intermittent signal recording failures, and later a complete failure of the device. It was likely caused during removal of the accelerometer, which was attached to the skin using skin-safe adhesive, or during accidental harsh interactions by participants. Furthermore, the remaining data exhibited a poor signal-to-noise ratio, possibly due to inadequate grounding or errors in the DAQ programming, particularly affecting the reliability of high-frequency data of interest.

Tribometer and Load Platform Limitations

Due to mechanical resonance around 90 Hz inherent to the structure of the platform, the tribometer data were restricted to low-frequency information, which limited the comprehensiveness of the mechanical data analysis. The use of a low pass filter limited the influence of the resonance on our measurements.

Data inclusion

These technical issues and equipment limitations resulted in the exclusion of most mechanical data, retaining only minimal insights from the platform data to preserve the integrity of the study and ensure the accuracy of its conclusions.

All included data from load sensor and tribometer are paired for statistical analysis. For missing data in one condition, the same trial number was excluded in the other condition for the same participant. Only datasets with 35 (70%) or more data entries in both conditions were included. A participant was excluded altogether if the resulting number of trials any condition was smaller than 70% of the total number of trials per experimental block.

In total, for tribometer data from the roughness-discrimination trials, data from 11 out of 15 participants were included in the analysis based on these criteria. This corresponded to 71% of the initial dataset. For the load cell data from the softness discrimination trials, data from 10 out of 15 participants were included in the analysis. This corresponds to 66% of the initial dataset.

G.2. Processing of Included Data

G.2.1. Description of the Data

The included raw mechanical data consisted of five data streams:

1. **Time stamps**: In seconds.
2. **Load cell stream**: Signal, in volts, from the force sensor embedded in the load cell platform and amplified. Used for the softness trials only. It recorded the normal force applied by the participant on the sample.
3. **Tribometer tangential force sensor stream**: Signal, in volts, from the force sensor embedded in the tribometer platform and amplified. Used for the roughness trials only. It recorded the tangential force of the interactions between the finger and the sample.
4. **Tribometer normal force sensor stream #1**: Signal, in volts, from the force sensor embedded in the tribometer platform and amplified. Used for the roughness trials only. It recorded the normal force applied to one of the extremities of the platform.
5. **Tribometer normal force sensor stream #2**: Signal, in volts, from the force sensor implemented in the tribometer cell platform and amplified. Used for the roughness trials only. It recorded the normal force applied at one of the extremities (opposite to the other normal force sensor) of the platform.

An 80 Hz first order low pass Butterworth filter was applied forward and backward to the platform signals, resulting in a zero phase shift second order filter.

G.2.2. APPLYING SENSOR SENSITIVITY TO RAW DATA

The sensor signals after amplification needed to be converted to physical values. Table G.1 gives the sensitivity and offset values to make the transformation.

Data Stream	Sensitivity (N/V)	Offset (N)
Load cell (amplified)	17.419	-3.136
Tribometer - tangential force (amplified)	2.5	-5
Tribometer - normal force (amplified)	0.625	0

Table G.1. From raw data to physical values

G.2.3. CALCULATED VARIABLES

Some variables were obtained by combining the data streams.

- **Position and velocity** of the finger on the tribometer platform: Using beam theory and general equilibrium theory with the three data streams from the tribometer it is possible to determine contact position in two ways. We computed an estimate of the center of pressure of the contact area between the finger an the sample by averaging the results from both position computation methods.

$$x_1 = \frac{L \cdot N_2 - h \cdot T}{N_1 + N_2}$$

$$x_2 = L - \frac{L \cdot N_1 + h \cdot T}{N_1 + N_2}$$

$$x_{est} = \langle x_1, x_2 \rangle$$

With L being the distance between the two normal force sensors, h the height difference between the tangential force sensor and the normal force sensors, N_1 and N_2 the normal force signals and T the tangential force signal.

- **The coefficient of friction** was obtained, for tribometer data, from the ratio between the tangential force and the resultant of the normal forces.

$$\mu = \frac{T}{N_1 + N_2}$$

Then the interaction velocity was obtained with a numerical derivative of the position.

G.2.4. SIGNAL STATISTICS

Statistics were applied on variables from each trial. The statistics applied were:
- Moment order 1 : average
- Moment order 2 : standard deviation
- Moment order 3 : skewness
- Moment order 4 : kurtosis

The variables they were applied to are:
- For roughness trials
  – Interaction velocity
  – Load applied
  – Coefficient of friction
- For softness trials
  – Peaks of load applied

All data processing was performed using MatLAB (version R2021b).

H

PARTICIPANT-WISE MODEL PREDICTIONS FOR CHAPTER 4
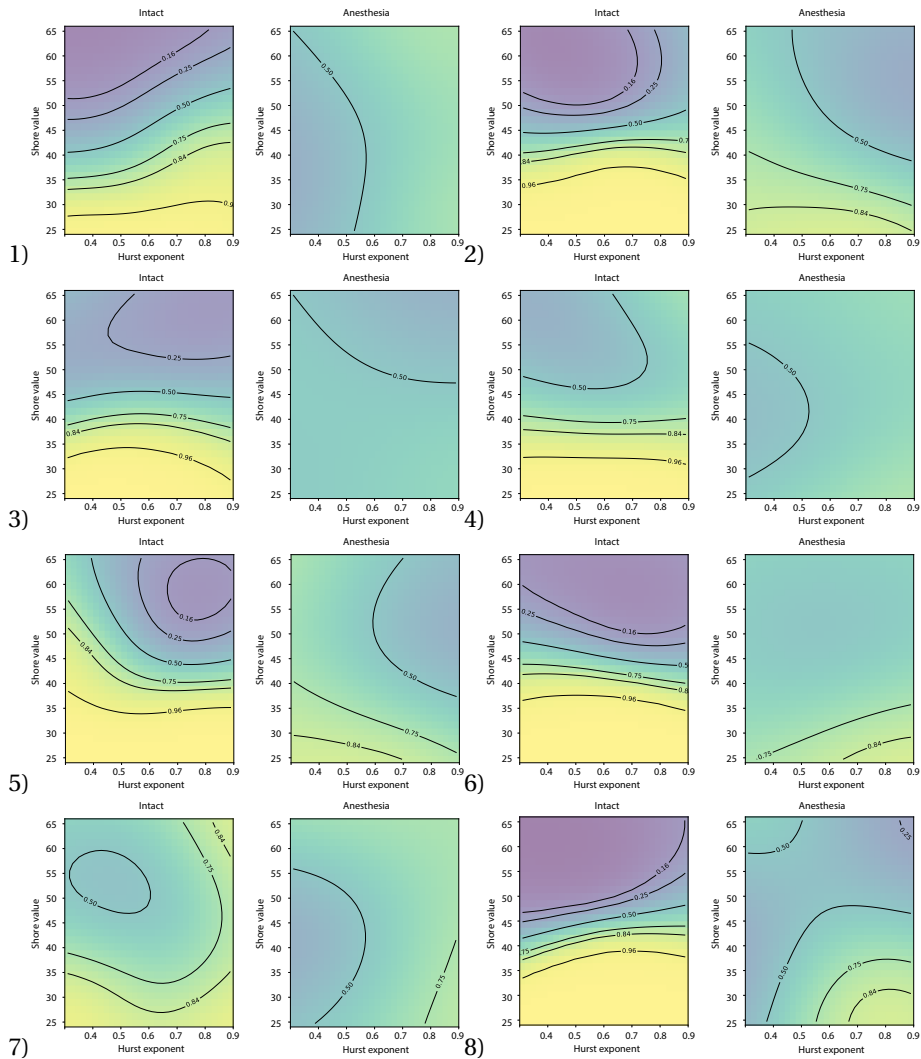
Figure H.1. Softness discrimination—Model predictions for each participant and condition (anesthesia/intact). Predictions were made on a dense grid of Hurst and Shore values. The background color indicates the probability that a stimulus would be rated as softer than a stimulus with the median Hurst/Shore values. Isocontours are plotted at 16%, 25%, 50%, 75%, 84%, and 96%. (continued on next page)
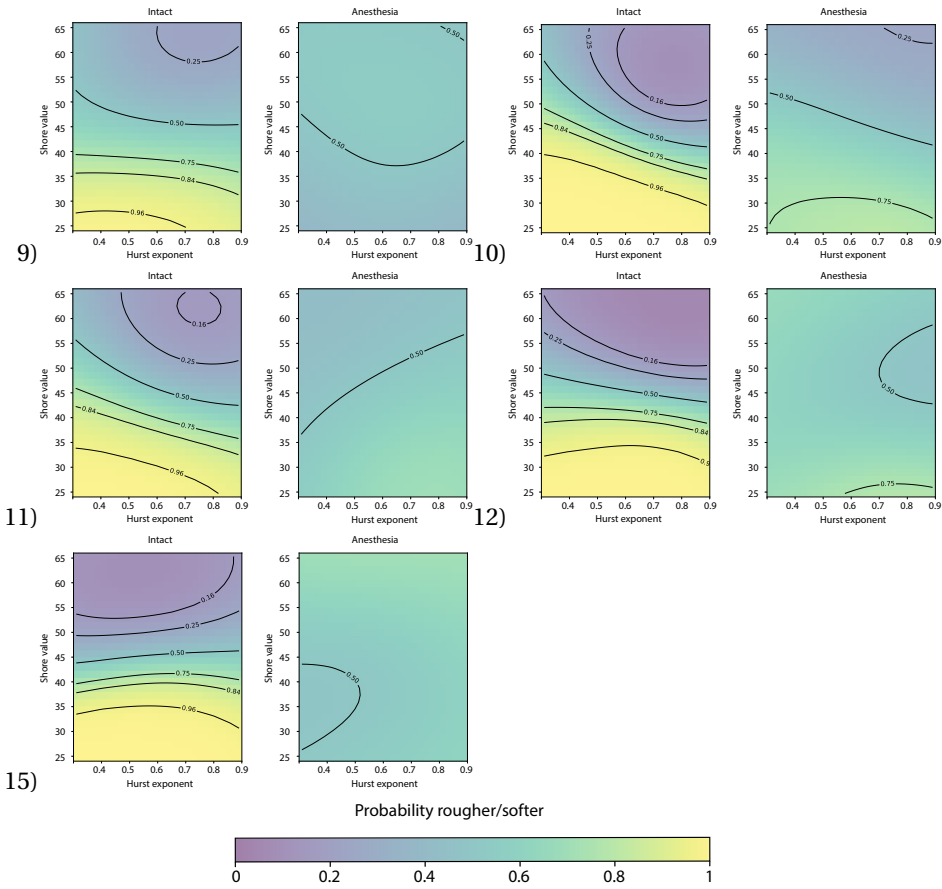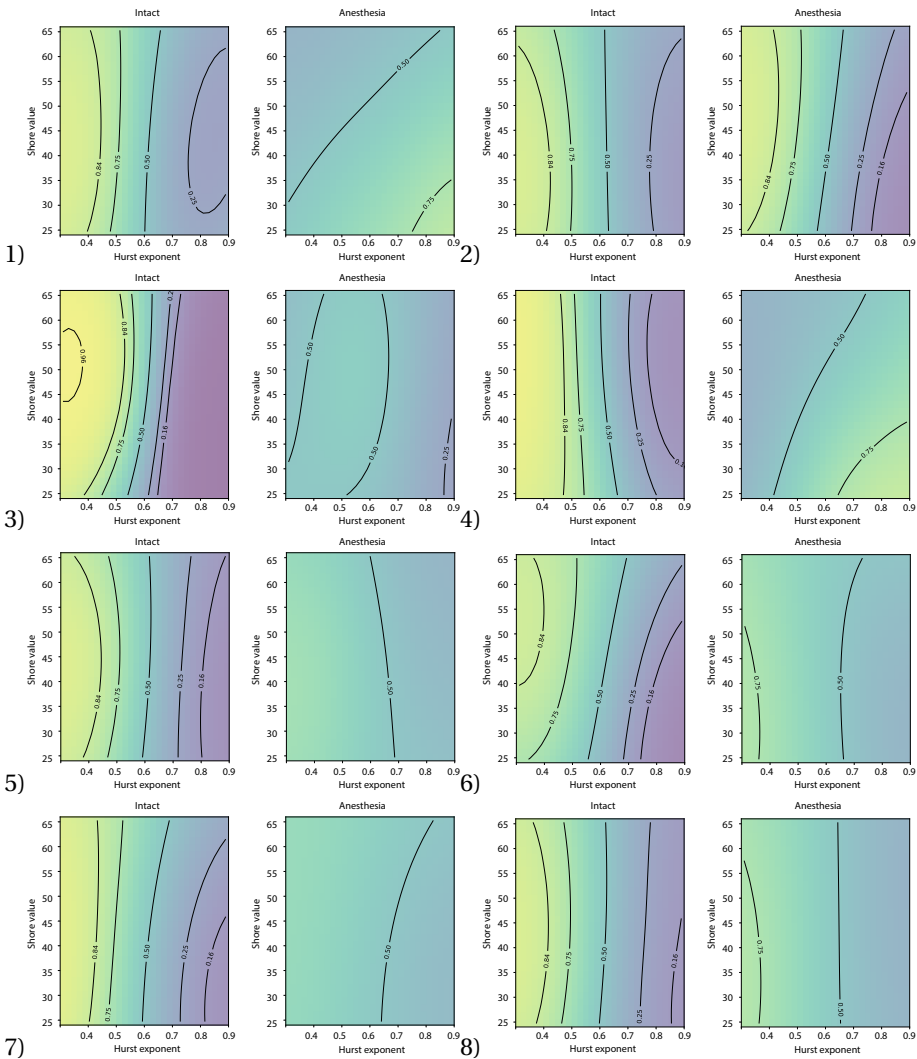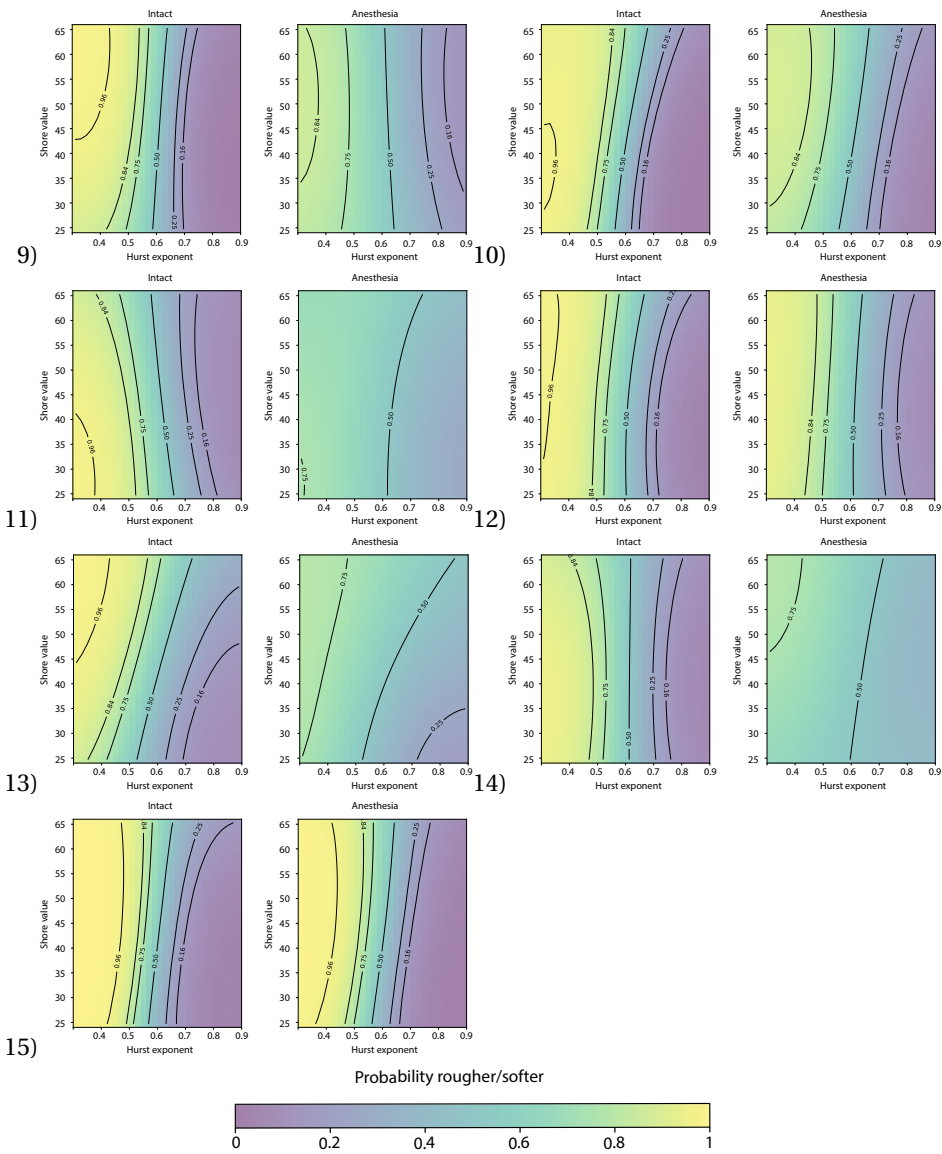
**Figure H.1.** (continued from previous page)

Figure H.2. Roughness discrimination—Model predictions for each participant and condition (anesthesia/intact). Predictions were made on a dense grid of Hurst and Shore values. The background color indicates the probability that a stimulus would be rated as more rough than a stimulus with the median Hurst/Shore values. Isocontours are plotted at 16%, 25%, 50%, 75%, 84%, and 96%. (continued on next page)

Figure H.2. (continued from previous page)

252
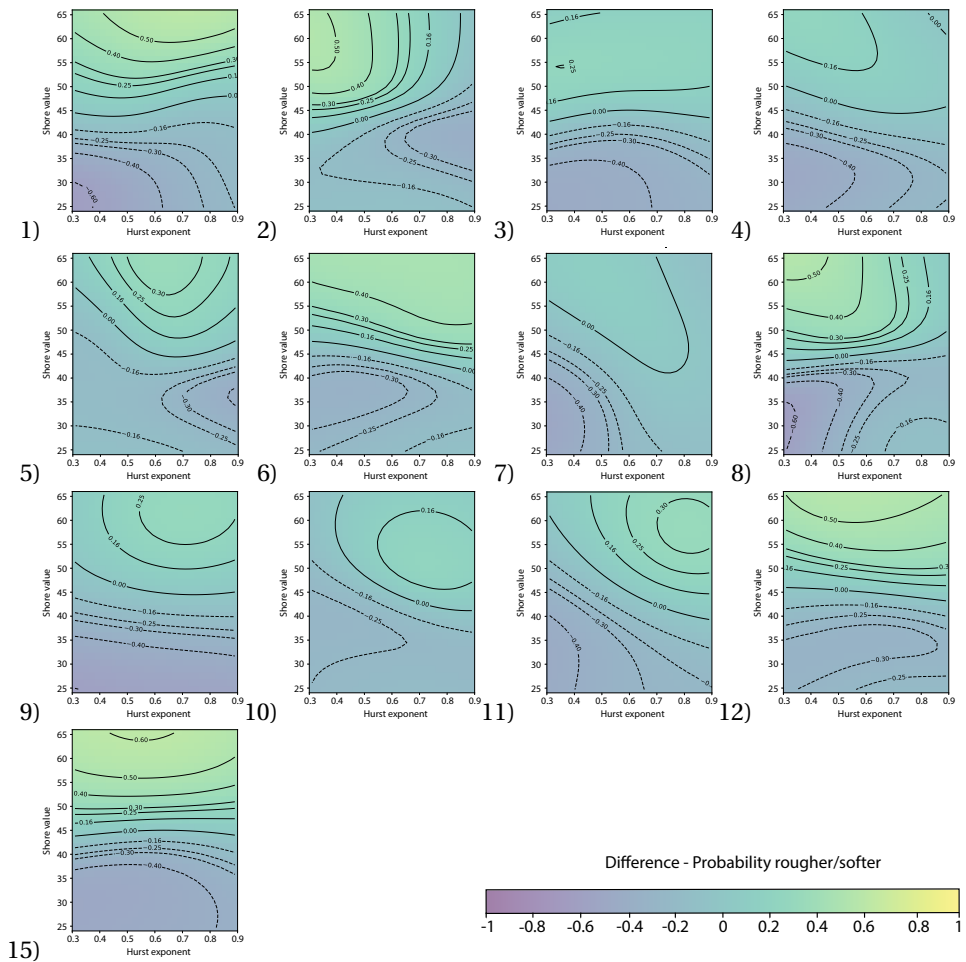
Figure H.3. Softness discrimination—Difference between Anesthesia and intact calculated as (a) the mean across all subjects and (b) for each individual subject. Isocontours are plotted at 16%, 25%, 50%, 75%, 84%, and 96% and here indicate the *difference* in probability of a sample being chosen as softer between the two conditions.

252
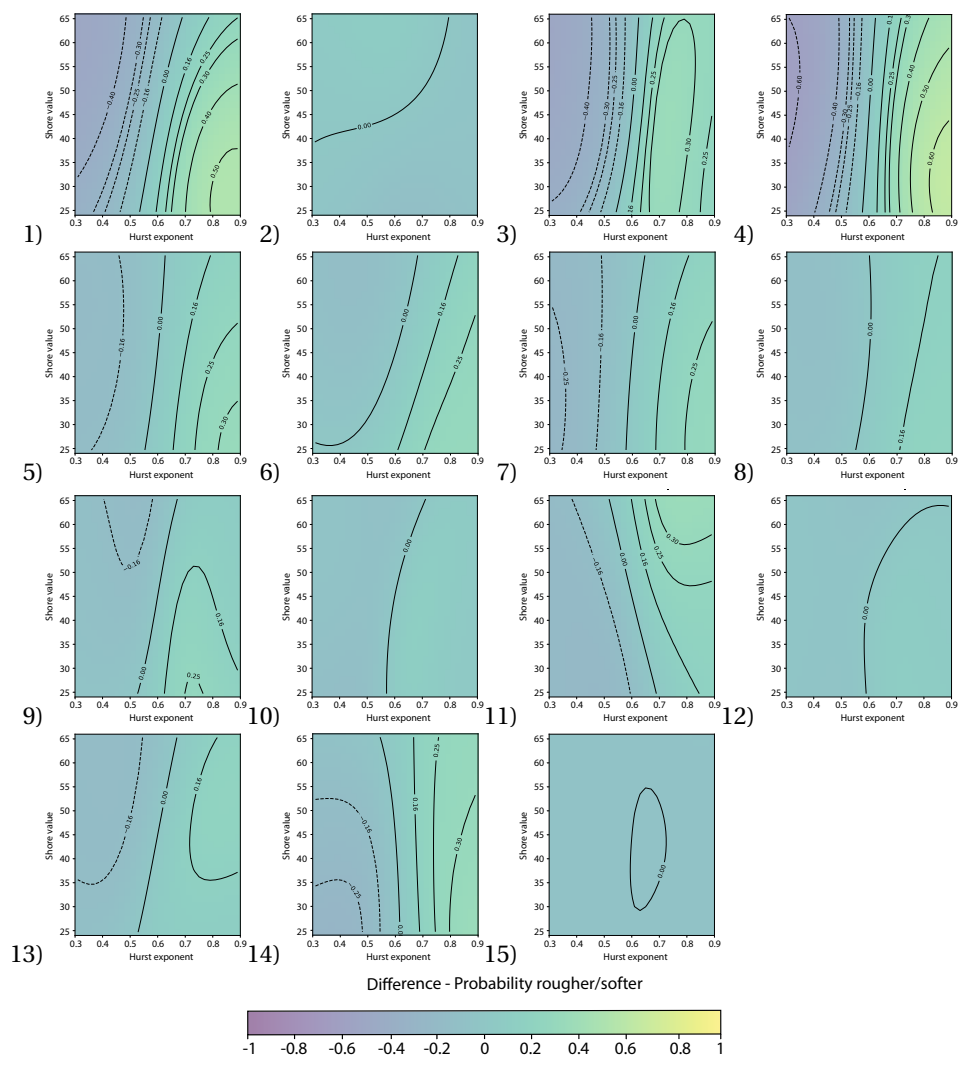
Figure H.4. Roughness discrimination—Difference between Anesthesia and intact calculated as (a) the mean across all subject and (b) for each individual subject. Isocontours are plotted at 16%, 25%, 50%, 75%, 84%, and 96% and here indicate the *difference* in probability of a sample being chosen as rougher between the two conditions. Dashed lines indicate a negative difference.
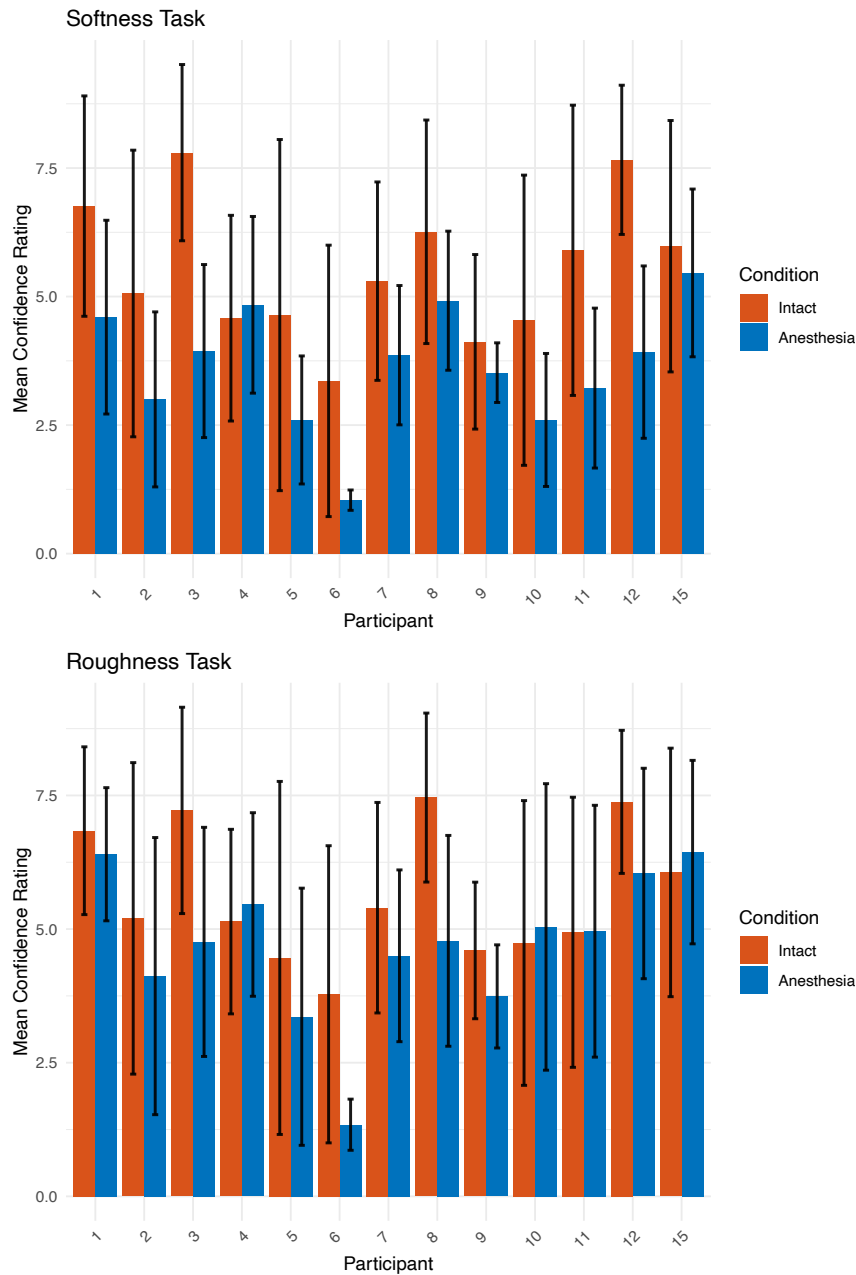
Figure H.5. Mean confidence ratings for the intact and anesthesia condition per participant for softness discrimination (top) and roughness discrimination (bottom). Error bars indicate the standard deviation from the mean.

H

I

PARTICIPANT-WISE INTERACTION PLOTS FOR CHAPTER 4

Figure I.1 shows the mean peak loads applied during softness discrimination. Figure I.2 displays the mean velocity as a function of the mean normal force for each condition and participant. The plots provide a visualization of how individual participants interactions with the samples differed between the two conditions. Figure I.3 shows the mean friction coefficient for each condition and participant, a measure that is commonly affected by both the velocity and normal force applied during an interaction, as well as changes in moisture content of the finger pad, which in the present study took place as a side effect of the local anesthesia (cf. Section 4.3.2).

The same data as outlined in Appendix G are included here.

(a) Participant 1

(b) Participant 3

(c) Participant 4

(d) Participant 6

(e) Participant 7

(f) Participant 8

(g) Participant 9

(h) Participant 10

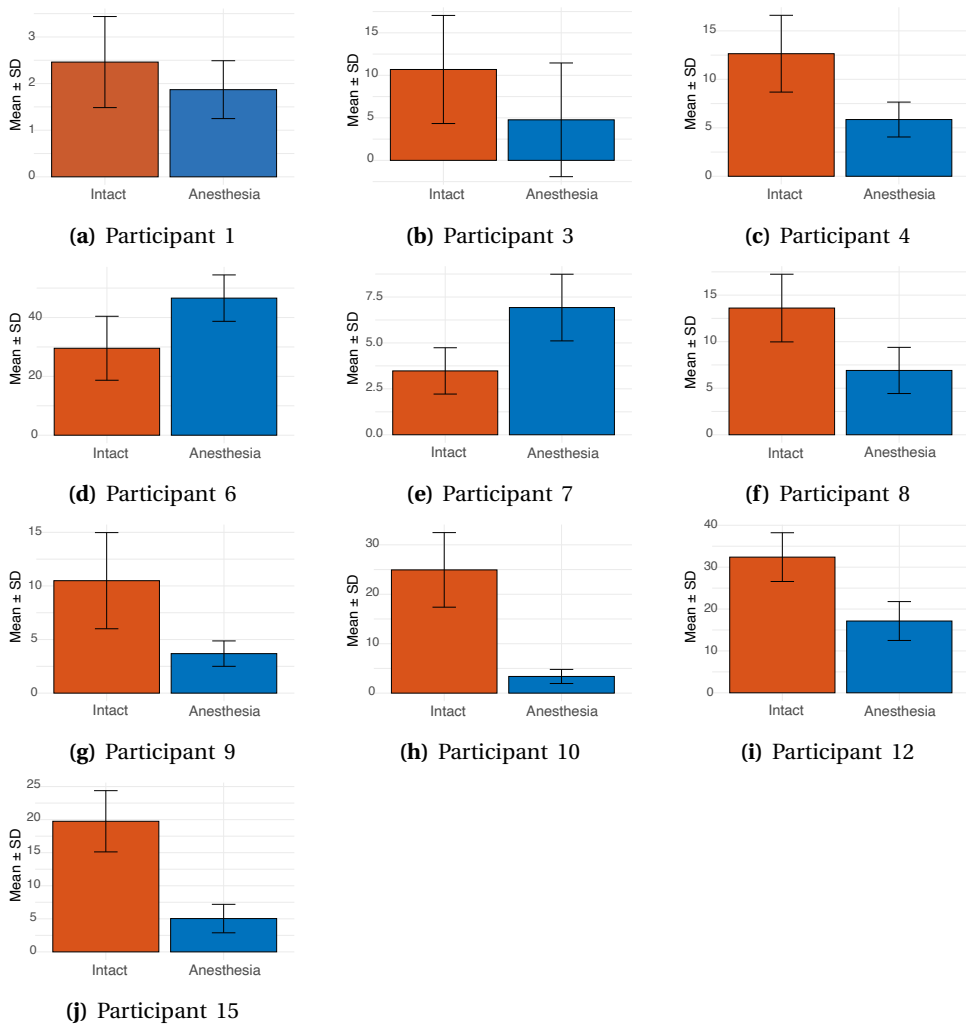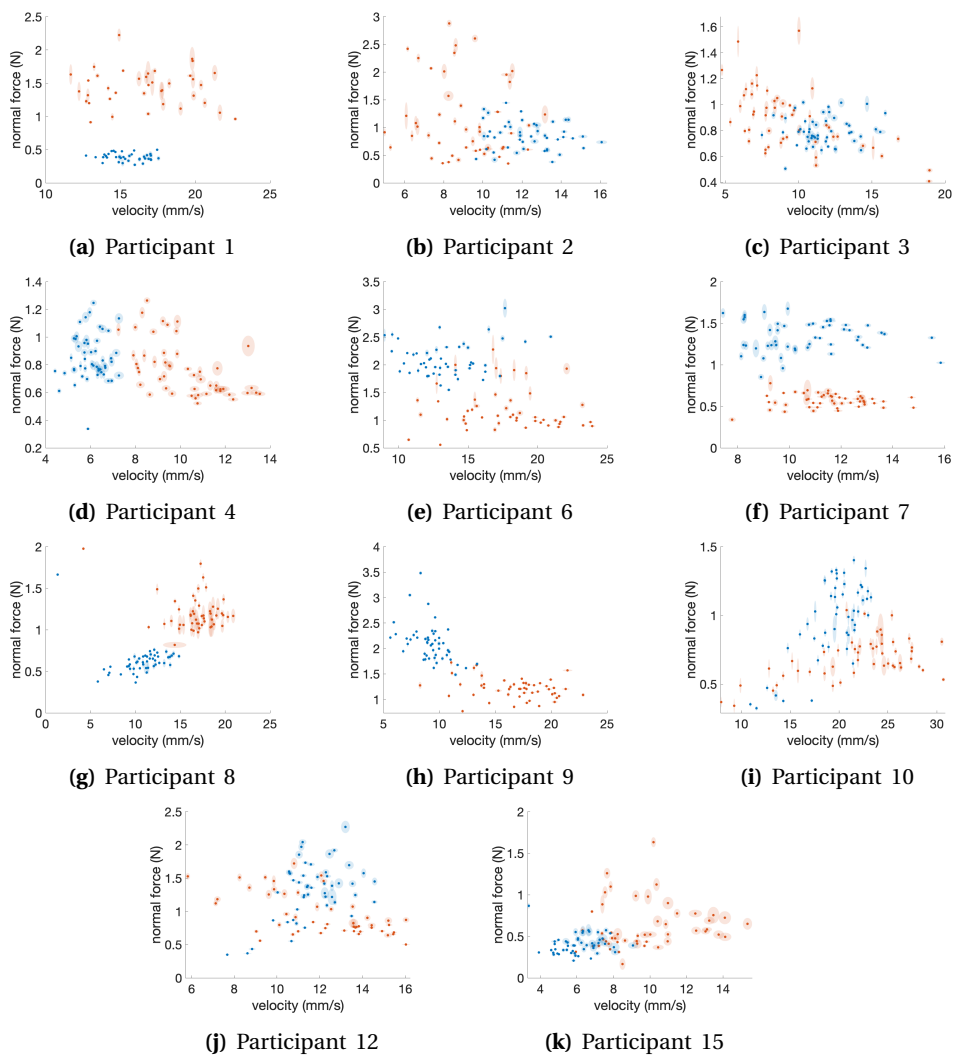**(i)** Participant 12

(j) Participant 15

Figure I.1. Softness discrimination: Participant-wise Peak load. Mean peak load applied applied for each condition (averaged across interactions with both samples within a trial). Error bars indicate standard deviation of means.

Figure I.2. Roughness discrimination: Participant-wise interaction scatter plots. Mean velocity as a function of mean normal force. Within each plot, a single point corresponds to the mean value of a single trial (averaged across interactions with both samples within a trial). The shaded area behind each point displays the standard deviation within this trial, providing insights into the range of different velocities (horizontal extent) and forces (vertical extent) applied during the trial. Red: Intact. Blue: Anesthesia.
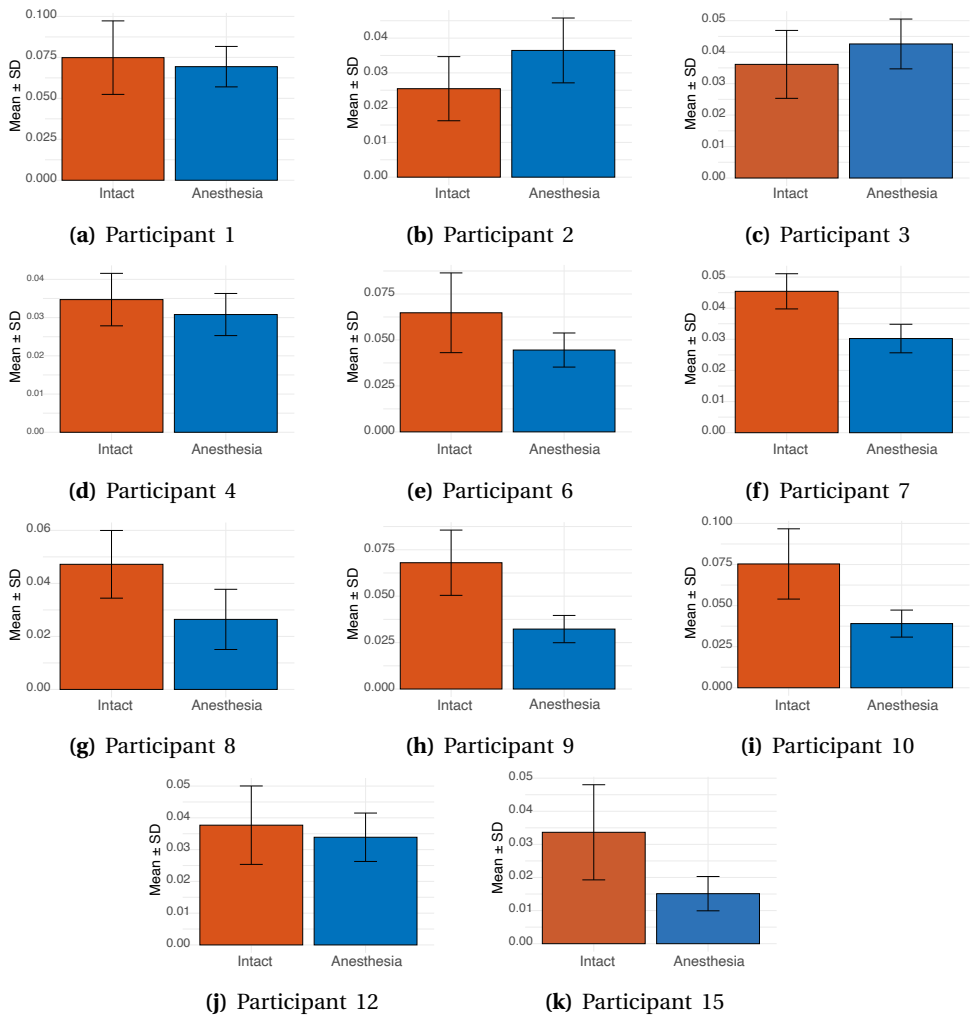
Figure I.3. Roughness discrimination: Participant-wise friction bar plots. Mean Coefficient of Friction for each condition (averaged across interactions with both samples within a trial). Error bars indicate standard deviation of means.

I

J

Ecoflex™ Mixing Ratios for Chapter 5

Ecoflex™ 00-30 is a two-part silicone elastomer, where parts A and B are mixed in equal proportions (a 1:1 ratio) to achieve a Shore-00 hardness of approximately 30. The Shore-00 scale measures the material's hardness, with higher values signifying increased hardness. Modifying the ratio of parts A to B allows for the tuning of the elastomer's hardness or elasticity. Typically, decreasing the amount of part B relative to part A leads to a harder material with a lower elasticity and higher shore value (e.g., [1]). Table J.1 documents the mixing ratios used for the stimuli created in Chapter 5, indicating the quantity of part B for every one part of A.

Table J.1. Silicone mixing ratio for the stimuli used in Chapter 5.

Elasticity Nr.	E1	E2	E3	E4	E5	E6	E7
Ratio part B per 1A	0.125	0.146	0.16	2	1	0.5	0.25
Shore-00 value	9	18	25	32	39	43	47

It is salient from Table J.1 that the relationship between the proportions of parts A and B, where a greater proportion of part A typically results in a higher Shore 00 value, inverts beyond a certain threshold. Specifically, when the amount of part B is significantly reduced relative to part A, the trend reverses, and a further decrease in part B result in specimens with a lower Shore value. Samples E1–E3 demonstrate this behavior. This phenomenon is further illustrated in Figure J.1.

To the best of our knowledge, this phenomenon has not been previously reported in the literature, yet it was consistently observed in our test samples and was therefore utilized to produce samples with especially-low elasticity in Chapter 5. It must finally be noted that the physical properties of Ecoflex™ elastomers can change over time, depending on factors such as UV-exposure, temperature, humidity and mechanical stress. Variations in measurements are thus common [1]. In the present study, Shore-00 hardness measurements for the stimulus set were conducted a few weeks post-fabrication, immediately following data collection. This timing may account for the relatively high Shore value of 39 for the 1:1 mixing ratio. Researchers
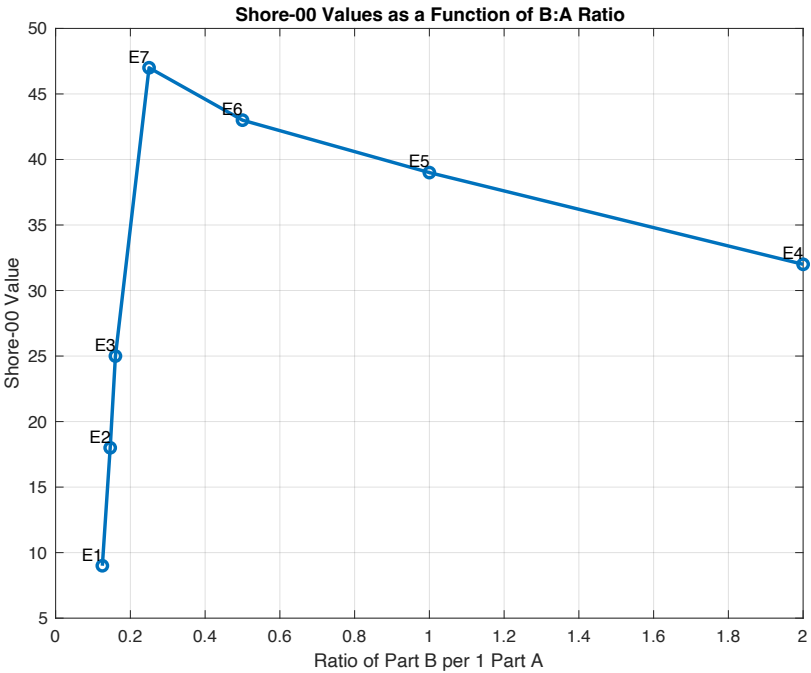
Figure J.1. Achieved shore-00 hardness as function of Ecoflex™ 00-30 mixing ratio for the stimuli used in Chapter 5.

should account for such potential material changes by conducting measurements and documentation close to perceptual data collection.

J

ACKNOWLEDGEMENTS

CURRICULUM VITÆ

Karina Kirk DRILLER

13-08-1991	Born in Flensburg, Germany.
2012–2015	BSc in Psychology, Aarhus University, Denmark
2015–2017	MSc in Psychology, Aarhus University, Denmark
2017-2018	Visiting Researcher at Humboldt University of Berlin Department of Psychology (Biological Psychology and Psychophysiology; w. Prof. Werner Sommer)
2019–2024	PhD in haptic perception, TU Delft & Sorbonne Université within the EU Horizon 2020 project H-Reality Joint supervision by: Jess Hartcher-O'Brien & Vincent Hayward Promotor: Richard Goossens

LIST OF PUBLICATIONS

- Driller, K. K., Fradet, C., Hayward, V., and Hartcher-O'Brien, J. "Conception and Design of a Dual-Property Haptic Stimuli Database Integrating Stochastic Roughness and Elasticity". In: Haptics: Understanding Touch; Technology and Systems; Applications and Interaction. Ed. by Kajimoto, H., Lopes, P., Pacchierotti, C., Basdogan, C., Gori, M., Lemaire-Semail, B., and Marchal, M. Springer Nature Switzerland, 2024, pp. 223–237. DOI: 10.1007/978-3-031-70061-3_19

- Driller, K. K., Fradet, C., Mathijssen, N., Kraan, G., Goossens, R., Hayward, V., and Hartcher-O'Brien, J. Increased temporal binding during voluntary motor task under local anesthesia. *Scientific Reports* **13** (2023). Number: 1 Publisher: Nature Publishing Group, 14504. DOI: 10.1038/s41598-023-40591-x

- Howard, T., Driller, K., Frier, W., Pacchierotti, C., Marchal, M., and Hartcher-O'Brien, J. Gap detection in pairs of ultrasound mid-air vibrotactile stimuli. *ACM Transactions on Applied Perception* **20** (Jan. 2023), 5:1–5:17. ISSN: 1544-3558. DOI: 10.1145/3570904

- Stephani, T., Kirk Driller, K., Dimigen, O., and Sommer, W. Eye contact in active and passive viewing: Event-related brain potential evidence from a combined eye tracking and EEG study. en. *Neuropsychologia* **143** (June 2020), 107478. ISSN: 00283932. DOI: 10.1016/j.neuropsychologia.2020.107478

- Driller, K., Frier, W., Pont, S., and Hartcher-O'Brien, J. Mid-Air Ultrasonic Stimulations of the Palm - The Influence of Frequency and Stimulus Duration on Perceived Intensity: WHC 2019 : IEEE World Haptics Conference. *World Haptics Conference, Tokyo, Japan* (2019). Ed. by Shinoda, H. and Kajimoto, H.

- Kirk Driller, K., Stephani, T., Dimigen, O., and Sommer, W. Large lateralized EDAN-like brain potentials in a gaze-shift detection task. en. *Psychophysiology* **56** (July 2019), e13361. ISSN: 0048-5772, 1469-8986. DOI: 10.1111/psyp.13361